DISSERTATION

ENGINEERING EFFECTIVE FIBROCARTILAGE REPLACEMENT TECHNOLOGIES USING NANOSTRUCTURE-DRIVEN REPLICATION OF SOFT TISSUE BIOMECHANICS IN THERMOPLASTIC ELASTOMER HYDROGELS

Submitted by

Jackson Tyler Lewis

Graduate Degree Program in Bioengineering

In partial fulfillment of the requirements

For the Degree of Doctor of Philosophy

Colorado State University

Fort Collins, Colorado

Spring 2018

Doctoral Committee:

Advisor: Travis S. Bailey
Co-Advisor: Tammy L. Haut Donahue

Susan P. James
Ketul C. Popat
Yan (Vivian) Li

ABSTRACT

ENGINEERING EFFECTIVE FIBROCARTILAGE REPLACEMENT TECHNOLOGIES USING NANOSTRUCTURE-DRIVEN REPLICATION OF SOFT TISSUE BIOMECHANICS IN THERMOPLASTIC ELASTOMER HYDROGELS

Synthesis of hydrogel networks capable of accurately replicating the biomechanical demands of musculoskeletal soft tissues continues to present a formidable materials science challenge. Current systems are hampered by combinations of limited moduli at biomechanically relevant strains, inefficiencies driven by undesirable hysteresis and permanent fatigue, and recovery dynamics too slow to accommodate rapid cycling prominent in most biomechanical loading profiles. This dissertation presents a new paradigm in hydrogel design based on prefabrication of an efficient nanoscale network architecture using the melt-state self-assembly of amphiphilic block copolymers. Rigorous characterization and preliminary mechanical testing reveal that swelling of these preformed networks produce hydrogels with physiologically relevant moduli and water compositions, negligible hysteresis, sub-second elastic recovery rates, and unprecedented resistance to fatigue over hundreds of thousands of compressive cycles. By relying only on simple thermoplastic processing to form these nanostructured networks, the synthetic complexities common to most solution-based hydrogel fabrication strategies are completely avoided. Described within this dissertation are a range of efforts, broadly focused on refining synthetic and post-synthetic processing techniques to improve the modulus, surface hydrophilicity, fatigue resistance and cytocompatibility of these thermoplastic elastomer hydrogels, with the ultimate goal of producing a material viable as a meniscal replacement.

TABLE OF CONTENTS

CHAPTER 1

MOTIVATION AND INSPIRATION FOR HYDROGELS AS A SYNTHETIC FIBROCARTILAGE REPLACEMENT

1.1 INTRODUCTION [1]

1.1.1 Osteoarthritis of the Knee

Nearly one in two people develop symptomatic OA of the knee by age 85[1], and among obese people, the rate rises to every two out of three.[1] Total knee replacements are one of the major treatment methods for severe OA of the knee, with over 500,000 replacements performed annually.[2] Due to an aging population, that rate is projected to grow to nearly 3.5 million by 2030.[2] One major effort to combat OA is to promote the healing of articular cartilage, the firm tissue found on the surface of articular joints. Articular cartilage is avascular and therefore does not possess the ability to heal effectively. One way to promote healing is by inducing injury in the vascularized subchondral bone using microfracture,[3] drilling,[4] or other abrasion techniques in order to stimulate the formation of a new blood supply.[4] Another means of repairing injured cartilage is through autologous chondrocyte implantation, which is done by taking cartilage from non-weight bearing portions of the bone, culturing the cells, and then injecting them into the damaged site under a periosteal cover.[5] There is also autologous implantation where a cartilage plug is directly transferred from a non-load bearing region to the damaged site.[5] Other more recent research has focused on approaches involving tissue engineering where chondrocytes are seeded into a scaffold to stimulate the growth of new tissue in the damaged region.[5] There are

[1] This chapter and its contents were written and prepared by Jackson Lewis.

several candidate materials for tissue engineering scaffolds including synthetic polymer scaffolds, hydrogel scaffolds, ECM component scaffolds and tissue-derived scaffolds.[6] However, balancing a myriad of factors including uniform cell infiltration, cell migration, scaffold degradation rates, and the preservation of mechanics have proven to be a very formidable challenge.[6]

While the effort to heal damaged cartilage is critical in the battle against OA, it would be ideal to prevent or postpone the onset of damage to articular cartilage in the first place. It is believed that excessive friction and stress concentrations are some of the leading causes in the acceleration of cartilage wear.[7] Healthy synovial joint friction mechanics are the product of both biomechanical and biomolecular factors.[7] Matej et al. note two major biomechanical contributors to the minimization of contact stresses on the cartilage extracellular matrix (ECM) (1) joint congruity and cartilage deformation, which effectively distribute the biomechanical load over a large contact area and (2) high water content and low hydraulic permeability, which allows for fluid pressurization to bear nearly 90% of the load.[7] Biomolecular factors on the other hand are largely attributed to the formation of effective joint lubrication. There are three major forms of joint lubrication (1) boundary lubrication (surface-surface) which is based on the properties of the uppermost layer of cartilage[8] (2) fluid film lubrication where a layer of synovial fluid separates the two articulating surfaces[8] and (3) a combination of boundary and fluid film lubrication often referred to as "mixed lubrication".[7] Maintaining fluid film generation is critical to minimizing the coefficient of friction within the joint and is the product of weeping lubrication (lubricating films are squeezed into dimples of cartilage) [9] acting in concert with boosted lubrication (dimples within cartilage contain enriched synovial fluid).[7, 10]

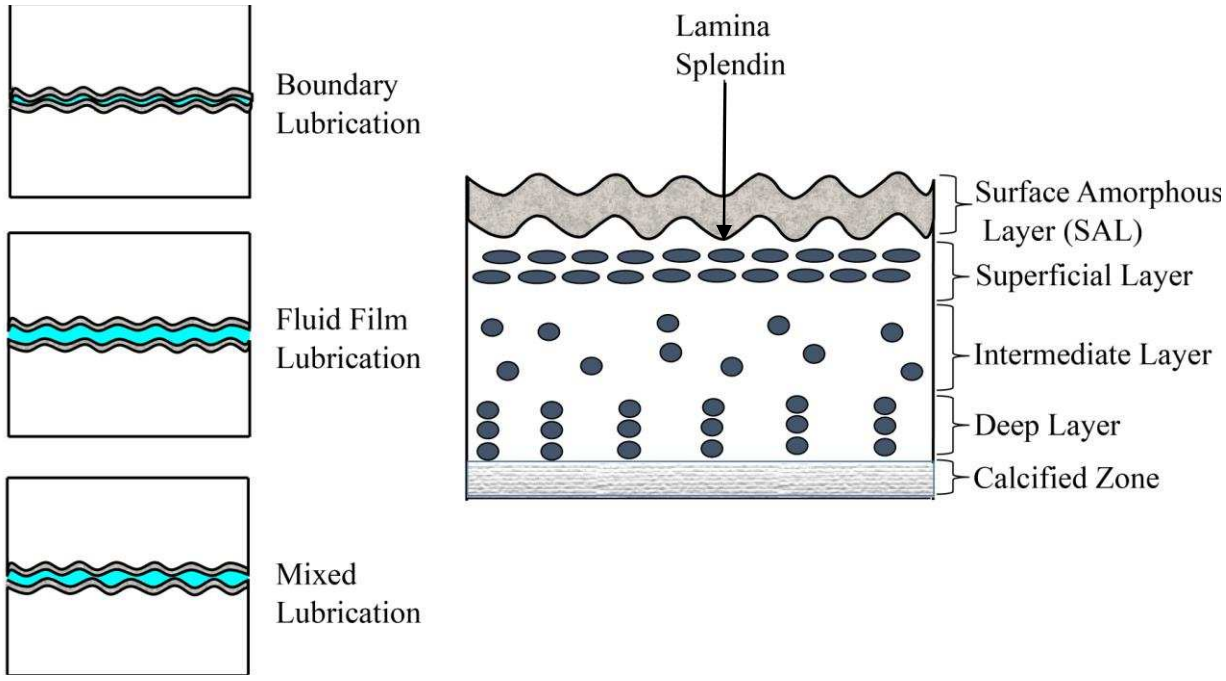

Figure 1.1: *Left:* There are three major forms of joint lubrication: (1) boundary lubrication (surface-surface), (2) fluid film lubrication (surfaces are separated by fluid), and (3) mixed lubrication (a combination of boundary and fluid film). *Right:* There are five distinct regions within cartilage with unique compositional, structural and cellular properties (from deepest layer to surface layer): (1) The calcified zone is distinguished by its high calcium salt concentrations and is where the cartilage attaches to the subchondral bone, (2) the deep layer consists of collagen and chondrocyte orientation perpendicular to the articulating surface, (3) the intermediate layer consists of spherical chondrocytes distributed throughout a randomly oriented collagen mesh, (4) the superficial layer is most resistant to wear and consists of flattened chondrocytes within a collagen matrix that runs tangential to the articulating surface and (5) the recently discovered gel-like acellular and nonfibrous surface amorphous layer which consists of adhered specialized molecules such as hyaluronic acid, lubricin, or surface-active phospholipids.

While cartilage is often discussed in terms of four distinct regions[11] with the once uppermost region being referred to as the lamina splenden[7], recent studies have revealed a thin (20 ± 10 μm) gel-like acellular and nonfibrous layer on top of the lamina splenden[12] of bound specialized molecules of the synovial fluid, in particular: hyaluronic acid, lubricin, and surface-active phospholipids[13] (**Figure 1.1**). This layer has been called the surface amorphous layer (SAL)[7]. It is believed that these highly hydrophilic molecules bind water tightly and result in the promotion of fluid-film lubrication which produces the incredibly low coefficients of friction

observed by articular cartilage (μ as low as 0.002) [14]. Stribeck curves of articular cartilage suggest a permanent "fluid-like" film at the surface of articular cartilage[7] which may be attributed to the SAL.

The knee meniscus protects and promotes an environment such that the biomechanical and biomolecular factors of cartilage can function optimally within the knee joint. The knee meniscus is a structurally complex soft tissue that increases joint stability, distributes axial load, and reinforces the lubrication mechanisms of the articular cartilage.[6, 15] The meniscus is often discussed in terms of two distinct regions (red-red and white-white) with a transition region between them (red-white).[6] The peripheral red-red region is vascularized (outer 10-30%), while the inner white-white region is largely avascular.[6] Unfortunately, like articular cartilage, the avascular nature of the white-white region makes healing in this region highly unlikely. Damage to the meniscus can occur from normal wear and tear,[16] aging,[17] or from a traumatic injury[18] and has been strongly linked to the formation of OA in the knee joint.[19]

The current treatment for damaged menisci is either a partial or full meniscectomy. However, this procedure is not an effective long-term solution, as removal of the protective fibrocartilage tissue may result in immediate pain relief, but it comes at the cost of an accelerated deterioration of the underlying articular cartilage.[6] Despite this, the meniscus's inability to heal combined with its high susceptibility to injury lead to 387,833 meniscectomies being performed in the US from 2005 to 2011.[20] A treatment or replacement for damaged menisci will therefore be critical in slowing or preventing the progression of OA in the knee joint.

1.1.2 Current Efforts to Engineer a Meniscus Replacement

The cellular, compositional and structural makeup between regions within the meniscus are distinct and act in concert to produce its unique mechanical and lubricating properties. The tissue is comprised of a highly hydrated (72% water by mass) and structurally intricate ECM (28% by mass).[6] Within this ECM is a unique class of cells, often characterized as "fibrochondrocytes" as they possess many of the characteristics of both fibroblasts and chondrocytes.[6] The ECM of the meniscus is primarily composed of collagen (75% by mass).[15] The type of collagen varies from region to region within the meniscus, with the red-red region being primarily composed of type I collagen (80%), while the white-white region is a mixture of type II (60%) and type I (40%).[15] These collagen fibers adopt a circumferential orientation in the deeper regions of the meniscus (**Figure 1.2**), eventually blending into the tibial surface via the meniscal horns.[15] At the surface, the collagen fibers adopt a radial orientation, this radial orientation also exists in the deeper layers of the tissue as "radial tie fibers" which provide structural integrity.[15] This structure when compressed converts axial forces into hoop stresses, effectively transmitting the axial load via tensile stresses on the circumferential fibers to the tibial plateau via the posterior horns.[15] The tissue's collagen structure results in mechanical anisotropy with a much higher modulus in tension (50 to 200 MPa [21]) than in compression (0.5 to 2 MPa[21]).

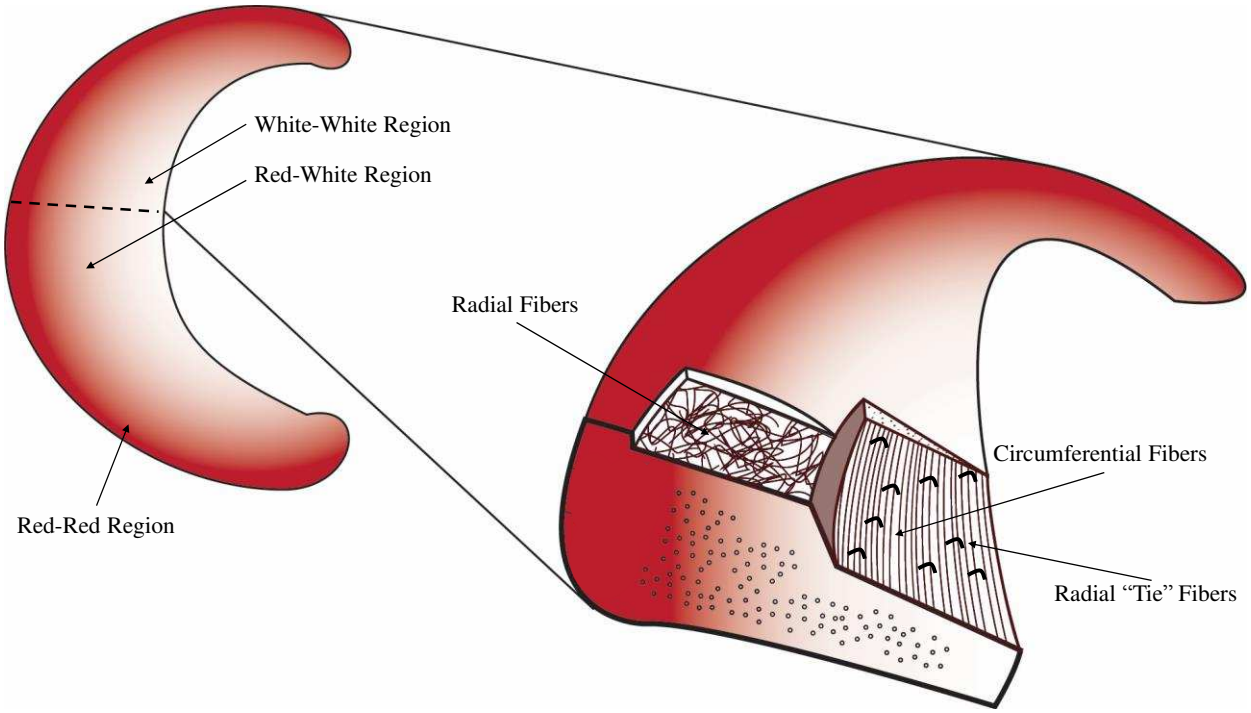

Figure 1.2: Collagen structure and vascularization within the knee meniscus. *Left*: Varying degrees of vascularization with the meniscus. Red-red region contains the majority of vascularization within the meniscus and constitutes approximately the outer one third. *Right*: Collagen orientation is circumferential within the deeper layers of the tissue with reinforcing radial tie fibers and consists of a lamellar surface layer with a more random collagen orientation.

Glycosaminoglycans (GAGs) constitute the next major contributor to the dry mass of the meniscus at approximately 17%. [15] The most prevalent GAGs in the meniscus are chondroitin-6-sulfate (40%), chondroitin-4-sulfate (10% to 20%), dermatan sulfate (20% to 30%), and keratin sulfate (15%).[15] Proteoglycans contribute approximately 1% to 2% of the dry mass of the meniscus and consist of a core protein decorated with one or more covalently linked GAGs.[15] Aggrecan, the most common proteoglycan in the meniscus, often forms aggregates via a non-covalent interaction between hyaluronic acid and link proteins.[15] Because of their high fixed-charge density and repulsion forces, these proteoglycans are attributed with providing the tissue with hydration and a resistance to compressive loads.[15] The large swelling pressure within the meniscus is counteracted by tension within the collagen matrix.[15] This hydrated polymer matrix

results in a unique viscoelastic mechanical loading profile and may play a critical role in joint nutrition and lubrication .[15] The lubricating properties of the meniscus have been attributed to the movement of synovial fluid to the surface of the meniscus via microcanals located close to the blood vessels, this synovial fluid is eventually compressed into the articular cartilage.[15] Notably, the role of the meniscus in lubrication in the knee joint is highly complex and not well understood.

The structural complexity and resulting biphasic nature and lubricating properties of the native tissue makes recreating its mechanical and biomolecular responses using traditional plastics or ceramics extremely difficult. Tienen et al. has postulated that there are two major classes of meniscal substitutes (1) resorbable implants that stimulate tissue regeneration and (2) non-resorbable implants to replace the meniscus (partially or fully).[22] For example, the NUsurface® meniscal implant is made from a composite of polycarbonate-urethane and UHMWPE. This implant is currently designed for patients who have suffered partial meniscal tears and functions as a permanent replacement in order to help the remaining tissue facilitate articulation in the joint.[22] However, the elastomeric nature of this implant does not demonstrate any relaxation upon loading associated with the biphasic composition of the natural tissue, which may ultimately limit its ability to replicate an accurate biomechanical response. Also, it may inhibit the natural lubricating mechanisms once maintained by the native tissue. Furthermore, it cannot function as a full meniscal replacement in its current form, as it relies on the meniscal rim to function.

Ideally, tissue engineering would one day enable us to repair and regrow the meniscus, however, these cell-seeded scaffolds have, as mentioned above, been unable to perform in the mechanically-demanding environment of the knee joint.[6] In the meantime, a synthetic meniscal

replacement must be further developed to, first and foremost, perform the function of the natural tissue: to protect the underlying articular cartilage and help facilitate healthy articulation in the joint. By first focusing on how we want the synthetic replacement to perform instead of directly mimicking the native tissue, we may be able to even improve upon some of the limitations of the native meniscus, especially its high susceptibility to tearing at low strains. An ideal replacement would possess the biphasic nature, lubrication mechanisms, cytocompatibility and mechanical robustness of the native tissue while being easily integrable during surgery.

1.1.3 Hydrogels as a Potential Fibrocartilage Replacement Technology

Hydrogels have been successfully implemented in many biomedical applications, due to their physiologically relevant water content, cytocompatibility, and biphasic mechanical properties similar to biological tissues. As a highly hydrated polymer matrix, hydrogels fundamentally exhibit many of the desirable biomechanical and biomolecular properties exhibited by both articular cartilage and the meniscus. Like solids, hydrogels deform when stressed, however, unlike solids and traditional elastomers, hydrogels can support fluid convection and diffusion. In regard to friction mechanics, water in hydrogels is very strongly solvated to the polymer network and therefore behaves, in many respects, similarly to polymer solutions. This phenomenon has led to a repulsion-adsorption model for hydrogel friction.[23] In this model, Gong et al. propose that a gel in contact with a solid in water is analogous in many ways to a polymer solution in contact with a solid.[23] The polymer network will be repelled from the surface if the interaction between the polymer matrix and the solid is repulsive, and will be adsorbed to the surface if it is attractive. In the repulsive case, a fluid layer will form between the polymer matrix and the solid and will be analogous to fluid film lubrication. In the attractive case, the friction will be constrained by elastic deformation of the polymer matrix and assisted by

the water coating of the solvated polymer network (**Figure 1.3**). Gong et al. have noted several contributing factors to hydrogel friction including: hydrophilicity, charge density, cross-link density, water content and elasticity.[23] Some of the key factors that were present in hydrogel systems that most closely mimicked the extremely low friction coefficients of animal tissue were, the maximization of surface hydrophilicity, a repulsive interaction between the two articulating surfaces (promoting the formation of a fluid film) and the presence of loose dangling chain ends at the surface.[23]

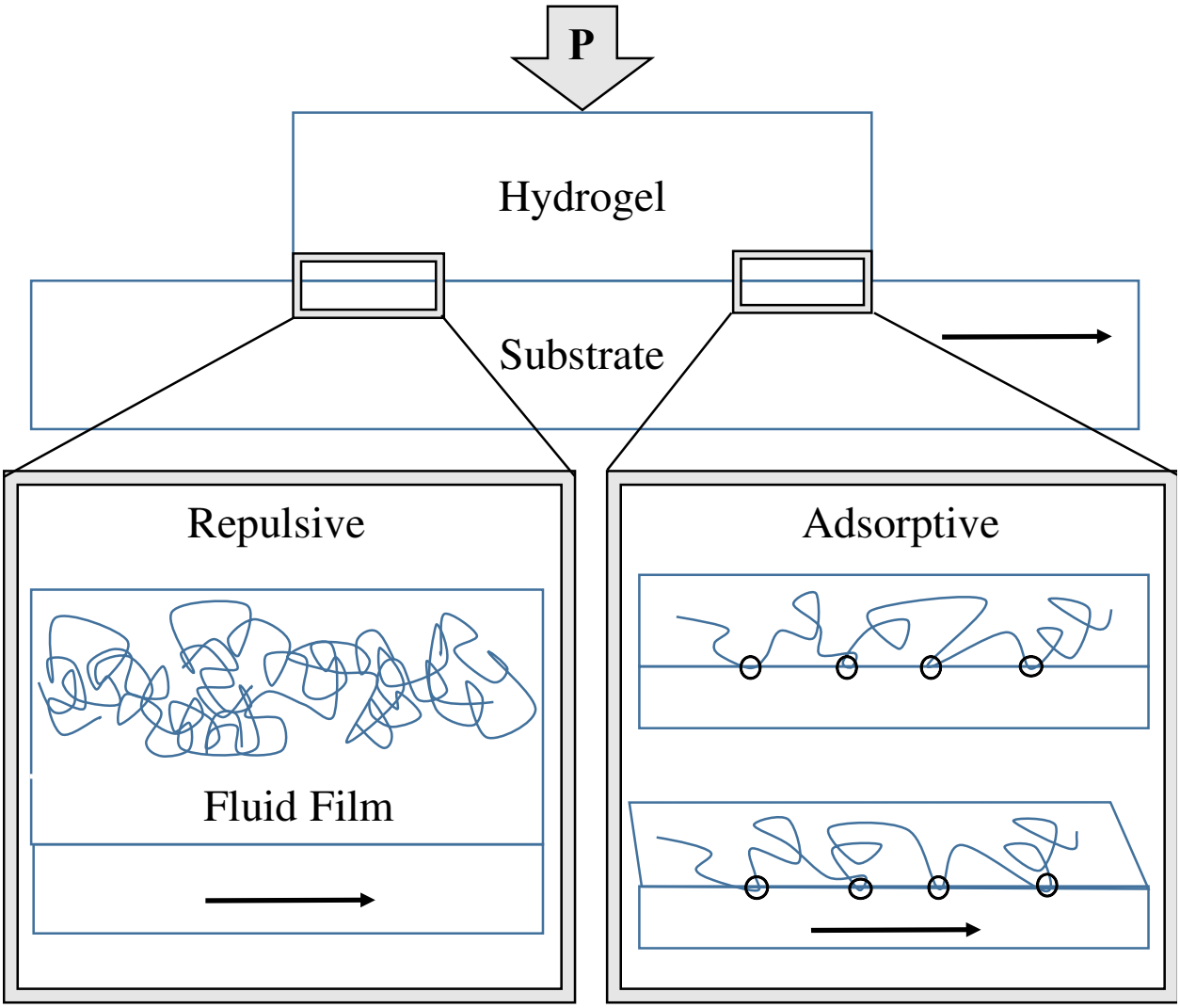

Figure 1.3: Repulsive-adsorptive model for hydrogel friction mechanics. As a hydrogel is moved across the surface of a solid substrate in solution, the lowest possible coefficient of friction is reliant on the interaction between the polymer network and the solid substrate being repulsive. This repulsive interaction promotes fluid film lubrication and minimizes elastic deformation of the polymer matrix.

Despite their lubrication mechanics and biphasic nature being similar to soft tissues like the meniscus and articular cartilage, hydrogels have only been successful in non-mechanically demanding environments. For example, conventional hydrogels formed from crosslinked polymer networks of polyethylene glycol (PEG) and polyvinyl alcohol (PVA)[24] have been used successfully in low-load bearing biomedical applications, including drug delivery,[25, 26] wound

dressings,[26, 27] and injectable fillers.[25] However, hydrogels have, as of yet, been unable to perform in more mechanically-demanding environments, such as the knee joint. These environments demand a relatively high modulus in both compression and tension, and perhaps more importantly, resistance to fatigue over millions of loading cycles at physiologically relevant rates (< 1 Hz). Not only have hydrogels been unable to produce any signs of fatigues resistance, but their moduli are often over several orders of magnitude lower than the native tissue (Table 1).

Table 1.1: Comparison of relevant material properties (compressive modulus, tensile modulus and water content) between human knee menisci and conventional hydrogels.

	Knee Meniscus	Conventional Hydrogels
Compressive Modulus	0.5 to 2 MPa[21]	10^{-3} to 10^{-1} MPa [28]
Tensile Modulus	50 to 200 MPa[21]	10^{-3} to 10^{-1} MPa [28]
Water Content	79% by mass[6]	50 - 99% by mass[28]

Low-load bearing conventional hydrogels are prone to fatigue because of the intrinsic heterogeneity and brittle nature of the polymer network.[28-30] During synthesis, the initial differences in reactivity between monomers and crosslinkers create densely crosslinked microgels, which later assemble into macrogels.[28] This inhomogeneous gel formation causes regions of high strain on the polymer system that are exacerbated during swelling.[28] Thus, the system has few mechanisms available to absorb energy effectively without breaking bonds, leading to low strain network failure or a brittle hydrogel. More recent advances aimed at the formation of more homogeneous networks in hydrogels involve tetra-arm PEG.[31] These efforts have resulted in more controlled and homogeneous crosslinking, yielding tougher materials able to reach much higher strains-at-break. While these materials possess a more homogeneous

network, their relatively limited modulus (approximate 40kPa)[31] makes them currently unsuitable for a potential meniscus surrogate.

Gong et al.[32] developed double network hydrogels (DN) to compensate for the brittleness and low modulus of conventional single network hydrogels by reinforcing them with a second interpenetrating network (IPN). This additional network is introduced at a reduced osmotic stress relative to the primary network.[32] In most configurations, a high initial stress state in the primary network is used to produce an enhanced modulus, while the secondary network absorbs energy and prevents crack propagation when the primary network begins to fail, allowing the material to reach much higher strains.[32] Using this architecture these DN hydrogels made from PAAm (poly(acrylamide)) and PAMPS (poly(2-acrylamido-2-methylpropanesulfonic acid) are able to reach a tensile strength of over 17.2 MPa.[33] Unfortunately, these DN hydrogel systems display very low levels of fatigue resistance following the first compressive or tensile loading cycle.[32, 34-36] This poor fatigue resistance has been attributed to failure of the primary network, which remains largely susceptible to the same failure modes associated with single network systems where the heterogeneity results in brittle failure. This irrecoverable brittle failure of the primary network has been demonstrated not only quantitatively by the poor fatigue resistance of the hydrogel, but also qualitatively through the observation of soft damage zones around the crack tip in mechanical testing.[37, 38] Although the heterogeneity of the primary network is the source of the low fatigue resistance, it is also a key structural element essential to the high modulus and high extension at break observed. These gains in modulus and ultimate strain are a result of the primary network's fragmentation into microgels which act effectively as sliding crosslinkers for the secondary network.[32]

It is paramount that a meniscal replacement has the ability to undergo very high levels of cyclic loading without fatigue while possessing lubrication mechanisms reminiscent of the natural tissue. The permanent mechanical hysteresis present in DN hydrogels is incompatible with such applications. Many labs are investigating healable primary networks[39, 40] which may remedy this issue if incorporated into a DN hydrogel. However, these recovery mechanisms are usually very slow, often taking over 12 hours,[39] making them impractical for the frequency of cyclic loading required by a meniscal replacement. The ideal hydrogel system would possess the modulus of these more modern DN hydrogels, while still being able to elastically recover under high levels of cyclic loading without experiencing permanent mechanical fatigue or hysteresis.

1.1.4 Advantages of Block Copolymer Based Hydrogels Over Traditional Brittle Hydrogels

In 2010, Guo et al. developed a simple, two component block copolymer based hydrogel platform which showed unusual elasticity, high modulus, and promising recovery rates over two compression cycles.[41] While the potential of this system to meet the demanding mechanical requirements of soft tissue were unknown (and unevaluated) at that time, these preliminary experiments suggested further investigations might be warranted. The origin of these unusual properties, when compared with existing hydrogel networks, were believed to be a product of the unique nanoscale network architecture created through a self-assembly process particular to the constituent block copolymer (BCP) species used.

Block copolymers consist of two or more homopolymers covalently linked to form a single macromolecule. In our lab, polyethylene oxide was anionically polymerized from a polystyrene macroinitiator to generate a linear diblock copolymer (polystyrene-*b*-poly(ethylene oxide) (P**S**-PE**O**, SO)). The covalent bond between these two thermodynamically incompatible homopolymers prevents macrophase separation and instead promotes microphase segregation.[42]

In this system, the small hydrophobic polystyrene (PS) block and much larger hydrophilic poly(ethylene oxide) (PEO) block drive phase segregation into distinct spherical domains of PS coated with large PEO coronal outer layers. These domains are often referred to as micelles or as having a micellar structure (**Figure 1.4**).

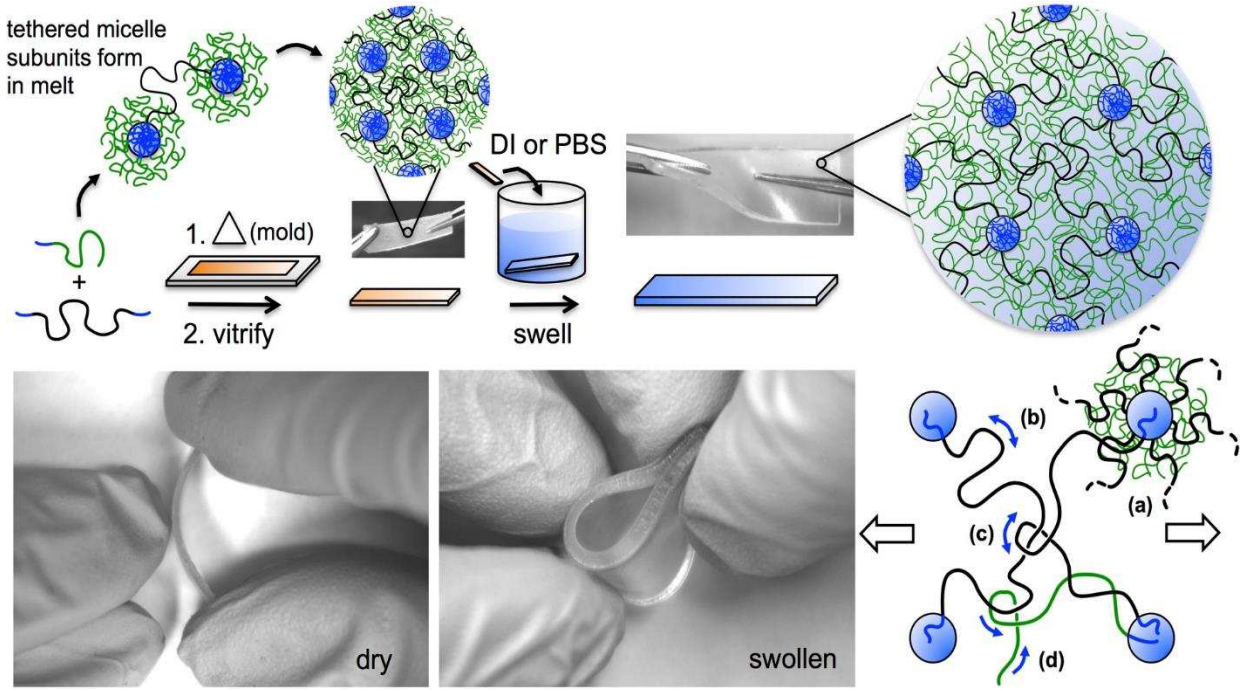

Figure 1.4: Hydrogel fabrication is accomplished using melt-state self-assembly of block copolymers. Blends of sphere forming polystyrene-poly(ethylene oxide) (PS-PEO, SO) diblock and PS-PEO-PS (SOS) triblock copolymer produce networks of tethered micelle-like domains when heated, which become fixed upon vitrification of the PS domains. Key features of the network structure (lower right) include (a) a low density of fixed junction points, each with high branch point functionality (f ~ 340), (b) large (Mn,PEO = 197 kDa) and narrowly distributed (PDI 1.06) molecular weights between junction points, (c) high densities of topologically fixed but mobile chain entanglements (thousands per fixed junction point) among tethering blocks, and (d) large numbers of dynamic entanglements between free diblock copolymer chain ends and other strands in the system. In combination, these features facilitate rapid and efficient homogenization of the stress fields in the sample

By coupling SO diblock at the PEO terminus via the coupling agent dibromoxylene (DBX) (Chapter 2), we can form a xylene bridge between SO molecules to form an SO-X-OS triblock copolymer (SOS). When this SOS triblock copolymer is blended with SO diblock copolymer, it forms a tether between micellar domains. Because the SOS is derived from the

coupling of SO, it also favors formation of spherical domains, with spatial (lattice) dimensions that are effectively "matched" to the SO diblock copolymer. These PS domains act as homogeneously distributed physical junction points in contrast with the heterogeneously distributed chemical junction points seen in conventional brittle hydrogels. The number of fixed junction points in this physically crosslinked system is actually far lower than those found in traditional single network or multi-network hydrogels. For example, the molecular weight between fixed junction points in a typical crosslinked PVA hydrogel[10] is on the order of 10^3 - 10^4 Da, where the SO/SOS network results in a molecular weight greater than 10^5 Da between junction points. Notably, each of these micelle-based junction points can have hundreds of network strands (i.e., SOS triblock copolymer chains) emanating from it, yielding a much higher effective junction (or branch) point functionality (f ~ 340) than conventional hydrogels (f ~ 3 to 4). This high branch point functionality, in combination with the large (~197 kDa) and narrowly distributed (PDI ~ 1.06) strand molecular weights gives rise to a high degree of chain entanglement among strands. The mobility of these trapped entanglements help distribute stored stress across the entire hydrogel matrix by acting similarly to the sliding "pulleys" used in slide-ring hydrogels. [43] Though there is chain stretching present in the SO/SOS hydrogel system, it is largely accommodated without failure by these sliding, topologically constrained (by tether fixation) entanglements, which allow the stress to be equally distributed without producing local stress concentrations. Additional network mobility is provided by relaxation of the free (not topologically constrained) chain ends of the SO diblock copolymer in the system. Having multiple mechanisms that contribute to the efficient distribution and storage of elastic energy without network failure is hypothesized to be the key for the production of an elastic, fatigue resistant hydrogel compatible with soft tissue replacement.

1.1.5 Progress Toward Engineering Effective Fibrocartilage Replacement Materials using Thermoplastic Elastomer Hydrogels: Thesis Overview

Guo et al. reported the first generation of thermoplastic elastomer (TPE) hydrogels in 2010.[41] In these original studies, there was an emphasis on understanding the minimum triblock copolymer necessary to create elastic, yet highly swollen hydrogels with maximized swelling ratios and moduli in the 10 – 100 kPa range. The original motivation was strongly influenced by a potential to apply such hydrogels in membrane-based separation of biological molecules, where the combination of porosities in the 90+% range and outstanding pore tortuosity were expected to be highly advantageous. Notably, all the samples used in that study were derived from diluting a single parent precursor containing a high concentration of SOS triblock copolymer. Data collected on this parent precursor hinted that samples containing such high concentrations of triblock copolymer, even with reduced swelling ratios compared with the membrane targeted samples, might be excellent candidates for applications for which water concentrations closer to 75 wt% and moduli in the 0.5 – 1.0 MPa range were more desirable. Such basic attributes were quickly recognized as being comparable to many soft biological tissues, and particularly reminiscent of the meniscal tissue of the knee in many respects.

The origin of my thesis was to explore this potential. Within, I describe a range of efforts, broadly focused on refining synthetic and post-synthetic processing techniques to improve the modulus, surface hydrophilicity, fatigue resistance and cytocompatibility of the originally developed hydrogels, with the ultimate goal of producing a material viable as a meniscal replacement. Chapter 2 begins to document this journey by describing some initial efforts dedicated to improving access to high purity, high triblock copolymer concentration samples, at bulk quantities necessary for extensive mechanical evaluation. Guo's published protocol showed

that SOS triblock copolymer could be formed from coupling SO, but the specific methodology was susceptible to high batch to batch variability in coupling efficiency (25 - 72 mol %). At that time, it was believed that achieving moduli in compression anticipated for tissues like the meniscus (> 1 MPa), would require significant improvement in SOS purity (> 90 mol %). In section 2.1 of Chapter 2, the development of a solvent and time intensive fractionation technique utilizing highly subtle differences in solubility between SOS and SO allowed us to reach SOS concentrations greater than 90 mol%. Although this fractionation technique gave us access to high concentration SOS samples for preliminary property investigations, the low yields associated with fractionation made production of quantities sufficient for thorough mechanical evaluation as a meniscal replacement largely impractical. This realization led to a rigorous evaluation of the coupling reaction methodology, from which a new and improved protocol reaching coupling efficiencies >90 mol % at large scale (> 10g) became possible. This improved protocol and how it was developed is described in section 2.2. During these studies, a high molecular weight impurity generated during the coupling reaction was also identified, and found to have significant negative impact on the fatigue resistance when present. Eventually, through another extensive investigation, the source of this impurity was able to be determined and an alternate protocol allowing production of high concentration SOS in a one pot reaction without impurity formation was developed. The details of this investigation and the one-pot protocol are described in section 2.2. Chapter 2 concludes with a final investigation aimed at reducing macroscopic (bubble) defects in melt pressed samples of the SOS/SO blends. Such small, often imperceptible bubbles, while largely innocuous with respect to accurate measurement of hydrogel compressive properties, were found serve as sites promoting localized stress concentration under tension, leading to non-structural, defect induced fracture at moderate

strains. Using magnetic resonance imaging (MRI) to observe such bubble defects, we were able develop an iterative heat, pump, cool process that promoted bubble removal and resulted in near 50 % improvement in mean strain at break. Unfortunately, this additional processing was somewhat time intensive, such that its use was only implemented for cases in which strain at break values were of primary interest.

Chapter 3 focuses on a preliminary mechanical characterization of these refined TPE hydrogels, particularly on samples containing SOS triblock copolymer concentrations between 22 and 72 mol%. This range of higher SOS concentrations had not been previously investigated, particularly for its ability to replicate the fundamental mechanical properties of meniscal tissue. These properties include physiologically appropriate moduli, negligible hysteresis, sub-second elastic recovery rates, and resistance to fatigue in compression.

With the basic properties of TPE hydrogels determined, and their promising potential to replicate the compressive behavior of the human meniscus established, we turned our attention to optimizing additional key attributes essential when considering these materials as a meniscal replacement. The particular attributes targeted included maximized surface hydrophilicity, cytocompatibility, enhanced moduli, improved toughness and mechanical anisotropy more consistent with meniscal tissue. Further still, there was a need to consider a practical a means of attachment of the would-be hydrogel implant to the tibial plateau (**Figure 1.5**). In developing strategies to incorporate these attributes into our TPE hydrogels, we discovered that the integration of a secondary network of hyaluronan (HA) would prove to be foundational. The benefits of introducing a secondary HA network were deemed to be largely three-fold. It would (1) further improve the modulus and toughness of our TPE hydrogels, (2) improve biologically relevant parameters such as surface lubricity (hydrophilicity) and cytocompatibility, and (3)

provide high concentrations of reactive functional groups through which the HA network could act as bonding intermediary between the TPE hydrogel and external material surfaces (e.g., reinforcing fibers).

Chapter 4 focuses on our development and assessment of a novel surface treatment in which an interpenetrating network (IPN) of HA could be efficiently introduced into our TPE hydrogels. While we discovered that the chain entanglement necessary to form an infinite covalent network of HA required molecular weights that would not diffuse far past the surface region of our TPE hydrogels at relevant time scales, the modification was still sufficient to significantly impact the hydrogel hydrophilicity, cytocompatibility and mechanical properties. Notably, although the original intent was to develop a method for bulk homogeneous incorporation of HA into our TPE hydrogels, it became clear that a surface modification technique would be sufficient to provide many of the desired attributes. Chapter 4 details the impact of using the developed HA surface modification technique to lower the water contact angle, reduce cell cytotoxicity, and increase compressive and tensile moduli. In addition, the influence of the surface treatment on the bulk fatigue resistance was assessed. One serendipitous consequence of being able to confine HA modification to the surface region, is the potential to limit impact to the bulk mechanical characteristics of the substrate being modified. As a result, we anticipate the methodology developed for our hydrogel systems has a strong potential to be applied to a range of future substrates.

While a uniform distribution of HA at the surface of our TPE hydrogels was beneficial for applications like a meniscal replacement, the ability to spatially pattern HA into specific surface regions was also of great interest. In particular, our group was interested in photopatterning HA at the surface of our TPE hydrogels for potential ocular lens applications.

Friction within the eye relies on similar lubrication mechanisms to cartilage to produce incredibly low coefficients of friction. Within the eye there is a layer of mucin that is maintained on the surface of the eye. [45] Mucin consists of high molecular weight extensively glycosylated glycoproteins that produce the same gel-like friction mechanics discussed above.[23, 45] HA is widely used in contact lenses to reduce friction and maintain hydration during wear[46]; however, it may impede the oxygen permeability of the lens if incorporated homogeneously on the surface. By patterning HA only into exclusive regions of interest—in this case, everywhere but the outer rim that touches the eye—the HA may maximize comfort without impeding oxygen permeability. In Chapter 5, we demonstrate an effective method to control the distribution of HA within our TPE hydrogels using photopatterning. The chapter documents the use of fluorescein-tagged HA modified with photo-crosslinkable methacrylate functionality, giving us the ability to control and observe where the crosslinking of HA took place. With this methodology, we were able to demonstrate precise control of where on the TPE hydrogel surface a secondary interpenetrating network of HA could be formed.

In Chapter 6, the potential of a secondary HA network to act as a binding intermediary between the TPE hydrogel and a non-absorbable nylon suture was investigated. It was hypothesized that the covalent incorporation of nylon sutures into the hydrogel would provide (1) the ability to recreate the mechanical anisotropy intrinsic to the meniscus and (2) a means of surgical attachment if extended through the anterior and posterior horns of a potential implant.

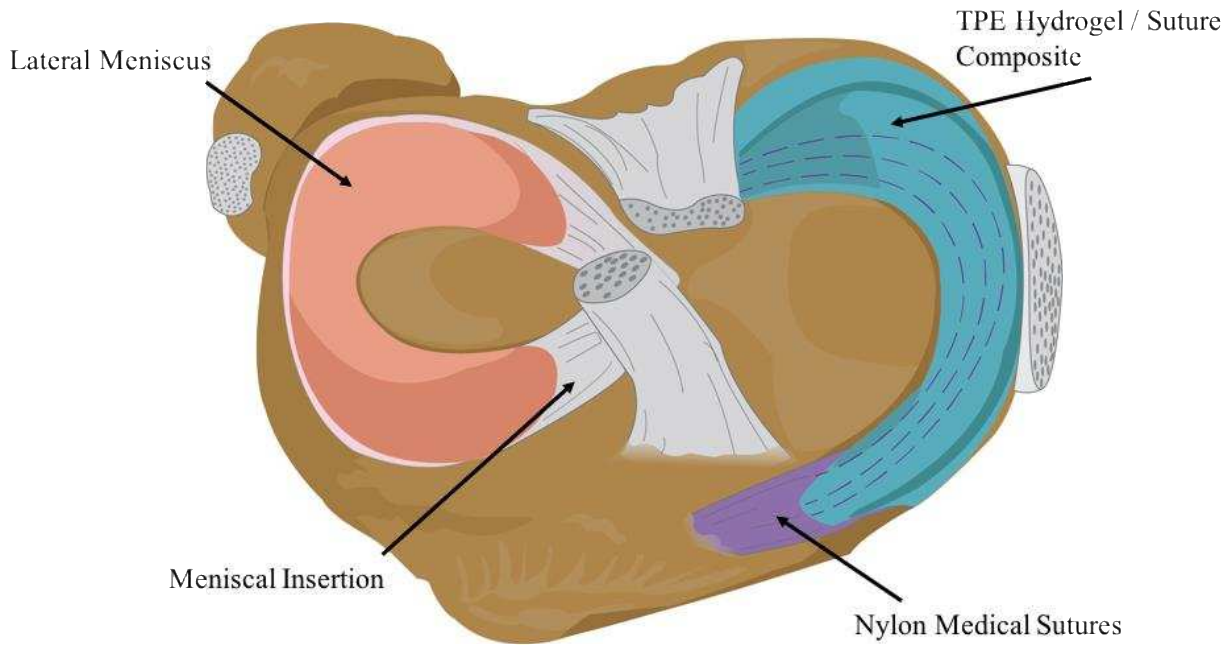

Figure 1.5: (*Left/Lateral*) Transverse view of tibial plateau demonstrating the natural transition from meniscal body to the insertions in the tibial plateau via the meniscal horn as it occurs in nature. (*Right/Medial*) Proposed approach of using surface treated medical sutures to reinforce the bulk surface treated hydrogel for a means of attachment to the tibial plateau. Surface modified medical sutures (purple) will be run in a circumferential orientation throughout the surface treated hydrogel and, after crosslinking, will form a covalent bond between the hydrogel and the suture.

Unfortunately, nylon is comprised of a sequence of very stable amide linkages, which do not accommodate covalent attachment without significant chemical modification. There was concern that modification techniques that could impact the bulk mechanical characteristics of the nylon sutures would be problematic, leading us to focus on strategies that limited modification to the surface. Plasma treatment is a very simple and effective way to add functionality to the surface of polymeric substrates. [44] It is safe, inexpensive, and an ideal method to quickly introduce multiple surface functionalities by simply changing the source gas for the plasma. We investigated water, ammonium, and alkyl amine as source gases for the plasma and characterized their efficacy at modifying nylon via X-ray photoelectron spectroscopy (XPS). Modified nylon sutures were incorporated into molten SOS/SO matrices and subjected to the HA surface

treatment developed in Chapter 4. The effectiveness of the HA network to act as a binding intermediary between the TPE hydrogel and the modified nylon sutures was assessed using pullout testing. The details of these tests are discussed in Chapter 6.

In Appendix 1, we further demonstrate the highly beneficial nature of the incorporation of a secondary network in our TPE hydrogels. In that work we showed that by coupling dangling SO diblock chain ends (using azide and alkyne click chemistry) in the micelle coronal layers post hydrogel swelling, a secondary network of tethers could be formed free of the osmotic stress imposed on the primary network. This secondary network produced substantial improvements in tensile properties (tensile modulus, toughness, strain at break, stress at break), including a 58-fold increase in mean toughness (to 361 kJ/m3) and a 19-fold increase in stress to break (to 169 kPa) in samples containing up to 95% (g/g) water. Importantly, these improvements could be realized without detriment to the water content, shape, dynamic shear moduli, and unconfined compressive properties of the original hydrogel. While this work focused on toughening low modulus materials more consistent with very soft tissues such as that found in the nucleus pulposis of the intervertebral disk, it directly established the potential for a passive secondary network to significantly enhance the properties of our SOS/SO hydrogel system.

REFERENCES

1. Murphy, L.; Schwartz, T. A.; Helmick, C. G.; Renner, J. B.; Tudor, G.; Koch, G.; Dragomir, A.; Kalsbeek, W. D.; Luta, G.; Jordan, J. M.,Lifetime risk of symptomatic knee osteoarthritis, *Arthritis Rheum* **2008,** 59, (9), 1207-13.

2. Kurtz, S.; Ong, K.; Lau, E.; Mowat, F.; Halpern, M.,Projections of primary and revision hip and knee arthroplasty in the United States from 2005 to 2030, *J Bone Joint Surg Am* **2007,** 89, (4), 780-5.

3. Mithoefer, K.; McAdams, T.; Williams, R. J.; Kreuz, P. C.; Mandelbaum, B. R.,Clinical Efficacy of the Microfracture Technique for Articular Cartilage Repair in the Knee An Evidence-Based Systematic Analysis, *American Journal of Sports Medicine* **2009,** 37, (10), 2053-2063.

4. Steadman, J. R.; Rodkey, W. G.; Rodrigo, J. J.,Microfracture: surgical technique and rehabilitation to treat chondral defects, *Clin Orthop Relat Res* **2001**, (391 Suppl), S362-9.

5. Bartlett, W.; Skinner, J. A.; Gooding, C. R.; Carrington, R. W.; Flanagan, A. M.; Briggs, T. W.; Bentley, G.,Autologous chondrocyte implantation versus matrix-induced autologous chondrocyte implantation for osteochondral defects of the knee: a prospective, randomised study, *J Bone Joint Surg Br* **2005,** 87, (5), 640-5.

6. Makris, E. A.; Hadidi, P.; Athanasiou, K. A.,The knee meniscus: structure-function, pathophysiology, current repair techniques, and prospects for regeneration, *Biomaterials* **2011,** 32, (30), 7411-31.

7. Daniel, M.,Boundary cartilage lubrication: review of current concepts, *Wien Med Wochenschr* **2014,** 164, (5-6), 88-94.

8. Wright, V.; Dowson, D.,Lubrication and cartilage, *J Anat* **1976,** 121, (Pt 1), 107-18.

9. Ateshian, G. A.,The role of interstitial fluid pressurization in articular cartilage lubrication, *J Biomech* **2009,** 42, (9), 1163-76.

10. Walker, P. S.; Dowson, D.; Longfield, M. D.; Wright, V.,"Boosted lubrication" in synovial joints by fluid entrapment and enrichment, *Ann Rheum Dis* **1968,** 27, (6), 512-20.

11. Freeman, M. A. R. e.,Adult Articular Cartilage, **1979**.

12. Crockett, R.; Roos, S.; Rossbach, P.; Dora, C.; Born, W.; Troxler, H.,Imaging of the surface of human and bovine articular cartilage with ESEM and AFM, *Tribology Letters* **2005,** 19, (4), 311-317.

13. Hills, B. A.; Crawford, R. W.,Normal and prosthetic synovial joints are lubricated by surface-active phospholipid - A hypothesis, *Journal of Arthroplasty* **2003,** 18, (4), 499-505.

14. Brinckmann P, F. W., Leivseth G.,Musculoskeletal Biomechanics, **2002**.

15. Fox, A. J.; Bedi, A.; Rodeo, S. A.,The basic science of human knee menisci: structure, composition, and function, *Sports Health* **2012,** 4, (4), 340-51.

16. Greis, P. E.; Bardana, D. D.; Holmstrom, M. C.; Burks, R. T.,Meniscal injury: I. Basic science and evaluation, *J Am Acad Orthop Surg* **2002,** 10, (3), 168-76.

17. Lohmander, L. S.; Englund, P. M.; Dahl, L. L.; Roos, E. M.,The long-term consequence of anterior cruciate ligament and meniscus injuries: osteoarthritis, *Am J Sports Med* **2007,** 35, (10), 1756-69.

18. Zhang, Y.; Jordan, J. M.,Epidemiology of osteoarthritis, *Clin Geriatr Med* **2010,** 26, (3), 355-69.

19. Hunter, D. J.; Arden, N.; Conaghan, P. G.; Eckstein, F.; Gold, G.; Grainger, A.; Guermazi, A.; Harvey, W.; Jones, G.; Hellio Le Graverand, M. P.; Laredo, J. D.; Lo, G.; Losina,

E.; Mosher, T. J.; Roemer, F.; Zhang, W.,Definition of osteoarthritis on MRI: results of a Delphi exercise, *Osteoarthritis Cartilage* **2011,** 19, (8), 963-9.

20. Abrams, G. D.; Frank, R. M.; Gupta, A. K.; Harris, J. D.; McCormick, F. M.; Cole, B. J.,Trends in Meniscus Repair and Meniscectomy in the United States, 2005-2011, *American Journal of Sports Medicine* **2013,** 41, (10), 2333-2339.

21. Fischenich, K. M.; Lewis, J.; Kindsfater, K. A.; Bailey, T. S.; Haut Donahue, T. L.,Effects of degeneration on the compressive and tensile properties of human meniscus, *J Biomech* **2015,** 48, (8), 1407-11.

22. Vrancken, A. C.; Buma, P.; van Tienen, T. G.,Synthetic meniscus replacement: a review, *Int Orthop* **2013,** 37, (2), 291-9.

23. Gong, J. P.,Friction and lubrication of hydrogels - its richness and complexity, *Soft Matter* **2006,** 2, (7), 544-552.

24. Peppas, N. A.; Merrill, E. W.,Crosslinked Polyvinyl-Alcohol) Hydrogels as Swollen Elastic Networks, *Journal of Applied Polymer Science* **1977,** 21, (7), 1763-1770.

25. Annabi, N.; Tamayol, A.; Uquillas, J. A.; Akbari, M.; Bertassoni, L. E.; Cha, C.; Camci-Unal, G.; Dokmeci, M. R.; Peppas, N. A.; Khademhosseini, A.,25th Anniversary Article: Rational Design and Applications of Hydrogels in Regenerative Medicine, *Advanced Materials* **2014,** 26, (1), 85-124.

26. Slaughter, B. V.; Khurshid, S. S.; Fisher, O. Z.; Khademhosseini, A.; Peppas, N. A.,Hydrogels in Regenerative Medicine, *Advanced Materials* **2009,** 21, (32-33), 3307-3329.

27. Aytimur, A.; Kocyigit, S.; Uslu, I.; Gokmese, F.,Preparation and Characterization of Polyvinyl Alcohol Based Copolymers as Wound Dressing Fibers, *International Journal of Polymeric Materials and Polymeric Biomaterials* **2015,** 64, (3), 111-116.

28. Naficy, S.; Brown, H. R.; Razal, J. M.; Spinks, G. M.; Whitten, P. G.,Progress Toward Robust Polymer Hydrogels, *Australian Journal of Chemistry* **2011,** 64, (8), 1007-1025.

29. Chen, Q.; Zhu, L.; Huang, L. N.; Chen, H.; Xu, K.; Tan, Y.; Wang, P. X.; Zheng, J.,Fracture of the Physically Cross-Linked First Network in Hybrid Double Network Hydrogels, *Macromolecules* **2014,** 47, (6), 2140-2148.

30. Y. Kawauchi, T. T., Hidemitsu Furukawa, Takayiki Kurokawa, Tasuku Nakajima, Yoshihito Osada, and Jian Ping Gong,Brittle, ductile, paste-like behaviors and distinct necking of double network gels with enhanced heterogeneity, *Journal of Physics: Conference Series* **2009,** 184, 012016.

31. Sakai, T.; Matsunaga, T.; Yamamoto, Y.; Ito, C.; Yoshida, R.; Suzuki, S.; Sasaki, N.; Shibayama, M.; Chung, U. I.,Design and fabrication of a high-strength hydrogel with ideally homogeneous network structure from tetrahedron-like macromonomers, *Macromolecules* **2008,** 41, (14), 5379-5384.

32. Gong, J. P.,Why are double network hydrogels so tough?, *Soft Matter* **2010,** 6, (12), 2583-2590.

33. Gong, J. P.; Katsuyama, Y.; Kurokawa, T.; Osada, Y.,Double-network hydrogels with extremely high mechanical strength, *Advanced Materials* **2003,** 15, (14), 1155-+.

34. Ducrot, E.; Chen, Y. L.; Bulters, M.; Sijbesma, R. P.; Creton, C.,Toughening Elastomers with Sacrificial Bonds and Watching Them Break, *Science* **2014,** 344, (6180), 186-189.

35. Webber, R. E.; Creton, C.; Brown, H. R.; Gong, J. P.,Large strain hysteresis and mullins effect of tough double-network hydrogels, *Macromolecules* **2007,** 40, (8), 2919-2927.

36. Sun, J. Y.; Zhao, X. H.; Illeperuma, W. R. K.; Chaudhuri, O.; Oh, K. H.; Mooney, D. J.; Vlassak, J. J.; Suo, Z. G.,Highly stretchable and tough hydrogels, *Nature* **2012,** 489, (7414), 133-136.

37. Yu, Q. M.; Tanaka, Y.; Furukawa, H.; Kurokawa, T.; Gong, J. P.,Direct Observation of Damage Zone around Crack Tips in Double-Network Gels, *Macromolecules* **2009,** 42, (12), 3852-3855.

38. Tanaka, Y.,A local damage model for anomalous high toughness of double-network gels, *Europhysics Letters* **2007,** 78, 56005.

39. Zhong, M.; Liu, X. Y.; Shi, F. K.; Zhang, L. Q.; Wang, X. P.; Cheetham, A. G.; Cui, H. G.; Xie, X. M.,Self-healable, tough and highly stretchable ionic nanocomposite physical hydrogels, *Soft Matter* **2015,** 11, (21), 4235-4241.

40. Sun, Y. N.; Liu, S.; Du, G. L.; Gao, G. R.; Fu, J.,Multi-responsive and tough hydrogels based on triblock copolymer micelles as multi-functional macro-crosslinkers, *Chemical Communications* **2015,** 51, (40), 8512-8515.

41. Guo, C.; Bailey, T. S.,Highly distensible nanostructured elastic hydrogels from AB diblock and ABA triblock copolymer melt blends, *Soft Matter* **2010,** 6, (19), 4807-4818.

42. Bates, F. S.,Polymer-Polymer Phase-Behavior, *Science* **1991,** 251, (4996), 898-905.

43. Bin Imran, A.; Esaki, K.; Gotoh, H.; Seki, T.; Ito, K.; Sakai, Y.; Takeoka, Y.,Extremely stretchable thermosensitive hydrogels by introducing slide-ring polyrotaxane cross-linkers and ionic groups into the polymer network, *Nature Communications* **2014,** 5.

44. Chu, P. K.; Chen, J. Y.; Wang, L. P.; Huang, N.,Plasma-surface modification of biomaterials, *Materials Science & Engineering R-Reports* **2002,** 36, (5-6), 143-206.

45. Sterner, O.; Karageorgaki, C.; Zurcher, M.; Zurcher, S.; Scales, C. W.; Fadli, Z.; Spencer, N. D.; Tosatti, S. G. P.,Reducing Friction in the Eye: A Comparative Study of Lubrication by Surface-Anchored Synthetic and Natural Ocular Mucin Analogues, *Acs Applied Materials & Interfaces* **2017,** 9, (23), 20150-20160.

46. Paterson, S. M.; Liu, L.; Brook, M. A.; Sheardown, H.,Poly(ethylene glycol)-or silicone-modified hyaluronan for contact lens wetting agent applications, *J Biomed Mater Res A* **2015,** 103, (8), 2602-10.

CHAPTER 2

OPTIMIZING MECHANICAL PROPERTIES IN THERMOPLASTIC ELASTOMER HYDROGELS THROUGH IMPROVED COUPLING EFFICIENCY AND PROCESSING TECHNIQUES

2.1 INTRODUCTION [2]

Guo et al. reported the first generation of thermoplastic elastomer (TPE) hydrogels in 2010.[1] In these original studies, there was an emphasis on understanding the minimum triblock copolymer content necessary to create elastic, yet highly swollen hydrogels with maximized swelling ratios and moduli in the 10 – 100 kPa range. The original motivation was strongly influenced by a potential to apply such hydrogels in membrane-based separation of biological molecules, where the combination of porosities in the 90+% range and outstanding pore tortuosity were expected to be highly advantageous. Notably, all the samples used in that study were derived from diluting a single parent precursor containing a high concentration of SOS triblock copolymer. Data collected on this parent precursor hinted that samples containing such high concentrations of triblock copolymer, even with reduced swelling ratios compared with the membrane targeted samples, might be excellent candidates for applications for which water concentrations closer to 75 wt% and moduli in the 0.5 – 1.0 MPa range were more desirable. Such basic attributes were quickly recognized as being comparable to many soft biological tissues, and particularly reminiscent of the meniscal tissue of the knee in many respects.

[2] This chapter was written and prepared by Jackson Lewis. All synthesis and chemical characterization was conducted by Jackson Lewis. MRI data collection and image processing was conducted by Benjamin Kohn. Cyclic compression data was collected by Kristine Fischenich.

Guo's published protocol for making initial hydrogel systems were based on the use of SOS triblock copolymer formed from coupling SO diblock copolymer. Notably, the coupling of SO diblock copolymer to form SOS triblock copolymer results in a highly desirable "latticed matched" system which allows the sphere size and morphological domain spacing during self-assembly to remain largely independent of blend composition. This coupling reaction consists of activating the hydroxyl terminus of the SO chain ends via titration followed by the addition of a bifunctional coupling agent. The activation of the SO chain end takes place after the addition of potassium naphthalenide (K-NAP), which deprotonates the hydroxyl terminus of SO resulting in an active nucleophilic potassium alkoxide. The addition of dibromoxylene (DBX) to the potassium alkoxide of SO results in an SN_2 substitution reaction, in which bromine is displaced from DBX as a result of nucleophilic attack by the activated SO forming a covalent bond between SO and the bromoxylene fragment. As DBX is a bifunctional coupling agent, eventual displacement of both bromine leaving groups produces a coupled SO polymer product, SOS (**Figure 2.1**). DBX and an activated SO reacting with each other to form SO-xylene bromide is much more kinetically favored than SO-xylene bromide reacting with another activated SO to form the desired SOS product. This difference in reactivity is primarily due to the much higher mobility of the small DBX molecule compared to the large SO-xylene bromide polymer chain. Because of this difference in rates, achieving maximal coupling efficiency requires, theoretically, the precise addition of exactly a half molar equivalent of DBX to the activated SO chains.

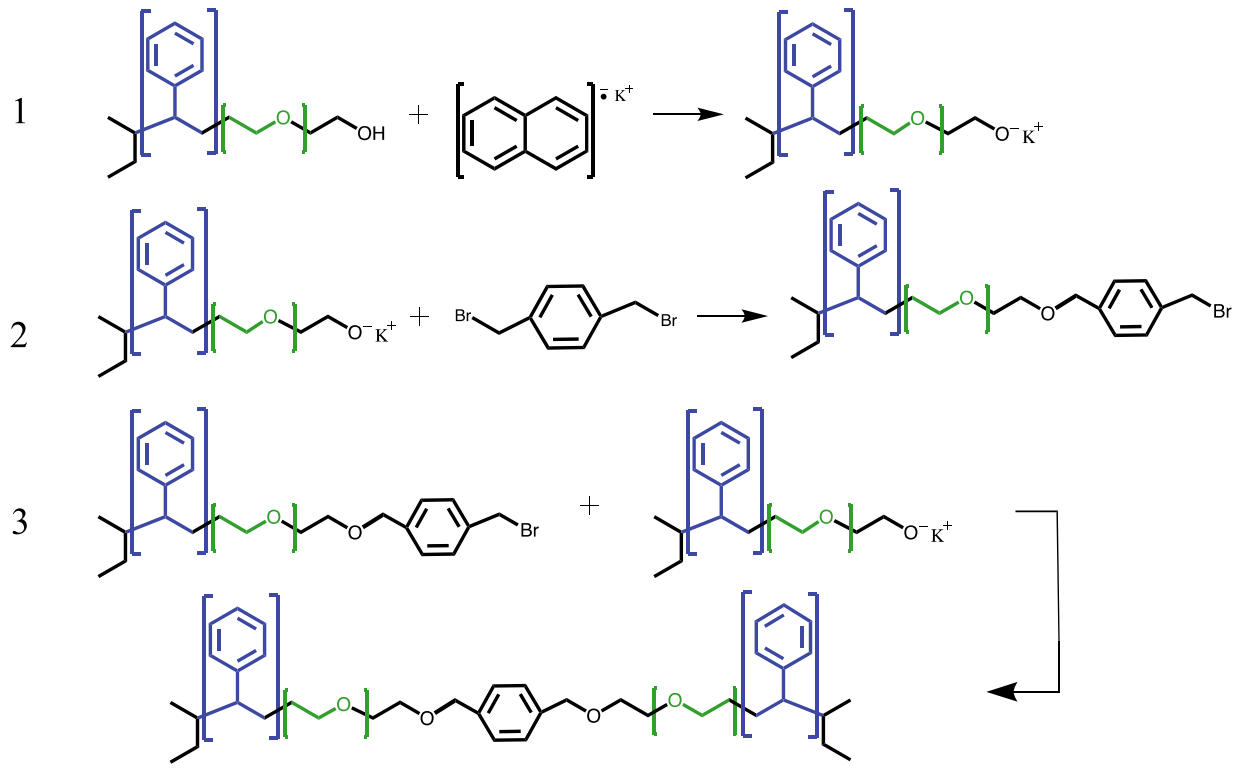

Figure 2.1: Proposed mechanism for the coupling of activated SO diblock copolymer to form SOS triblock copolymer via an SN_2 substitution reaction with the coupling agent DBX. (1) Activation of SO chain end to produce a potassium alkoxide through the deprotonation of the terminal primary alcohol via the addition of K-NAP. (2) SN_2 substitution reaction between potassium alkoxide and dibromoxylene to form SO-xylene bromide. (3) SO-xylene bromide reacting through the same SN_2 substitution reaction with another activated SO chain end to form the desired product, SOS.

One hundred mol % coupling efficiency is difficult to achieve in this reaction without an exact knowledge of the amount of SO being coupled. Molecular weight and PDI of polymers can only be approximated using methods such as GPC or NMR. Instead, the original protocol developed by Guo et al. used rate controlled addition of DBX to maximize coupling efficiency by slowly adding DBX via a syringe pump.[1] This maximized the time that SO-xylene bromide had to find another unmodified and activated SO chain end. If the addition of DBX is slow enough, then in theory, excess DBX would not inhibit the formation of the desired coupled product. This permits a small excess to be added to account for inaccuracy in the half molar

equivalent calculations without fear of reducing coupling efficiencies. Thus, the original protocol recommended addition of a 0.6x molar equivalent of DBX (to the approximated number of SO chains calculated via GPC and NMR) over 8 to 12 hours. Notably, this reaction must be done in an air and moisture free environment, as any proton source as well as other reactive species could result in the re-protonation, modification, or termination of the activated SO chains. Several precautions were taken to ensure that the solvent, reactor vessels, SO, K-NAP, and DBX were all dry and air-free. Despite this controlled and slow addition of DBX, the methodology was susceptible to high batch-to-batch variability in coupling efficiency (25 - 72 mol %). Importantly, it was believed that achieving the moduli in compression anticipated for tissues like the meniscus (> 1 MPa), would require significant improvements in SOS purity (> 90 mol %).

This chapter focuses on refining synthetic and post-synthetic processing techniques to improve the modulus and fatigue resistance of the originally developed hydrogels, with the ultimate goal of producing a material that could act as a meniscal replacement. The work described documents the progress made toward this goal by describing initial efforts dedicated to improving access to high purity, high triblock copolymer concentration samples at quantities necessary for preliminary mechanical evaluation. As coupling efficiencies following the original protocol were so variable, isolating SOS from the crude SOS/SO mixtures produced from the coupling reaction was initially accomplished using a solvent-based separation technique known as fractionation. This fractionation technique utilizes subtle differences in solubility between SOS and SO polymers to promote selective precipitation of SOS, allowing us to gain access to samples with SOS concentrations greater than 90 mol%.

Polymers spontaneously mix with a solvent (dissolve) when the Gibb's free energy of mixing is negative.[2] When polymers dissolve they have a much higher chain mobility resulting

in an increase in entropy, making mixing favorable. [2] The energy that keeps polymers in contact with themselves instead of interacting with the solvent (mixing) is known as the interaction energy and is analogous to the heat of vaporization.[2] The more similar the interaction energy between polymer chains and the solvent being used, the more likely the two molecules will mix as this reduces the enthalpic resistance to mixing.[2]

$$\Delta G_m = \Delta H_m - T\Delta S_m \text{ (Equation 1)}$$

The Flory-Huggins interaction parameter (χ) for polymers in solution is an enthalpy related term that describes the thermal energy required for molecular exchange between one solvent molecule and one polymer segment of equivalent solvent volume and is described by Equation 2 (where z is the coordination number; Δw is the difference in interaction energy between a mixture of the solvent and the polymer segment and the complementary, unmixed state; k is the Boltzmann constant; and T is the temperature) [2].

$$\chi = \frac{z\Delta w}{kT} \text{ (Equation 2)}$$

In fact, the enthalpy of mixing term in the Flory Huggins expression can be redefined in terms of χ (Equation 3) where ϕ_1 is the volume fraction of solvent, N is the degree of polymerization, m_2 is the number of polymer molecules, k is the Boltzmann constant, and T is temperature [2].

$$\Delta G_m = \phi_1 N m_2 \chi kT - T\Delta S_m \text{ (Equation 3)}$$

Therefore, an increase in χ results in an increase in the enthalpy of mixing term, helping to drive the system toward spontaneous de-mixing. The enthalpy of mixing term is not a fixed parameter and is proportional to the MW of the polymer (N), the polymer segment/solvent

interaction energies, and the relative polymer/solvent composition.[2] It is assumed that SOS and SO are identical in their polymer segment and solvent interaction energies as their molecular compositions are identical. The key difference in the enthalpy of mixing term between the two lies in their respective molecular weight, as SOS is approximately double the molecular weight of SO. By utilizing this difference in the enthalpy of mixing between the two polymers one can tune the solvent conditions to create an environment where SOS precipitates more preferentially than SO. Similarly, the gains in entropy which favor mixing are also molecular weight dependent, being smaller for SOS than SO. This difference therefore also intrinsically favors preferential precipitation of SOS over SO, particularly as the temperature drops.

By first dissolving the SOS/SO mixture in a "good" solvent for both species (chloroform) and then progressively adding a "poor" solvent for both species (n-hexane), we are slowly increasing the enthalpy of mixing term for both SOS and SO. This effective increase in the enthalpy of mixing will eventually produce an environment where both SOS and SO would rather be in contact with other SOS or SO chains than with the solvent, resulting in precipitation. However, since the molecular weight of SOS is greater than that of SO, its enthalpy of mixing overcomes the entropic driving force of mixing before that of the SO chains, and selectively precipitates first. One can recover multiple layers of precipitant with progressively decreasing concentrations of SOS using this technique by either (1) continuing to add the poor solvent and increasing the enthalpic penalty for mixing; or (2) decreasing the temperature in the system, which decreases the entropic driving force for mixing. Both techniques continue to favor precipitation of the higher molecular weight SOS species, but the fraction of SO chains that also precipitates increases due to their naturally increasing (relative) abundance in the solution layer. Each sample of collected precipitate can then also be subjected to the fractionation process once

again, to further improve purity. However, as purity of the high molecular weight species is increased using successive fractionations, the amount recovered becomes smaller and smaller.

Ultimately, purification through fractionation is not ideal to produce pure SOS as it is a very time- and solvent-intensive process with diminishing returns as purity is maximized. Therefore, a thorough investigation of the coupling reaction was conducted in an attempt to reliably produce pure SOS from SO, without requiring additional purification steps such as the fractionation process described above. During these investigations, a high molecular weight impurity generated during the coupling reaction was also identified, and found to have significant negative impact on the fatigue resistance when present. Investigations aimed at identifying the source of this impurity are described below. These investigations importantly led to the development of an alternate coupling protocol, allowing for the production of SOS/SO blends with high concentrations of SOS in a convenient one-pot reaction without impurity formation.

This chapter concludes with a final investigation aimed at reducing macroscopic (bubble) defects in melt pressed samples of the SOS/SO blends. Such small, often imperceptible bubbles, while largely innocuous with respect to accurate measurement of hydrogel compressive properties, serve as sites promoting localized stress concentrations under tension leading to defect induced fracture at moderate strains unrelated to failure modes specific to the network nanostructure itself. Using magnetic resonance imaging (MRI) to observe such bubble defects, we document the development an iterative heat, pump, cool process promoting bubble consolidation and removal to improve the hydrogel's mean strain at break.

2.2 RESULTS AND DISCUSSION

2.2.1 High Coupling Efficiency of SO Diblock Copolymer

Figure 2.2 below demonstrates a typical coupling reaction following the original protocol reported by Guo et al.[1], resulting in a coupling efficiency of ~22 mol%. When the theoretical and actual coupling efficiencies are plotted against percent molar equivalents of DBX added per SO chain end (approximated via NMR) we observe a lower coupling efficiency than that predicted by theory throughout the metered addition of DBX (0.0625 molar equivalents per hour over 8 hours) (**Figure 2.2a**). Excess DBX was added (beyond a 0.5 molar equivalence) after no additional coupling was observed for several hours at the 0.5 molar equivalence point. This additional DBX had no impact on improving the coupling efficiency, indicating that the low coupling efficiencies observed were not likely the result of a deficiency in coupling agent. Notably, by the 12-hour point, the reactor pressure had decreased from a positive pressure of 5 psi down to atmospheric pressure, indicating that there was a slow leak. Such leaks seem to be the product of the sustained placement of the syringe pump needle in the rubber septa over such extended reaction times, perhaps coupled with repetitive sampling during this specific experiment. Because this reaction is so sensitive to moisture (each adventitious water molecule results in a deactivated SO chain) and/or the introduction of other contaminants, compromised seals like this, as well as the purity of the solvent, SO, or DBX, could all be the cause of the lower coupling efficiencies observed.

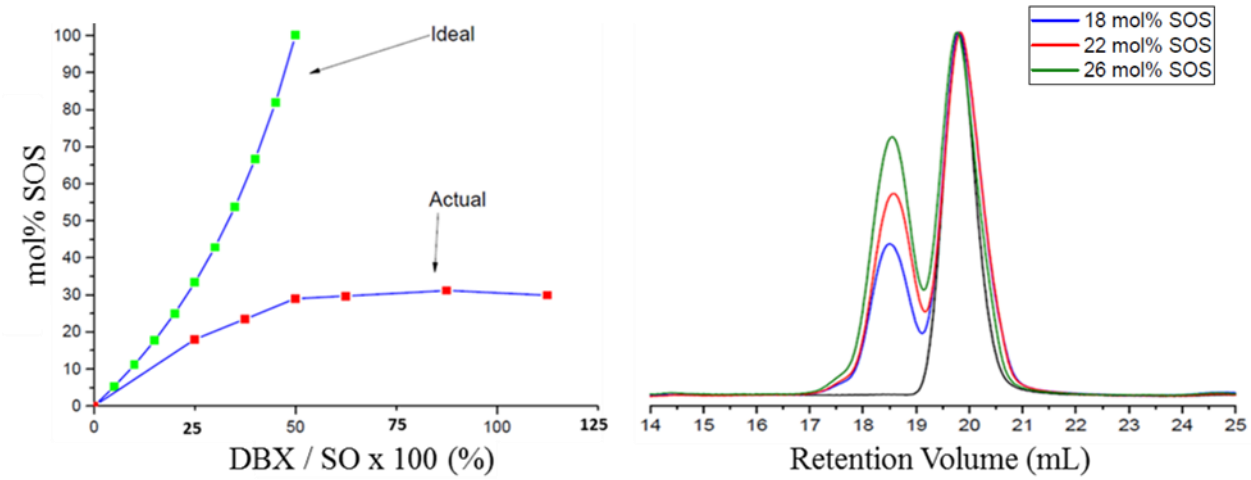

Figure 2.2: (a) Theoretical (green squares) vs. actual (red squares) mol% SOS as a function of the percent molar equivalents of DBX to SO added to the reactor. The figure shows a strong deviation between the theoretical and actual coupling efficiencies observed. (b) Representative gel permeation chromatography data showing the relative ratios of SOS to SO sampled at different time points throughout the addition of DBX to the reactor.

In fact, the presence of contaminants in the solvent or SO precursor was strongly supported by the need to use two to three stoichiometric equivalents of K-NAP (relative to the approximated number of SO chain ends) to completely titrate the contents of the reactor. These additional titratable groups, likely water or residual impurities left following the SO polymerization step, appear to negatively influence the formation of SOS. It was theorized that by adding a half molar equivalent of DBX relative to the total titratable groups, as opposed to the approximated number of SO chains, one might be able to promote higher rates of SO coupling. This hypothesis was initially based on the assumption that the small molecular weight contaminants, due to their much higher mobility in solution, would more rapidly consume the excess DBX, resulting in an SO coupling environment rid of reactive contaminants.

Adding a half molar equivalent of DBX to the total titratable groups (2.4x predicted number of SO chains) did indeed result in a higher coupling efficiency (44 mol% vs. 22 mol%), however, the kinetic data (**Figure 2.4**: black dots) curiously did not seem to support the theory of

rapid consumption of the DBX by small molecule contaminants. If this theory were true, one would expect very little to no SOS formation during the initial stages of DBX addition (**Figure 2.4**: blue) until a half stoichiometric equivalent of the contaminant was reached. In contrast, the data appears to indicate that when stoichiometric amounts of DBX to titratable groups are added there is competitive consumption of DBX by the contaminant and SO at the rate of addition chosen. Again, it was found that a typical septum could only maintain positive pressure for approximately 8 hours after being punctured by the DBX delivery needle. The deviation observed in the third data point in **Figure 2.2** (open black dot) was taken when the reactor pressure had reached atmospheric pressure, where premature termination of the activated SO chain ends had been previously observed.

Interestingly, the coupling rate seemed to be consistent with kinetics under which you would have reached 100% coupling had premature termination from compromised reactor pressure did not occur. This suggested that DBX consumption by a contaminant would have to occur under conditions in which no permanent termination of the active SO chains were occurring. We considered several models under which this could be true. One possible theory was that the system precludes cross-coupling i.e. DBX reacting with a contaminant will always react with another contaminant and never an SO chain. Such exclusivity seemed unlikely from a chemical reactivity standpoint, and was not considered further.

A more plausible explanation for the reaction kinetics observed, before the reactor leak, is that the contaminant possesses bifunctionality and is being incorporated into the SO chain, before being eventually capped by another SO chain. This may explain how parallel consumption of DBX by the small molecular weight contaminant and SO does not result in the termination of the SO chain. This behavior can be modeled much like a step-growth

polymerization if three species are assumed to exist: SO (SO-A), small molecular weight contaminant (A-A) and dibromoxylene (B-B) (**Figure 2.3**). In this model, SO-A is a monofunctional monomer and acts to terminate the step growth polymerization and control molecular weight. Because the molar concentration of SO-A is comparable with the B-B molar concentration, the chain capping reaction by SO-A is prevalent and severely limits the number of growth steps. That is, the molecular weight of the formed SO-abb(aabb)$_i$a-OS (i = 0, 1, 2…) (SOS) is dominated by the molecular weight of the capping SO-A chains (Note on notation: once a covalent bond has formed between an A and a B they are denoted in the lowercase a and b). This model makes three notable assumptions (1) that the reactivity of the contaminant with DBX is the same as the reactivity of an active chain end with DBX and (2) that all DBX in the reactor will be consumed by either an active chain-end or the small MW contaminant (3) the small molecular weight impurity is bifunctional.

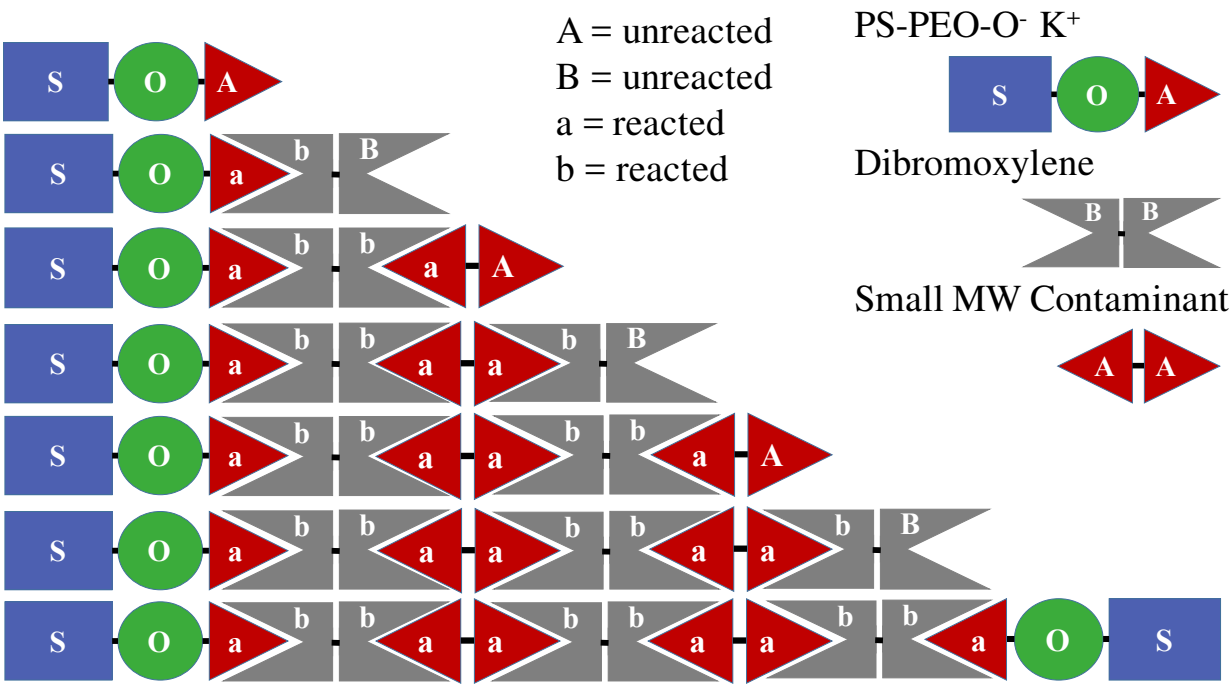

Figure 2.3: Pictorial representation of step growth model to account for small molecular weight contaminant incorporation into SOS formation. Small MW contaminants react with DBX to form dimers, trimers and oligomers of the small MW contaminant before eventually being terminated on both ends by an active SO chain.

We can calculate, using relative probabilities, the relative ratio of all SO-abb(aabb)$_i$ (SO) to SO-abb(aabb)$_i$a-OS (SOS) as DBX (B-B) is added as follows:

1. We first define the fraction of A groups in the small MW bifunctional contaminants as ρ (Equation 4),

$$\rho = \frac{v_{A-A}}{v_A} = \frac{v_{A-A}}{v_{A-A} + v_{SO-A}} = \frac{V_t * \frac{m_K}{MW_K * V_{THF}} - \frac{m_{SO}}{MW_{SO}}}{V_t * \frac{m_K}{MW_K * V_{THF}}} \qquad \text{(Equation 4)}$$

where v_{A-A} is the total number of A's in bifunctional groups and v_A is the total number A groups, including those in monofunctional SO-A. The terms v_{A-A} and v_A can be further defined into known experimental values, where V_t is the volume of K-NAP needed to titrate reactor, m_K is the total mass potassium in the K-NAP solution, MW_K is the molecular weight of potassium,

V_{THF} is the total volume tetrahydrofuran used to make the K-NAP solution, m_{SO} is the total mass of SO-A and MW_{SO} is the molecular weight of SO-A.

2. We can then define the fraction of A groups that have reacted in terms of *p*, the ratio of total B groups to total A groups (Equation 5),

$$p = \frac{v_B}{v_A} = \frac{v_{B-B}}{v_{A-A} + v_{SO-A}} = \frac{2 * V_{DBX} * \frac{m_{DBX}}{MW_{DBX} * V_{THF}}}{V_t * \frac{m_K}{MW_K * V_{THF}}} \qquad \text{(Equation 5)}$$

where m_{DBX} is the total mass DBX in coupling solution, MW_{DBX} is the molecular weight of DBX, and V_{THF} is the total volume of tetrahydrofuran in coupling solution.

With these two terms defined we can begin to develop a probability table (Table 1). This probability table finds the probability that, if we locate any SO chain in solution, that it is also capped by a second SO (i.e. SOS). As is shown in Table 1, the initial probability of an SO-A chain reacting to form SO-ab-B (SO-xylene bromide) is simply *p*. The probability that the SO-ab-B will react with a small molecular weight contaminant instead of another SO-A is ρ. This stepwise addition of small molecular weight contaminants can eventually be distilled into a final cumulative probability.

Table 2.1: Step and cumulative probability table summarizing the probability that, if we locate any SO chain in solution, that it is also capped by a second SO. A capital "A" or "B" represents an unreacted species while a lowercase "a" or "b" represents its reacted form. This model assumes (1) identical reactivity between the SO chain end (SO-A) and the small MW contaminant (A-A) with DBX (B-B), (2) small MW contaminants are bifunctional and (3) all DBX in the reactor will react. The fraction of the total A groups (SO-A + A-A) that are small MW contaminants is denoted by "ρ" and the fraction of total "A" groups that have reacted is denoted by "*p*".

SO-A	Step	Cumulative
SO-a	p	p
SO-ab-B	1	p*(1)
SO-ab-ba	1	p *(1)*(1)
SO-ab-ba-A	ρ	p *(1)*(1)*ρ
SO-ab-ba-a	p	p_2*(1)*(1)*ρ
SO-abb(aabb)$_i$-a	(1)*(1)	p_2*ρ
SO-abb(aabb)$_i$-a-A	ρ	p_2*ρ_2
SO-abb(aabb)$_i$-a-a	p	p_3*ρ_2

3. The final cumulative probability of finding an SO chain which is also currently capped by a second SO chain regardless of the number of contaminant molecules incorporated (SO-abb(aabb)$_i$a-OS where i = 0, 1, 2…), α_{SOS} , is:

$$\alpha_{SOS} = \sum_{i=0}^{\infty} p(p\rho)^i(1-\rho) = \frac{p(1-\rho)}{1-p\rho} \qquad \text{(Equation 6)}$$

By incorporating This can then be further expanded into experimental terms to generate Equation 7,

$$\alpha_{SOS} = \frac{\frac{2 * mol_{DBX}}{mol_K} - \frac{2 * mol_{DBX} * (mol_K - mol_{SO})}{{mol_K}^2}}{1 - \frac{2 * mol_{DBX} * (mol_K - mol_{SO})}{{mol_K}^2}} \qquad \text{(Equation 7)}$$

where mol_{DBX} is the total moles of DBX added to the reactor, mol_K is the total moles of potassium added to the reactor to titrate the reactor, and mol_{SO} is the total moles of SO in the reactor at the start of the coupling reaction. Equation 7 is plotted against the experimental data collected (**Figure 2.4**: gold) and is shown to predict the data the most accurately of the theories proposed.

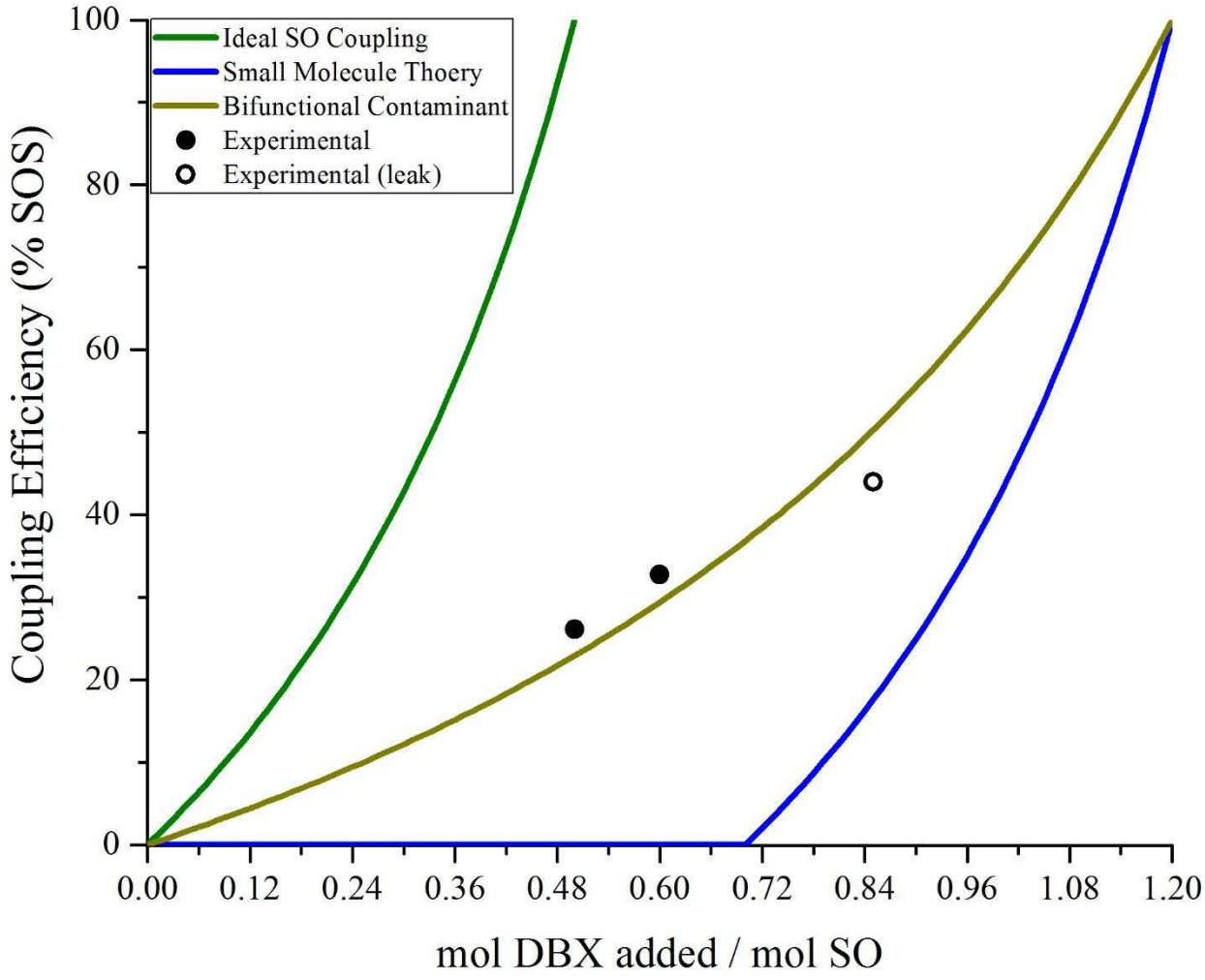

Figure 2.4: Three proposed theoretical mechanisms for coupling reaction kinetics for the coupling of SO in the presence of small molecule contaminants (1 SO: 1.4 small MW contaminant). shown via coupling efficiency (%) vs. mol DBX/ mol SO compared to actual experimental data (BLACK DOTS). (Green) Ideal coupling i.e. no influence on the reaction kinetics of SO coupling by small molecule contaminants. (Blue) Rapid consumption of DBX by small molecular weight contaminants inhibiting SOS formation until all small molecular weight contaminants have reacted. (Gold) Coupling reaction assuming the contaminant possesses bifunctionality and is following step-growth polymerization.

While a more thorough investigation would be necessary to validate the theory of a bifunctional contaminant, say by assessing the composition inside of the reactor at a sequence of time points, the challenges of efficiently sampling the reactor without compromising the reactor seal made this difficult. Therefore, in lieu of an elaborate kinetic study, it was decided to test this

theory by allowing the reaction go to completion without sampling along the way to see if the final product, if not interrupted by the compromising effects of sampling, could reach a coupling efficiency of near 100 mol%.

In the original protocol, the slow rate of addition of DBX was used because an accurate amount of chain ends could only be approximated. In this new protocol, the exact amount of titratable groups as well as how they react is known, therefore we can increase the rate of addition of DBX in order to minimize the impact of a reactor seal leak. To summarize, the knowledge of an exact amount of titratable groups and how those titratable groups (SO and other small molecules) react together in the formation SOS allowed for an exact amount of DBX (0.5 molar equivalents to total titratable groups) to be added at an accelerated rate. By implementing this methodology for coupling, a coupling efficiency of over 90 mol % was achieved (**Figure 2.5**). A detailed protocol for the coupling reaction (**Figure 2.5**) can be found in the experimental section.

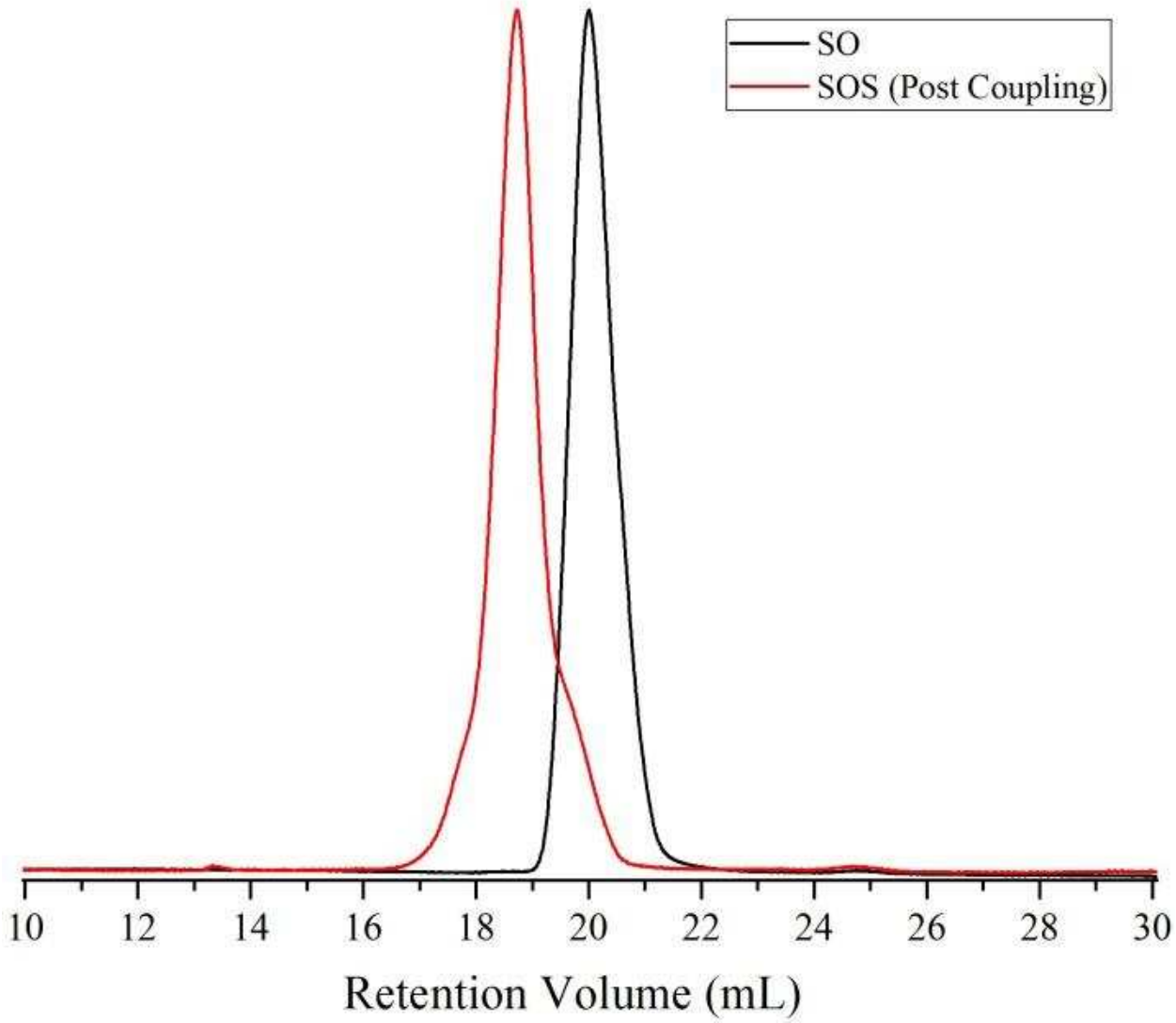

Figure 2.5: PSPEO before (black) and after (red) coupling by adding DBX in half molar equivalence to the number of potassium ions added for titration. This technique results in a much higher coupling efficiency (over 90 mol%) compared to adding DBX in a half molar equivalent to the theoretical number of SO chains.

2.2.2 Discovery, Impact, And Removal of High Molecular Weight Contaminant

As seen above in **Figure 2.5**, even after achieving high coupling efficiency, small, high molecular weight shoulders were visible in the GPC data. These high molecular weight species, while small when considered against the composition of directly coupled product, were discovered to have considerable negative impact on mechanical properties of the hydrogel. Due to its larger molecular weight than SOS (as well as its molecular composition likely being

similar), it was theorized that this high molecular weight species would precipitate before SOS in fractionation. This was indeed the case as is shown in below in **Figure 2.6**, where two different polymer products produced from independent coupling reactions (22 and 46 mol% SOS) are compared to the first precipitated layer from the fractionation of the 46 mol% SOS sample. When the high molecular weight impurity was attributed to the SOS, it produced an integrated peak of "80 mol% SOS". In order to assess the mechanical impact of this high molecular weight species on the mechanical properties of the hydrogel, the hydrogel was subjected to cyclic compression testing (10,000 cycles @ 12 % strain).

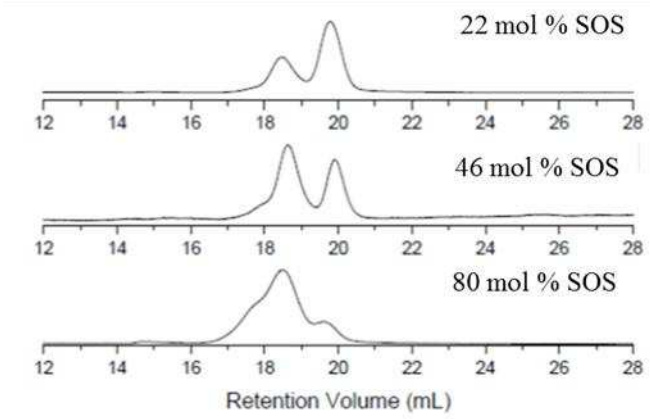

Figure 2.6: Gel permeation chromatography of SOS/SO blends resulting from coupling reactions following the protocol developed by Guo et al. The number displayed in the upper right denotes the mol % SOS. Samples labeled "22" and "46" were recovered directly from the coupling reaction, while sample "80" was the first recovered layer after fractionating sample "46".

Cyclic compression testing found that hydrogels produced from SOS/SO mixtures containing this shoulder on the SOS peak were softer and less fatigue resistant than samples with no shoulder on the SOS peak even when the overall integration of the high molecular weight peak was much higher (Table 2). Therefore, investigation into the cause of this high molecular weight impurity was needed in order to minimize its impact on the modulus and the fatigue resistant properties in our hydrogels.

Table 2.2: Summary of initial and mean modulus as well as % decay in modulus after 10,000 12% strain cycles for 22, 46 and "80" mol% SOS samples. Samples that contain a lower relative amount of the high molecular weight impurity to the SOS peak demonstrated higher initial and mean moduli as well as a greater resistance to decay

	Initial Modulus ± STD (MPa)	Mean Modulus ± STD (MPa)	Full Cycle Decay ± STD(%)
22	0.19 ± 0.017	0.15 ± 0.013	22 ± 3.8
46	0.44 ± 0.087	0.37 ± 0.090	16 ± 5.2
80	0.33 ± 0.12	0.23 ± 0.069	35 ± 6.1

Removing and isolating the impurity from Impurity/SOS/SO via successive fractionations was conducted in order to (1) see if the impurity could be removed without damaging the SOS or SO and (2) assess its chemical composition in order potentially discover its cause. Removing the impurity to see if an SOS/SO mixture could be recovered rid of the high molecular weight impurity was accomplished in two distinct phases. (1) Dissolve the mixture in a good solvent for all three species (chloroform) and then adding the minimum amount of poor solvent (n-hexane) necessary to initiate initial precipitation. Once the highest molecular weight precipitate (containing the highest conc. of the impurity) had settled the solvent containing the more desirable SOS/SO mixture with a lower conc. of the impurity was recovered. (2) This solvent was placed into the fridge and allowed to cool. Lowering the temperature of the solution induces further precipitation of the remaining polymer species by decreasing the entropic drive for mixing. The precipitant layer generated from cooling the system was recovered, and the solution was again placed into the fridge. This process was repeated to recover multiple layers of precipitant with progressively decreasing concentrations of the high molecular weight impurity (**Figure 2.7**).

A Gaussian fit of the crude coupled product directly from the coupling reaction, as well as the multiple layers of precipitant generated from fractionation, confirmed the presence of a third unknown high molecular weight impurity with an approximate MW, calculated via GPC, of

500kDa (**Figure 2.7** A-C). Notably, after approximately half of the total polymer had been recovered via fractionation, all subsequent precipitation layers that formed did not contain the high molecular weight impurity (**Figure 2.7 D**).

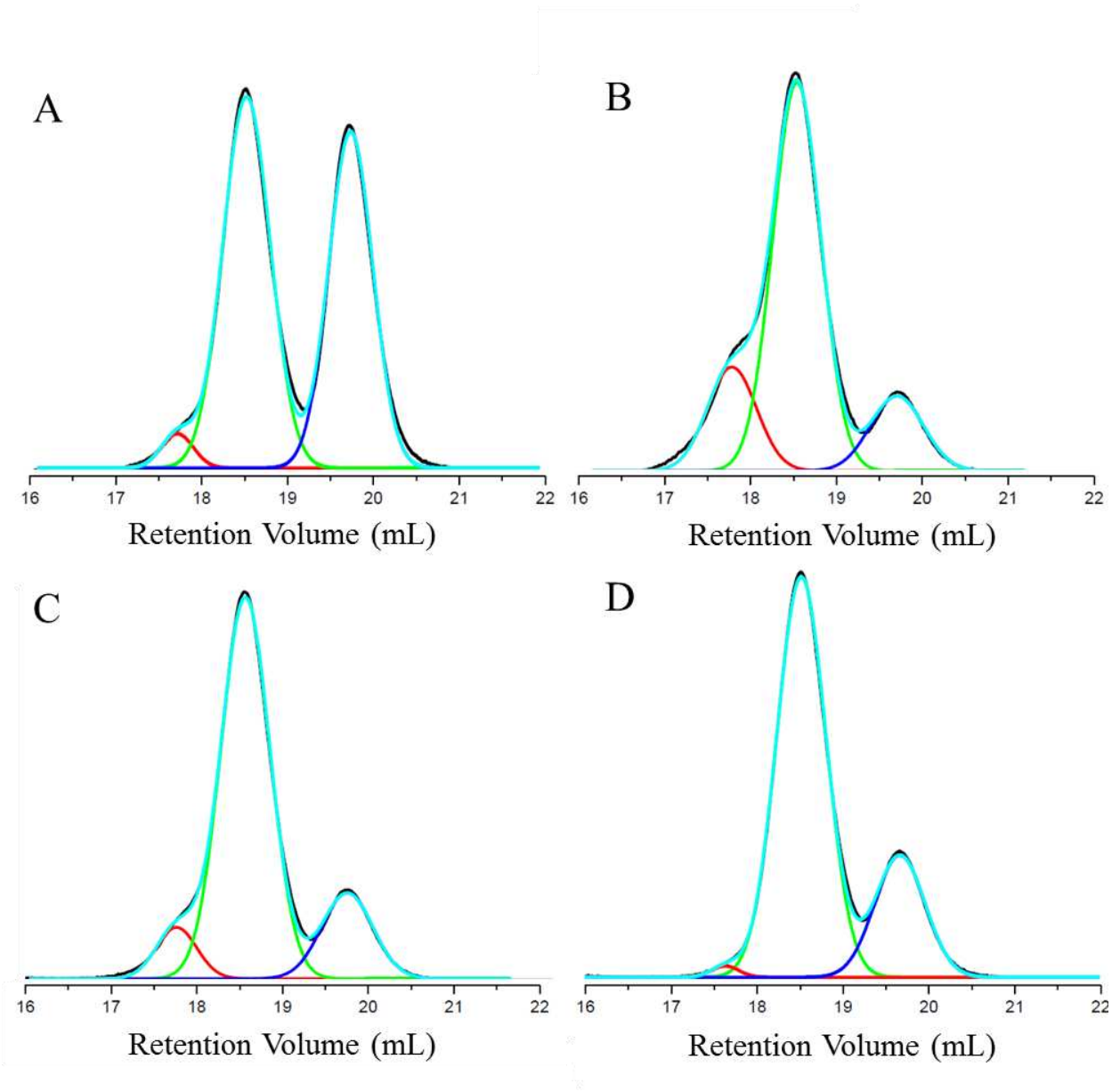

Figure 2.7: Isolation of SOS from the crude product of a coupling reaction following the original protocol developed by Guo containing SO/SOS/High MW Impurity. (A) Original crude product formed from coupling reaction (B) First layer of fractionation by adding n-hexane (C) Second layer of fractionation produced by placing upper layer of first fractionation in fridge for 24 hrs (D) Third layer of fractionation produced by placing upper layer of second fractionation in fridge for 24 hrs displays a product that does not contain the high molecular weight impurity.

While this high molecular weight impurity was initially detrimental to the mechanical integrity of the hydrogels, once removed via fractionation the moduli and fatigue resistant properties of its resulting hydrogels recovered to levels consistent with hydrogels of the same

SOS content without the impurity (i.e. the purification process did not damage the SOS/SO). While this impurity made up only approximately 1.2 mol % of the crude coupling product, its presence resulted in negative impacts on the mechanical integrity of the hydrogels produced from blends containing it. Also, fractionation resulted in a purification technique to remove the impurity without compromising the existing SOS or SO. While using fractionation to produce a polymer free of the mechanically detrimental high molecular weight impurity was effective, it was not efficient. Fractionating coupled product to isolate SOS/SO from its impurity would often result in losing well over half of the polymer from the crude coupling reaction.

Generating higher molecular weight species than SOS using this reaction led us initially to theorize potential impurities in DBX. Xylenes that possessed more than bifunctionality would result in the production of sites where more than two SO chains could join. Multiple manufacturers of DBX were tested and purified via recrystallization. No changes in the production of the high MW impurity were observed

Therefore, an investigation was conducted to try to isolate this impurity in an effort to design a coupling reaction that would not produce it. The initial layer, with the highest concentration of the impurity was recovered, dissolved, re-fractionated and a precipitant layer with even higher concentration of the impurity was recovered. After repeating this process for four successive fractionations of subsequent initial layers, this high molecular weight species was concentrated and characterized via NMR to reveal a disproportionately higher concentration of PEO relative to PS when compared to SO or SOS (**Figure 2.8**).

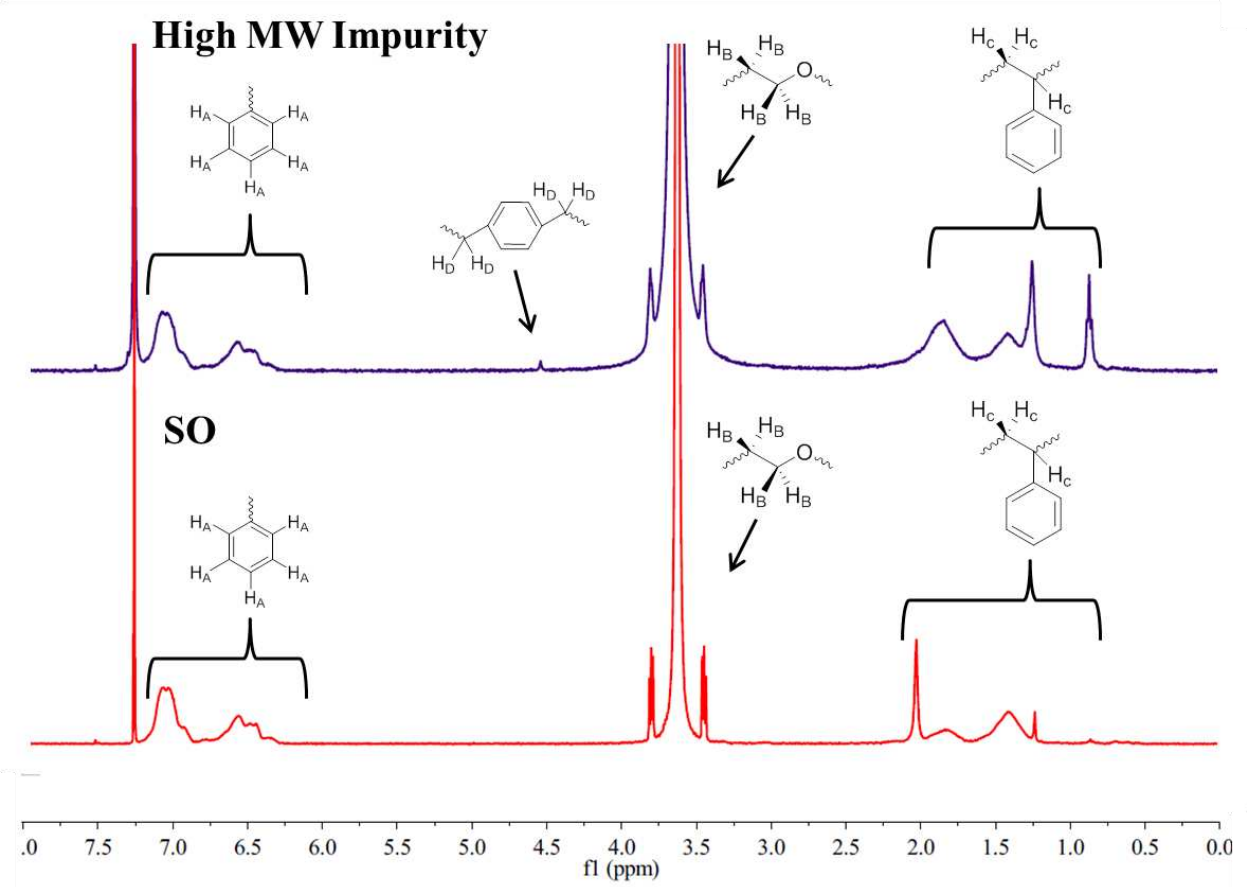

Figure 2.8: NMR of SO (bottom) and an ~50/50 mass % of SOS and the high molecular weight impurity (top) in deuterated chloroform revealing a much higher relative integration of polyethylene oxide relative to polystyrene in the sample containing higher concentrations of the impurity.

It was also theorized that the coupling agent itself, being a xylene, may yield a potential site for radical generation resulting in an eventual degradation of the polymer chain. If chain scission were to take place in the PEO block (the majority block) than you could create a bifunctional homopolymer of PEO that could be incorporated between two SO chains. This may explain the higher relative amount of PEO present in the high MW species. Therefore, two other coupling agents were tested (diiodobutene and dibromobutene) but resulted in a much lower coupling efficiency (~5 mol%) and the amount of impurity produced, if any, was not measurable.

These low of coupling efficiencies were not practical for our objectives. The dryness, as well as how closed the system was, were of particular concern as air may introduce chain degenerative compounds. Multiple factors were tested including: repacking solvent columns, drying the solvent further using molecular sieves, replacing Ar air filters, using different septa manufacturers, and using different reactor vessels. All of these variances had no impact on the production of the high MW impurity. Finally, the source of the impurity was found upon investigation of the SO diblock copolymer synthesis . Older SO that was manufactured in 2010 did not produce this impurity when coupled. Therefore, the problem was in the current methods used to synthesize SO diblock.

Multiple parameters were evaluated in the synthesis of SO diblock copolymer and its eventual impact, after coupling, in the production of the high molecular weight impurity. These methods included: different polystyrene molecular weights, different amounts of solvent, different drying agents for the ethylene oxide monomer (butylmagnesium chloride and dibutyl magnesium), and different numbers of distillations in the purification of ethylene oxide monomer. None of these changes resulted in the elimination of the impurity when the produced SO was eventually coupled. Finally, we discovered that the rubber septa used in the distillation of ethylene oxide (EO) monomer were not used in the original synthesis of SO. Once these rubber septa were removed from the purification step of EO monomer, the SOS that resulted from coupling this SO did not contain the high molecular weight impurity. The likely reason that using a rubber septum in the distillation of ethylene oxide eventually results in the production of a high molecular weight impurity is due to the formation of peroxides from the ethylene oxide monomer reacting with the rubber septa. This peroxide may have either eventually degraded the SO to form poly(ethylene oxide) (PEO) homopolymer or produced a bifunctional initiation site,

that resulted in the polymerization of PEO homopolymer. Because PEO homopolymer possesses bifunctionality, DBX can react at both termini which are eventually capped by an SO chain. This would result in the formation of an SOS impurity with much higher relative ethylene oxide composition.

To summarize, during synthesis of SO diblock copolymer do not create an environment in which ethylene oxide monomer comes into contact with rubber. This can be accomplished through direct condensation of the monomer without distillation (if the monomer is pure enough (99+%)) or by using purification flasks for the distillation that do not require a rubber septum. Notably, due to the necessity of doing so many of these polymerizations followed by coupling, these studies resulted in the realization that SOS could be generated from polystyrene using a one pot synthesis. Because our synthesis consists of titration of the ethylene oxide terminated polystyrene with K-NAP to initiate the polymerization of PEO, it was theorized that you could simply add the DBX to the reactor following the polymerization of PEO off of PS to generate SOS, which would eliminate the need for precipitation of SO before re-dissolving, re-titrating and coupling with DBX. The below one pot reaction (**Figure 2.9**) which uses ethylene oxide monomer directly condensed into an air-tight graduated cylinder, resulted in the elimination of the high molecular weight impurity but produced a lower coupling efficiency (~50 mass%). A detailed protocol for this one pot synthesis can be found in the experimental section. It is theorized that if a second and controlled re-initiation of any terminated chains through slow reactor leaks following the PEO polymerization with KNAP was implemented after the polymerization of the SO diblock and before the addition of the coupling agent DBX, that a one pot reaction resulting in the production of pure SOS from styrene, without the formation of the impurity, could be achieved.

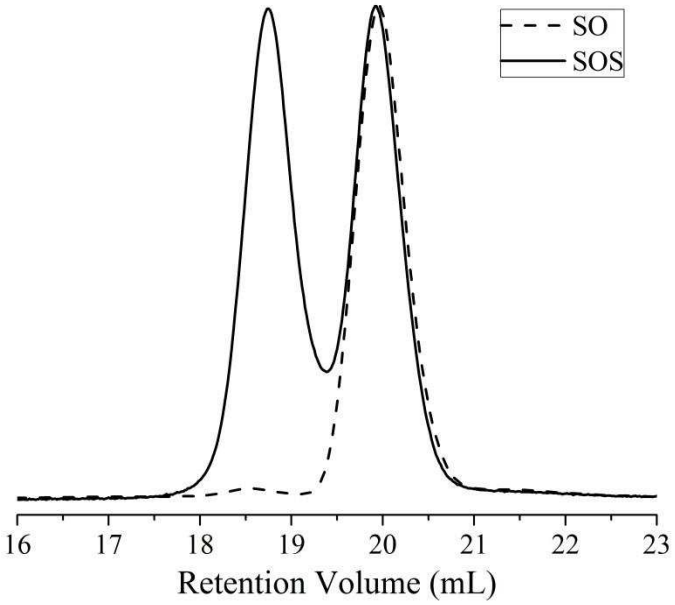

Figure 2.9: Gel permeation chromatography of SO (dash) and post coupling (SOS) using modified protocol. The GPC reveals no observable high molecular weight impurity after coupling.

2.2.3 Discovery, Impact, And Removal of Macroscopic Bubble Defects

While being able to synthesize SOS in large volumes at a high purity is paramount to the eventual mechanical capability of the swollen hydrogel, manufacturing techniques used to promote effective self-assembly and reduce macroscopic defects in the hydrogel are also of great importance to the overall mechanical robustness of these TPE hydrogels. Briefly, the original protocol for melt processing consisted of packing the dry SOS/SO polymer into a steel mold between two Kapton sheets and placing it into a hot press at 150°C for five minute. However, upon closer examination of the swollen hydrogels that resulted from this melt processing technique using MRI (**Figure 2.10**), significant air bubble defects were detected. In order to remove these bubbles, a vacuum processing technique was employed. This technique involved placing the Kapton/ steel mold / SOS/SO polymer assembly into a sealed plastic bag and applying a vacuum to it. The vacuum was applied while the polymer was in the molten state and

during cooling. This process was repeated and resulted in the removal of many of these macroscopic defects in the eventual swollen hydrogel. Removing these defects resulted in noticeable increases in mean extension at break as is shown in **Figure 2.10**. The observation of increased strain at break is likely due to the removal of stress concentrations inside of the hydrogel caused by the air bubble defects. These stress concentrations produce fracture sites that easily propagate through the hydrogel causing premature catastrophic failure.

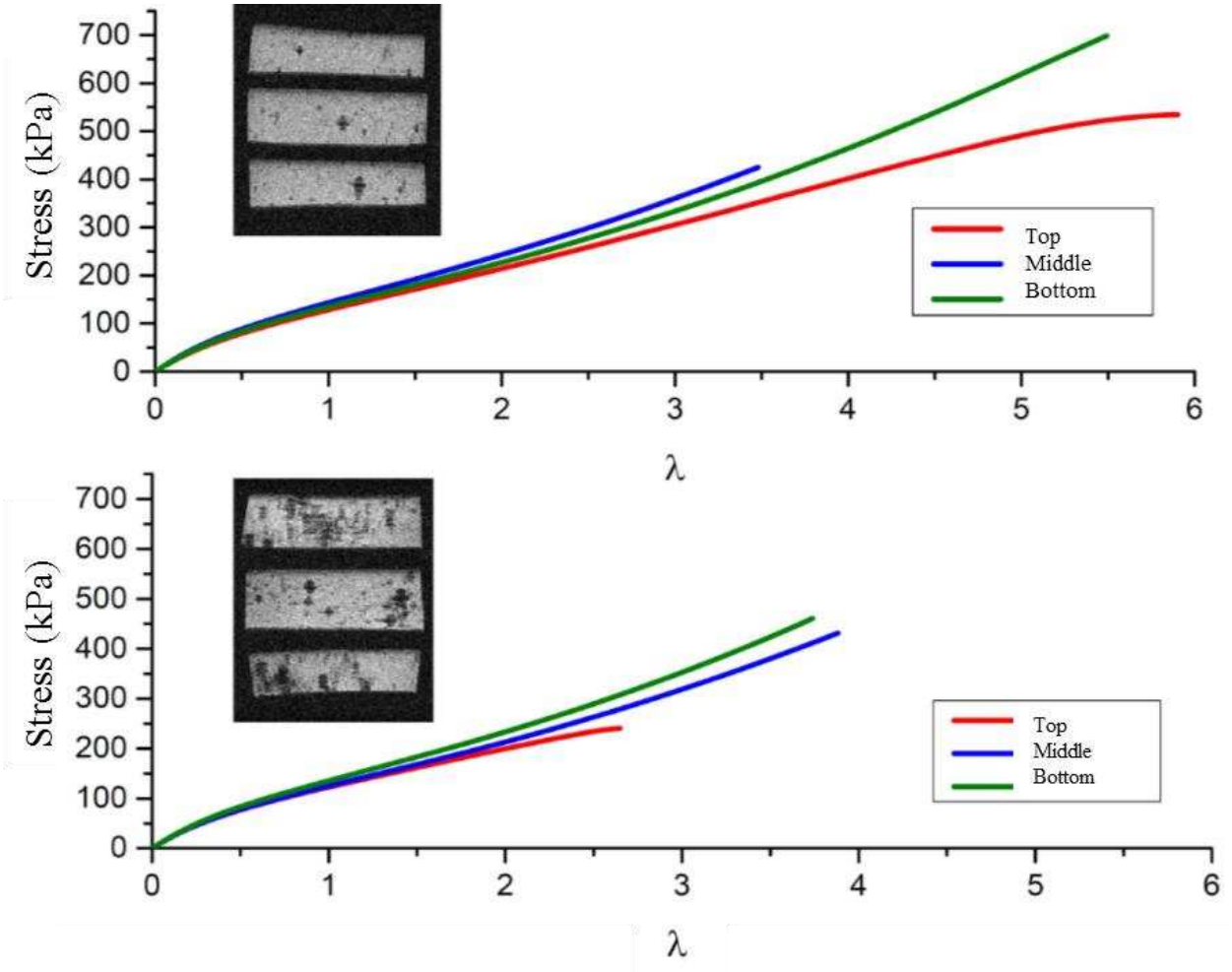

Figure 2.10: Tensile testing of samples that underwent melt processing under vacuum (top) and in air (bottom). MRI images (black and white) demonstrate a dramatic reduction in bubbles and tensile testing reveals a much higher average strain at break.

2.3 CONCLUSIONS

After a rigorous study we have developed methodologies which allow for much higher coupling efficiencies to be reached (90+ mol%) than those originally reported by Guo et al.[1] Also, we discovered that SO synthesized from EO monomer that has come into contact with rubber septa resulted in the formation of a high molecular weight contaminant upon coupling with DBX. Notably, this high MW contaminant severely diminished the modulus and fatigue resistant properties of our TPE hydrogels. Utilizing fractionation, we were able to discover the source of this high molecular weight contaminant and have developed a protocol for a one pot reaction that yields SOS from polystyrene without the production of the contaminant. The way in which these polymers are processed and manufactured has shown to be equally as important to their purity in regard to their mechanical ability, particularly in the mean extension at break. We have further developed a new processing technique in which samples were melt processed under vacuum through an iterative pump-heat-cool process which sinters the grains and removes bubble defects from the system. The combination of high SOS concentrations without high molecular weight contaminants and improved processing techniques to reduce sintering defects and bubbles now provide access to hydrogels that possess a higher moduli and a much greater resistance to fatigue. These improvements in mechanical properties, in turn, have produced hydrogel systems more mechanically appropriate for the demanding environment seen by the meniscus.

2.4 EXPERIMENTAL

Materials and Synthesis

Materials and Characterization Styrene (99%, 4-tert-butylcatechol inhibitor, Aldrich) and ethylene oxide (99.5+%, compressed gas, Aldrich) monomer were each purified by successive vacuum distillations (10–20 mTorr) from dried di-n-butylmagnesium (1.0 M solution in heptane, Aldrich) before use. Both purified styrene and ethylene oxide monomer were stored in glass burettes in the dark, at room temperature (styrene) and 3 °C (ethylene oxide), respectively, before use (typically less than 24 h). Argon degassed cyclohexane (CHX) was purified by passing the solvent over activated alumina followed by Q-5-like supported copper catalyst (Glass Contour, proprietary). Argon degassed tetrahydrofuran (THF) was purified by passing the solvent over activated alumina. High-purity argon (99.998%, Airgas) was passed through additional oxygen and moisture traps prior to use. Glassware and polymerization reactors were flamed under vacuum and backfilled with argon multiple times. All other reagents were used as received. ^{1}H NMR spectra were collected at room temperature in $CDCl_3$ on a Varian Inova 400 MHz Spectrometer (n = 32, delay = 30 s). Size exclusion chromatography (SEC) was performed on a Viscotek GPC-Max chromatography system fitted with three 7.5 x 340 mm Polypore^{TM} (Polymer Laboratories) columns in series, an Alltech external column oven, and a Viscotek differential refractive index (RI) detector. Measurements were performed using a DMF (55 °C) mobile phase (1 mL/min) with PS standards (Polymer Laboratories). Final SO/SOS compositions were confirmed via relative peak integrations in the SEC chromatograms of these blends.

Synthesis of potassium naphthalenide Place a rubber septum and two CHEM-CAP® valves into a solvent flask. Flame the solvent flask while under vacuum to remove moisture. Once

flamed perform 5 argon backfills with vacuum on the solvent flask. Seal the flask and then attach the flask to solvent columns and perform an additional 5 argon backfills on the stem of the flask to remove excess moisture. Collect approximately 150 ml of dry and oxygen free tetrahydrofuran from the solvent column and then seal the flask.

Place a rubber septum and a CHEM-CAP® valve into a graduated cylinder containing a glass stir bar. Flame the graduated cylinder while under vacuum to remove moisture. Once flamed perform 5 argon backfills with vacuum on the graduated cylinder. Seal the graduated cylinder and record its mass under vacuum. Attach the graduated cylinder back to the vacuum line and perform 5 additional argon backfills only on the stem of the graduated cylinder. Put the graduated cylinder under positive argon pressure.

Take a 100 ml beaker and place 50 ml of pentane into the beaker. Bubble argon into the pentane in the beaker for 5 minutes. Cut a piece of potassium metal inside of the pentane removing all of the oxidized metal sides to reveal a shiny surface. The amount of potassium metal should be enough to produce a 100 ml solution with enough potassium to titrate approximately 10x the number of free chain ends that will be coupled (ex. For 1g of SO diblock at a MW of 100kDa you would need approximately Xg of potassium metal). While under positive argon pressure, with argon flowing into the graduated cylinder, quickly add the piece of potassium metal to the graduated cylinder and then seal the cylinder. Pull vacuum on the cylinder for 5 minutes to remove any pentane that is coating the potassium metal. Perform 5 additional argon backfills on the graduated cylinder. Place the graduated cylinder under vacuum, seal the cylinder and then record its mass. Attach the graduated cylinder back to the vacuum line and perform 5 argon backfills on the stem of the cylinder. Place the graduated cylinder under positive argon pressure. Calculate the mass of potassium metal inside of the graduated cylinder by taking the difference

in mass of cylinder before and after the addition of the metal. Mass 1.2 molar equivalence of naphthalene to the dry potassium. While under positive argon pressure, with argon flowing into the graduated cylinder, quickly add the naphthalene to the graduated cylinder and then seal the cylinder. Perform 5 argon backfills with vacuum on the graduated cylinder and then pull vacuum on the cylinder for 10 minutes. Seal the graduated cylinder under positive argon pressure.

Attach the solvent flask containing the dry tetrahydrofuran to the vacuum line. Perform 5 argon backfills with vacuum on the stem of the solvent flask. Place the solvent flask under positive argon pressure with argon flowing. Place cannula into the solvent flask without going into the solution and check to ensure that argon is flowing out of the cannula. Place the other end of the cannula into the graduated cylinder. Push the cannula into the tetrahydrofuran inside of the solvent flask. Turn on the stir plate underneath the graduated cylinder. Take a needle and bleed argon from the graduated cylinder which will allow for the flow of tetrahydrofuran from the solvent flask into the graduated cylinder. The solution should turn a dark green immediately. Stop the flow of solvent at the 100 ml mark to ensure an accurate calculation of the potassium concentration. Allow the solution to stir overnight. Note: due to imperfect seals be sure to use the resulting potassium naphthalenide solution the following day to minimize the introduction of atmospheric moisture.

ω-Hydroxy-polystyrene (S-OH). Purified styrene monomer (120 g, 1.14 mol, 20°C) was added to a stirring solution of sec-butyl lithium (10.23 mL, 1.3 M in cyclohexane, Aldrich) and dry, air-free cyclohexane (1 L, 20 °C) in a 2 L reaction vessel. The solution was then raised to 40°C and stirred continuously for 8 hours. At a reduced pressure of 1 psig, purified ethylene oxide (6.6 g, 0.15 mol, 0 °C, liquid) was added to the reaction vessel. The reaction was held at 40°C for an

additional 24 hours, after which all excess ethylene oxide was removed from the reactor under a constant argon flow. The reaction was terminated by acidic methanol (50 mL). The polymer was precipitated in methanol (5 L total), producing a fluffy white solid, and dried under vacuum at room temperature over a 48 h period (yield 116 g, 97%, M_n= 8370 g/mol, PDI = 1.03).

ω-Hydroxy-polystyrene-b-poly(ethylene oxide) (SO). S-OH (7 g, 0.836 mmol) was added to a 2 L reaction vessel containing a glass coated magnetic stir bar. The reactor was evacuated and backfilled with purified argon before adding 1 L of dry, air-free tetrahydrofuran (THF). Concentrated potassium naphthalenide in THF was added to the polymer solution via cannula until a light green color persisted for 30 minutes. Ethylene oxide monomer (99.5%) was directly condensed into a burette without drying! The temperature of the reaction mixture was raised to 40 °C and purified ethylene oxide monomer (78.7 g, 1.78 mol, 0 °C) was added under argon (1 psi) to the stirring solution for 48 hours. The reaction was terminated by a stoichiometric equivalent of HCl in methanol (50 mL) and the polymer was precipitated in 4 L of pentane, producing a fluffy white solid. The polymer was dried under vacuum at room temperature for 48 hours. (M_n= 107,000 g/mol, PDI = 1.07, f_{PS} = 0.085).

polystyrene-b-poly(ethylene oxide)-b-polystyrene (SOS) from SO using original protocol SO (29 g, 0.271 mmol) was placed into a 2 L round bottom reactor vessel that was evacuated and backfilled with purified argon. SO was allowed to dry under vacuum overnight. The SO was then dissolved in dry THF. A concentrated potassium naphthalenide solution in dry THF was titrated into the reactor until the solution maintained a green color for 30 minutes. α,α′-dibromo-p-xylene (35.8 mg, 0.136 mmol, 0.5 eq) in THF (1.5 mL) was then injected into the reactor over a 12 hour

period at a rate of 0.125 mL hr^{-1} using a syringe pump and a 2.5 mL glass syringe. Coupled polymer was recovered through precipitation in 5 L of pentane followed by vacuum filtration. The precipitated polymer was dried overnight under vacuum to produce a fluffy white solid as a blend of coupled (SOS) and uncoupled (SO) block copolymer (52 mol% SOS).

polystyrene-b-poly(ethylene oxide)-b-polystyrene (SOS) from SO using modified protocol

Place a rubber septum and two CHEM-CAP® valves into a purification flask with a glass stir bar. Flame the purification flask while under vacuum to remove moisture. Once flamed perform 5 argon backfills with vacuum on the purification flask. Place purification flask under positive argon pressure with argon flowing and add 1g of SO diblock copolymer into the purification flask and reseal the flask. Perform 5 argon backfills with vacuum on the purification flask containing the SO diblock copolymer. Leave the flask under vacuum for 24 hours to remove any moisture from the polymer.

Place a rubber septum and two CHEM-CAP® valves into a solvent flask. Flame the solvent flask while under vacuum to remove moisture. Once flamed perform 5 argon backfills with vacuum on the solvent flask. Seal the flask and then attach the flask to solvent columns and perform an additional 5 argon backfills on the stem of the flask to remove excess moisture. Collect approximately 150 ml of dry and oxygen free tetrahydrofuran from the solvent column and then seal the flask. Attach the solvent flask containing the dry tetrahydrofuran to the vacuum line. Perform 5 argon backfills with vacuum on the stem of the solvent flask. Place the solvent flask under positive argon pressure with argon flowing. Place cannula into the solvent flask without going into the solution and check to ensure that argon is flowing out of the cannula. Place the other end of the cannula into the purification flask. Push the cannula into the tetrahydrofuran

inside of the solvent flask. Turn on the stir plate underneath the purification flask. Take a needle and bleed argon from the purification flask which will allow for the flow of tetrahydrofuran from the solvent flask into the purification flask. Add approximately 100 ml of dry tetrahydrofuran per gram of SO diblock copolymer. Stir the solution of tetrahydrofuran and SO diblock copolymer until the polymer is completely dissolved.

Attach the sealed graduated cylinder containing the solution of potassium naphthalenide to the vacuum line. Perform 5 argon backfills with vacuum on the stem of the graduated cylinder. Place the graduate cylinder under positive argon pressure with argon flowing. Note the initial volume of potassium naphthalenide inside of the graduated cylinder. Place cannula into the graduated cylinder without going into the potassium naphthalenide solution and check to ensure that argon is flowing out of the cannula. Place the other end of the cannula into the purification flask containing the dry and dissolved SO diblock copolymer. Push the cannula into the potassium naphthalenide solution inside of the graduated cylinder. While stirring in the purification flask, take a needle and very slowly bleed argon from the purification flask which will allow for the flow of potassium naphthalenide from the graduated cylinder into the purification flask. Continue to titrate the potassium naphthalenide solution into the purification flask containing the SO diblock copolymer until a light green color persists for at least 30 minutes. Note the final volume of potassium naphthalenide inside of the graduated cylinder. Calculate the number of moles of potassium that were added to the purification flask by multiplying the molar concentration of potassium inside of the potassium naphthalenide solution by the volume added. Once this value is calculated further titrate the SO diblock copolymer solution until a medium green color persists for 30 minutes.

Place a rubber septum and two CHEM-CAP® valves into a second purification flask with a glass stir bar. Flame the purification flask while under vacuum to remove moisture. Once flamed perform 5 argon backfills with vacuum on the purification flask. Seal the flask under vacuum and record its initial mass. Place purification flask under positive argon pressure with argon flowing and add enough dry dibromoxylene into the purification flask to produce a 20 ml solution of dibromoxylene in tetrahydrofuran at a concentration where 2 ml contains 0.5 molar equivalence to the moles of potassium needed for the light green color to persist for 30 minutes and then reseal the flask. For example, if it took x ml of potassium naphthalenide solution for a light green color to persist for 30 minutes, and the concentration of potassium in your potassium naphthalenide solution was x mol K/ ml, then you would add x mg of dibromoxylene to the purification flask. Perform 5 argon backfills with vacuum on the purification flask containing the dibromoxylene. Pull vacuum on the purification flask for 30 minutes. Seal the flask and record its mass.

Using the calculated amount of dibromoxylene added to the purification flask, you will need to calculate how much tetrahydrofuran you need so that a 2 ml solution of dibromoxylene in tetrahydrofuran contains 0.5 molar equivalence to the moles of potassium needed for the light green color to persist for 30 minutes and then reseal the flask. Assemble a 10 ml air-tight glass syringe with Teflon at the interface between the syringe and the needle. Pull argon into the syringe and expel the argon from the syringe 3 times to minimize the amount of oxygen and moisture in the syringe. Pull up the calculated amount of tetrahydrofuran into the syringe and add it to the second purification flask containing the dry dibromoxylene. Stir the solution until the dibromoxylene is completely dissolved.

Assemble a new 5 ml air-tight glass syringe with Teflon at the interface between the syringe and Teflon tubing and attach a needle to the end of the Teflon tubing. Pull argon into the syringe and expel the argon from the syringe 3 times to minimize the amount of oxygen and moisture in the syringe. Place the syringe into the purification flask containing the dibromoxylene solution and draw up 4 ml of dibromoxylene solution. Be sure to remove all bubbles from the syringe, tubing and needle. Remove the needle from the dibromoxylene solution and place the needle into the purification flask containing the medium green colored potassium naphthalenide titrated SO diblock copolymer. Place the glass syringe into a syringe pump. Choose the manufacturer of the syringe (Hamilton, 5 ml), the volume of solution to be added (2 ml), and the time for the addition (8 hours). Allow the syringe to add 2 ml of dibromoxylene solution (0.5 molar equivalence to all titratable groups) to the purification flask over the designated 8-hour period and allow the solution to react overnight. Place 500 ml of pentane into a 1 L beaker with a large Teflon stir-bar. Stir the pentane inside of the beaker at a rate that generates a gentle vortex. Pour the contents of the purification flask, containing the SOS triblock copolymer, into the middle of the vortex of pentane inside of the 1 L beaker. This should result in the production of a white (or slightly yellow) and fluffy precipitate. Using a filter funnel and filter paper pour the contents of the beaker through the filter to isolate the polymer from the solution. Collect the damp SOS triblock copolymer and place into a drying holm and pull vacuum to remove any pentane and tetrahydrofuran.

One pot synthesis of polystyrene-b-poly(ethylene oxide)-b-polystyrene (SOS) from S-OH using modified protocol The first step involved synthesis of a hydroxyl-terminal polystyrene macroinitator (3.6 g PS, $M_{n,PS}$ = 8064 g mol^{-1}, $M_{w,PS}/M_{n,PS}$ = 1.05, SEC (polystyrene standards)).

The PS was added to a 2.5L reactor was evacuated and backfilled (5x) with purified argon before adding 1 L of dry, air-free tetrahydrofuran (THF). Concentrated potassium naphthalenide in THF was added to the polymer solution via cannula until a light green color persisted for 30 minutes. Ethylene oxide monomer (99.5%) was directly condensed into a burette without drying! The temperature of the reaction mixture was raised to 40 °C and purified ethylene oxide monomer (26.74 g, 0.607 mol, 0 °C) was slowly added under argon (1 psi) to the stirring solution and allowed to react for 48 hours. Half of the solution was terminated by transferring half of the reactor contents into a stoichiometric equivalent of HCl in methanol (50 mL) and the polymer was precipitated in 4 L of pentane, producing a fluffy white solid. The polymer was dried under vacuum at room temperature for 48 hours. Because 10.5 ml of concentrated potassium naphthalenide ($5.88*10^{-5}$ mol K/ml) was needed in order for a light green color to persist, and half of the contents of the reactor were removed for precipitation, 2.0 ml of a THF solution containing a total of $1.54*10^{-4}$ mol of DBX was added via a glass syringe over 4 hours and allowed to react overnight. The coupled product was precipitated into 4L of pentane and dried over-night under vacuum for 48 hours. The volume fraction of the PS block in the final diblock copolymer was determined to be 0.124 (using nominal densities at 140 ˚C) with an overall M_n = 73800 g mol^{-1} (M_w, SO, /M_n, SO = 1.04. SEC (polystyrene standards)) calculated using the measured M_n, PS and the relative 1 H NMR integrations.

SO/SOS Fractionation. To achieve higher SOS concentrations than the 52 mol% produced during the SO coupling reaction, fractionation was performed. Dry SO/SOS polymer (4 g) was dissolved in chloroform (400 ml) and heated to 45 °C. N-hexane (920 ml) was added slowly, keeping the temperature above 40°C. The SOS precipitated and the solution turned cloudy. Upon

cooling to room temperature, the solution turned transparent. The solution contained the majority of the SO while the SOS existed as a precipitate. The SOS precipitate was recovered and allowed to dry under vacuum overnight, while the SO in solution was recovered by placing the solution into the fridge and collecting precipitant layers every 24 hours. Even higher SOS concentrations were achieved through successive fractionations of precipitated SOS.

Preparation of SO/SOS hydrogel samples. Dry polymer for the different SOS blend compositions (22, 46, and 80 mol%) were compacted into a circular steel washers (8 mm diameter × 0.73 mm deep) or rectangular steel cutouts (assorted dimensions × 1 mm deep) and sandwiched between two sheets of Teflon coated Kapton™. These assemblies were then placed into a Carver Press and heated to 150°C under an applied pressure of ~500 psi for 5 minutes. In some cases multiple compressions were used to remove visible bubbles. Samples were allowed to cool to room temperature before swelling. Samples taken from circular washer molds were used for indentation relaxation testing, swelling analysis, and tensile testing. For tensile testing, test strips (3 mm × 8 mm × 1.25 - 1.5 mm deep) were cut from the swollen disks. Samples taken from the rectangular cutouts were used for fatigue and overloading compressions tests. In all cases, 8 mm or 6 mm diameter testing plugs were punched from swollen rectangular hydrogels using a biopsy punch.

Fatigue testing of SO/SOS hydrogels. Fatigue tests were initially run on hydrogels fabricated using three concentrations of SOS triblock copolymer (22, 46, and 80 mol% SOS). The three disk shaped samples (SOS 22, SOS 46, and SOS 80) were swollen in DI water (8 mm diameter), mounted (Loctite Super Glue Ultragel Control, Henkel Corporation, Rocky Hill, CT) on one side

to a polished aluminum platen, submerged in a DI bath, and compressed using a secondary aluminum plate. The sample was preloaded to 20 g and then compressed to 12% strain at a frequency of 1 Hz for 10,000 cycles using an MTS Bionic Model 370.02 (MTS Corp, Eden Prairie, MN) configured with a 908 g load cell (Futek LSB200, Irvine, California). **Analysis.** MATLAB (Mathworks, Natick,MA) was used to analyze the resulting data. Maximum and minimum compressive force and displacement for each cycle were determined and a linear fit between strains nearest 2-10% was used to ascertain the compressive mean modulus.

Tensile testing of SO/SOS hydrogels. Tensile testing was performed on an ARES-rheometer (TA Instruments, DE) at room temperature. Testing strips were placed into torsion rectangular grips (TA Instruments, DE) with a layer of sand paper between the grip and the hydrogel to reduce slippage. The hydrogels were clamped and pulled until a force of 5 g was reached to ensure the hydrogel was taut. The hydrogel was then extended to a mid-substance failure at a strain rate of 2% s^{-1}.

REFERENCES

1. Guo, C.; Bailey, T. S.,Highly distensible nanostructured elastic hydrogels from AB diblock and ABA triblock copolymer melt blends, *Soft Matter* **2010,** 6, (19), 4807-4818.

2. Sperling, L. H., *Introduction to Physical Polymer Science*. 4th ed.; Wiley: 1979; p 845.

CHAPTER 3

NANOSTRUCTURE-DRIVEN REPLICATION OF SOFT TISSUE BIOMECHANICS IN A THERMOPLASTIC ELASTOMER HYDROGEL

3.1 INTRODUCTION [3]

With a biphasic composition reminiscent of biological tissues, synthetic hydrogel networks have long been embraced as a foundation from which biomechanically accurate musculoskeletal soft tissue surrogates might be engineered. Reduction to practice, however, has been plagued by the gap in mechanical performance that continues to differentiate biological and synthetic systems. The most prominent advances in hydrogel design have employed the inclusion of interpenetrating networks,[1] hydrophobic interactions,[2, 3] ionic interactions,[4, 5, 6] deformable domain structures,[7] sliding junction points,[8, 9, 10] and multifunctional macromers of prescribed structure[2, 11, 12] to produce intriguing network designs pushing the boundaries of mechanical achievement. These designs are responsible for stunning demonstrations of modulus, [4, 6] stretchability, [3, 5, 6, 8, 9] ultimate strength,[1, 2, 11] and overall toughness [3, 5, 6, 8, 9] that were inconceivable less than two decades ago. However, most of these systems are plagued by combinations of limited moduli at small strain, unacceptably high levels of energy dissipation

[3] The following chapter is the result of highly collaborative efforts between the groups of Travis S. Bailey and Tammy Haut-Donahue and is adapted from a recently submitted manuscript. Jackson T. Lewis performed all the syntheses, chemical and structural characterization of the materials used in this study, and uniaxial extension tests of the hydrogels. Kristine M. Fischenich performed all uniaxial compression tests and the accompanying numerical and statistical analysis of that data. Travis S. Bailey conceived and designed the hydrogel architecture. Jackson T. Lewis, Kristine M. Fischenich, Travis S. Bailey and Tammy L. Haut-Donahue conceived and designed the experiments and contributed to the writing of the manuscript. The authors would like to thank Alyssa Winter for assistance with X-ray scattering measurements.

and fatigue, or slow and incomplete elastic recovery that are incompatible with the cyclic biomechanical loading profiles of most musculoskeletal soft tissues. Intrinsic susceptibility to permanent covalent bond rupture and significant plastic deformation[13, 14, 15, 16, 17, 18] preclude a network from returning elastically to its original configuration, while recovery dynamics in the minutes to hours range[5, 6] preclude it from doing so at physiologically relevant (often sub-second) time scales. Unfortunately, none of these advanced systems would yet be acceptable, for example, as substitutes for the fibrocartilage comprising menisci of the knee, the annulus fibrosis of the intervertebral disc, or connective tissue of the cardiovascular system, which rely on high levels of elasticity to rapidly absorb and transfer (not dissipate) strain energy into efficient body movement or pulsatile blood flow.[13, 14, 15]. Fatigue in typical non-swollen elastomeric polymers often considered for biomaterials applications tends to begin after hundreds of thousands of cycles.[16, 17, 18, 19] Swollen systems, in contrast, tend to be rather brittle and have not been able to produce a comparable benchmark.[20] The brittleness derives from both the reduced areal density of polymer chains compared with their non-swollen counterparts, and the tendency of swelling to exaggerate strand length heterogeneity and localized stress concentrations, facilitating bond rupture.[21] Unfortunately, the development of higher modulus, fatigue-free hydrogel systems that can demonstrate a sustained ability to absorb and store energy elastically have not received the attention that tough dissipative systems have been afforded.[20, 22] Two important contributions, however, have come from the groups of Sakai[11, 12] and Ito,[9, 10] who have pioneered synthetic approaches for removing strand heterogeneity and promoting uniformity in the dispersal of stress. Sakai and coworkers used exact reaction stoichiometry and monodisperse tetra-arm macromonomers[2, 11, 12] to produce materials supporting very large compressive strains (99+%), which they attribute to the near absence of "spatial inhomogeneities and trapped entanglements"

in the network.[11] In a somewhat contrary approach, Ito used topologically trapped but freely movable junctions to form "slide-ring gels", which allow the network to autonomously adjust strand lengths and use a "pulley effect" to redistribute local stress concentrations.[8, 9, 10] Notably, while each of these innovative networks has the potential to enhance elasticity while minimizing

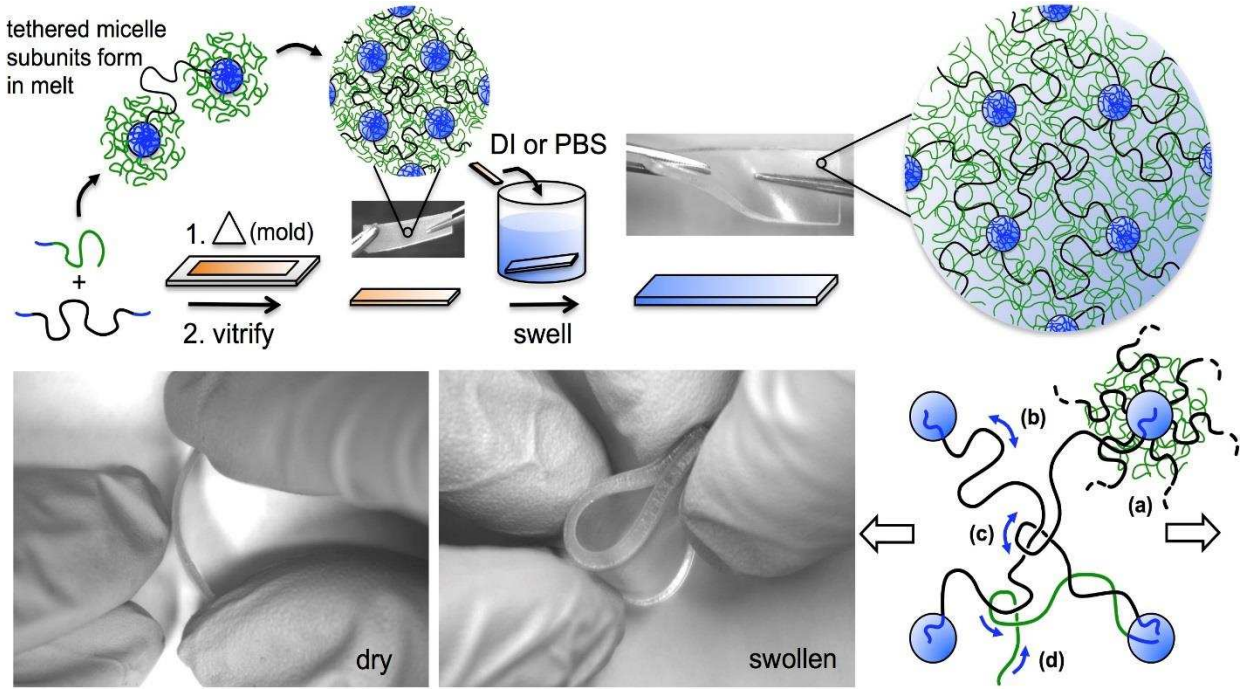

Figure 3.1: Hydrogel fabrication is accomplished using melt-state self-assembly of block copolymers. Blends of sphere forming polystyrene-poly(ethylene oxide) (PS-PEO, SO) diblock and PS-PEO-PS (SOS) triblock copolymer produce networks of tethered micelle-like domains when heated, which become fixed upon vitrification of the PS domains. Selective solvation of the PEO matrix by water or phosphate buffered saline (PBS) produces hydrogels with outstanding mechanical properties and equilibrium water compositions typically between 80 and 98 wt%. Importantly, the modulus and water content can be tuned simply using the ratio of SO diblock and SOS triblock copolymer added to the blend. Images depict hydrogel fabricated with 61 mol% SOS containing 85 wt% PBS buffer. Key features of the network structure (lower right) include (a) a low density of fixed junction points, each with high branch point functionality (f ~ 340), (b) large (Mn,PEO = 197 kDa) and narrowly distributed (PDI 1.06) molecular weights between junction points, (c) high densities of topologically fixed but mobile chain entanglements (thousands per fixed junction point) among tethering blocks, and (d) large numbers of dynamic entanglements between free diblock copolymer chain ends and other strands in the system. In combination, these features facilitate rapid and efficient homogenization of the stress fields in the sample, while promoting sub-second recovery rates.

hysteresis, the specific materials synthesized in these examples were generally quite soft (compressive moduli in the tens of kPa). That is, they were not necessarily designed to produce a biomechanically appropriate modulus, particularly over the small strain ranges relevant during standard physiological compression of many musculoskeletal soft tissues (e.g., meniscus ~ 12%,[23, 24, 25] intervertebral disc ~ 10%,[26, 27] articular cartilage ~ 5 to 30%[28, 29]). Regardless, these groundbreaking studies demonstrate the importance of utilizing network architectures that promote homogenization of the stress field, if elasticity without fatigue is to be achieved. In that vein, we report here a simple two-component block copolymer hydrogel, synthetically designed to be conveniently processable as a thermoplastic prior to swelling, and characterized by a network nanostructure (**Figure 3.1**) that imparts both a physiologically relevant modulus and an unprecedented ability to distribute stress, resist fatigue, rapidly recover, and avoid catastrophic failure even under extreme degrees of compressive strain.

Network efficiency through melt-state self-assembly

As shown in **Figure 3.1**, we use melt blends of AB diblock and ABA triblock copolymers, synthetically designed with average block molecular weights ($M_{n,A}$ or $M_{n,B}$), polydispersity indicies (PDIs), and volume fractions (f_A or f_B) that favor formation of the classic block copolymer sphere morphology upon heating,[30, 31] to produce a physically cross-linked network of tethered micelle-like units. During melt-state self-assembly, A blocks form spherical aggregates composed of hundreds of chains, while the B blocks form a coronal brush layer which behaves as a matrix in which the spherical A domains reside.[32, 33, 34, 35] Hydrogel fabrication entails heating the blend to induce self-assembly, vitrifying the sample to trap the developed morphology, and the selectively swelling the B blocks through submersion in aqueous media. Each bridging ABA triblock copolymer thus functions as a tether, mechanically linking adjacent

spherical domains. Hydrogel formation relies on two important phenomena that dictate the choice of A and B blocks. One, the A blocks must form a vitrified solid upon cooling. Polystyrene (PS) was used in this study, with a glass transition temperature near 80 ˚C ($M_{n,PS}$ = 8.4 kDa).[36] Two, the B blocks must be selectively soluble in the swelling media, while the A blocks remain impervious to it. Poly(ethylene oxide) (PEO) was selected as the water soluble B block.

In terms of network nanostructure, this method of hydrogel fabrication produces key architectural features (**Figure 3.1a-d**) believed to be critical for eliminating fatigue, producing a high modulus, and ensuring rapid recovery. First, strand length homogeneity is ensured by keeping the density of fixed junction points (glassy spherical PS domains) low, and the strand molecular weight adjoining them both high ($M_{n,\,PEO}$ = 197 kDa) and narrowly distributed (PDI < 1.07). This construction would normally favor soft, weak materials, but each junction point in these systems has an intrinsic branch point functionality in the hundreds, with each spherical aggregate containing approximately 340 chains (SAXS model fits, **Supplementary Figure A2.1**). Thus, even moderate triblock copolymer compositions produce large numbers of bridging strands emanating from each sphere. In addition, because assembly takes place in the melt, the density of topologically trapped entanglements among these bridging (and looping) triblock copolymers is intrinsically maximized. Given the small entanglement molecular weight for PEO (M_e ~ 1.6 kDa),[37] the number of topologically fixed entanglements per fixed junction point are estimated to be in the thousands. The shear number of these highly mobile entanglements, which act much like primitive versions of the freely movable junction points introduced in rotaxane-based slide-ring gels,[9, 10] simultaneously produce both a significant modulus and an ability to rapidly redistribute localized stress. Notably, the PS-PEO-PS (SOS) triblock copolymer

synthesized is purposefully "latticed matched" to the PS-PEO (SO) diblock copolymer, such that the sphere size and morphological domain spacing remains largely independent of blend composition (SAXS data fits, **Supplementary Figure A2.1**). This novel approach allows the relative amounts of triblock copolymer in the blends to be easily changed, and thus the fixed entanglement density, without significantly changing the density of fixed junction points formed during melt-state self-assembly. Controlling entanglement density during self-assembly, in turn, allows direct control over the equilibrium swelling and modulus (vide infra) in the final swollen systems.[32] Importantly, the liquid content of these hydrogels at equilibrium, whether swollen in DI water or phosphate buffered saline (PBS) (**Supplementary Figure A2.2**) is inherently always greater than 80 wt%. Nominally, this quantity exceeds that of many biological tissues (~70 wt%).[38, 39, 40]

3.2 RESULTS AND DISCUSSION:

3.2.1 Elasticity, Recovery and Resistance to Fatigue

The compression data of **Figure 3.2** underscores the exceptional ability of the hydrogel nanostructure to absorb and distribute strain energy. It depicts an overlay of two successive compression cycles to 99% strain (strain rate = 2% s^{-1}) performed on a submerged hydrogel disc (6 mm × 1.6 mm) fabricated using 61 mol% SOS triblock copolymer (85 wt% PBS buffer). In this case, the strain rate was limited to reduce surface stress at the hydrogel-platen interface, such

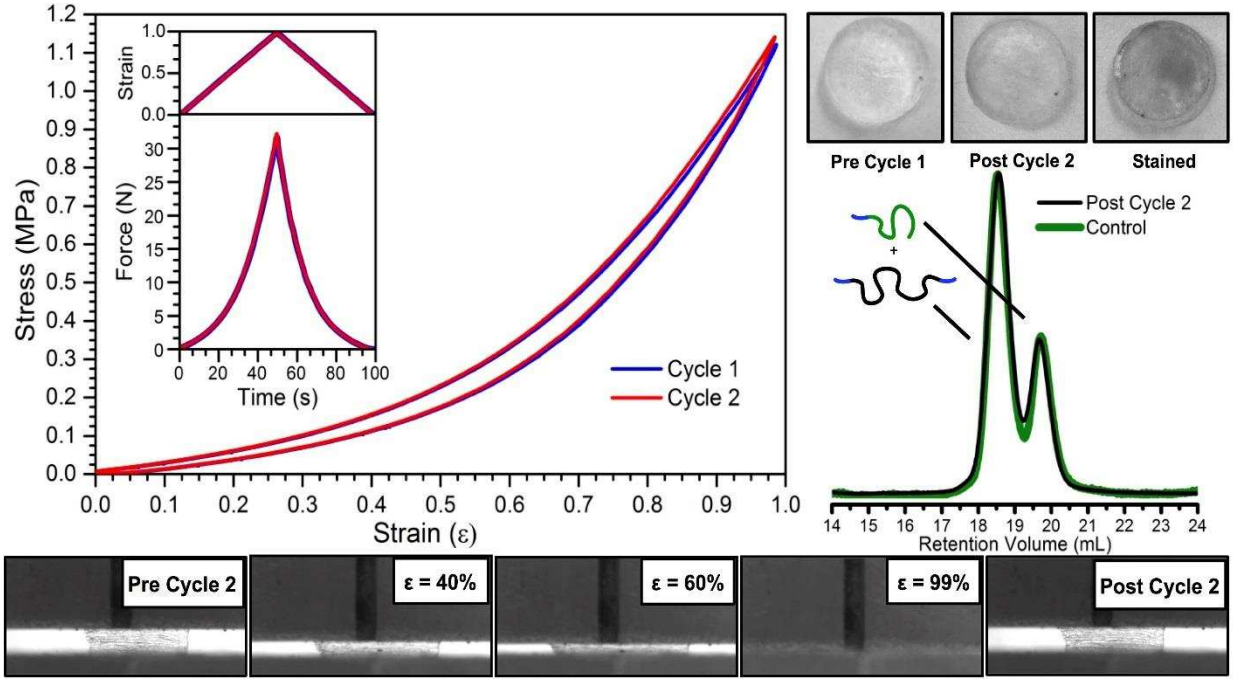

Figure 3.2: Extreme degrees of compressive strain can be accommodated without evidence of failure. An example overlay of the stress vs. strain data (left) from two successive compression cycles to 99% strain (strain rate = 2% s-1) for a submerged hydrogel (6 mm × 1.6 mm, 85 wt% PBS) containing 61 mol% SOS triblock copolymer is shown. Overlaid SEC data (right) depicts the molecular weight distributions of the constituent block copolymers comprising an untested hydrogel and one that experienced the two consecutive compression cycles to 99%. Photographs depict the hydrogel dimensions and visible surface before and after compression. Staining with India ink was used to highlight any microcrack formation. Video stills (bottom) depict the progression of the second compression cycle.

that each full cycle was performed over a 100 s interval. The near coincidence of the first and second stress-strain cycles confirms the ability of the network to accommodate extreme degrees of strain without plastic deformation. Video stills from the second cycle visually capture the full shape recovery, and photographs of the disc before and after the second cycle compression confirm the absence of any visible evidence of fracture, even after staining (India ink). Finally, **Figure 3.2** includes size exclusion chromatography (SEC) data confirming the molecular weight distributions of the SO diblock and SOS triblock copolymer comprising the hydrogel, both before and after the consecutive compression cycles to 99% strain, are identical. This SEC data, in combination with the coincident stress-strain data, supports the hypothesis that the prescribed

network architecture is able to efficiently absorb and distribute extreme degrees of compressive strain without succumbing to permanent chain pullout or mid-chain bond rupture. Additionally, the ability to disassemble the hydrogel post-testing, and evaluate the molecular weight distributions of the constituent block copolymers via SEC, underscores the thermoplastic nature of the system and emphasizes the ability of the network nanostructure to dictate mechanical properties in the absence of permanent chemical cross-links. The rapid recovery rate and minimal hysteresis intrinsic to the network under more moderate, physiological strains is captured in **Figure 3.3a.** The data depicted in the stress vs. strain plot correspond to an overlay of 120 consecutive compression cycles performed on a similarly submerged hydrogel disc (6 mm × 1.5 mm) fabricated using 61 mol% SOS triblock copolymer (85 wt% PBS buffer). Compression was carried out to 12% strain at a cycle frequency of 1 Hz, with every 11^{th} cycle overloaded to 50% strain. The inset captures the mean compressive modulus (K) between 2 and 10% strain (K ~ 0.54 MPa) for each of the 120 cycles, and that between 40 – 48% strain (K ~ 1.2 MPa) for the 10 overload cycles. In the 0.5 s interval in which the unloading leg of each cycle is performed, the network demonstrates a clear ability to fully recover its original configuration, and reproduce the stress-strain behavior identically in the next cycle, even after experiencing the overload to 50% strain. It is also notable that each cycle is accompanied by an extremely small degree of hysteresis between the loading and unloading legs, indicative that minimal energy is dissipated.[20] This result, in combination with cycle repeatability, suggests that the dissipation that does occur is primarily the result of transient phenomena like strain-induced convective flow, bond rotation, and/or chain reptation (in the diblock copolymer population) that have no permanent impact on the network architecture and subsequent mechanical performance.

Consistently, SEC data confirm the molecular weight distributions of the SO diblock and SOS triblock copolymer remain detectably unchanged following the 120-cycle compression test.

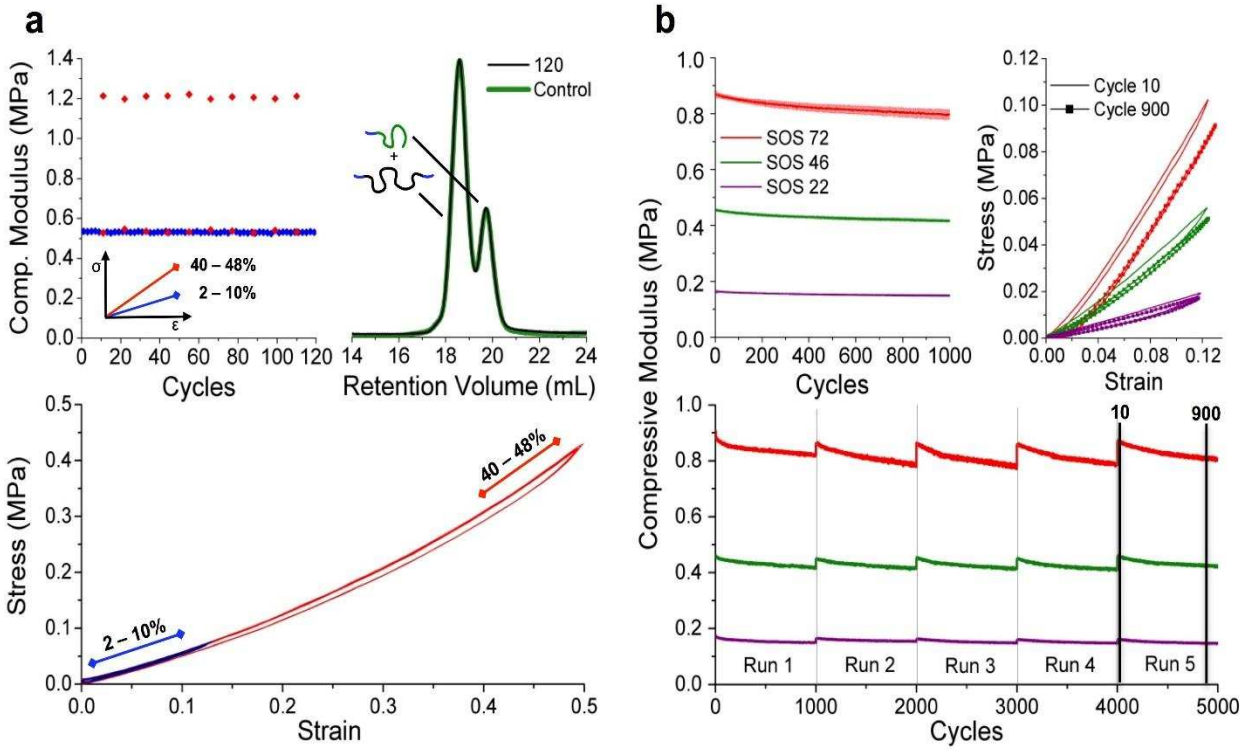

Figure 3.3: Compression at biomechanically relevant frequencies demonstrates rapid recovery and resistance to fatigue at multiple SOS triblock copolymer compositions. a. An overlay of 120 successive compression cycles performed on a submerged hydrogel (6 mm × 1.5 mm, 85 wt% PBS) containing 61 mol% SOS triblock copolymer demonstrates minimal hysteresis and rapid recovery. Compression cycles were carried out at 1 Hz and 12% peak strain, with an increase to 50% peak strain each 11th cycle. Mean moduli (upper left) span 0.5 to 1.2 MPa across the boundaries of the 50% strain range. SEC data indicate the molecular weight distributions for tested and untested hydrogels remained indistinguishable (upper right). b. Fatigue tests carried out on submerged hydrogels of different blend compositions (22, 46, and 72 mol% SOS triblock copolymer, 94, 90, and 86 wt% DI) highlight the facile control over modulus possible and persistence of fatigue resistance across compositions. Each hydrogel was subjected to five consecutive 1,000 cycle runs (1 Hz, 12% strain), separated by one-hour "rest" periods in which no load was applied. Relaxation appears to be the result of slight decreases in modulus and diminishing cycle hysteresis (upper right). The average of the five runs plotted with one standard deviation (upper left) confirms repeatability of the relaxation behavior run to run, and the absence of any permanent fatigue.

The sub-second recovery times exhibited by the 61 mol% SOS sample extend to other diblock and triblock copolymer compositions, as well. **Figure 3.3b** shows data compiled during

a fatigue experiment in which submerged hydrogels of 3 different blend compositions (22, 46 and 72 mol% SOS; 94, 90, and 86 wt% DI water; 6 mm × 2.4, 2.2, and 1.9 mm) were each subjected to five consecutive 1000 cycle runs (1 Hz, 12% strain), separated by 1 hour "rest" periods in which no load was applied. The blend composition allows for simple control over the material modulus without impacting the elastic recovery intrinsic to the network, at least on the 1 Hz time scale probed by the fatigue experiment. Notably, the range of moduli defined by these three samples falls within that of many soft fibrocartilage tissues.[41, 42, 43, 44, 45] The inset in the upper right of **Figure 3.3b** shows representative stress-strain data for cycles 10 and 900, extracted from the fifth run at each blend composition. These data capture the tendency for the modulus of the hydrogel to undergo a subtle decay with increasing cycle number. This decay appears to be at least partly associated with a diminishing degree of hysteresis, as well as a change in the actual stiffness of the material. However, full recovery of the original modulus (and hysteresis) is achieved following a "rest" period between runs, indicating the observed decay is not a consequence of plastic deformation or permanent fatigue, but of transient phenomena associated with cyclic loading and unloading. The ability to reproducibly return to its original state following rest is highlighted in the upper left panel of **Figure 3.3b**, in which the mean modulus and standard deviation over all five runs are plotted as a function of cycle number. We speculate that both the reduced hysteresis and relaxation in the modulus are the consequence of deformation-induced changes in fluid structure[46, 47] and flow (poroelastic flow), for which the 1 Hz cycle frequency is nominally too quick to permit full recovery in the strictest sense. The deficiencies produced are exceedingly small when considered cycle to cycle (thousandths to ten thousandths of a percent), but become conspicuous when compounded over many successive cycles. Indentation relaxation data collected on hydrogels fabricated across this

range of SOS compositions support this hypothesis of flow driven relaxation (**Supplementary Figure A2.3**). Notably, such relaxation at physiological frequencies such as the 1 Hz used here, followed by full recovery with rest, is prototypical behavior for musculoskeletal soft tissues and a natural consequence of the biphasic composition shared with these hydrogel systems.[42, 45, 48]

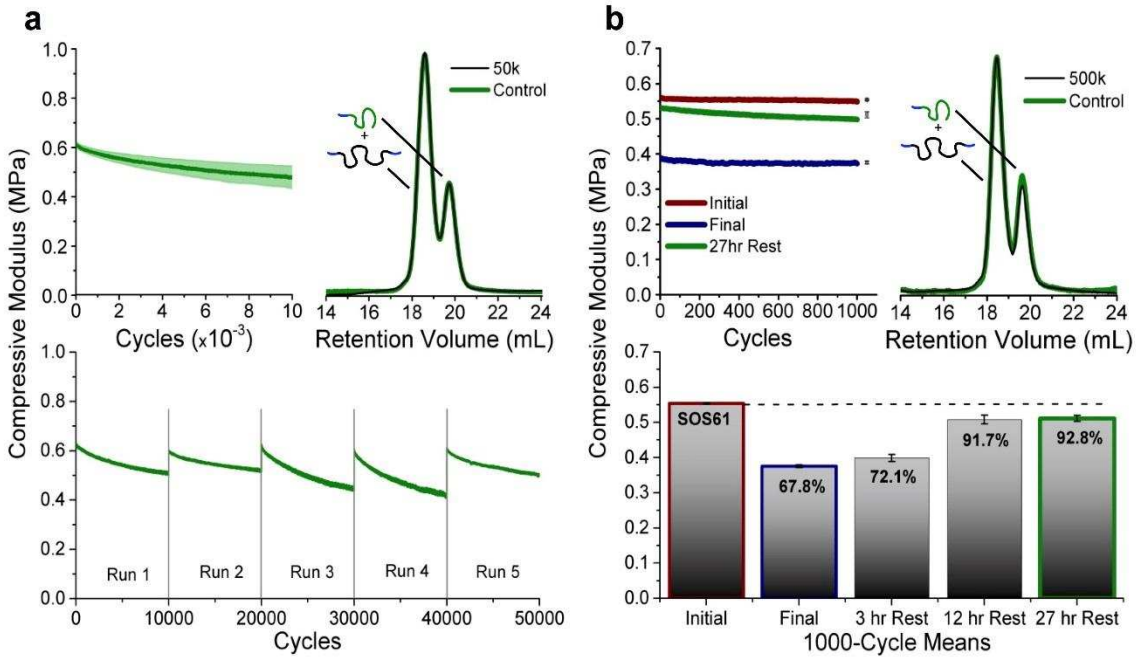

Figure 3.4: Extended fatigue tests emphasize network resilience. Tests were carried out on submerged hydrogels containing of 61 mol% SOS triblock copolymer (85 wt% PBS). a. Five consecutive 10,000 cycle runs (1 Hz, 12% strain), separated by overnight "rest" periods in which no load was applied. The average of the five runs plotted with one standard deviation (upper left) confirms repeatability of the relaxation behavior run to run, and suggests the absence of any permanent fatigue. SEC data indicate the molecular weight distributions of tested and untested hydrogels remained indistinguishable (upper right). b. Compiled data describe effects of one continuous run of 500,000 cycles. The bar chart depicts the mean moduli (and one standard deviation) over the initial and final 1,000 cycles, and over an additional 1,000 cycles applied following three, 12, and 27 hours of rest. Incomplete recovery to only 94.8% of the initial modulus (92.8% of the 1,000 cycle averages) after 27 hours rest indicates a small degree of permanent fatigue is likely present after 500,000 compression cycles. Modulus as a function of cycle number for the initial and final 1,000 cycles, and after 27 hours rest, give a sense of the relative magnitudes of relaxation present during various stages of the fatigue experiment (upper left). SEC data again indicate virtually identical molecular weight distributions in tested and untested hydrogels (upper right).

Recovery rates on the order of approximately one second open up considerable experimental flexibility with regard to examining the fatigue resistance limits of these unique hydrogel materials. Consequently, **Figure 3.4a** expands upon the fatigue experiments described by **Figure 3.3b** by increasing the number of consecutive cycles (1 Hz, 12% strain) performed in each of the five runs to 10,000. In this case, the submerged hydrogel (61 mol% SOS triblock copolymer, 85 wt% PBS, 6 mm × 1.8 mm) was allowed to rest in the unloaded state overnight following the conclusion of each 10,000-cycle run. Again, the hydrogel shows a clear relaxation of modulus, with a mean final relaxation of about 22.1% when the mean of the initial and final 1,000 cycles are compared. However, after each run, the hydrogel regained its original configuration, producing a pooled mean modulus over the first ten cycles of each run that is extremely narrowly distributed (0.614 ± 0.012 MPa). The SEC data comparing tested and untested samples also confirm that even after 50,000 cycles, there is no detectable difference in the molecular weight distribution in the loaded hydrogel. We believe this extraordinary demonstration of fatigue resistance in a synthetic hydrogel with this intrinsic stiffness (K ~ 0.6 MPa) and degree of swelling (80+ wt% PBS) is entirely unprecedented.

In a final test designed to challenge the limit of fatigue resistance in these hydrogels, we exposed a set of submerged hydrogel samples (61 mol% SOS triblock copolymer, 85 wt% PBS, 6 mm × 1.6 mm) to 500,000 consecutive compression cycles (1 Hz, 12% strain) without rest. In total, five samples were used to evaluate the potential fatigue in mechanical response. The first of these five samples was used to establish the baseline mechanical performance over the initial 1000 compression cycles. The remaining four samples were simultaneously and collectively subjected to 500,000 consecutive compression cycles over a nearly six-day period. Of these four, one was used to establish the average mechanical response over the final 1000 cycles, while

remaining three samples were used to evaluate the mechanical response following rest periods of three, 12, and 27 hours, respectively. As shown in **Figure 3.4b**, the immediate effect following the conclusion of the 500,000 compression cycles was a net 32.2% decay in mean modulus between the initial and final 1000 cycles of the run. Following 27 hours of rest, the cycled hydrogel produced an instantaneous modulus (measured over the first few cycles) equal to 94.8% of that measured for the pristine hydrogel, and a mean modulus over 1000 cycles equivalent to 92.3% of the initial 1000-cycle mean value. These results suggest that under the continuous loading experienced over the six-day period, some residual fatigue in mechanical properties does remain after rest. A comparison of the moduli as a function of cycle number (**Figure 3.4b, upper left**) suggests the cycled samples may also exhibit a faster rate of relaxation once exposed to such extensive cyclic loading. Despite these apparent indicators signifying the onset of fatigue, the SEC data before and after loading continues to show limited to no observable change in molecular weight distribution. This may indicate that physical mechanisms such as chain pullout, and not chemical bond rupture are largely responsible for the small, yet emergent decline in

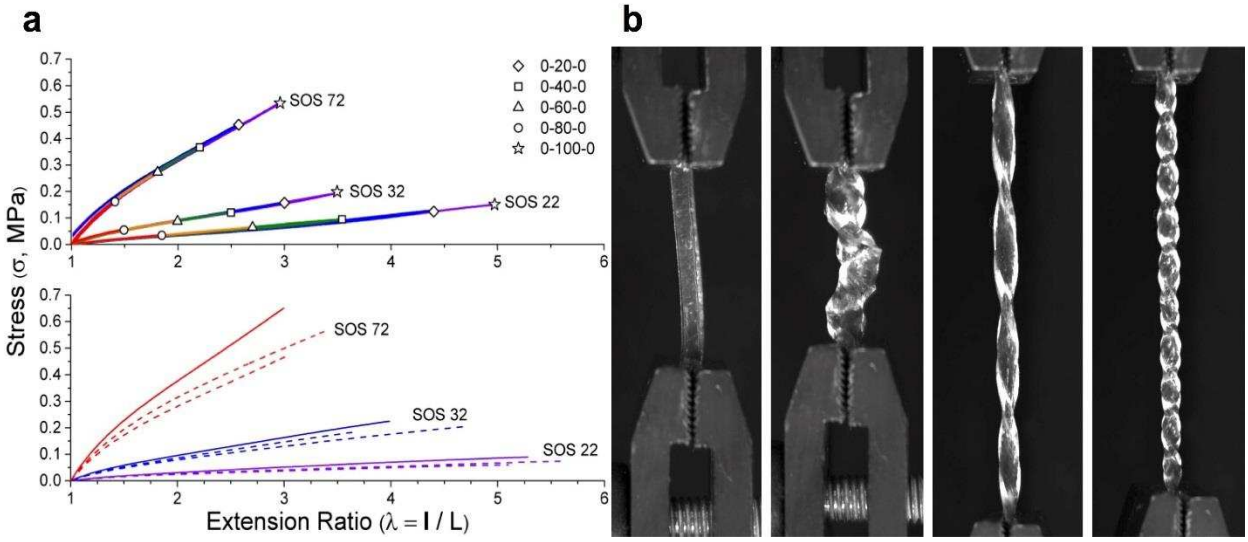

Figure 3.5: Uniaxial extension indicates comparable elasticity and an overall absence of hysteresis at moderate tensile strains, but susceptibility to brittle fracture at higher strains common in elastomeric materials. a. Uniaxial extension performed directly (lower) and progressively (upper) to failure (strain rate 2% s-1) for hydrogels fabricated from three blend compositions (22, 32, and 72 mol% SOS triblock copolymer; 94, 91 and 86 wt% DI). Progressive cycling over increments defined by 20% of the mean strain at failure for each composition confirms the absence of hysteresis and any plastic deformation prior to failure. b. At moderate strains, hydrogels are able to handle coupled extension and torsion without failure (hydrogel containing 61 mol% SOS triblock copolymer (85 wt% PBS) is shown). From left to right: $\lambda = 1$, $\phi rot = 0$; $\lambda = 0.9$, $\phi rot = 4\pi$; $\lambda = 2.4$, $\phi rot = 4\pi$; $\lambda = 2.25$, $\phi rot = 10\pi$.

mechanical performance. While the extent to which this decline will progress with continued cycling is currently unknown, post-assembly crosslinking of the hydrophobic core domains[49, 50] may offer an opportunity to push the suppression of fatigue to even more extreme cycle numbers. The final study examines the behavior of these hydrogels under uniaxial extension. As shown in **Figure 3.5a**, the hydrogels of various diblock and triblock copolymer blend compositions (22, 32, 72 mol% SOS triblock copolymer; 94, 91, 86 wt% DI) can reach moderate (several hundred percent), but by no means extraordinary degrees of extension prior to failure. Progressive loading demonstrates the fundamental absence of hysteresis throughout, indicating, as with compression, an ability to elastically absorb strain energy without dissipation. At moderate extensions, these hydrogels also demonstrate excellent flexibility, and an ability to handle more dimensionally

complex stress fields such as those created during coupled extension and torsion as shown in **Figure 3.5b**. Not unexpectedly, failure under tensile loading in these hydrogels is strongly correlated to fracture initiated at local defects (such as bubbles left during melt processing), where the inability to efficiently dissipate stress amplification results in crack formation, rapid propagation and eventual catastrophic failure. So while the clear absence of any plastic deformation prior to failure during progressive tensile cycling (**Figure 3.5a**) emphasizes the favorable fatigue resistance of these hydrogels, the abrupt failure at higher extensions emphasizes a latent susceptibility to brittle fracture in the presence of network defects. The latter, of course, is a phenomenon not uncommon to many elastomeric polymers and biological tissues alike, observable for example, in the sudden rupture of nitrile gloves, the bursting of balloons with the prick of a pin, or the tearing of the menisci during injury to the knee. Importantly, strains required of soft musculoskeletal tissues are not excessive, and rarely reach values higher 30% under ordinary biomechanical loading.[23, 24, 25, 26, 27, 28, 29] Thus, an excessively high extension ratio is not a particularly relevant target for biomechanical applications of a hydrogel surrogate. However, an ability to prevent fracture in the event of microcrack formation *is*, and that requires that a hydrogel can efficiently dissipate strain energy in the amplification zone near a nucleating crack tip.

3.3 CONCLUSIONS

This trade-off between fatigue and fracture resistance highlights one of the major challenges facing hydrogel engineering for musculoskeletal soft tissue replacement materials. An ideal mechanical surrogate would possess the exceptional elasticity, fatigue resistance, and rapid recovery at low to moderate strains, but be able to autonomously dissipate excess strain energy above a critical threshold, such that fracture could likewise be efficiently suppressed. We believe

that the unprecedented level of intrinsic fatigue resistance and rapid recovery demonstrated by these thermoplastic hydrogel systems establishes a new benchmark in hydrogel design, and provides a solid foundation from which future materials, such as those with threshold triggered dissipative capabilities, might one day be developed. As recently suggested by Zhao,[20] the effective integration of dissipative elements into elastic systems will likely require the use of multi-mechanism, multi-scale strategies. We expect this will prove to be particularly true for hydrogels designed as musculoskeletal soft tissue replacements, for which the dissipative mechanisms integrated to fight fracture must come without compromise to the elasticity, recovery dynamics, and fatigue resistance of the system.

3.4 EXPERIMENTAL

Materials and Synthesis

Materials and Characterization. Styrene (99%, 4-tert-butylcatechol inhibitor, Aldrich) and ethylene oxide (99.5+%, compressed gas, Aldrich) monomer were each purified by successive vacuum distillations (10–20 mTorr) from dried di-n-butylmagnesium (1.0 M solution in heptane, Aldrich) before use. Both purified styrene and ethylene oxide monomer were stored in glass burettes in the dark, at room temperature (styrene) and 3 °C (ethylene oxide), respectively, before use (typically less than 24 h). Argon degassed cyclohexane (CHX) was purified by passing the solvent over activated alumina followed by Q-5-like supported copper catalyst (Glass Contour, proprietary). Argon degassed tetrahydrofuran (THF) was purified by passing the solvent over activated alumina. High-purity argon (99.998%, Airgas) was passed through additional oxygen and moisture traps prior to use. Glassware and polymerization reactors were flamed under vacuum and backfilled with argon multiple times. All other reagents were used as received. ^{1}H NMR spectra were collected at room temperature in $CDCl_3$ on a Varian Inova 400 MHz Spectrometer (n = 32, delay = 30 s). Size exclusion chromatography (SEC) was performed on a Viscotek GPC-Max chromatography system fitted with three 7.5 x 340 mm Polypore™ (Polymer Laboratories) columns in series, an Alltech external column oven, and a Viscotek differential refractive index (RI) detector. Measurements were performed using a DMF (55 °C) mobile phase (1 mL/min) with PS standards (Polymer Laboratories). Final SO/SOS compositions were confirmed via relative peak integrations in the SEC chromatograms of these blends.

ω-Hydroxy-polystyrene (S-OH). Purified styrene monomer (120 g, 1.14 mol, 20°C) was added to a stirring solution of sec-butyl lithium (10.23 mL, 1.3 M in cyclohexane, Aldrich) and dry, air-

free cyclohexane (1 L, 20 °C) in a 2 L reaction vessel. The solution was then raised to 40°C and stirred continuously for 8 hours. At a reduced pressure of 1 psig, purified ethylene oxide (6.6 g, 0.15 mol, 0 °C, liquid) was added to the reaction vessel. The reaction was held at 40°C for an additional 24 hours, after which all excess ethylene oxide was removed from the reactor under a constant argon flow. The reaction was terminated by acidic methanol (50 mL). The polymer was precipitated in methanol (5 L total), producing a fluffy white solid, and dried under vacuum at room temperature over a 48 h period (yield 116 g, 97%, M_n= 8370 g/mol, PDI = 1.03).

ω-Hydroxy-polystyrene-b-poly(ethylene oxide) (SO). S-OH (7 g, 0.836 mmol) was added to a 2 L reaction vessel containing a glass coated magnetic stir bar. The reactor was evacuated and backfilled with purified argon before adding 1 L of dry, air-free tetrahydrofuran (THF). Concentrated potassium naphthalenide in THF was added to the polymer solution via cannula until a light green color persisted for 30 minutes. The temperature of the reaction mixture was raised to 40 °C and purified ethylene oxide monomer (78.7 g, 1.78 mol, 0 °C) was added under argon (1 psi) to the stirring solution for 48 hours. The reaction was terminated by methanol (50 mL) and the polymer was precipitated in 4 L of pentane, producing a fluffy white solid. The polymer was dried under vacuum at room temperature for 48 hours. (M_n= 107,000 g/mol, PDI = 1.07, f_{PS} = 0.085).

Polystyrene-b-poly(ethylene oxide)-b-polystyrene (SOS). SO (29 g, 0.271 mmol) was placed into a 2 L round bottom reactor vessel that was evacuated and backfilled with purified argon. The SO was allowed to dry under vacuum overnight. The SO was then dissolved in dry THF. A concentrated potassium naphthalenide solution in dry THF was titrated into the reactor until the

solution maintained a green color for 30 minutes. α,α′-dibromo-p-xylene (35.8 mg, 0.136 mmol, 0.5 eq) in THF (1.5 mL) was then injected into the reactor over a 12 hour period at a rate of 0.125 mL hr^{-1} using a syringe pump and a 2.5 mL glass syringe. Coupled polymer was recovered through precipitation in 5 L of pentane followed by vacuum filtration. The precipitated polymer was dried overnight under vacuum to produce a fluffy white solid as a blend of coupled (SOS) and uncoupled (SO) block copolymer (52 mol% SOS).

SO/SOS Fractionation. To achieve higher SOS concentrations than the 52 mol% produced during the SO coupling reaction, fractionation was performed. Dry SO/SOS polymer (4 g) was dissolved in chloroform (400 ml) and heated to 45 °C. N-hexane (920 ml) was added slowly, keeping the temperature above 40°C. The SOS precipitated and the solution turned cloudy. Upon cooling to room temperature, the solution turned transparent. The solution contained the majority of the SO while the SOS existed as a precipitate. The SOS precipitate was recovered and allowed to dry under vacuum overnight, while the SO in solution was recovered through rotary evaporation. Even higher SOS concentrations were achieved through successive fractionations of precipitated SOS.

Hydrogel Fabrication and Swelling Analysis

Preparation of SO/SOS hydrogel samples. Dry polymer for the different SOS blend compositions (22 - 87 mol%) were compacted into a circular steel washers (8 mm diameter × 0.73 mm deep) or rectangular steel cutouts (assorted dimensions × 1 mm deep) and sandwiched between two sheets of Teflon coated Kapton™. These assemblies were then placed into a Carver Press and heated to 150°C under an applied pressure of ~500 psi for 5 minutes. In some cases

multiple compressions were used to remove visible bubbles. Samples were allowed to cool to room temperature before swelling. Samples taken from circular washer molds were used for indentation relaxation testing, swelling analysis, and tensile testing. For tensile testing, test strips (3 mm × 8 mm × 1.25 - 1.5 mm deep) were cut from the swollen disks. Samples taken from the rectangular cutouts were used for fatigue and overloading compressions tests. In all cases, 8 mm or 6 mm diameter testing plugs were punched from swollen rectangular hydrogels using a biopsy punch.

Swelling analysis of SO/SOS hydrogels. Dry polymer disks were all massed prior to swelling and were then allowed to swell in DI water or phosphate buffered saline (1x PBS, composition: 11.9 mM phosphates, 137 mM sodium chloride and 2.7 mM potassium chloride in DI water, diluted from 10x PBS, Fisher Scientific) for 24 hours allowing the hydrogels to reach a swelling equilibrium. Once swollen, the hydrogels were removed from the solution and gently patted dry to remove any excess water or PBS using a Kim wipe. Swelling ratio of the hydrogels was determined gravimetrically (g solution/g polymer) at 3 different temperatures (10, 22, and 37 °C). The solutions for swelling were brought to the appropriate temperature using a temperature controlled water bath or oil bath for cooling and heating respectively. Swelling ratio was calculated by the difference of the swollen hydrogel and dry polymer disk divided by the mass of the dry polymer disk.

Hydrogel Mechanical Testing

Overloading and ramp to failure of SO/SOS hydrogels. Overloading and ramp-to-failure experiments were performed on disk shaped hydrogel samples containing 61 mol% SOS triblock copolymer (SOS 61) swollen in PBS (8 mm diameter x 1.5 mm). The overloading sample was

mounted (Loctite Super Glue Ultragel Control, Henkel Corporation, Rocky Hill, CT) on one side to a polished aluminum platen, submerged in a PBS bath, and compressed using a secondary aluminum plate. A preload of 20 g was then applied to ensure contact with the sample. The hydrogel was compressed to 12% strain at 1 Hz for 10 cycles followed by 1 cycle of 50% strain at 1 Hz. This 11-cycle regiment was repeated 10 times using a Bionic Model 370.02 servo hydraulic testing system (MTS Corp, Eden Prairie, MN) configured with a 908 g load cell (Futek LSB200, Irvine, California).

The ramp-to-failure experiment was performed on a hydrogel disk containing 61 mol% SOS triblock copolymer (SOS 61) swollen in PBS (6 mm diameter x 1.6 mm). The swollen sample was placed unfixed between the two platens, preloaded to 200 mN, and submerged in a PBS bath. Compression was ramped at 2% s^{-1} up to 99% strain, and unloaded at the same rate using an MTS Bionic Model 370.02 (MTS Corp, Eden Prairie, MN) configured with a 908 g load cell (Futek LSB200, Irvine, California). The sample was then inspected for defects and rerun under the same conditions a second time, after which it was stained with India ink for better visualization of possible microcrack formation.

Fatigue testing of SO/SOS hydrogels. Fatigue tests were initially run on hydrogels fabricated using three concentrations of SOS triblock copolymer (22, 46, and 72 mol% SOS). The three disk shaped samples (SOS 22, SOS 46, and SOS 72) were swollen in DI water (8 mm diameter x 2.4, 2.2, and 1.9 mm, respectively), mounted (Loctite Super Glue Ultragel Control, Henkel Corporation, Rocky Hill, CT) on one side to a polished aluminum platen, submerged in a DI bath, and compressed using a secondary aluminum plate. The sample was preloaded to 20 g and then compressed to 12% strain at a frequency of 1 Hz for 1,000 cycles using an MTS Bionic

Model 370.02 (MTS Corp, Eden Prairie, MN) configured with a 908 g load cell (Futek LSB200, Irvine, California). The sample was then unloaded and left submerged in DI for one hour before being retested under the same conditions for four additional sets of 1,000 cycles.

An extended fatigue test was subsequently run on a disk shaped hydrogel sample containing 61 mol% SOS triblock copolymer. The SOS 61 sample was swollen in PBS (6 mm diameter x 1.8 mm), mounted (Loctite Super Glue Ultragel Control, Henkel Corporation, Rocky Hill, CT) on one side to a polished aluminum platen, submerged in a PBS bath, and compressed with a secondary aluminum plate. The sample was preloaded to 20 g and then compressed to 12% strain at a frequency of 1 Hz for 10,000 cycles using an MTS Bionic Model 370.02 (MTS Corp, Eden Prairie, MN) configured with a 908 g load cell (Futek LSB200, Irvine, California). The hydrogel was then unloaded and left submerged in PBS for the balance of 24 hours before being retested under the same conditions for four additional sets of 10,000 cycles.

Lastly, five 6 mm diameter disk shaped plugs of SOS 61 swollen in PBS with an average 1.6 mm thickness were used to assess the mechanical integrity of the hydrogel over 500,000 cycles. Due to the extended duration of the experiment, the applied loading was performed in a custom built material testing system designed to allow simultaneous axial displacements of up to six samples[1] while the mechanical measurements were performed using an MTS Bionic Model 370.02 (MTS Corp, Eden Prairie, MN) configured with a 908 g load cell (Futek LSB200, Irvine, California). The first of the five samples were used to establish the baseline mechanical performance over the initial 1000 cycles. This sample was mounted (Loctite Super Glue Ultragel Control, Henkel Corporation, Rocky Hill, CT) on one side to a polished aluminum platen, submerged in a PBS bath, and compressed with a secondary aluminum plate. The sample was preloaded to 20 g and compressed to 12% strain at a frequency of 1 Hz for 1,000 cycles. The remaining four samples

were simultaneously and collectively subjected to 500,000 consecutive compression cycles over a nearly six-day period. Samples were not fixed in the home built testing system. At the conclusion of the 499,000 cycles, one of the four samples was immediately removed and transferred to the MTS to establish the baseline mechanical performance over the final 1000 cycles. The remaining three samples completed their final 1000 cycles in the home built system, after which they were evaluated on the MTS using an additional 1000 cycle test following rest periods of three, 12, and 27 hours, respectively. Samples tested on the MTS were all mounted on one side during testing.

Analysis. MATLAB (Mathworks, Natick,MA) was used to analyze the resulting data. Maximum and minimum compressive force and displacement for each cycle were determined and a linear fit between strains nearest 2-10% was used to ascertain the compressive mean modulus. For the overloading experiment, the same method was used to fit a linear function across the 2-10% strain range of all cycles and 40-48% strain range for the overloading cycles. For the 500,000-cycle experiment, the mean modulus of each cycle recorded was determined similarly, and then averaged across the 1000 cycle segments recorded.

Tensile testing of SO/SOS hydrogels. Tensile testing was performed on an ARES-rheometer (TA Instruments, DE) at room temperature. Testing strips were placed into torsion rectangular grips (TA Instruments, DE) with a layer of sand paper between the grip and the hydrogel to reduce slippage. The hydrogels were clamped and pulled until a force of 5 g was reached to ensure the hydrogel was taut. The hydrogel was then extended to a mid-substance failure at a strain rate of 2% s^{-1}. Once the mean strain at break (progressively over cycles of

increasing strain from 20%λ_f) was determined new samples of the same size were strained progressively over cycles of increasing strain from 20%λ_f strain to λ_f (i.e. 0-20-0-40-0-60…0-100 % λ_f,) at a strain rate of 2% s^{-1}.

Indentation Relaxation Testing of SO/SOS hydrogels. Specimens were kept hydrated in DI water or PBS before and during indentation relaxation tests, which were run on an MTS Bionic Model 370.02 servo hydraulic test system (MTS Corp, Eden Prairie, MN). The water or PBS bath containing the sample was attached to a multi degree of freedom camera mount, and an x-y plate fixture allowing for the indentation surface to be oriented normal to the indenter and centered on the specimen respectively. A spherical tip with a diameter of 1.59 mm was used as an indenter, and loads were recorded using a 908 g load cell (Futek LSB200, Irvine, California). Due to the time dependent nature of the compressive properties of hydrated materials both the equilibrium and instantaneous moduli were computed. All samples were preloaded to 2 g, and preliminary tests determined a relaxation time of 300 seconds resulted in near-equilibrium conditions. Specimens were indented to a strain of 12% s^{-1}. A Hertzian contact model was applied and used to determine both the instantaneous and equilibrium moduli.

$$E_1 = \frac{(1 - {v_1}^2)}{\frac{4d^{3/2}\,R^{1/2}}{3F} - \frac{(1 - {v_2}^2)}{E_2}}$$

The contact equation assumes contact between an elastic half space and a sphere where F is the force, R is the radius of the indenter, d is the indentation depth, E_1 and υ_1 are the elastic modulus and Poisson's ratio of the hydrogel respectively, and E_2 and υ_2 are the elastic modulus and Poisson's ratio of the indenter. The indenter tip had an elastic modulus and Poisson's ratio of

210 GPa and 0.3, respectively. The elastic modulus of the hydrogel was calculated assuming the Poisson's ratio of the hydrogel was approximately 0.5 at small strains.

Photography. Images were taken using a Point Grey Flea3 camera (model FW-14S3M-C) equipped with a Fujinon 1:1.4/25mm lens (model HF25HA-1B). Initial images were saved in the jpeg format at a resolution of 1280x960 pixels and a bit depth of 8. The lens allows for a focal length of 25mm and depending on the situation objects were imaged at varying distances. Images were taken under regular laboratory fluorescent lighting with the aid of additional lamps in the case of the more extreme compression images (providing more side light when the sample was placed under shadow due to the fixturing). Various materials including black felt and both white and colored paper were used for uniform and contrasting backgrounds, which were needed to see the nearly clear hydrogel. Once acquired, images were imported into ImageJ (US National Institutes of Health, Bethesda, MD) where they were cropped to the desired size for figures.

REFERENCES

1. Gong JP, Katsuyama Y, Kurokawa T, Osada Y. Double-network hydrogels with extremely high mechanical strength. *Adv Mater* 2003, **15**(14)**:** 1155-+.

2. Kamata H, Akagi Y, Kayasuga-Kariya Y, Chung UI, Sakai T. "Nonswellable" hydrogel without mechanical hysteresis. *Science* 2014, **343**(6173)**:** 873-875.

3. Li WB, An HY, Tan Y, Lu CG, Liu C, Li PC*, et al.* Hydrophobically associated hydrogels based on acrylamide and anionic surface active monomer with high mechanical strength. *Soft Matter* 2012, **8**(18)**:** 5078-5086.

4. Henderson KJ, Zhou TC, Otim KJ, Shull KR. Ionically Cross-Linked Triblock Copolymer Hydrogels with High Strength. *Macromolecules* 2010, **43**(14)**:** 6193-6201.

5. Sun JY, Zhao X, Illeperuma WR, Chaudhuri O, Oh KH, Mooney DJ*, et al.* Highly stretchable and tough hydrogels. *Nature* 2012, **489**(7414)**:** 133-136.

6. Sun TL, Kurokawa T, Kuroda S, Bin Ihsan A, Akasaki T, Sato K*, et al.* Physical hydrogels composed of polyampholytes demonstrate high toughness and viscoelasticity. *Nat Mater* 2013, **12**(10)**:** 932-937.

7. Brown AEX, Litvinov RI, Discher DE, Purohit PK, Weisel JW. Multiscale Mechanics of Fibrin Polymer: Gel Stretching with Protein Unfolding and Loss of Water. *Science* 2009, **325**(5941)**:** 741-744.

8. Bin Imran A, Esaki K, Gotoh H, Seki T, Ito K, Sakai Y*, et al.* Extremely stretchable thermosensitive hydrogels by introducing slide-ring polyrotaxane cross-linkers and ionic groups into the polymer network. *Nature communications* 2014, **5:** 5124.

9. Ito K. Novel cross-linking concept of polymer network: Synthesis, structure, and properties of slide-ring gels with freely movable junctions. *Polym J* 2007, **39**(6)**:** 489-499.

10. Okumura Y, Ito K. The polyrotaxane gel: A topological gel by figure-of-eight cross-links. *Adv Mater* 2001, **13**(7)**:** 485-+.

11. Sakai T, Akagi Y, Matsunaga T, Kurakazu M, Chung U, Shibayama M. Highly Elastic and Deformable Hydrogel Formed from Tetra-arm Polymers. *Macromol Rapid Comm* 2010, **31**(22)**:** 1954-1959.

12. Sakai T, Matsunaga T, Yamamoto Y, Ito C, Yoshida R, Suzuki S*, et al.* Design and fabrication of a high-strength hydrogel with ideally homogeneous network structure from tetrahedron-like macromonomers. *Macromolecules* 2008, **41**(14)**:** 5379-5384.

13. Andrews S, Shrive N, Ronsky J. The shocking truth about meniscus. *Journal of Biomechanics* 2011, **44**(16)**:** 2737-2740.

14. Cortes DH, Elliott DM. The Intervertebral Disc: Overview of Disc Mechanics. In: Shapiro IM, Risbud MV (eds). *The Intervertebral Disc: Molecular and Structural Studies of the Disc in Health and Disease*. Springer Vienna: Vienna, 2014, pp 17-31.

15. Wagenseil JE, Mecham RP. Vascular Extracellular Matrix and Arterial Mechanics. *Physiological reviews* 2009, **89**(3)**:** 957-989.

16. El Fray M, Prowans P, Puskas JE, Altstadt V. Biocompatibility and fatigue properties of polystyrene-polyisobutylene-polystyrene, an emerging thermoplastic elastomeric biomaterial. *Biomacromolecules* 2006, **7**(3)**:** 844-850.

17. Miller AT, Safranski DL, Smith KE, Guldberg RE, Gall K. Compressive cyclic ratcheting and fatigue of synthetic, soft biomedical polymers in solution. *J Mech Behav Biomed Mater* 2016, **54:** 268-282.

18. Puskas JE, Dos Santos LM, Fischer F, Gotz C, El Fray M, Altstadt V*, et al.* Fatigue testing of implantable specimens: Effect of sample size and branching on the dynamic fatigue properties of polyisobutylene-based biomaterials. *Polymer* 2009, **50**(2)**:** 591-597.

19. Puskas JE, El Fray M, Tomkins M, Dos Santos LM, Fischer F, Altstadt V. Dynamic stress relaxation of thermoplastic elastomeric biomaterials. *Polymer* 2009, **50**(1)**:** 245-249.

20. Zhao XH. Multi-scale multi-mechanism design of tough hydrogels: building dissipation into stretchy networks. *Soft Matter* 2014, **10**(5)**:** 672-687.

21. Long R, Hui CY. Fracture toughness of hydrogels: measurement and interpretation. *Soft Matter* 2016, **12**(39)**:** 8069-8086.

22. Naficy S, Brown HR, Razal JM, Spinks GM, Whitten PG. Progress Toward Robust Polymer Hydrogels. *Aust J Chem* 2011, **64**(8)**:** 1007-1025.

23. Freutel M, Seitz AM, Galbusera F, Bornstedt A, Rasche V, Tate MLK*, et al.* Medial Meniscal Displacement and Strain in Three Dimensions Under Compressive Loads: MR Assessment. *J Magn Reson Imaging* 2014, **40**(5)**:** 1181-1188.

24. Jones RS, Keene GCR, Learmonth DJA, Bickerstaff D, Nawana NS, Costi JJ*, et al.* Direct measurement of hoop strains in the intact and torn human medial meniscus. *Clin Biomech* 1996, **11**(5)**:** 295-300.

25. Tissakht M, Ahmed AM. Tensile Stress-Strain Characteristics of the Human Meniscal Material. *Journal of Biomechanics* 1995, **28**(4)**:** 411-422.

26. Costi JJ, Stokes IA, Gardner-Morse M, Laible JP, Scoffone HM, Iatridis JC. Direct measurement of intervertebral disc maximum shear strain in six degrees of freedom: Motions that place disc tissue at risk of injury. *Journal of Biomechanics* 2007, **40**(11)**:** 2457-2466.

27. Stokes IAF. Surface Strain on Human Intervertebral Disks. *J Orthopaed Res* 1987, **5**(3)**:** 348-355.

28. Armstrong CG, Bahrani AS, Gardner DL. Invitro Measurement of Articular-Cartilage Deformations in the Intact Human Hip-Joint under Load. *J Bone Joint Surg Am* 1979, **61**(5)**:** 744-755.

29. Guterl CC, Gardner TR, Rajan V, Ahmad CS, Hung CT, Ateshian GA. Two-dimensional strain fields on the cross-section of the human patellofemoral joint under physiological loading. *Journal of Biomechanics* 2009, **42**(9)**:** 1275-1281.

30. Bates FS. Polymer-Polymer Phase-Behavior. *Science* 1991, **251**(4996)**:** 898-905.

31. Bates FS, Fredrickson GH. Block copolymers - Designer soft materials. *Phys Today* 1999, **52**(2)**:** 32-38.

32. Guo C, Bailey TS. Highly Distensible Nanostructured Elastic Hydrogels from AB Diblock and ABA Triblock Copolymer Melt Blends. *Soft Matter* 2010, **6**(19)**:** 4807-4818.

33. Guo C, Bailey TS. Tailoring Mechanical Response through Coronal Layer Overlap in Tethered Micelle Hydrogel Networks. *Soft Matter* 2015, **11**(37)**:** 7345-7355.

34. Guo C, Lewis JT, Scalfani VF, Schwartz MM, Bailey TS. Dangling-End Double Networks: Tapping Hidden Toughness in Highly Swollen Thermoplastic Elastomer Hydrogels. *Chemistry of Materials* 2016, **28**(6)**:** 1678–1690.

35. Wijayasekara DB, Cowan MG, Lewis JT, Gin DL, Noble RD, Bailey TS. Elastic free-standing RTIL composite membranes for CO2/N2 separation based on sphere-forming triblock/diblock copolymer blends. *Journal of Membrane Science* 2016, **511:** 170-179.

36. Fox TG, Flory PJ. The Glass Temperature and Related Properties of Polystyrene - Influence of Molecular Weight. *J Polym Sci* 1954, **14**(75)**:** 315-319.

37. Fetters LJ, Lohse DJ, Richter D, Witten TA, Zirkel A. Connection between Polymer Molecular Weight, Density, Chain Dimensions, and Melt Viscoelastic Properties. *Macromolecules* 1994, **27**(17)**:** 4639-4647.

38. Bollet AJ, Nance JL. Biochemical Findings in Normal and Osteoarthritic Articular Cartilage .2. Chondroitin Sulfate Concentration and Chain Length Water and Ash Content. *J Clin Invest* 1966, **45**(7)**:** 1170-1177.

39. Marinelli NL, Haughton VM, Munoz A, Anderson PA. T(2) Relaxation Times of Intervertebral Disc Tissue Correlated With Water Content and Proteoglycan Content. *Spine* 2009, **34**(5)**:** 520-524.

40. Mow VC, Arnoczky SP, Jackson DW (eds). *Knee Meniscus: Basic and Clinical Foundations*. Raven Press: New York, 1992.

41. Athanasiou KA, Rosenwasser MP, Buckwalter JA, Malinin TI, Mow VC. Interspecies Comparisons of Insitu Intrinsic Mechanical-Properties of Distal Femoral Cartilage. *J Orthopaed Res* 1991, **9**(3)**:** 330-340.

42. Chia HN, Hull ML. Compressive moduli of the human medial meniscus in the axial and radial directions at equilibrium and at a physiological strain rate. *J Orthop Res* 2008, **26**(7)**:** 951-956.

43. Joshi MD, Suh JK, Marui T, Woo SLY. Interspecies Variation of Compressive Biomechanical Properties of the Meniscus. *J Biomed Mater Res* 1995, **29**(7)**:** 823-828.

44. Mow VC, Gu WY, Chen FH. Chapter 5: Structure and Function of Articular Cartilage and Meniscus. In: Mow VC, Huiskes R (eds). *Basic Orthopaedic Biomechanics & Mechano-biology*, 3rd edn. Lippincott Williams & Wilkins, 2005, pp 181-258.

45. Treppo S, Koepp H, Quan EC, Cole AA, Kuettner KE, Grodzinsky AJ. Comparison of biomechanical and biochemical properties of cartilage from human knee and ankle pairs. *J Orthopaed Res* 2000, **18**(5)**:** 739-748.

46. Dormidontova EE. Role of Competitive PEO−Water and Water−Water Hydrogen Bonding in Aqueous Solution PEO Behavior. *Macromolecules* 2002, **35**(3)**:** 987-1001.

47. Lee J, Lee H, Andrade J. Blood compatibility of polyethylene oxide surfaces. *Progress in Polymer Science* 1995, **20**(6)**:** 1043-1079.

48. Fischenich KM, Lewis J, Kindsfater KA, Bailey TS, Haut Donahue TL. Effects of Degeneration on the Compressive and Tensile Properties of Human Meniscus. *Journal of Biomechanics* 2015, **48**(8)**:** 1407-1411.

49. Scalfani VF, Bailey TS. Thermally Stable Photocuring Chemistry for Selective Morphological Trapping in Block Copolymer Melt Systems. *Chemistry of Materials* 2010, **22**(21)**:** 5992-6000.

50. Scalfani VF, Bailey TS. Access to Nanostructured Hydrogel Networks through Photocured Body-Centered Cubic Block Copolymer Melts. *Macromolecules* 2011, **44**(16)**:** 6557-6567.

CHAPTER 4

IMPROVING CYTOCOMPATABILITY AND HYDROPHILICITY OF THERMOPLASTIC ELASTOMER HYDROGELS VIA A HYALURONAN SURFACE TREATMENT

4.1 INTRODUCTION [4]

Hyaluronan, an anionic glycosaminoglycan, is a major constituent of the extracellular matrix[1] and is widely distributed throughout the body[2] including skin,[1] synovial fluid [2] and the vitreous humor of the eye.[3] Hyaluronan's highly hydrophilic nature is thought to help maintain a fluid layer that, along with lubricin, supports reduced friction in joint articulation.[4] Hyaluronan is also believed to play a critical role in inflammation[5] and the wound healing cascade.[6] Because of its role in the reduction of friction as well as its highly cytocompatible nature, hyaluronan has been widely used in multiple applications including coatings for contact lenses[7, 8] and orthopedic joint replacements,[9, 10, 11] tissue engineering scaffolds,[12] and as a filler in the cosmetic industry.[13] Hyaluronan is broken down in the body very rapidly (requiring high turnover) by a class of enzymes known as hyaluronidases, which makes it difficult to use hyaluronan in long term applications without modification.[1] In order to restrict the enzyme's ability to break down hyaluronan in vivo as well as promote the formation of an infinite network, crosslinking

[4] This chapter was written and prepared by Jackson Lewis. Jackson Lewis, Travis S. Bailey, Susan P. James, Ketul C. Popat and Tammy Haut-Donahue contributed significantly to the development and design of the experiments. Jackson Lewis was involved in all data collection and analysis with key assistance from Rachael Simon Walker, and Hieu Bui. Jackson Lewis performed all syntheses, processing and hyaluronan surface treatment of TPE hydrogels in the study. Rachael Simon Walker assisted with cytotoxicity testing and the accompanying numerical and statistical analysis of the assay data collected. Hieu Bui assisted with the captive bubble testing and the accompanying numerical and statistical analysis of the contact angle data collected.

strategies have been implemented. Crosslinking produces covalent attachments between hyaluronan repeat units that are not as susceptible to the enzyme's natural mechanism for chain scission.[14, 15] If the degree of chain entanglement and crosslinking is great enough to form an infinite network, it results in a relatively stable hydrogel when placed in water.[15]

Notably, crosslinking should prevent dissolution and chain scission in vivo without inhibiting hyaluronan's innate ability to reduce friction and increase biocompatibility. There are many crosslinking strategies for hyaluronan using chemical crosslinkers such as glutaraldehyde, divinyl sulfone, ethylene-glycol diglycidyl ether[15] and 1,4-butanediol diglycidyl ether.[13] However, some of these chemical crosslinking strategies, particularly glutaraldehyde, often produce a cytotoxic response due to the presence of residual aldehydes.[16] Efforts to reduce or remove such residual aldehydes have led to the development of alternate treatment strategies including vapor deposition in conjunction with rinsing.[17] Much effort is being taken to reduce the amount of residual compounds and harmful solvents used in chemical crosslinking. Lee et al.[18] and others[19, 20] have begun to use enzymes such as horseradish peroxidase, a natural enzyme extracted from horseradish, to facilitate crosslinking in tyramine functionalized hyaluronan. This strategy results in a very rapid (from 1s to 20 min) and bio-friendly mechanism for the formation of a highly crosslinking HA network.[18] UV crosslinking is another attempt at a bio-friendly strategy for crosslinking that works by exposing hyaluronan modified with light sensitive functionalities, such as methacrylate,[21, 22] to UV light. The use of UV light to trigger crosslinking has the added benefit of the user being able to spatially photopattern hyaluronan onto other substrates, such as hydrogels.[22, 23] This technique of photopatterning light sensitive HA into hydrogels will be discussed in detail in Chapter 5.

While strategies involving light irradiation or enzymatic chemistry have produced more bio-friendly mechanisms for covalent crosslinking, they still require HA to be functionalized or chemically modified before crosslinking can take place. This involves additional synthetic steps and characterization of the HA before it can be used, as well as potential exposure to cytotoxic solvents in the modification process. For its efficacy and wide use as a coupling reaction used to crosslink HA[14, 15, 24] and many other biological molecules, a modified Steglich reaction using the water soluble carbodiimide 1-Ethyl-3-(3-dimethylaminopropyl) carbodiimide (EDC) was chosen as the means of infinite network formation in this study. Water soluble EDC, as compared with the traditional dicyclohexylcarbodiimide (DCC) originally reported by Steglich,[25] permits crosslinking of unmodified HA directly in an aqueous environment. Importantly, a byproduct of this crosslinking reaction, a substituted urea derivative, can be easily removed by the body and as a result the crosslinking reaction is shown to be largely non-cytotoxic.[26, 27] In addition, this reaction is catalyzed in mildly acidic (0.01M HCl) aqueous conditions. Crosslinking using EDC takes place when a carboxylate anion within the hyaluronic acid main chain attacks a protonated EDC molecule to form an activated ester. This activated ester then reacts with a primary alcohol of a nearby hyaluronic acid repeat unit to form an ester linkage within (intra-chain crosslink) or between (inter-chain crosslink) hyaluronan chains Fig.1.

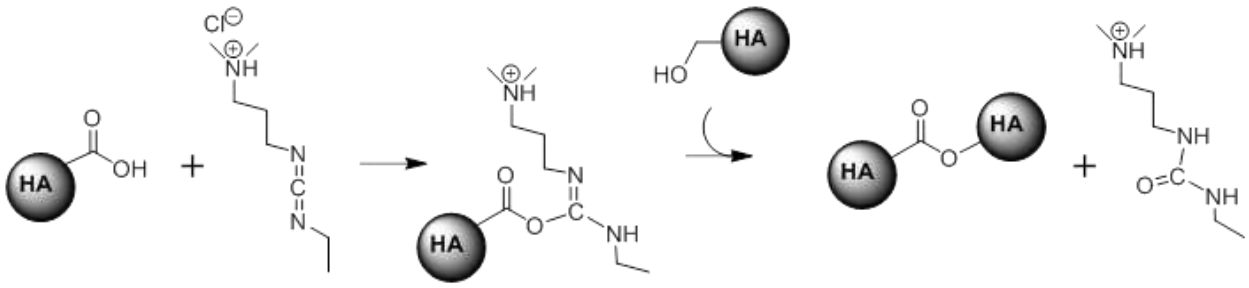

Figure 4.1: Reaction scheme for hyaluronan crosslinking using EDC.[15]

While all of these strategies for crosslinking, including those employing EDC, are effective at preventing hydrogel dissolution and retarding enzymatic degradation, without sacrificing cytocompatibility, they typically produce mechanically weak stand-alone hydrogels.[28] This is why hyaluronan is very often integrated with substrates such as silicone,[7, 8, 29] polyethylene,[30] or with other more conventional hydrogels such as those derived from polyethylene glycol, [31, 32, 33, 23] polyvinyl alcohol, [34, 35] or polylactic acid.[36]

Much of the current research focusing on the incorporation of HA into conventional hydrogel systems is predicated on strategies in which hyaluronan is incorporated homogeneously throughout the material. This is often accomplished via random solution-based crosslinking of dispersed HA with the monomer or oligomer of the reinforcing hydrogel network. Solution-based crosslinking has the benefits of being injectable, providing a low modulus, being amenable to degradable chemistries and facilitating cell incorporation.[26, 37] Systems like these are thus advantageous for tissue engineering applications for soft tissues like cartilage [12, 27, 37-39] or in facilitating nerve regeneration[23]. However, when degradation is not desirable and only the surface of the material interacts with the biological environment, such as in orthopedic replacements or in contact lenses, a stable and largely non-degradable modification of the surface with HA is often desirable. In contrast to homogeneous bulk incorporation of HA, treatments that can be constrained to only modify a surface can help limit impact on the bulk mechanical, chemical, or mass transport characteristics of the substrate being modified.

Recently, our group has been successful in designing a thermoplastic elastomer (TPE) based hydrogel system with compressive moduli comparable to fibrocartilage soft tissue and a demonstrated resistance to fatigue over hundreds of thousands of compressive cycles at physiologically relevant strains and strain rates (Chapter 3). [40] The block copolymer blends that

make up this TPE hydrogel consist of polystyrene-*b*-poly(ethylene oxide) (SO) diblock copolymer and polystyrene-*b*-poly(ethylene oxide)-*b*-polystyrene (SOS) triblock copolymer (**Figure 4.2a**). The remarkable properties of these hydrogels are produced utilizing self-assembly of the BCP blend in the melt to generate a highly homogeneous distribution of spherical polystyrene domains that are physically tethered to one another via the poly(ethylene oxide) bridge of the SOS triblock copolymer (**Figure 4.2b**). This nanoscale network architecture, once swollen (**Figure 4.2c**) is intrinsically able to efficiently distribute stress while limiting strain induced covalent bond breakage responsible for fatigue in most traditional hydrogel systems. [41] This ability to resist fatigue at a high modulus is a result of a network predicated on a high degree of chain mobility, a large density of chain entanglements, and a relatively minimal crosslink density.

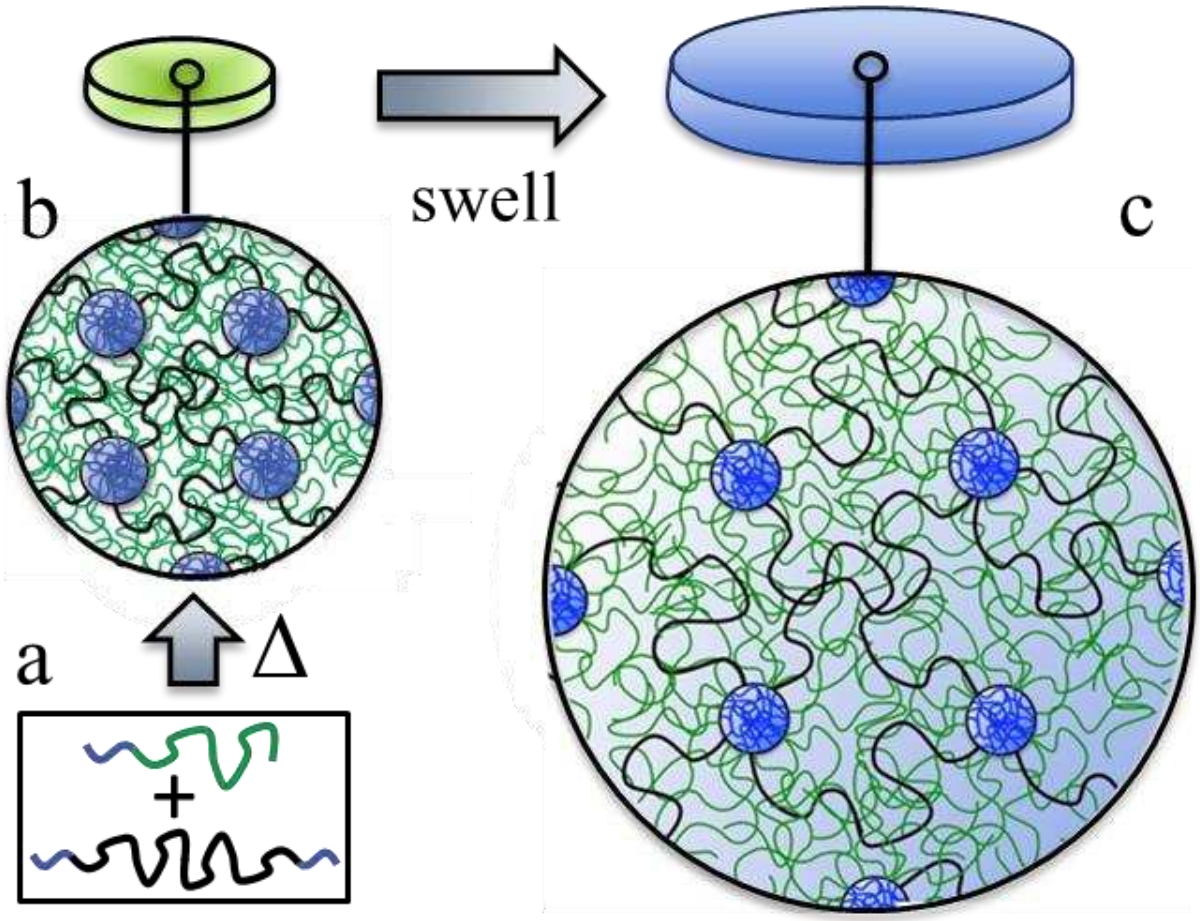

Figure 4.2: (a) SOS triblock copolymer within SOS/SO block copolymer blends forms (b) poly(ethylene oxide) tethers (black) connecting polystyrene micellar domains (blue) when heated. (c) The network architecture is conserved upon vitrification of the heated samples. Swelling through the selective solvation of the poly(ethylene oxide) matrix (green/black) in water expands the network while the vitrified polystyrene domains (blue) act as highly-branched, fixed junction points.

The intrinsic mechanical capability of these hydrogels has inspired their consideration as a permanent synthetic fibrocartilage replacement for tissues such as the meniscus or intervertebral disk (Chapter 3).[40] While undergoing high levels of cyclic loading without fatigue is often critical when considering hydrogels for these applications, it is equally important that the material surface is compatible with the native environment of the replaced tissue. For example, the knee meniscus needs to maintain the lubricity (via improved hydrophilicity) necessary for

repetitive articulation and a chemical composition that minimizes inflammatory response in the surrounding tissue.

In this context, we have developed a surface treatment for our TPE hydrogels, designed to efficiently introduce an interpenetrating network of hyaluronan within the SO/SOS tethered micelle framework. This novel treatment protocol was inspired by a bulk film casting technique originally developed by Ikada et. al. to produce a single network hydrogel from hyaluronan homopolymer.[42] In this original protocol, dried hyaluronan thin films cast from aqueous media were exposed to acetone or isopropanol solutions containing a crosslinking agent. The organic/aqueous solutions were employed to restrict dissolution of the hyaluronan as crosslinking took place. This technique demonstrated that even crosslinkers of limited efficiencies can be effective at forming hyaluronan networks if sufficiently high degrees of chain entanglement are maintained throughout the crosslinking process. However, in the context of using such a technique to modify our underlying TPE hydrogel, the presence of organic solvent solutions proved deleterious, compromising the integrity of the vitreous polystyrene cores critical to network stability.

Here, a modified method for introducing an interpenetrating hyaluronan network into our TPE hydrogels free of organic solvents and other harmful small molecules is reported. In the following study we assessed the impact of this HA surface treatment on general cytocompatibility, hydrophilicity, and the compressive and tensile properties of our TPE hydrogels.

4.2 RESULTS AND DISCUSSION

4.2.1 Formation of an HA Hydrogel From an HA Film Using A Modified Film Casting Technique

In order to form a stable HA hydrogel, sufficiently high degrees of chain entanglement must be maintained during the crosslinking process. Thus swelling of the HA film, which is required to deliver the crosslinking agent, must be balanced against the need to maintain high chain overlap. Ikada et al. were able to achieve minimal swelling of the HA film during crosslinking by combining aqueous crosslinker solution with a miscible organic "non-solvent" for HA (e.g, acetone or isopropanol). This allowed the HA film to preferentially imbibe the aqueous component of crosslinking mixture needed for delivery of the crosslinking agent, while the organic "non-solvent" prevented large-scale HA dissolution. Because of the interference of the organic non-solvent with the integrity of our SOS/SO hydrogel systems, we proposed a modified protocol eliminating the need for the organic solvent additives. In our modified protocol, high degrees of chain entanglement during crosslinking were instead achieved by adding just enough aqueous swelling solution to deliver the desired amount of crosslinking agent while restricting overall swelling ratios. In development of this protocol, it was hypothesized that air could effectively act as the "non-solvent" for the HA film while the crosslinking reaction takes place, thus eliminating the need for organic non-solvents. The merit of this approach is based on ensuring a significant differential exists between swelling (fast) and crosslinking (slow) rates, favoring homogeneity in crosslink density.

Before incorporating HA into our TPE hydrogels using this modified film casting technique, its efficacy forming a stable HA hydrogel using EDC as a crosslinker was assessed. Briefly, an HA/DI water solution was poured onto a glass slide and allowed to dry overnight to

produce an HA film. Just enough aqueous crosslinking solution was then added to the film to produce a "swelling ratio" of approximately 1.5 to maximize chain entanglement during crosslinking. The partially swollen HA film was then sealed in a vial to minimize evaporation, crosslinked for 24 hours, and then rinsed (soaked) in excess DI water for an additional 48 hours to remove any unreacted EDC or isourea byproducts. 700kDa HA was shown to produce sufficient chain entanglement during crosslinking and after rinsing to form an HA hydrogel that was stable in solution for long periods of time (> 1 month). Notably, lower molecular weight (MW) HA (40kDa) was also assessed for its ability to form a stable hydrogel, in anticipation that variability in molecular weight would provide a means of tuning penetration depth when ultimately applied to the modification of the SOS/SO hydrogels. However, 40kDa HA possessed insufficient chain entanglement to form an infinite network and resulted in considerable HA dissolution during rinsing (>1 hour). While there are likely MWs of HA between 40kDa and 700kDa that would result in the formation of a stable hydrogel upon rinsing, our primary objective of creating a surface network of HA was achievable using the 700kDa HA and thus determination of the minimum MW required for sufficient entanglement was not pursued.

Figure 4.3a below shows a typical dry 700 kDa HA film (inside of the dashed circle) following film casting but prior to crosslinking. The image captures the typical transparency and flexibility of dry HA films produced through casting. **Figure 4.3b** shows the same film after crosslinking using the modified film casting protocol. These swollen, crosslinked films could be easily handled and physically manipulated. The films did tend to fold in on themselves easily, which produces the appearance of texture in the image of **Figure 4.3b**. However, if unfolded, the swollen hydrogel was identical in shape to its dry film counterpart, but an increased size consistent with a swelling ratio of approximately 10.

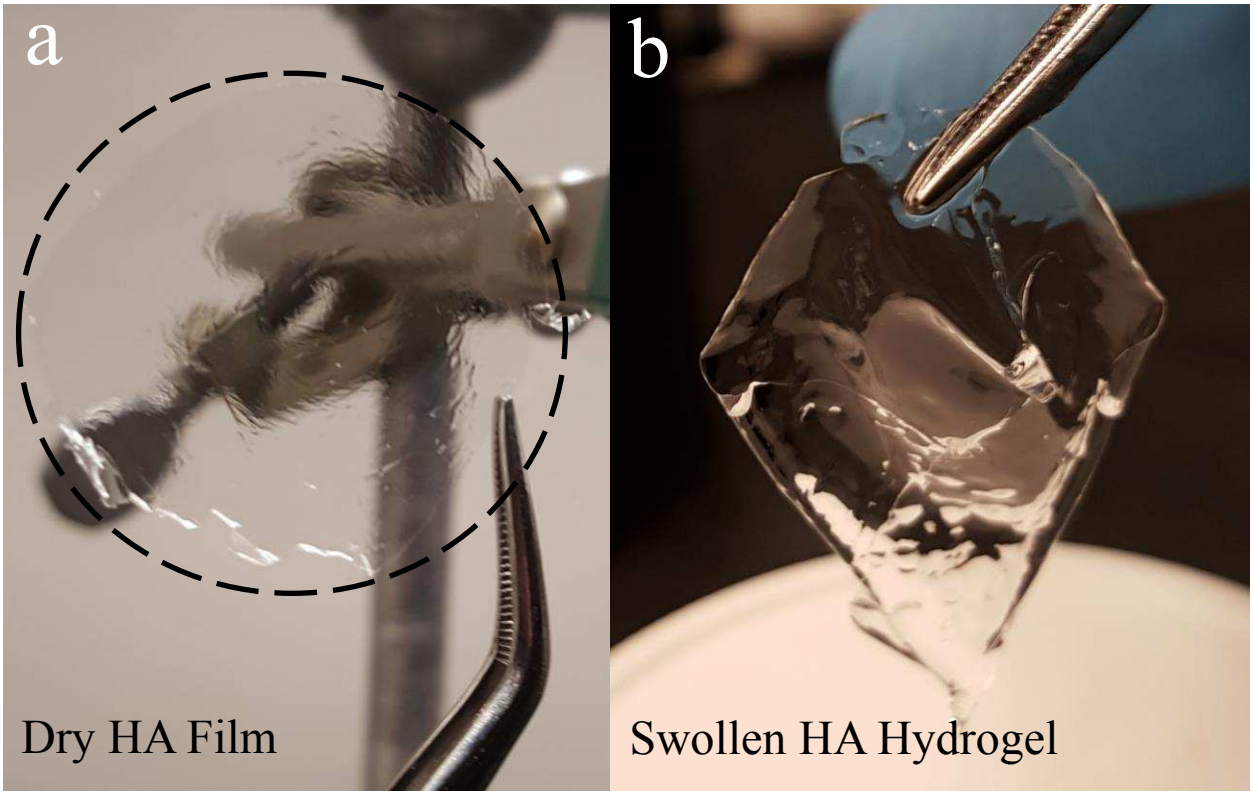

Figure 4.3: (a) Dry 700kDa hyaluronan film before crosslinking (b) 700kDa hyaluronan hydrogel after crosslinking with EDC and after rinsing in DI water for 24 hours.

4.2.2 HA surface treatment of TPE hydrogels using modified film casting technique

Once it was confirmed that this modified film-casting technique could produce a stable HA hydrogel, the protocol was then adapted for surface modification of our TPE hydrogels (**Figure 4.4**). Briefly, a dry SOS/SO polymer blend was swollen to equilibrium over 48 hours in a 1.5 wt.% solution of 700kDa HA in DI water. The hyaluronan chains interpenetrate with the poly(ethylene oxide) chains at the surface of the SOS/SO hydrogel during swelling. The HA exposed SOS/SO hydrogel is then dried, resulting in a thin, interpenetrating film of HA decorating the surface of the dried SOS/SO network. Crosslinking takes place by adding just enough crosslinking solution (adjusted to contain 4 molar equivalent EDC per repeat unit of HA in an aqueous solution of 0.01M HCl) to produce a reduced (relative to equilibrium) swelling

ratio of 1.5 g crosslinking solution per g dry polymer (SOS/SO/HA). The hydrogel was allowed to crosslink for 24 hours and then rinsed in an excess volume of DI water for 48 hours in order to remove any uncrosslinked HA, EDC, and isourea byproduct.

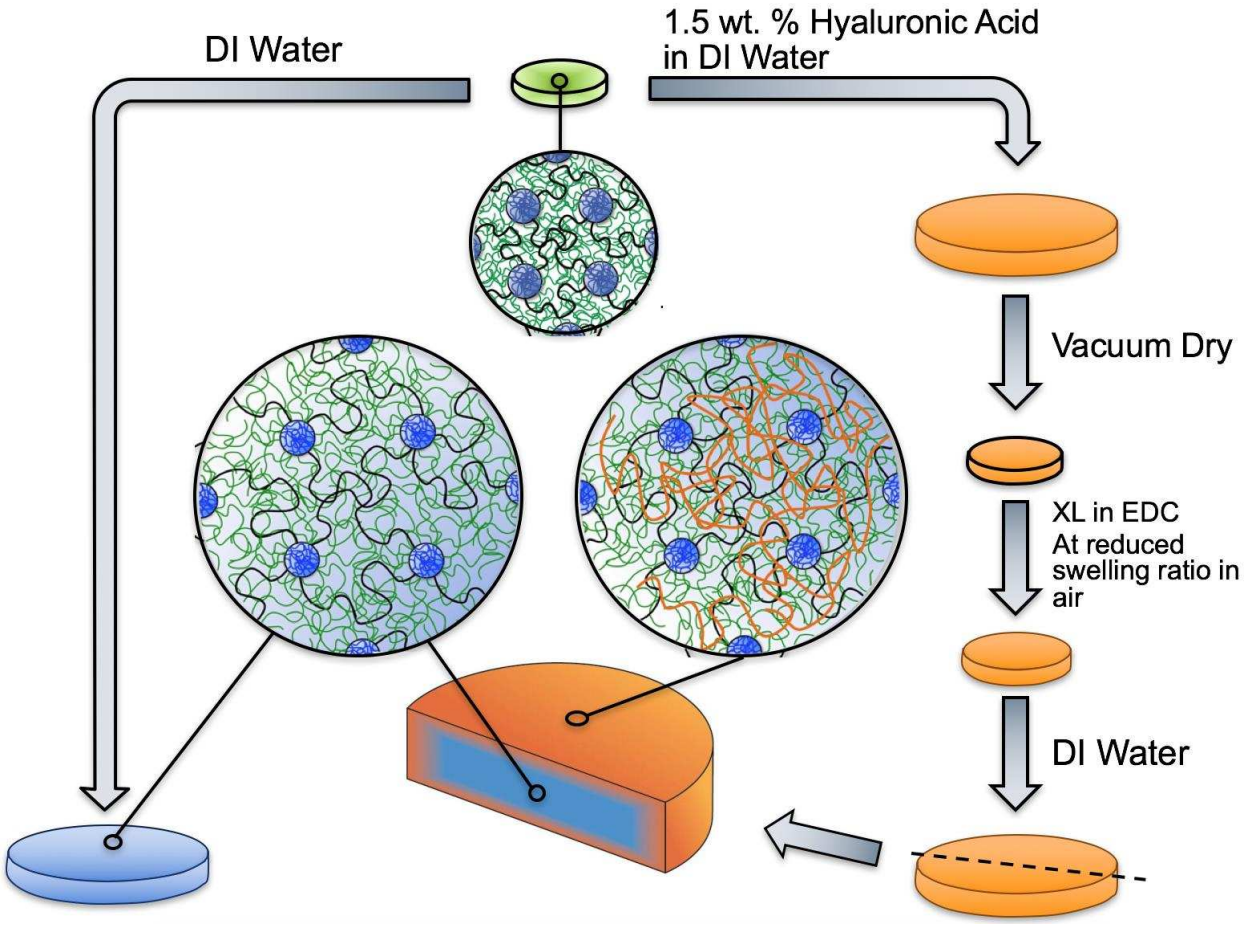

Figure 4.4: Schematic representation of the hyaluronan surface treatment process (right). The melt-processed, unswollen SOS/SO disk (green) is shown undergoing the HA surface treatment protocol to produce an interpenetrating network of HA at the surface of the swollen TPE hydrogel. The HA surface treatment protocol consists of swelling in a 1.5 wt % HA solution (orange), drying to produce an HA film at the surface of the TPE hydrogel, crosslinking at a reduced swelling ratio to ensure sufficient chain entanglement and then rinsing in DI water to remove any uncrosslinked HA, EDC or isourea byproducts. The HA surface treated hydrogel is bisected to demonstrate that this HA treatment is limited to the surface region as a result of the HA's slow rate of diffusion into highly entangled TPE hydrogel network, and that the center of the hydrogel remains structurally consistant with an untreated TPE hydrogel swollen only in DI water (left).

4.2.3 Approximating the amount and location of HA within treated TPE hydrogels

The amount of HA inside of the surface treated TPE hydrogels was initially determined gravimetrically by measuring the dry mass of the SOS/SO polymer disk both before and after the surface treatment (via a bench-top mass balance). The relative contributions to mass were then analyzed using thermal gravimetric analysis (TGA). **Figure 4.5** shows an example series of TGA thermograms conducted on a 700kDa HA film, SOS/SO polymer sample, and an HA surface treated SOS/SO polymer sample. The untreated SOS/SO polymer sample was stable until the onset of degradation at ~375°C. Degradation of mass occurred rapidly in a single stage with only a minimal amount of non-volatile carbon residue left after ~450°C. The HA film decomposition pattern was much more complex, occurring in approximately three phases. Initial heating was characterized by an asymptotic mass loss into a stable plateau followed by a second, more rapid mass loss starting at ~220°C. However, by ~250°C degradation slows significantly with the remaining ~50% mass decreasing to only ~20% over the next 550°C. The HA treated SOS/SO dry polymer sample demonstrated a clear superposition of these two thermograms. Quantitative analysis of the TGA for this hydrogel sample predicted that HA comprised approximately 10.8 wt% of the total dry polymer mass following treatment. This value is comparable to the 9.6 wt% predicted using a simple gravimetric measurement. This level of agreement in calculated HA compositions between these two gravimetric methods was typical for all samples examined, confirming that the drying step was sufficient to minimize the amount of residual water and permit the use of gravimetric methods in calculating reaction stoichiometry.

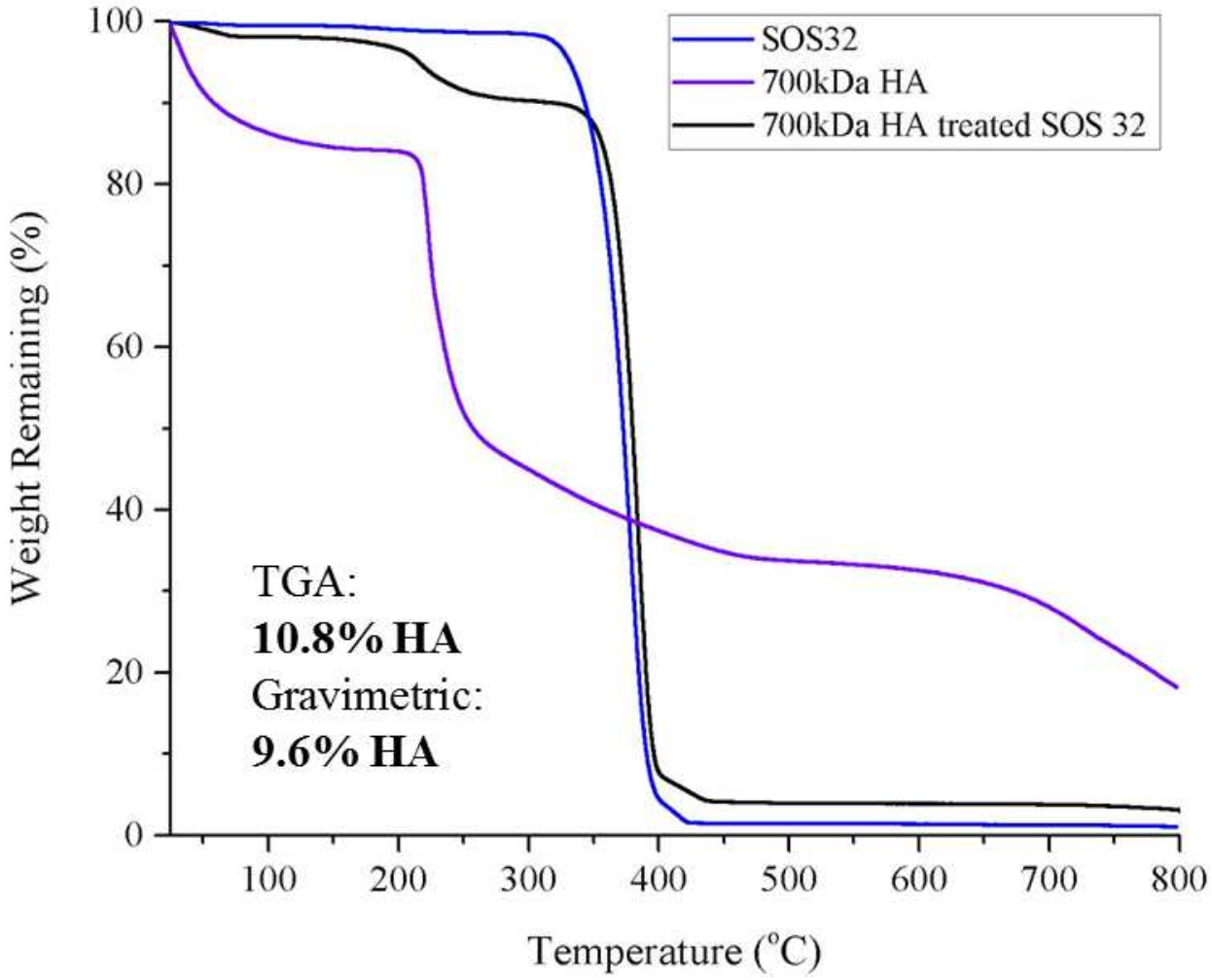

Figure 4.5: Thermal gravimetric analysis (TGA) showing weight remaining vs. temperature of a neat 700kDa HA film (purple), dry SOS/SO polymer (blue), and a dry HA modified SOS/SO polymer after rinsing (black). Comparison of values showing the dry mass % of HA determined by comparison of dry masses before and after swelling and TGA is shown in the lower left.

The successful incorporation of HA into SOS/SO hydrogels was further confirmed via attenuated total reflection Fourier transform infrared spectroscopy (ATR-FTIR). This surface characterization technique works at a penetration depth of ~ 2 μm. A neat 700kDa HA film, neat SOS/SO polymer, and an HA surface treated SOS/SO polymer were all analyzed. Two distinct functionalities that are unique to HA, and apparent in ATR-FTIR, when compared to SOS/SO are the amide (~1675 cm^{-1}) and hydroxyl stretching (~3300 cm^{-1}). These functionalities do not exist in neat SOS/SO systems as shown in **Figure 4.6** below. However, in the SOS/SO hydrogels

that were treated with HA these functionalities become apparent and suggest the presence of HA, at least within the first 2 μm of the HA modified hydrogel.

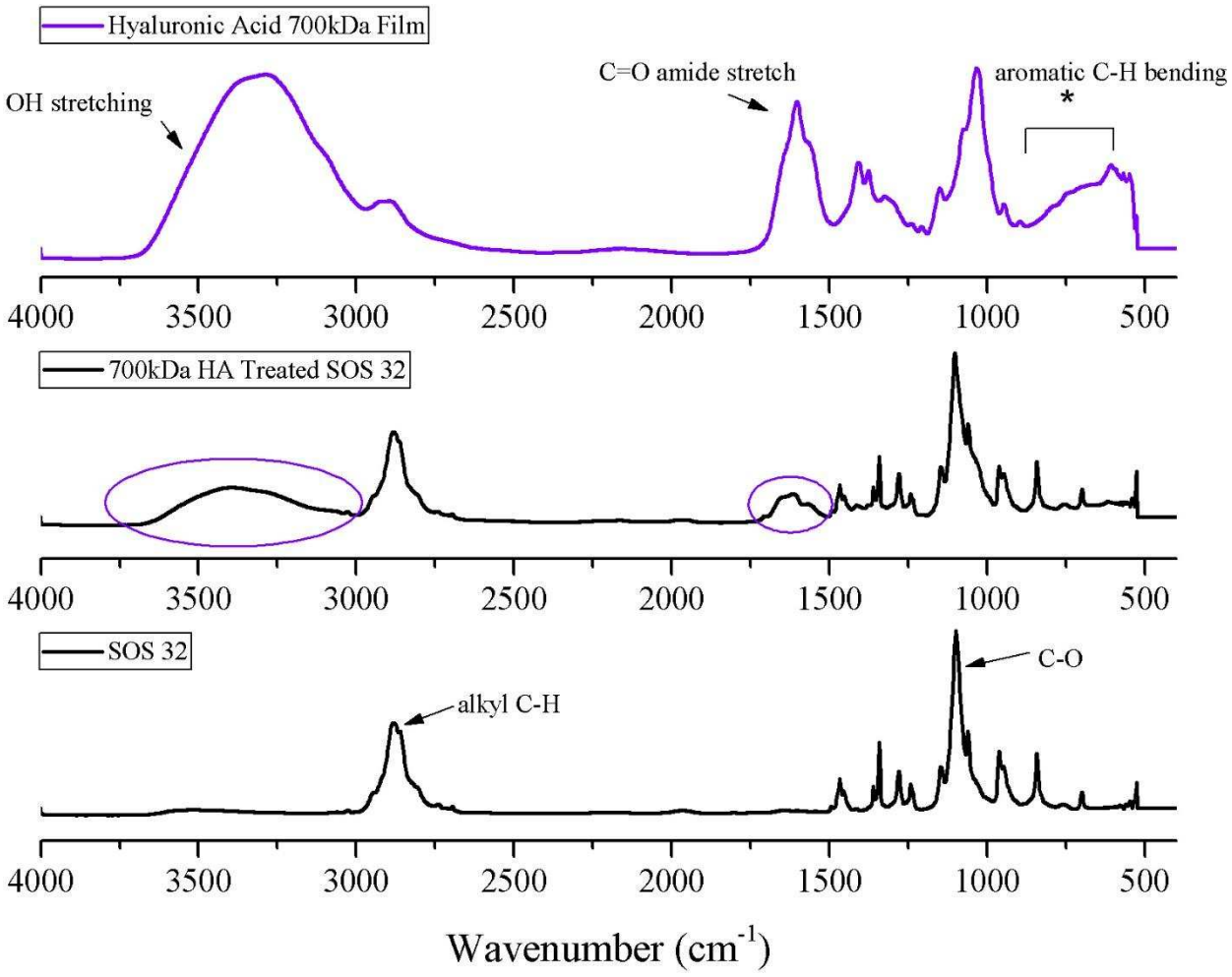

Figure 4.6: ATR-FTIR measurements of neat 700kDa HA film (top), HA surface modified SOS 32 (middle), and neat SOS 32 (bottom). Two unique peaks to HA that are not present in SOS samples are amide (~1675 cm^{-1}) and hydroxyl stretching (~3300 cm^{-1}). Amide and hydroxyl stretching are however observed in HA treated samples after rinsing, suggesting the presence of HA in HA treated SOS/SO samples.

The relative concentration of HA at the surface compared to the center of these hydrogels was assessed by scanning the surface of the HA treated SOS/SO dry polymer, followed by bisecting the sample and scanning it on its side. **Figure 4.7** demonstrates the much higher absorbance values, for the peaks that were unique to HA (hydroxyl and amide stretching), at the

surface vs. the interior of the HA treated samples. In fact, when scanned on its side the HA treated sample is nearly indistinguishable from its unmodified counterpart.

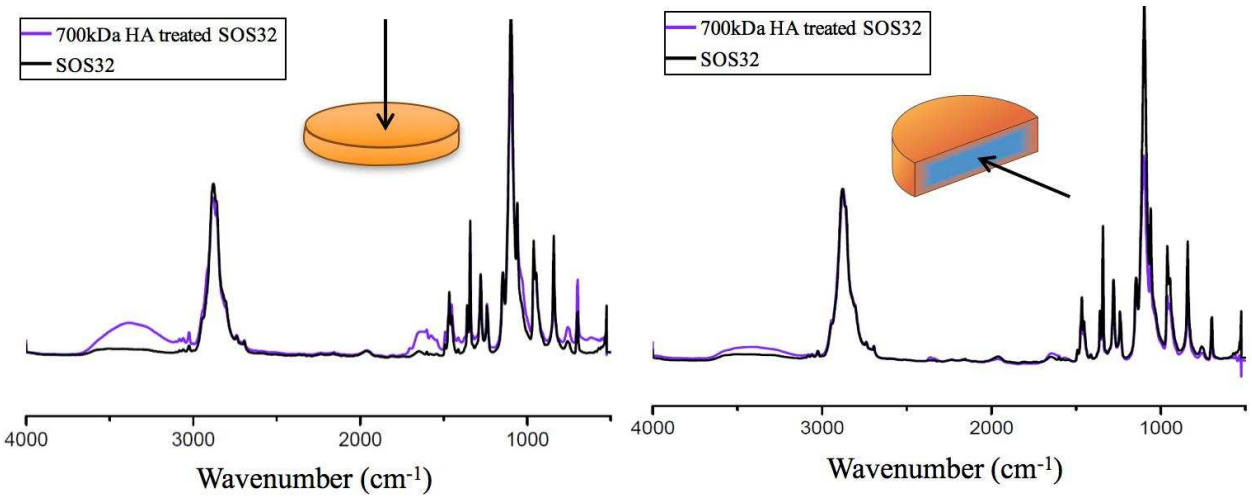

Figure 4.7: (Top) ATR-FTIR of the surface of a dry HA modified hydrogel (purple) compared to the surface of a dry unmodified hydrogel (black). (Bottom) ATR-FTIR of a dry and bisected HA modified hydrogel turned on its side (purple) compared to a dry and bisected unmodified hydrogel turned on its side (black).

4.2.4 Measuring the impact of the HA surface treatment on the compressive and tensile properties of the HA treated TPE hydrogels

The impact of the HA surface treatment on the mechanical properties of the hydrogel under compression was assessed through progressive compressive loading. Samples were loaded and unloaded in successive cycles that increased by 10% each cycle at a strain rate of 2 %/sec until a final strain of 80% was reached (0-10-0-20-0-30…) (**Figure 4.8**). The incorporation of HA at the surface of the hydrogel results in a near doubling of compressive modulus. This gain in compressive modulus does not have any impact on the materials ability to elastically recover upon successive cycling all the way to the final tested strain of 80%. This dramatic gain in modulus by incorporating a highly crosslinking HA matrix on the surface could be from multiple sources including: a resistance to the movement of fluid inside of the hydrogel through the formation of a stiff outer layer of HA, or perhaps it is due to the formation of higher degree of

tethering between spheres via a hyaluronan bridge. Prior research in our group shows that when there is an increase in micellar coronal overlap this results in an increase in chain entanglement and therefore modulus. Because the SO in the SOS/SO blends used in this study have an end terminus with a primary alcohol functionality, they could, theoretically, react with the activated ester of HA in the same way that the primary alcohols of HA. This would result in a graft copolymer of HA with SO attached via the carboxylic acid at various sites along the backbone effectively linking micellar domains together. Although the domain spacing between micelles would be much different in this type of crosslinking when compared to the native SOS, it would increase chain entanglement and could effectively result in the higher modulus values observed below.

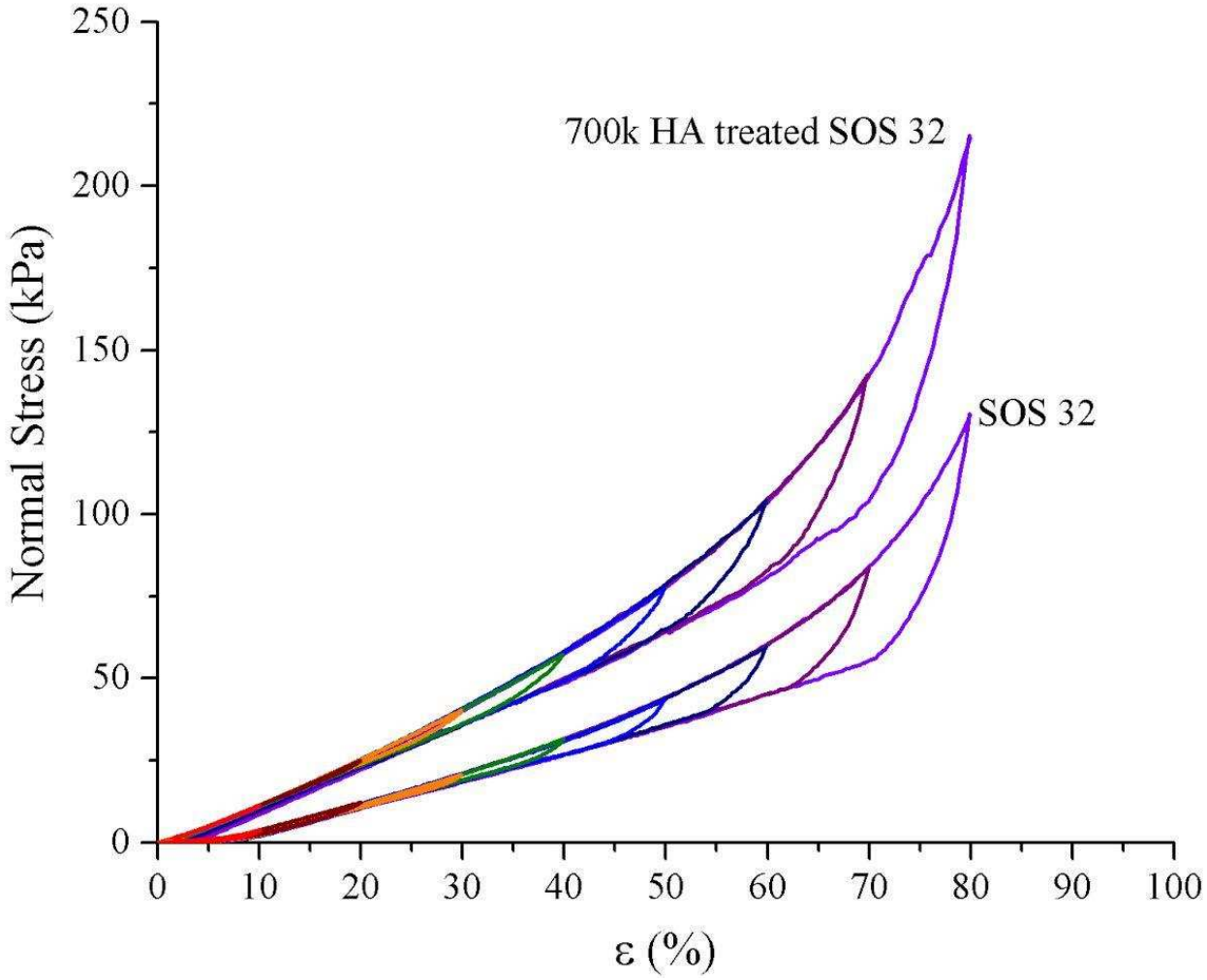

Figure 4.8: Progressive compressive mechanical testing of HA surface treated and untreated SOS/SO hydrogels. Samples were loaded and unloaded in successive cycles that increased by 10% each cycle at a strain rate of 2 %/sec until a final strain of 80% was reached (0-10-0-20-0-30…). Mechanical loading profiles indicate that the HA surface treatment results in an increase in modulus with impacting the materials ability to resist fatigue.

A similar mechanical analysis was performed in tension, where samples were loaded and unloaded in successive cycles that increased by 50% strain until the mean extension at break of the untreated hydrogel was reached (determined from prior testing, see Chapter 3). Tensile testing revealed that the HA surface treated hydrogels produced a slightly higher tensile modulus than their untreated counterpart, much like in compression (**Figure 4.9**). However, the successive cycles above 100% strain, or after the hydrogel had doubled its original length, were unable to

recover and demonstrate the loading profile of the prior cycle. In fact, all successive cycles above 100% strain followed the unloading curve of the prior cycle, until the hydrogel was strained past its' prior cycles max strain. The hydrogel's inability to elastically recover and perform similarly to prior cycles in these high strain regions suggests that the mechanism that is providing the additional modulus in the system is brittle compared to the primary TPE hydrogel. The HA surface treatment is likely performing similarly to traditional chemically crosslinked hydrogels in that it is prone to the same brittle failure mechanisms at high strain due to stress concentrations formed from inhomogeneous crosslinking (Chapter 3). This suggests that the modulus gained in tension from the HA surface treatment is likely beneficial for applications that do not require elastic performance above ~100% strain. Notably, physiological loading conditions are far lower than 100% strain in tension, where the hydrogel performs with minimal cycle to cycle fatigue. That is, these hydrogels may perform elastically under standard physiological loading conditions, particularly over the small strain ranges relevant during standard physiological compression of many musculoskeletal soft tissues (e.g., meniscus ~ 12%,[43-45] intervertebral disc ~ 10%,[46, 47] articular cartilage ~ 5 to 30%[48, 49]). Also, the HA surface treated hydrogel never drops below the modulus of its unmodified counterpart.

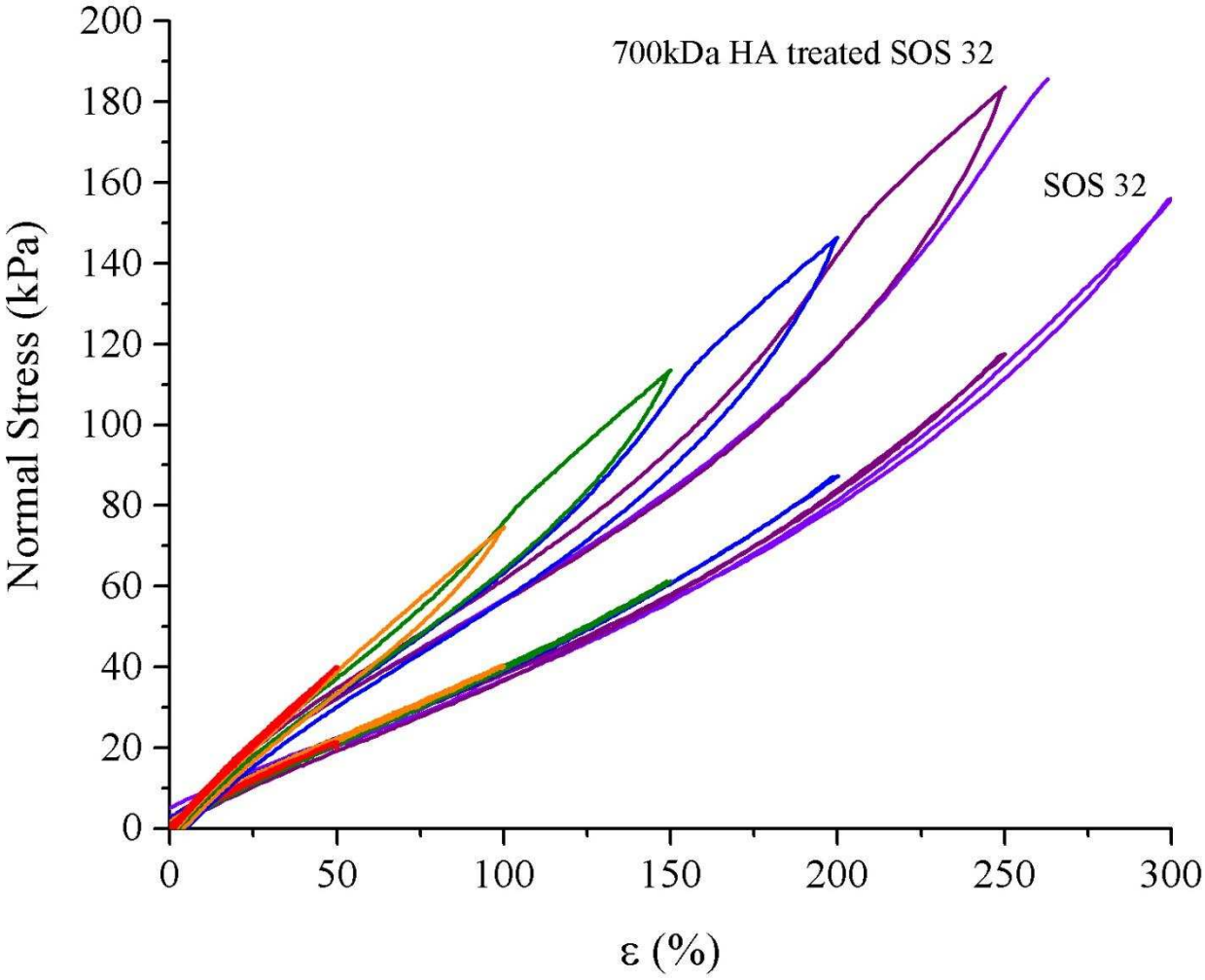

Figure 4.9: Progressive tensile mechanical testing of HA surface treated and untreated SOS/SO hydrogels. Samples were loaded and unloaded in successive cycles that increased by 50% each cycle at a strain rate of 2 %/sec until either the mean extension at failure (300%) or actual failure was reached. Mechanical loading profiles indicate that the HA surface treatment results in an increase in overall modulus and is prone to irrecoverable damage upon successive loading above ~100%.

4.2.5 Impact of the HA surface treatment on the contact angle of HA surface treated TPE hydrogels

Hydrophilicity was tested using captive bubble goniometry, due to the already highly hydrophilic nature of all hydrogel systems, to measure changes in contact angle between untreated TPE hydrogels and HA surface treated TPE hydrogels. In order to see if any changes in

hydrophilicity between HA treated and untreated hydrogels were stable after mechanical loading, a third group of HA surface treated TPE hydrogels was subjected to 5000 compressive cycles at 12% strain at a cycling rate of 1Hz. Contact angles of the hydrogel with water were calculated by taking the supplementary angle to the contact angle of the air bubble on the surface of the hydrogel (**Figure 4.10**).

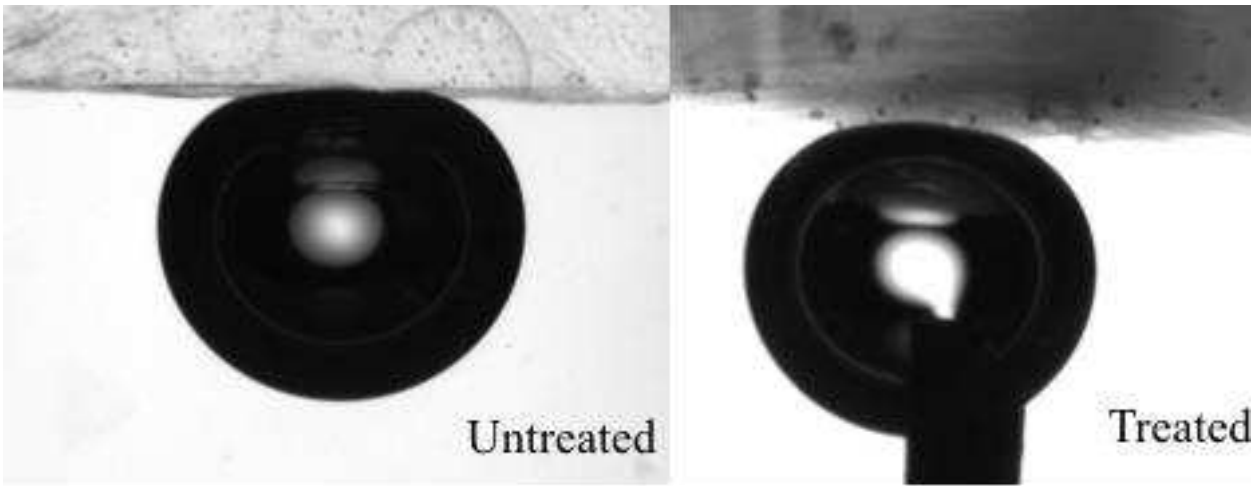

Figure 4.10: Photograph of a typical untreated (left) and HA treated (right) hydrogel in DI water with a captive air bubble resting on the surface. These photos demonstrate the highly hydrophilic nature of the system both before and after treatment as well as the relatively higher hydrophilicity of the HA treated group.

The static, advancing and receding contact angles were measured by expanding and collapsing the air bubbles until a stable contact angle was obtained. HA surface treated hydrogels resulted in statistically insignificant changes in static contact angle ($p = 0.283$) and receding contact angle ($p = 0.682$) between all groups. The receding contact angle ($p = 0.072$) and the contact angle hysteresis ($p = 0.072$) showed a more significant difference between the HA surface treated group and the other two groups. Testing also revealed that after 5000 successive compressive loading cycles the HA treated hydrogels performed almost identically to their unmodified counterpart (Table 1). The difference in contact angle hysteresis between the HA treated group suggests an increase in either chemical or physical homogeneity being produced

along the surface of the hydrogel. The fact that the reduction in surface heterogeneities is not maintained after high levels of cyclic loading suggests that this surface treatment is being modified, rearranged, or broken apart when exposed to high levels of cyclic loading.

Table 4.1: Summary of average and standard deviation values for static, receding and advancing contact angles as well as contact angle hysteresis for unmodified and HA modified hydrogels before (HA) and after (HAM) mechanical loading (5000 compressive cycles at 12% strain at 1Hz). The table suggests an increase in hydrophilicity and homogeneity from treating the surface with HA and that this increase is not sustained after mechanical loading.

	Contact Angle (°)	Static	Receding	Advancing	Hysteresis
SOS	mean	21	14	47	33
	stdev.	2.1	3.2	6.4	6.1
SOS HA	mean	19	12	31	20
	stdev.	1.0	3.9	6.7	9.2
SOS HA (M)	mean	21	13	45	32
	stdev.	2.7	3.9	5.6	5.9

4.2.6 Impact of HA surface treatment on cytotoxicity in HA surface treated TPE hydrogels

The impact of the HA surface treatment on cytotoxicity was assessed via a lactate dehydrogenase (LDH) assay. HA treated (HA) untreated SOS/SO hydrogels (SOS) were compared to a positive control of tissue culture polystyrene (PS) and a negative control where all of the cells were chemically lysed using Triton X (Triton X). Another group assessed the mechanical robustness of any changes in cytotoxicity by subjecting the HA treated hydrogels to compressive loading consisting of compression to 12% strain at 1 Hz for 10 cycles, followed by 1 cycle of 50% strain at 1 Hz. This 11-cycle regime was repeated 10 times using a servo hydraulic testing system. Although the unmodified SOS/SO hydrogels had a higher relative toxicity than the PS it was not significantly higher, suggesting that the unmodified SOS/SO hydrogels are largely non-cytotoxic (**Figure 4.11**). This may be a result as the major constituent of these hydrogels is poly (ethylene oxide) which is chemically identical to the well-known and

largely cytocompatible polyethylene glycol (PEG). Perhaps more exciting is the significant reduction in relative cytotoxicity between the HA treated and untreated TPE hydrogels (**Figure 4.11**). This significant reduction in cytotoxicity is maintained even after mechanical loading (**Figure 4.11**).

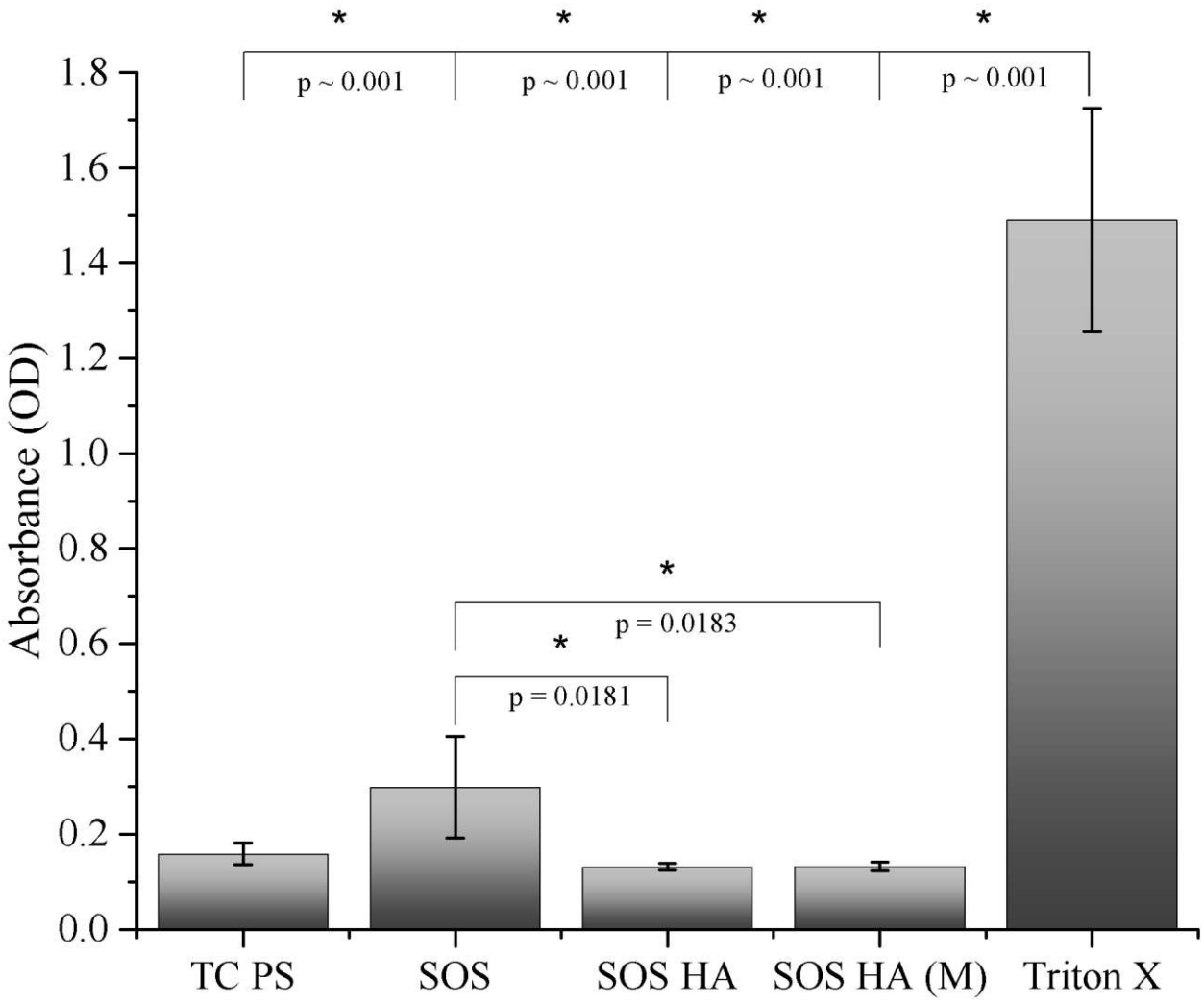

Figure 4.11: Results of lactate dehydrogenase assay showing relative absorbance between controls and different treatment groups: tissue culture polystyrene (PS), neat SOS/SO TPE hydrogel (SOS), HA modified SOS/SO TPE hydrogel (SOS HA), mechanically loaded HA modified SOS/SO TPE hydrogel (SOS HA (M)), and triton X (Triton X).

4.3 CONCLUSIONS

This simple and effective surface treatment of our TPE hydrogel results in an increase in modulus in both compression and tension as well as improvements in hydrophilicity and cytocompatibility. Compressive and tensile moduli appear to maintain the fatigue resistance present in the unmodified TPE hydrogel under high strains in compression (80%) and moderate strains in tension (100%). However, successive loading cycles in tension higher than ~100% result in an irrecoverable reduction in tensile modulus suggesting a brittle failure of the HA surface treatment at high strains. The surface treatment resulted in an increase in hydrophilicity and a reduction in contact angle hysteresis suggesting that the surface of the hydrogel is more homogenous in either chemical potential or surface topography. This may have implications in the surface treatment's ability to reduce friction and further testing is needed to confirm this potential. Notably, these gains in hydrophilicity and contact angle hysteresis are not maintained after 5000 successive compressive cycles @ 12% strain and 1 Hz. The treatment also results in a decrease in cytotoxicity determined from an LDH assay using adipose derived stem cells. These improvements in biologically relevant properties without hindering the hydrogels mechanical ability suggest that this surface treatment may improve the hydrogel's potential candidacy as a synthetic fibrocartilage replacement. Importantly, chemical crosslinking often results in inhomogeneous stress distributions and brittle failure and this treatment appears to be no exception to this. In future studies installing the network at a higher swelling ratio or a lower crosslink density may provide more chain mobility and a more robust surface treatment that is not as susceptible to brittle failure in high strain tensile testing. This technique could provide useful as many of the substrates being using in biological applications are sensitive to harsh solvents and highly acidic conditions and only require a modification of the surface of the

material with HA. This approach also has the added benefit of taking place without the need to modify the surface of the substrate or the hyaluronan.

4.4 EXPERIMENTAL

Materials and Synthesis

Materials: Styrene (99%, 4-tert-butylcatechol inhibitor, Aldrich) and ethylene oxide (99.5+%, compressed gas, Aldrich) monomer were each purified by successive vacuum distillations (10–20 mTorr) from dried di-n-butylmagnesium (1.0 M solution in heptane, Aldrich) before use. Both purified styrene and ethylene oxide monomer were stored in glass burettes in the dark, at room temperature (styrene) and 3 °C (ethylene oxide), respectively, before use (typically less than 24 h). Argon degassed cyclohexane (CHX) was purified by passing the solvent over activated alumina followed by Q-5-like supported copper catalyst (Glass Contour, proprietary). Argon degassed tetrahydrofuran (THF) was purified by passing the solvent over activated alumina. High-purity argon (99.998%, Airgas) was passed through additional oxygen and moisture traps prior to use. Glassware and polymerization reactors were flamed under vacuum and backfilled with argon multiple times. ^{1}H NMR spectra were collected at room temperature in $CDCl_3$ on a Varian Inova 400MHz Spectrometer (n=32, delay=30 s). Size exclusion chromatography (SEC) was performed on a Viscotek GPC-Max chromatography system fitted with three 7.5 x 340 mm Polypore^{TM} (Polymer Laboratories) columns in series, an Alltech external column oven, and a Viscotek differential refractive index (RI) detector. Measurements were performed using a DMF (55 °C) mobile phase (1 mL/min) with PS standards (Polymer Laboratories). Final SO/SOS compositions were confirmed via relative peak integrations in the SEC chromatograms of these blends. Sodium Hyaluronate (700kDa (500 kDa-749 kDa), Lifecore Biomedical), 1-Ethyl-(3-dimethylaminopropy)carbodiimide (EDC) (99.80%, Chem-Impex International, Hydrochloric Acid (N/10, Fisher Chemical).

ω-Hydroxy-polystyrene (S-OH) Purified styrene monomer (120 g, 1.14 mol, 20°C) was added to a stirring solution of sec-butyl lithium (10.23 mL, 1.3 M in cyclohexane, Aldrich) and dry, air-free cyclohexane (1 L, 20 °C) in a 2 L reaction vessel. The solution was then raised to 40°C and stirred continuously for 8 hours. At a reduced pressure of 1 psig, purified ethylene oxide (6.6 g, 0.15 mol, 0 °C, liquid) was added to the reaction vessel. The reaction was held at 40°C for an additional 24 hours, after which all excess ethylene oxide was removed from the reactor under a constant argon flow. The reaction was terminated by methanol (50 mL). The polymer was precipitated in methanol (5 L total), producing a fluffy white solid, and dried under vacuum at room temperature over a 48h period (yield 116 g, 97%, M_n= 8370 g/mol, PDI = 1.03).

ω-Hydroxy-polystyrene-b-poly(ethylene oxide) (SO). S-OH (7 g, 1.14 mol) was added to a 2 L reaction vessel containing a glass coated magnetic stir bar. The reactor was evacuated and backfilled with purified argon before adding 1 L of dry, air-free tetrahydrofuran (THF). Concentrated potassium naphthalenide in THF was added to the polymer solution via cannula until a light green color persisted for 30 minutes. The temperature of the reaction mixture was raised to 40 °C and purified ethylene oxide monomer (78.7 g, 1.78 mol, 0 °C) was added under argon (1 psi) to the stirring solution for 48 hours. The reaction was terminated by methanol (50 mL) and the polymer was precipitated in pentane (4 L), producing a fluffy white solid. The polymer was dried under vacuum at room temperature for 48 hours. (M_n= 107,000 g/mol, PDI = 1.07, f_{PS} = 0.085).

Polystyrene-b-poly(ethylene oxide)-b-polystyrene (SOS) SO (8 g) was placed into a 250 ml round bottom reactor vessel which was evacuated and backfilled with purified argon. The SO was allowed to dry under vacuum overnight. The SO was then dissolved in dry THF (100 ml). A concentrated potassium naphthalenide solution in dry THF was titrated into the reactor until the solution maintained a green color for 30 minutes. α,α′-dibromo-p-xylene (0.099g) in THF (5.0 mL) at a 0.5 molar equivalent to the SO was then injected into the reactor over a 8 hour period at a rate of 0.0625 mL/hour using a syringe pump and a 2.5 mL glass syringe. Coupled polymer was recovered through precipitation in 5 L of pentane followed by vacuum filtration. The precipitated polymer was dried overnight under vacuum to produce a fluffy white solid as a blend of uncoupled (SO) and coupled (SOS) block copolymer (32 mol% SOS and 68 mol% SO).

Preparation of dry SO/SOS disks Dry 32 mol% SOS polymer was placed into a steel washer (8mm x 0.73mm thick) and sandwiched between two sheets of Kapton. This assembly was then placed into a Carver Press and was heated to 150°C and compressed at ~500 psi for 5 minutes. Samples were removed and allowed to cool to room temperature and their masses were recorded before swelling.

Hyaluronan surface treatment (HA/SOS) Dry 32 mol% SOS samples were either swollen in DI water or a solution containing 1.5 wt% sodium hyaluronate in DI water for 24 hours at 4°C. Samples were then removed from their respective swelling solutions, patted dry with a Kimwipe, allowed to dry in air for 24 hours, and their masses were recorded. The amount of hyaluronan inside of the hydrogel was determined gravimetrically by taking the difference of the dry mass of the polymer before and after being subjected to a swelling and drying cycle. EDC crosslinking

solutions consisted of a 4:1 molar equivalence of EDC: hyaluronan repeat unit in 0.01M HCl. Enough solution was added to the dry polymer to produce a swelling ratio of 1.5. These partially swollen hydrogels were then allowed to crosslink for 24 hours. After crosslinking the hydrogels were placed into a semi-infinite solution of DI water for 7 days to remove any loose unbound HA. Thermogravimetric analysis (TGA) was performed using a TA Instruments Thermogravimetric Analyzer (TGA Q500) at a temperature ramp rate of 10°C/min from 25 °C to 800 °C. Unmodified dry SOS/SO polymer, a 700kDa HA film, and a HA modified dry SOS/SO polymer were all subjected to TGA.

Determining Contact Angle Via Captive Bubble Technique Unmodified (n = 6), HA modified (n = 6), and HA modified hydrogels that had been subjected to 5000 cycles @ 12% strain and 1 Hz (n = 6) were assessed to determine any changes in surface hydrophilicity via a captive bubble technique using a goniometer (260-F4 Ramé-Hart Instrument). All hydrogels were kept in DI water for at least 48 hours before testing in order to reach swelling equilibrium as well as rinse off any unbound HA in the applicable groups. All samples were then superglued to a glass slide which was clamped on either side. The glass slide and clamp assembly was then inverted and suspended in an acrylic box and completely submerged in DI water. Static contact angle was measured by introducing an air bubble via a syringe. Receding and advancing contact angles were determined by measuring the angle between the solid-liquid interface when the air bubble reached a stable value when being either expanded or contracted respectively. All results were evaluated using a one-way analysis of variance (ANOVA) with a Tukey's HSD. Statistical significance was considered at $p < 0.05$.

Cytotoxicity assay Cytocompatibility of polystyrene pucks (6mm diameter x ~ 1 mm in thickness) (n = 5), unmodified TPE hydrogels (n = 5), HA modified TPE hydrogels (n = 5), and HA modified TPE hydrogels that had been subjected to 5000 cycles @ 12% strain and 1 Hz (n = 5) were assessed using a commercially available lactase dehydrogenase assay (LDH) (Quantichrom C2LD-100). All samples were placed into a 96 well plate with each row containing 5 samples from each group. Samples were sterilized by placing this 96 well plate into a cell culture hood and exposing the plate containing all the samples to UV light for 30 minutes. All samples in the 96 well plate were then turned over using tweezers and exposed for an additional 30 minutes to UV light. The manufacturer's protocol for the Quantichrom C2LD-100 LDH assay was followed. Adipose derived stem cells were cultured on sample materials for 24 hours in cell media (20,000 cells were seeded). 10 µl of cell media exposed to samples from each well was then transferred to a 96 well plate. 10 µl of deionized water was used for control wells, and 10 µl 20 % Triton X in cell media containing cells was used for the total lysis control group. 160 µl of reagent was then added to all wells and the wells were allowed to incubate for 10 mins. Results were then analyzed using spectrophotometry at 500 nm. All results were evaluated using a one-way analysis of variance (ANOVA) with a Tukey's HSD. Statistical significance was considered at $p < 0.05$.

REFERENCES

1. Stern, R. *Eur J Cell Biol* **2004,** 83, (7), 317-25.

2. Fraser, J. R.; Laurent, T. C.; Laurent, U. B. *J Intern Med* **1997,** 242, (1), 27-33.

3. Kasdorf, B. T.; Arends, F.; Lieleg, O. *Biophys J* **2015,** 109, (10), 2171-81.

4. Daniel, M. *Wien Med Wochenschr* **2014,** 164, (5-6), 88-94.

5. Noble, P. W. *Matrix Biol* **2002,** 21, (1), 25-9.

6. Weigel, P. H.; Fuller, G. M.; LeBoeuf, R. D. *J Theor Biol* **1986,** 119, (2), 219-34.

7. Bettuelli, M.; Trabattoni, S.; Fagnola, M.; Tavazzi, S.; Introzzi, L.; Farris, S. *J Biomed Mater Res B Appl Biomater* **2013,** 101, (8), 1585-93.

8. Lin, C. H.; Cho, H. L.; Yeh, Y. H.; Yang, M. C. *Colloids Surf B Biointerfaces* **2015,** 136, 735-43.

9. Pitarresi, G.; Palumbo, F. S.; Calascibetta, F.; Fiorica, C.; Di Stefano, M.; Giammona, G. *Int J Pharm* **2013,** 449, (1-2), 84-94.

10. Zhang, M.; King, R.; Hanes, M.; James, S. P. *J Biomed Mater Res A* **2006,** 78, (1), 86-96.

11. Zhang, M.; Pare, P.; King, R.; James, S. P. *J Biomed Mater Res A* **2007,** 82, (1), 18-26.

12. Hwang, H. D.; Cho, H. J.; Balakrishnan, P.; Chung, C. W.; Yoon, I. S.; Oh, Y. K.; Byun, Y.; Kim, D. D. *Colloids and Surfaces B-Biointerfaces* **2012,** 91, 106-113.

13. De Boulle, K.; Glogau, R.; Kono, T.; Nathan, M.; Tezel, A.; Roca-Martinez, J. X.; Paliwal, S.; Stroumpoulis, D. *Dermatol Surg* **2013,** 39, (12), 1758-66.

14. Collins, M. N.; Birkinshaw, C. *Journal of Applied Polymer Science* **2008,** 109, (2), 923-931.

15. Collins, M. N.; Birkinshaw, C. *Journal of Applied Polymer Science* **2007,** 104, (5), 3183-3191.

16. Lai, J. Y. *Int J Mol Sci* **2012,** 13, (9), 10970-85.

17. Ramires, P. A.; Milella, E. *J Mater Sci Mater Med* **2002,** 13, (1), 119-23.

18. Lee, F.; Chung, J. E.; Kurisawa, M. *Soft Matter* **2008,** 4, (4), 880-887.

19. Loebel, C.; D'Este, M.; Alini, M.; Zenobi-Wong, M.; Eglin, D. *Carbohydrate Polymers* **2015,** 115, 325-333.

20. Kurisawa, M.; Lee, F.; Wang, L. S.; Chung, J. E. *Journal of Materials Chemistry* **2010,** 20, (26), 5371-5375.

21. Baier Leach, J.; Bivens, K. A.; Patrick, C. W., Jr.; Schmidt, C. E. *Biotechnol Bioeng* **2003,** 82, (5), 578-89.

22. Zawko, S. A.; Suri, S.; Truong, Q.; Schmidt, C. E. *Acta Biomater* **2009,** 5, (1), 14-22.

23. Leach, J. B.; Bivens, K. A.; Collins, C. N.; Schmidt, C. E. *J Biomed Mater Res A* **2004,** 70, (1), 74-82.

24. Lu, P. L.; Lai, J. Y.; Ma, D. H.; Hsiue, G. H. *J Biomater Sci Polym Ed* **2008,** 19, (1), 1-18.

25. Neises, B.; Steglich, P. D. W. *Angewandte Chemie* **1978,** 17, (7), 522-524.

26. Zhang, F.; He, C.; Cao, L.; Feng, W.; Wang, H.; Mo, X.; Wang, J. *Int J Biol Macromol* **2011,** 48, (3), 474-81.

27. Wu, W.; Mao, T.; Feng, X. *Zhongguo Xiu Fu Chong Jian Wai Ke Za Zhi* **2007,** 21, (4), 401-5.

28. Collins, M. N.; Birkinshaw, C. *Journal of Materials Science-Materials in Medicine* **2008,** 19, (11), 3335-3343.

29. Paterson, S. M.; Liu, L.; Brook, M. A.; Sheardown, H. *J Biomed Mater Res A* **2015,** 103, (8), 2602-10.

30. Oldinski, R. A.; Cranson, C. N.; James, S. P. *J Biomed Mater Res B Appl Biomater* **2010,** 94, (2), 441-6.

31. Hwang, H. D.; Cho, H. J.; Balakrishnan, P.; Chung, C. W.; Yoon, I. S.; Oh, Y. K.; Byun, Y.; Kim, D. D. *Colloids Surf B Biointerfaces* **2012,** 91, 106-13.

32. Calles, J. A.; Tartara, L. I.; Lopez-Garcia, A.; Diebold, Y.; Palma, S. D.; Valles, E. M. *International Journal of Pharmaceutics* **2013,** 455, (1-2), 48-56.

33. Nimmo, C. M.; Owen, S. C.; Shoichet, M. S. *Biomacromolecules* **2011,** 12, (3), 824-830.

34. Ding, J.; He, R.; Zhou, G.; Tang, C.; Yin, C. *Acta Biomaterialia* **2012,** 8, (10), 3643-3651.

35. Kodavaty, J.; Deshpande, A. P. *Defence Science Journal* **2014,** 64, (3), 222-229.

36. Antunes, J. C.; Oliveira, J. M.; Reis, R. L.; Soria, J. M.; Gomez-Ribelles, J. L.; Mano, J. F. *Journal of Biomedical Materials Research Part A* **2010,** 94A, (3), 856-869.

37. Skaalure, S. C.; Dimson, S. O.; Pennington, A. M.; Bryant, S. J. *Acta Biomater* **2014,** 10, (8), 3409-20.

38. Kim, I. L.; Mauck, R. L.; Burdick, J. A. *Biomaterials* **2011,** 32, (34), 8771-82.

39. Kang, J. Y.; Chung, C. W.; Sung, J. H.; Park, B. S.; Choi, J. Y.; Lee, S. J.; Choi, B. C.; Shim, C. K.; Chung, S. J.; Kim, D. D. *International Journal of Pharmaceutics* **2009,** 369, (1-2), 114-120.

40. Jackson T. Lewis, K. M. F., Tammy L. Haut-Donahue and Travis S. Bailey. *Submitted for Review at Nature Communications* **2017**.

41. Naficy, S.; Brown, H. R.; Razal, J. M.; Spinks, G. M.; Whitten, P. G. *Australian Journal of Chemistry* **2011,** 64, (8), 1007-1025.

42. Tomihata, K.; Ikada, Y. *J Biomed Mater Res* **1997,** 37, (2), 243-51.

43. Freutel, M.; Seitz, A. M.; Galbusera, F.; Bornstedt, A.; Rasche, V.; Tate, M. L. K.; Ignatius, A.; Durselen, L. *Journal of Magnetic Resonance Imaging* **2014,** 40, (5), 1181-1188.

44. Jones, R. S.; Keene, G. C. R.; Learmonth, D. J. A.; Bickerstaff, D.; Nawana, N. S.; Costi, J. J.; Pearcy, M. J. *Clinical Biomechanics* **1996,** 11, (5), 295-300.

45. Tissakht, M.; Ahmed, A. M. *Journal of Biomechanics* **1995,** 28, (4), 411-422.

46. Costi, J. J.; Stokes, I. A.; Gardner-Morse, M.; Laible, J. P.; Scoffone, H. M.; Iatridis, J. C. *Journal of Biomechanics* **2007,** 40, (11), 2457-2466.

47. Stokes, I. A. F. *Journal of Orthopaedic Research* **1987,** 5, (3), 348-355.

48. Armstrong, C. G.; Bahrani, A. S.; Gardner, D. L. *Journal of Bone and Joint Surgery-American Volume* **1979,** 61, (5), 744-755.

49. Guterl, C. C.; Gardner, T. R.; Rajan, V.; Ahmad, C. S.; Hung, C. T.; Ateshian, G. A. *Journal of Biomechanics* **2009,** 42, (9), 1275-1281.

CHAPTER 5

PHOTOPATTERNING HYALURONAN INTO THERMOPLASTIC ELASTOMER HYDROGELS

5.1 INTRODUCTION [5]

Hyaluronic Acid (HA) plays many roles in the healthy functioning of the eye, including an ability to stimulate corneal epithelial cell migration[1], protect against oxidative damage to cells [2] and increase corneal wettability due to enhanced water retention. [3, 4] These properties and many others have inspired the use of HA in a multitude of ophthalmic applications including vitreous replacement and corneal protection in ocular surgeries.[4] HA is also a key component in rewetting or comfort drops for not only its ability to increase wettability[4] but also decrease protein adsorption and lysozyme activity[5], thereby supporting a healthy tear film and creating relief for dry eyes. Unfortunately, this relief from dry eyes is very temporary as the drops are quickly lost to the nasolacrimal duct or absorbed by the eye resulting in at least a 90% loss of the drop after each application.[6]

Contact lens wearers are particularly susceptible to dry eye condition with five times as many reported symptoms as spectacle wearers and twelve times that of clinical emmetropes (those with perfect vision).[7] For a more sustained relief to dry eyes for contact lens wearers, as well as an increase in comfort, much research is being done in order to modify the surface of contact lens materials to enhance their surface wettability, particularly in silicone-based contact lenses.[5, 8, 9] Silicone contact lenses have a much higher permeability to oxygen than their

[5] The following chapter documents a preliminary study on the incorporation of photosensitive hyaluronan into TPE hydrogels. This chapter was written and prepared by Jackson Lewis.

traditional hydrogel lens competitors, however this comes at the cost of increased hydrophobicity due to the siloxane groups.[9] This lack of hydrophilicity has led to the copolymerization of polydimethylsiloxane (PDMS) with more conventional hydrogel materials such as poly(ethylene glycol) methacrylate to produce block copolymers with increased hydrophilicity while maintaining much of the oxygen permeability of the silicone lens.[9] There are several other approaches that have been employed in order to enhance surface wettability on silicone-based contact lenses such as surfactants and demulcents, however, a front runner for its added benefits in the reduction of protein adsorption and lysozyme activity are HA surface treatments.[5] These surface treatments consist of crosslinking HA onto the surface of these silicone lenses by using more traditional methods such as thiol-ene "click" chemistry[10] or even by using layer by layer deposition[9] and have resulted in lenses with higher wettability, lower protein adsorption and higher cytocompatibility. Some of the key factors in modifying the surface of these contact lenses with HA is to maximize wettability, cytocompatibility and comfort while minimizing protein fowling in order to support a healthy pre and post-lens tear film all without compromising the oxygen permeability of the silicone substrate.[6, 4, 5] Unfortunately, adding a homogenous layer of HA to the surface of the contact lens will likely lead to a compromised permeability to oxygen which has led to attempts to make the thickness of these HA surface treatments as thin as possible.[9]

Notably, the outer rim of the contact lens is in the most direct contact with the eye. Therefore, many of the benefits of HA may be achieved while allowing maximal oxygen permeability if HA is restricted to only the outer rim of the lens. Chapter 4 discussed the relevance and benefits of incorporating hyaluronan (HA) homogeneously throughout the surface region of our TPE hydrogels for meniscal applications in particular. These benefits included an

increase in modulus in both compression and tension as well as increased cytocompatibility and hydrophilicity. While the methodology to produce a homogeneous distribution of HA in the surface region is beneficial for many applications, such as in the development of a synthetic meniscus, creating a method to incorporate HA into exclusive regions of interest on the surface of our TPE hydrogels may be beneficial for contact lens surface treatments. Perhaps of equal interest is to adapt this protocol to make it suitable for the surface modification of a more desirable substrates such as silicone. This study will focus on the development of this surface treatment methodology on our TPE hydrogels as an initial proof of concept.

This controlled distribution of HA on the surface of our TPE hydrogels was thought to be achievable using photopatterning. Photopatterning allows for region controlled crosslinking by initiating a crosslinking reaction between light sensitive functionalities only in regions exposed to UV light. Unlike the traditional chemical crosslinking that took place in the HA surface treatment of our TPE hydrogels in Chapter 4, photopatterning takes place via a radical polymerization, and is therefore very rapid and short-lived, thereby confining infinite network formation only to regions exposed to UV light and the very immediate surroundings. Thus, region specific formation of an infinite network may be achievable through the use of an attenuating mask, which blocks specific regions of the hydrogel from exposure to UV light. In order to utilize this technique, polymers that are not inherently sensitive to UV light, such as HA, must be chemically modified with light sensitive functionalities. In order to add light sensitivity to HA it is often functionalized with an acrylate or methacrylate functionality.

The photopatterning of methacrylate functionalized HA into traditional hydrogels is of great interest for many unique biomedical applications. For example, Schmidt et al. have photo-patterned HA into conventional poly(ethylene glycol) (PEG) hydrogels to generate soft tissue

scaffolds for directed cell growth.[11] However, in these studies conventional solution-based crosslinking techniques are employed for the initial network formation. Schmidt's procedure involves the mixing photo-sensitive HA with oligomer solutions of PEG or PVA.[12] These solutions are then chemically crosslinked between PEG groups using solution based network formation before exposure to UV light.[12, 13] The photosensitive HA, now homogeneously mixed throughout the inside of the PEG hydrogel, is then exposed to UV light through an attenuating mask to trigger the crosslinking of HA into specific regions. [12] This type of methodology results in the photo-sensitive HA being patterned not just at the surface of the exposed regions but throughout the chemically crosslinked PEG hydrogel. The hydrogel is then placed into water and the HA inside of regions that were not exposed to light are easily rinsed from the hydrogel. [12]

This study presented here uses similar protocols to modify the HA with the photosensitive functionality methacrylate[11], but with TPE hydrogels the modified-HA, due to the use of high molecular weight HA (1MDa) in conjunction with the small pore size and high tortuosity present in the TPE hydrogel, it is largely confined to the immediate surface region at the swelling time scales used (24 - 48hrs) just like what was observed in Chapter 4. Once the TPE hydrogel is swollen in a modified-HA solution containing a photoinitiator, it can then be exposed to UV light through an attenuating mask, ultimately resulting in the formation of an interpenetrating network of HA only on the surface and only in the regions exposed to UV. The hydrogel is then rinsed and all of the uncrosslinked HA in the unexposed regions diffuse out of the hydrogel.

To qualitatively confirm the presence and location of HA in our TPE hydrogel, we initially used a traditional toluidine blue (TBO) polysaccharide stain. However, this technique proved insufficient, as it also stained the PEO matrix of the TPE hydrogel which made it difficult

to distinguish HA from the PEO matrix. Therefore, HA was modified with the fluorescent tag 5-aminofluoroscein before being modified with the photosensitive functionality methacrylate. This tag allowed us to more confidently observe the presence and position of HA inside the hydrogel matrix throughout the incorporation, crosslinking and rinsing process.

Figure 5.1 below shows how the photopatterning of HA into our TPE hydrogels at the surface takes place. Briefly, hyaluronan is modified with the fluorescent tag (green) 5 aminofluorescein, as well as with glycidyl methacrylate (black). Our melt processed and dry polystyrene-*b*-poly(ethylene oxide) (SO) and polystyrene-*b*-poly(ethylene-oxide)-*b*-polystyrene (SOS) disk (polystyrene: grey and poly(ethylene oxide): red) is then swollen in an aqueous solution containing the modified hyaluronan as well as a photoinitiator (Irgacure 2959). The HA swollen hydrogel (green) is then exposed to UV light through an attenuating mask (CSU ram pattern). In the regions of the swollen hydrogel that were exposed to the UV light, photopolymerization takes place locally, covalently binding adjacent methacrylate groups along the HA backbone, resulting in the formation of an interpenetrating covalent network (IPCN) of HA at the surface of the TPE hydrogel in the exposed regions. In the regions not exposed to UV light the HA remains unaltered and upon rinsing is removed from the hydrogel via the same diffusion mechanism from swelling, ultimately resulting in a TPE hydrogel with an infinite network of HA only in regions exposed to UV light.

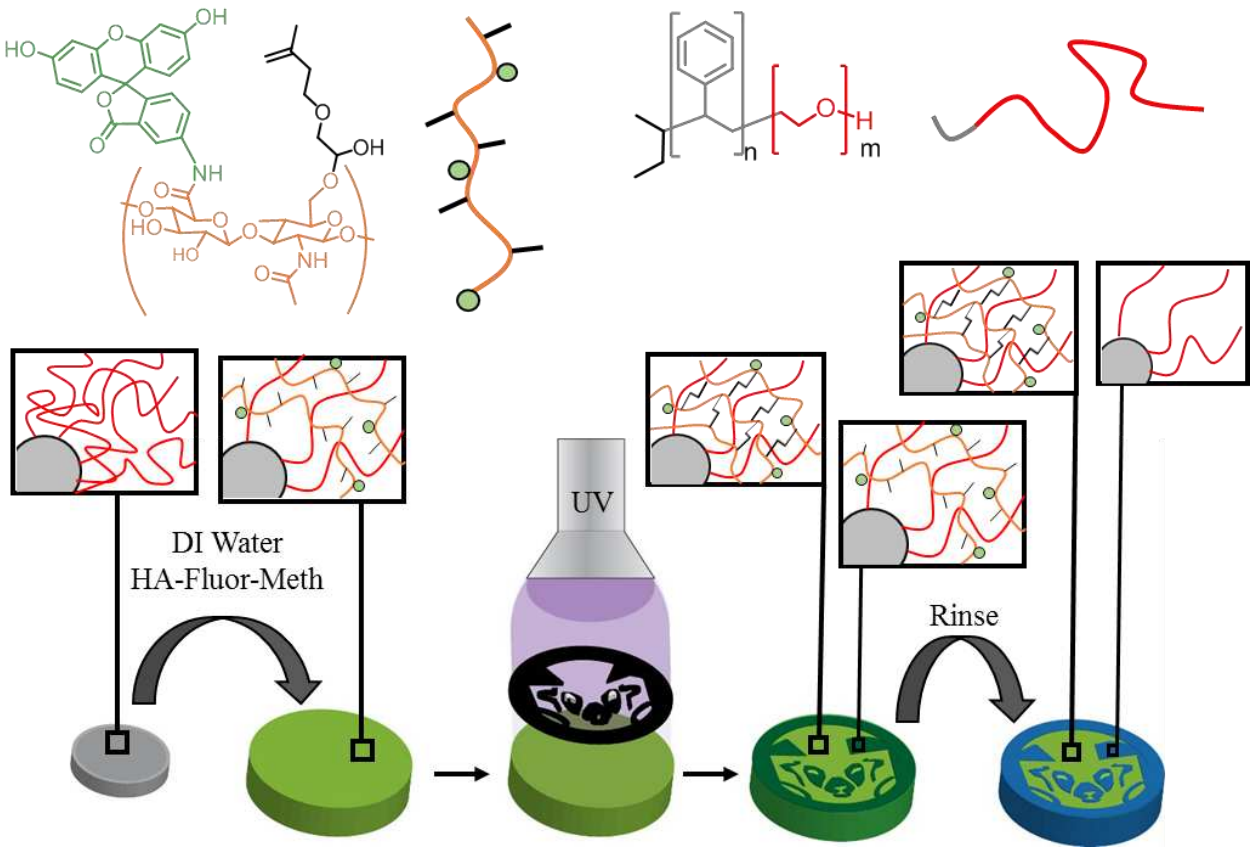

Figure 5.1: The incorporation of the fluorescently tagged (green circles) and methacrylate functionalized (black lines) HA via swelling into the thermoplastic elastomer. UV exposure through an attenuating mask (CSU Ram pattern), triggering a photopolymerization of the methacrylate functionalities, thereby forming an infinite network of modified HA in regions exposed to light. DI water rinse, removing unexposed HA from the hydrogel and revealing the controlled pattern of photopolymerized HA at the surface.

The following study will demonstrate our ability to modify HA with a fluorescent tag, further modify it with a photosensitive methacrylate group, and then pattern this modified HA into surface regions of interest in our TPE hydrogels through controlled exposure to UV light.

5.2 RESULTS AND DISCUSSION

5.2.1 Tagging Hyaluronic Acid with 5-aminofluorescein (HA-F)

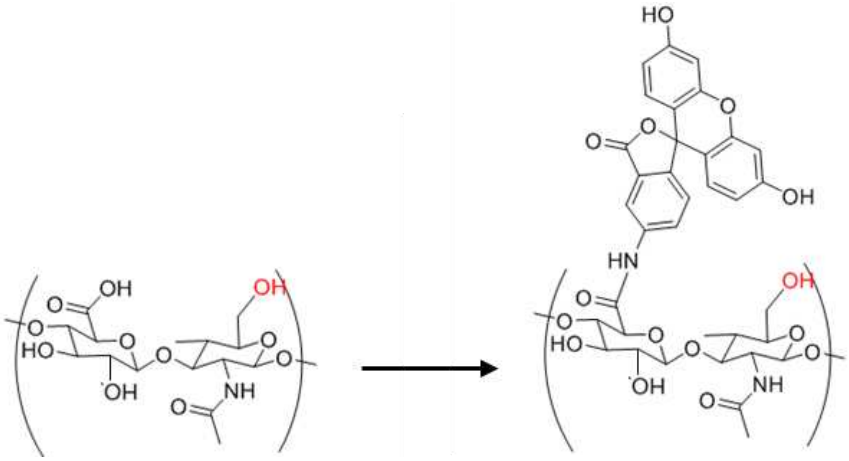

Figure 5.2: Change in the chemical structure of HA after modification with 5-aminofluorescein.

Hyaluronic Acid was first fluorescently labeled with 5-aminofluorescein according to protocols developed by Bryant et. al. [14] Briefly, HA was dissolved in hydrochloric acid / pyridine solution, mixed with 5-aminofluorescein and EDC, and allowed to react overnight. Following the reaction, the solution was dialyzed, precipitated, centrifuged, and re-dissolved in water. It was then re-precipitated and dried into a pellet of fluorescently-labeled HA (HA-F) using lyophilization.

The efficiency of the addition of 5-aminoflurescein to HA is very low [14]; therefore, it does not produce a significant signal when subjected to NMR, making it difficult to quantify. Also, the concentrations of HA-F necessary to run NMR proved too high with the limited quantities of HA used for this preliminary investigation (100 mg). However, because its primary purpose in this experiment is to allow for qualitative observation using a 365nm lamp, a simple experiment was conducted to confirm its presence. Two TPE hydrogels were swollen in two different solutions. The first hydrogel was swollen in an HA-F / DI water solution and the other

was swollen in an unmodified HA / DI water solution and allowed to reach equilibrium. The hydrogels were then examined under a handheld lamp with a 365nm filter (**Figure 5.3**).

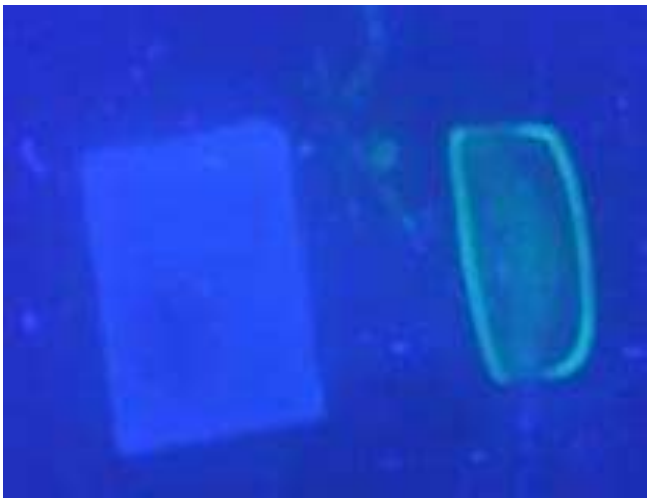

Figure 5.3: Two swollen SOS/SO hydrogels, swollen in unmodified HA (left) and HA-F (right) aqueous solutions beneath a handheld 365 nm lamp.

The SOS/SO hydrogel that was swollen in the HA-F solution fluoresces under the 365nm light source and produces a distinct green color, while the gel that was swollen in the unmodified HA solution does not. Because of the extensive dialysis and centrifugation that was performed to ensure there was no loose fluorescent tag, we can confidently say that the fluorescence that is observed is due to the presence of fluorescently tagged HA inside of the TPE hydrogel.

5.2.2 Adding methacrylate functionality to HA-F (HA-FM) using glycidyl methacrylate

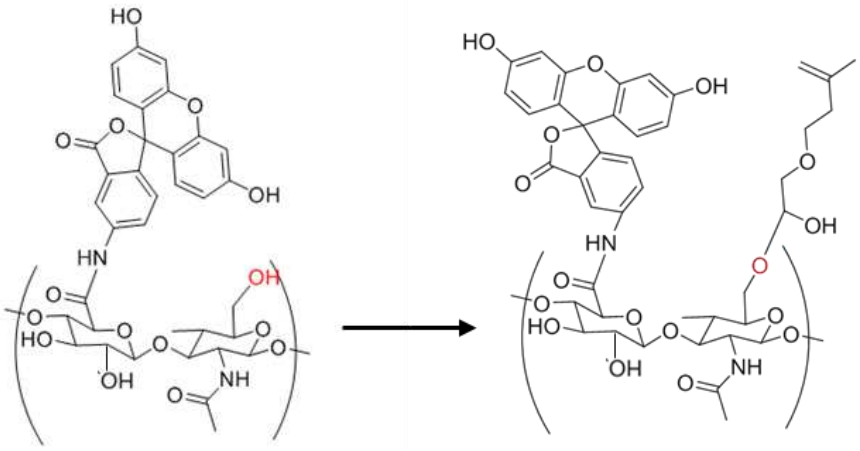

Figure 5.4: Change in the chemical structure of HA-F after reaction with glycidyl methacrylate.

The aforementioned HA-F was further modified through the addition of a methacrylate functionality using glycidyl methacrylate (HA-FM). This was done according to procedures developed by Schmidt et. al. {Leach, 2004 #4} and was chosen due to the semi-aqueous conditions used in the protocol for modification, limiting the exposure of HA to harsh solvents. Briefly, HA-F was dissolved in a mixture of acetone and water. Triethylamine and glycidyl methacrylate were added and the solution was allowed to stir overnight. The resulting HA-FM was then precipitated, re-dissolved, and recovered through lyophilization. The HA-FM was then subjected to NMR.

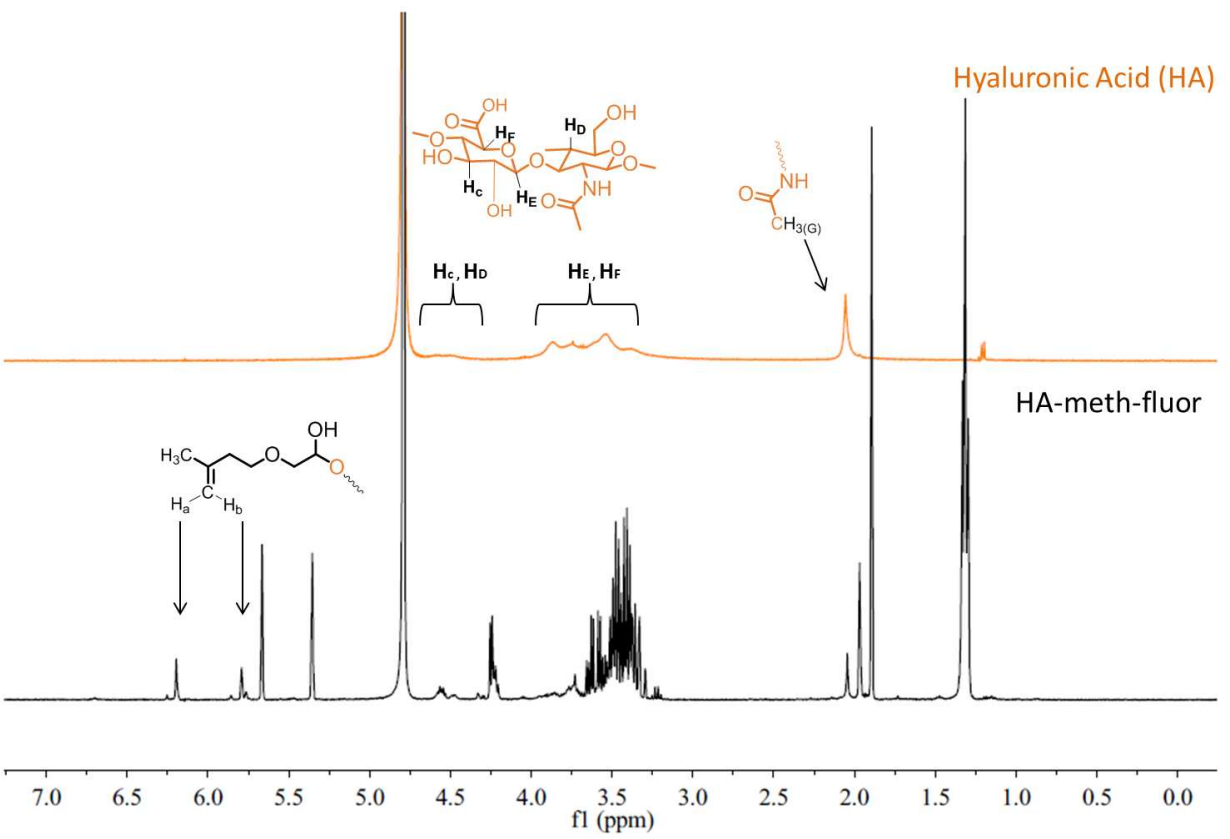

Figure 5.5: 1H-NMR of unmodified HA (top) and HA-FM (bottom).

The presence of peaks at ~5.75 and ~6.2 ppm in the HA-FM indicate the successful modification of HA with glycidyl methacrylate. Notably, there is also a change in the peaks that represent the hydrogens on the cyclic carbons of HA at ~3.5 ppm. This change in signal is likely due to a change in environment seen by those hydrogens caused by the presence of the new functionalities (fluorescein and methacrylate).

5.2.3 Formation of an infinite network of HA-FM on the surface of TPE hydrogels through exposure of UV light

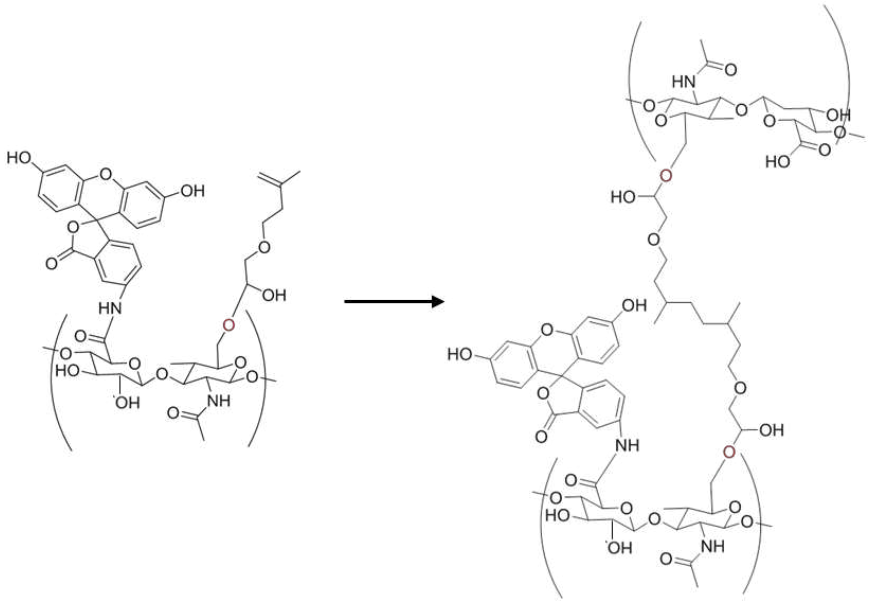

Figure 5.6: Polymerization of adjacent methacrylate functionalities on the backbone of HA-FM forming a covalent link between HA repeat units.

The formation of a second interpenetrating covalent network of HA-FM from exposure to UV was assessed through the following experiment. Two SOS/SO hydrogels were swollen in a DI water / HA-FM / Irgacure 2959 solution for 24 hours. One of the two hydrogels was then exposed to UV light for 5 minutes; the other was not exposed. The two hydrogels were then placed in water and rinsed in the dark for 60 hours. After 0, 36, and 60 hours of rinsing, photographs were taken with the hydrogels side by side, under a 365nm handheld lamp (**Figure 5.7**).

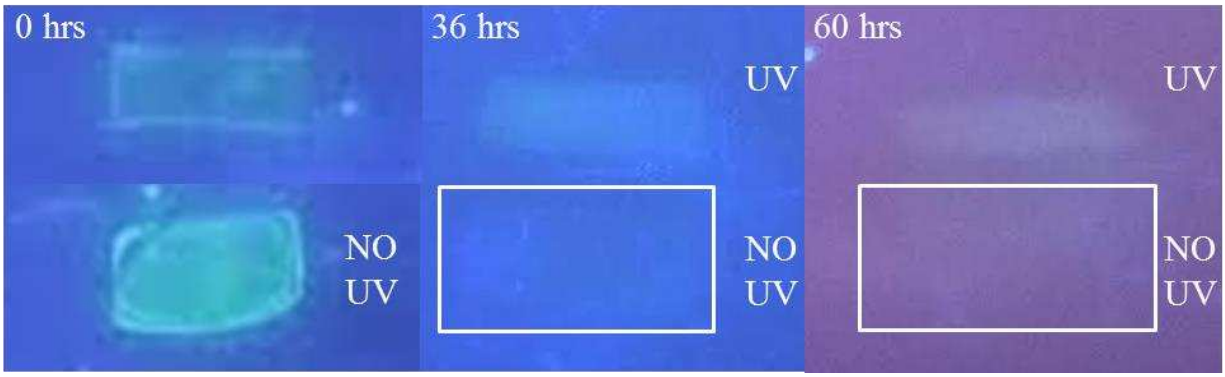

Figure 5.7: Image of two swollen SOS/SO hydrogels, swollen in a fluorescently tagged and methacrylate functionalized HA / Irgacure 2959 / DI water solution. The hydrogel that was exposed to UV light for 5 minutes (top) is compared to the hydrogel not exposed to UV light (bottom). The successive images captured under 365nm handheld lamp at the intervals before rinsing (0hrs) as well as 36 and 60 hrs of rinsing. The images show that the sample that was exposed to UV light was able to maintain its green color, indicating the presence of HA-FM, even after rinsing while the sample not exposed to UV was unable to maintain its green color upon rinsing, indicating that the HA-FM was removed from the TPE hydrogel.

Figure 5.7 reveals that the samples exposed to UV light maintained their fluorescence after rinsing, while those not exposed to UV light did not. This qualitatively suggests that photopolymerization of the HA-FM is taking place only when the samples are exposed to UV light, thus forming an infinite network of HA-FM, preventing it from leaving the hydrogel upon rinsing.

5.2.4 Photopatterning HA-FM on the surface of a hydrogel

The following experiment evaluates the ability of an attenuating mask to photopattern HA-FM on the surface of our TPE hydrogels. Hydrogels were again swollen in a DI water / HA-FM / Irgacure 2959 solution. Once swollen, the hydrogel was placed between two glass microscope slides with the attenuating mask—a CSU Ram logo printed on a transparency using a laser jet desktop printer—on top. The assembly was then placed under a UV light source for 8 minutes (**Figure 5.8**).

Figure 5.8: (Top) Glass slide, HA-FM swollen hydrogel and attenuator assembly. (Bottom) UV light source used to photopattern HA-FM into TPE hydrogel.

The observed effect was a controlled delivery of UV light. Unfortunately, the intensity and exposure time of the light caused photo-bleaching of the fluorescein tag in the HA-FM. This is clear because the photopattern emerges before rinsing (**Figure 5.9B**). Following the exposure to UV light the sample was placed into water in order to rinse any HA-FM that was not photopolymerized. After 60 hours of rinsing the pattern was still present on the gel. This is indicative that the dark portion of the mask was letting in enough light to photo-polymerize the HA-FM without photobleaching the fluorescein tag (**Figure 5.9**).

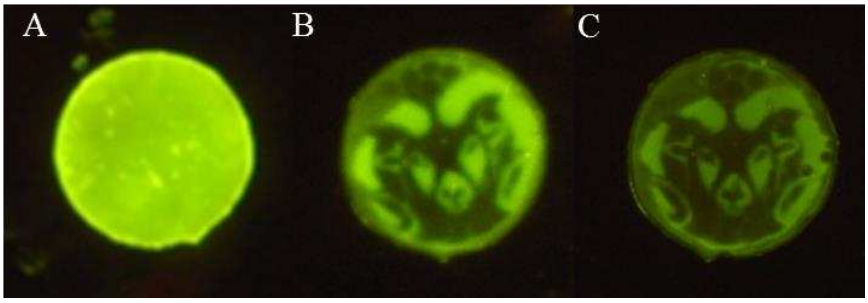

Figure 5.9: Image of SOS/SO hydrogel swollen in HA-FM / DI water under a 365 nm handheld lamp (A) before exposure to UV (B) immediately after exposure to UV and (C) after exposure to UV and subsequent 60-hour rinse in DI water.

In order to create optimal conditions that avoided photobleaching the fluorescein of the HA-FM, while still exposing the HA-FM to enough UV light to induce photopolymerization of the methacrylate functionality, a new attenuating mask was created. This experiment was repeated with a new attenuating mask that consisted of two distinct layers: one layer of ink the same opacity as the "dark" regions in the previous experiment and a square piece of duct tape to block as much UV light as possible in that region (**Figure 5.10**).

Figure 5.10: Attenuating masks placed in a window sill in order to demonstrate qualitatively the relative amounts of light passing through. The second attenuator which was printed "dark" across the whole mask and then a square piece of duct tape placed over the center in order to better block the light.

The experiment was repeated with the new attenuating mask. **Figure 5.11A** is an image of the hydrogel before exposure to UV light and **Figure 5.11B** is an image immediately after exposure to UV light and before rinsing. The identical and homogeneous glow between the

hydrogel in **Figure 5.11A** and **5.11B** show that minimal photobleaching took place. Once the sample was allowed to rinse for 3 hours the region that was under the duct tape lost all fluorescence while the rest of the hydrogel remained fluorescent. This is likely demonstrating, qualitatively, that the region that was not exposed to UV light (under the duct tape) did not crosslink the HA-FM and thus rinsed out when placed into water, while the remaining HA-FM that was exposed to UV light remained even after rinsing. It appears that the remaining HA-FM has been photopolymerized, resulting in an infinite network, and is therefore unable to leave the SOS/SO hydrogel.

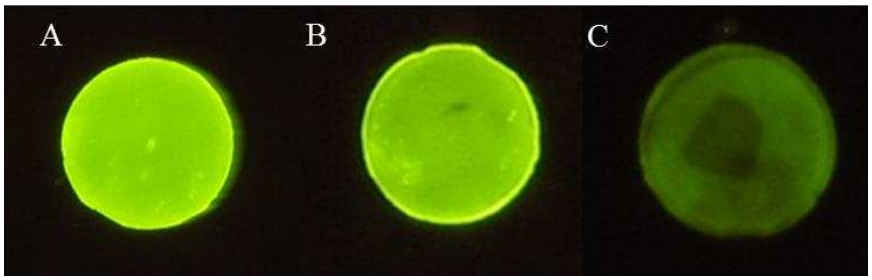

Figure 5.11: Image of SOS/SO hydrogel swollen in HA-FM / DI water (A) before exposure to UV (B) after exposure to UV and (C) after exposure to UV and subsequent 3-hour rinse in DI water. The emergence of the attenuator's pattern (square piece of duct tape) on the hydrogel after rinsing signifies that the HA-FM in this region, that was not exposed to UV light, was not photopolymerized and was therefore easily removed from the hydrogel via rinsing.

This experiment was repeated with the more complex pattern of the CSU Ram logo. This was done by printing multiple layers of ink over the transparency. The first layer of ink was homogeneously printed over the transparency sheet to act as an attenuator to prevent photobleaching. The second layer of ink was printed over the transparency sheet in the pattern of the CSU Ram logo (**Figure 5.12 top**).

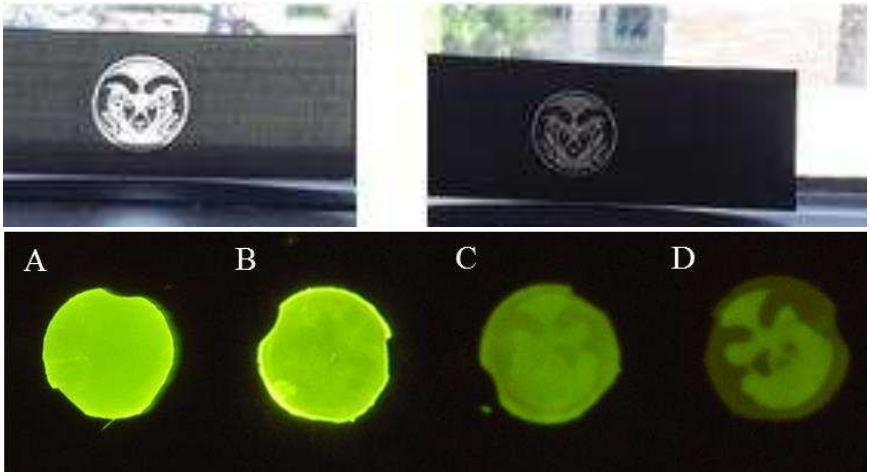

Figure 5.12: TOP: (left) initial attenuating mask that let too much light in the transparent regions and just enough in the dark regions (right) second attenuating mask where the transparent region is equivalent to the initial dark region and the dark region consists of an additional layer of ink. BOTTOM: Image of SOS/SO hydrogel swollen in HA-FM / DI water solution (A) before exposure to UV (B) After exposure to UV (C) after exposure to UV and subsequent 3-hour and (D) 60-hour rinse in DI water. The emergence of the attenuator's pattern (CSU Ram logo) on the hydrogel after rinsing signifies that the HA-FM in this region, that was not exposed to UV light, was not photopolymerized and was therefore easily removed from the hydrogel via rinsing.

This experiment showed minimal observable photobleaching, demonstrated by the same homogeneous fluorescence between the samples before (**Figure 5.12A**) and after (**Figure 5.12B**) exposure to UV light. Following exposure, the sample was placed in DI water and rinsed for 3 hours (**Figure 5.12C**) and finally 60 hours (**Figure 5.12D**). The emergence of the CSU Ram logo upon rinsing reinforces the conclusion reached from the crude duct tape mask attenuator. The lack of resolution in the image could be due to several factors including: scattering of light due to the ink attenuator, the mask allowing small amounts of light through in "dark" areas, inhomogeneity in the light source intensity and bleeding and scattering of light inside of the hydrogel.

5.2.5 Assessing potential degradation of SOS/SO hydrogel due to prolonged UV exposure

One of the major obstacles when working with UV light is UV degradation. It is critical to use enough UV exposure to initiate the polymerization of the methacrylate functionality, but

not so much UV exposure as to trigger a radical degradation of either the SOS/SO hydrogel or the hyaluronic acid. The next experiment evaluated the effect of various durations of UV exposure on the same hydrogel swollen in the HA-FM / DI water solution. A black mask (that allowed no measurable amount of UV light) was placed on top of the rectangular hydrogel to initially block 2/3 for 9 minutes and then 1/3 of the hydrogel for 1 minutes from UV at a 22mW/cm^2 intensity. Notably, the hydrogel in **Figure 5.13A** appears to have a lower concentration of HA-F in the upper 2/3 of the sample, however this is an illusion created by water adhesion in those darker regions.

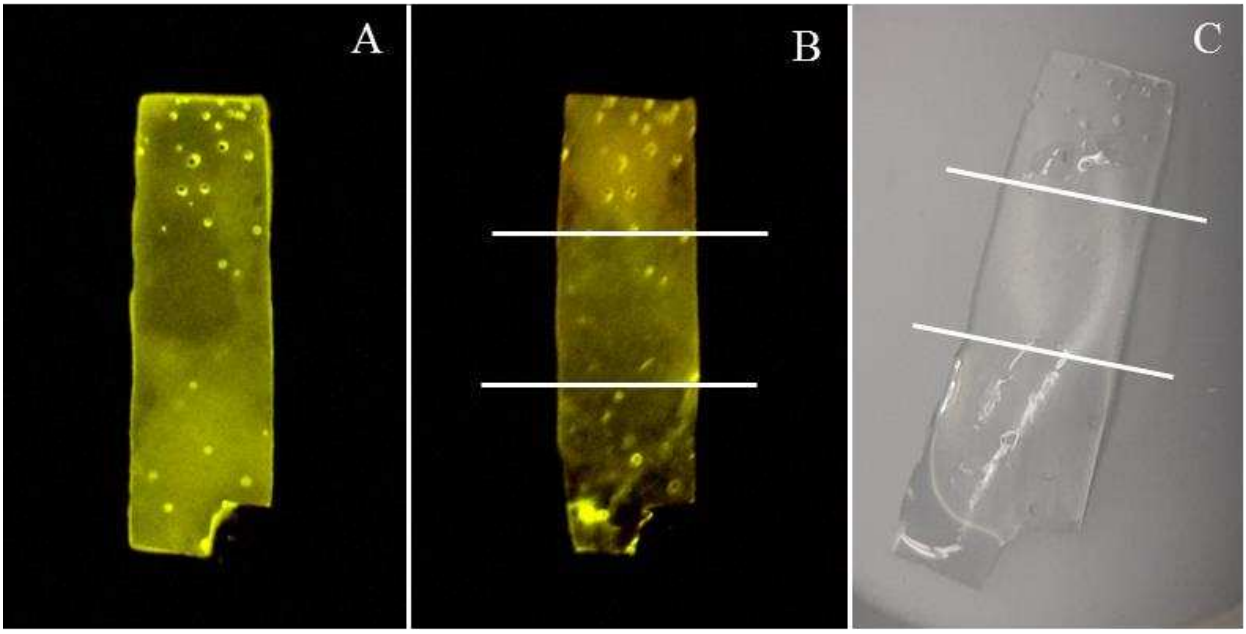

Figure 5.13: Rectangular hydrogel swollen in the HA-FM / DI water solution. (A) Swollen hydrogel before exposure to UV light under 365 nm lamp. (B) Swollen hydrogel after exposure to UV light under 365 nm lamp. (C) Swollen hydrogel after exposure to UV light and subsequent rinse in DI water under normal lighting.

In the region of the hydrogel that was exposed to UV light for the longest amount of time (10 minutes) there is a clear increase in equilibrium swelling ratio that becomes apparent after the hydrogel is rinsed in DI water. This may be due to the presence of the highly hydrophilic HA

in that region causing that region to swell more. This increased swelling could more likely be due to degradation in the SOS/SO network due to UV degradation. This damage would likely take place at the dibromoxylene linkage, as alkenes are more likely to produce radicals leading to chain scission. This will likely need to be assessed further in order to tune the amount of UV exposure to initiate crosslinking without degradation of the SOS/SO network. This phenomena of the degradation of SOS at the DBX linkage after prolonged exposure to UV light was observed by work done by Huq et al. where a reduction of up to 5 mol% SOS was observed after 40 min of UV exposure at similar intensities.

5.3 CONCLUSIONS AND FUTURE WORK

The ability to incorporate HA into our TPE hydrogels has already demonstrated many advantages including improvements in modulus and cytocompatibility (Chapter 4). This added ability to photopattern HA into our TPE hydrogels may give us access to new and exciting methodology that could open the door to many unique applications including those involving contact lenses. This ability to selectively reinforce regions of interest in our TPE hydrogels may also give us access to controlled mechanical anisotropy. This study demonstrated qualitatively that through the modification of HA with a light sensitive methacrylate functionality we were able to control and direct crosslinking of the HA inside of the TPE hydrogel.

Additional characterization is needed in order to provide quantitative measurements to confirm the presence and amount of HA that is present inside of the system before and after rinsing. This can be accomplished through ATR-FTIR and TGA as was discussed in Chapter 5. ATR-FTIR may provide the unique opportunity to probe regions that were exposed and not exposed to UV light and demonstrate region-specific differences. While using ink as an attenuator in order to prevent photobleaching was sufficient to prove the principle, these

experiments likely need to be repeated with darker “dark” regions and a more controlled light source. The photobleaching problem may be remedied by finding exposure times and intensities that do not cause photobleaching but are still able to crosslink HA sufficiently. It would also be of great benefit to select a fluorescent tag that is more resistant to photobleaching in order to better track the position of HA.

It is also important to compare the method by which the infinite network of HA is formed (e.g. chemical crosslinking with EDC vs. a photopatterning approach with a methacrylate functionality) and the impact on the desirable properties of HA, such as cytotoxicity, hydrophilicity and lubricity. The impact of incorporating HA in a specific pattern to promote region specific stiffening still needs to be assessed via mechanical testing. This may be done by creating attenuators in vertical or horizontal stripe patterns and running tensile testing in parallel or perpendicular to the stripes. The susceptibility of the SOS/SO hydrogel to UV degradation at the dibromoxylene site must also be further assessed in order to find SOS/SO as well as HA’s tolerance to UV exposure. This analysis may lead to the conclusion that different coupling agents for SO diblock to form SOS triblock should be employed that are not as susceptible to radical degradation.

5.4 EXPERIMENTAL

Materials: Styrene (99%, 4-tert-butylcatechol inhibitor, Aldrich) and ethylene oxide (99.5+%, compressed gas, Aldrich) monomer were each purified by successive vacuum distillations (10–20 mTorr) from dried di-n-butylmagnesium (1.0 M solution in heptane, Aldrich) before use. Both purified styrene and ethylene oxide monomer were stored in glass burettes in the dark, at room temperature (styrene) and 3 °C (ethylene oxide), respectively, before use (typically less than 24 h). Argon degassed cyclohexane (CHX) was purified by passing the solvent over activated alumina followed by Q-5-like supported copper catalyst (Glass Contour, proprietary). Argon degassed tetrahydrofuran (THF) was purified by passing the solvent over activated alumina. High-purity argon (99.998%, Airgas) was passed through additional oxygen and moisture traps prior to use. Glassware and polymerization reactors were flamed under vacuum and backfilled with argon multiple times. ^{1}H NMR spectra were collected at room temperature in $CDCl_3$ on a Varian Inova 400MHz Spectrometer (n=32, delay=30 s). Size exclusion chromatography (SEC) was performed on a Viscotek GPC-Max chromatography system fitted with three 7.5 x 340 mm Polypore^{TM} (Polymer Laboratories) columns in series, an Alltech external column oven, and a Viscotek differential refractive index (RI) detector. Measurements were performed using a DMF (55 °C) mobile phase (1 mL/min) with PS standards (Polymer Laboratories). Final SO/SOS compositions were confirmed via relative peak integrations in the SEC chromatograms of these blends. Sodium Hyaluronate (1MDa, Lifecore Biomedical), Dialysis Tubing, 5-aminofluorescein (Sigma Aldrich), glycidyl methacrylate (Sigma Aldrich), Irgacure 2959 (Sigma Aldrich).

Synthesis of polystyrene, polystyrene-*b*-poly(ethylene oxide) and polystyrene-*b*-poly(ethylene oxide)-*b*-polystyrene were all conducted on samples synthesized from prior experiments whose chemical synthesis is described in chapter 3.

Preparation of dry SO/SOS disks Dry 32 mol% SOS / 68 mol% SO polymer was placed into a steel washer (8mm x 0.73mm thick) and sandwiched between two sheets of Kapton. This assembly was then placed into a Carver Press and was heated to 150°C and compressed at ~500 psi for 5 minutes. Samples were removed and allowed to cool to room temperature and their masses were recorded before swelling.

Adding fluorescein functionality to hyaluronic acid (HA-F) Hyaluronic acid was fluorescently labeled with 5-aminofluorescein according to protocols developed by Bryant et. al. 48mg of 1 MDa hyaluronic acid was dissolved in 12ml of a hydrochloric acid /pyridine solution (75/25 wt.%) containing 70.5mg of 5-aminofluorescein and 0.965g of EDC, this mixture produced a dark orange color and was allowed to react overnight.

Following the reaction, the HA solution was transferred to (100kDa MW cutoff) cellulose dialysis tubing and was dialyzed against 3.5L of DI water. The 3.5L of DI water containing the small molecular weight species (<100 kDa) was replaced with fresh DI water every 12 hours for 48 hours. Once the dialysis was complete, the fluorescently tagged HA was precipitated by pouring the HA solution into chilled ethanol (4°C) with 1.25 wt.% sodium acetate (25 ml). The ethanol solution containing the precipitated and fluorescently tagged HA was then transferred to a centrifuge tube and centrifuged for 10 minutes. The recovered fluorescently tagged HA pellet was then re-dissolved in water, re-precipitated and re-centrifuged. The fluorescently tagged HA

pellet recovered from the second centrifugation was re-dissolved in water and dried via lyophilization.

Qualitative comparison of relative fluorescence between HA-F swollen and HA swollen TPE hydrogels The recovered hyaluronic acid tagged fluorescein was then dissolved in water at a concentration of 5mg HA-F/6mL (0.083 wt. % HA-F). One dry and melt processed SOS/SO disk (0.015g) was then swollen in the HA-F solution for 24 hours in parallel with another SOS/SO disk (0.015g) swollen in a 0.083 wt. % solution of unmodified HA, both were removed from the solution and dabbed dry. The gels were then examined under a handheld lamp with a 365nm filter

Adding methacrylate functionality to fluorescently functionalized hyaluronic acid (HA-FM) Briefly, HA (1MDa) (100 mg) was dissolved in a 50/50 wt. % mixture of acetone and water. 20 molar equivalence per repeat unit of HA of triethylamine (0.595g) and glycidyl methacrylate (0.836g) were added and the solution was allowed to stir overnight. The methacrylate functionalized HA was precipitated into acetone (20 ml) The HA was then re-dissolved in water (1 ml) and precipitated (20 ml) in an effort to further remove any small molecular weight contaminants and dried via lyophilization for 24 hrs.

Photopatterning HA-FM into SOS/SO hydrogel A SOS/SO melt processed polymer disk (0.015 g) was placed into a 0.1 wt. % solution of HA-FM containing the photoinitiator Irgacure 2959 (1 mg HA-FM/ 5mg Irgacure 2959 /ml DI water) and allowed to swell and reach equilibrium for 24 hours. Once swollen, the hydrogel was placed between two glass microscope slides with an attenuating mask (transparency with laser jet printed CSU ram pattern) placed on top of the top microscope slide. The assembly was then placed under 365 nm filtered at an intensity of 22 W / cm^2 using a UV light source for 8 minutes. Following the exposure to UV light, the sample was placed into DI water and rinsed for 60 hours with pictures taken under a 365 nm lamp at 0, 3 and 60 hrs.

REFERENCES

1. Inoue, M.; Katakami, C.,The effect of hyaluronic acid on corneal epithelial cell proliferation, *Invest Ophthalmol Vis Sci* **1993,** 34, (7), 2313-5.

2. Presti, D.; Scott, J. E.,Hyaluronan-Mediated Protective Effect against Cell-Damage Caused by Enzymatically Produced Hydroxyl (Oh-Center-Dot) Radicals Is Dependent on Hyaluronan Molecular-Mass, *Cell Biochemistry and Function* **1994,** 12, (4), 281-288.

3. Lapcik, L.; Lapcik, L.; De Smedt, S.; Demeester, J.; Chabrecek, P.,Hyaluronan: Preparation, structure, properties, and applications, *Chemical Reviews* **1998,** 98, (8), 2663-2684.

4. Rah, M. J.,A review of hyaluronan and its ophthalmic applications, *Optometry-Journal of the American Optometric Association* **2011,** 82, (1), 38-43.

5. Van Beek, M.; Jones, L.; Sheardown, H.,Hyaluronic acid containing hydrogels for the reduction of protein adsorption, *Biomaterials* **2008,** 29, (7), 780-789.

6. Fonn, D.,Targeting contact lens induced dryness and discomfort: What properties will make lenses more comfortable, *Optometry and Vision Science* **2007,** 84, (4), 279-285.

7. Nichols, J. J.; Ziegler, C.; Mitchell, G. L.; Nichols, K. K.,Self-reported dry eye disease across refractive modalities, *Investigative Ophthalmology & Visual Science* **2005,** 46, (6), 1911-1914.

8. Van Beek, M.; Weeks, A.; Jones, L.; Sheardown, H.,Immobilized hyaluronic acid containing model silicone hydrogels reduce protein adsorption, *Journal of Biomaterials Science-Polymer Edition* **2008,** 19, (11), 1425-1436.

9. Lin, C. H.; Cho, H. L.; Yeh, Y. H.; Yang, M. C.,Improvement of the surface wettability of silicone hydrogel contact lenses via layer-by-layer self-assembly technique, *Colloids and Surfaces B-Biointerfaces* **2015,** 136, 735-743.

10. Korogiannaki, M.; Zhang, J. F.; Sheardown, H.,Surface modification of model hydrogel contact lenses with hyaluronic acid via thiol-ene "click" chemistry for enhancing surface characteristics, *Journal of Biomaterials Applications* **2017,** 32, (4), 446-462.

11. Leach, J. B.; Bivens, K. A.; Collins, C. N.; Schmidt, C. E.,Development of photocrosslinkable hyaluronic acid-polyethylene glycol-peptide composite hydrogels for soft tissue engineering, *Journal of Biomedical Materials Research Part A* **2004,** 70A, (1), 74-82.

12. Zawko, S. A.; Suri, S.; Truong, Q.; Schmidt, C. E.,Photopatterned anisotropic swelling of dual-crosslinked hyaluronic acid hydrogels, *Acta Biomaterialia* **2009,** 5, (1), 14-22.

13. Suri, S.; Schmidt, C. E.,Photopatterned collagen-hyaluronic acid interpenetrating polymer network hydrogels, *Acta Biomaterialia* **2009,** 5, (7), 2385-2397.

14. Skaalure, S. C.; Dimson, S. O.; Pennington, A. M.; Bryant, S. J.,Semi-interpenetrating networks of hyaluronic acid in degradable PEG hydrogels for cartilage tissue engineering, *Acta Biomaterialia* **2014,** 10, (8), 3409-3420.

CHAPTER 6

PROGRESS TOWARD SUTURE MODIFICATION AND INCORPORATION INTO THERMOPLASTIC ELASTOMER HYDROGELS AND FUTURE WORK

6.1 INTRODUCTION [6]

This chapter investigates the plasma surface modification of nylon medical sutures and subsequent attempts to covalently attach these sutures to a thermoplastic elastomer (TPE) hydrogel via an interpenetrating covalent network (IPCN) of hyaluronic acid acting as a bonding intermediary. It was hypothesized that the covalent attachment between these surface modified nylon medical sutures and a TPE hydrogel would (1) mechanically reinforce the hydrogel in tensile loading and (2) provide a potential means of surgical attachment if extended through the anterior and posterior horns of a potential implant. This chapter assesses the effectiveness of plasma treatment in generating the reactive chemical functionalities necessary for covalent attachment. This chapter will then evaluate if any additional resistance to suture pullout from the hydrogel occurred as a result of any covalent attachment between the suture and the hydrogel. Finally, the chapter will conclude with an appraisal of the validity this approach in achieving a suture / hydrogel composite.

As was discussed in previous chapters, hydrogels have long been considered as ideal candidates for a myriad of biomedical applications due to their high water content and biologically relevant properties.[1] However, hydrogels have not yet demonstrated the mechanical

[6] This chapter was written and prepared by Jackson Lewis. Michelle Mann ran all plasma treatment and subsequent characterization via XPS. Jackson Lewis performed all chemical syntheses and also ran all corresponding mechanical pullout testing.

viability necessary for many mechanically demanding conditions such as those seen by the knee meniscus. In particular, conventional hydrogels possess insufficient moduli, elasticity, toughness and resistance to fatigue for applications such as these.[1] While our TPE hydrogels have demonstrably overcome many of these mechanical limitations that have prohibited hydrogels from being considered as synthetic meniscus replacements, including producing a high compressive modulus (1 MPa), recoverability at extreme tensile ($\lambda > 5$) and compressive strains (99%), and an unprecedented resistance to fatigue (> 100k loading cycles at a 1 Hz cycle frequency), these TPE hydrogels still remain one to two orders of magnitude lower in tensile modulus when compared to native meniscal tissue (50-200 MPa).[2]

In order to mechanically reinforce conventional hydrogels, particularly in tensile loading, many groups have developed hydrogel / polymer fiber composite materials. These composites use traditional hydrogels such as polyvinyl alcohol (PVA)[3], polyampholyte[4], poly (2-hydroxyethylmethacrylate) (PHEMA)[5], and polyethylene glycol (PEG)[6] and reinforce them with natural and synthetic polymer fibers such as cellulose[6], polycaprolactone (PCL)[5], polyurethane[4], and ultra-high molecular weight polyethylene (UHMWPE)[3]. Crosslinking these conventional hydrogels to underlying fibers to generate composite materials has often resulted in over an order of magnitude increase in tensile modulus and toughness.[3] However, the lack of assessment of these brittle hydrogel / fiber composites in high cycle loading regimes may suggest that many of the same brittle failure mechanisms associated with the neat conventional hydrogels are still present in these composite materials.

It is hypothesized that if these tensile reinforcing fibers are successfully incorporated and covalently attached within our TPE hydrogels it will not only mimic the tensile reinforcement observed in these conventional hydrogel / polymer fiber composites, but will do so while

preserving the compressive modulus, toughness, elasticity and fatigue resistance observed in the neat TPE hydrogel. Additionally, the successful incorporation of medical sutures into our TPE hydrogel may provide an effective and easily integrable attachment method of the would-be synthetic meniscal replacement to the tibial plateau that is familiar to surgeons (**Figure 6.1**).

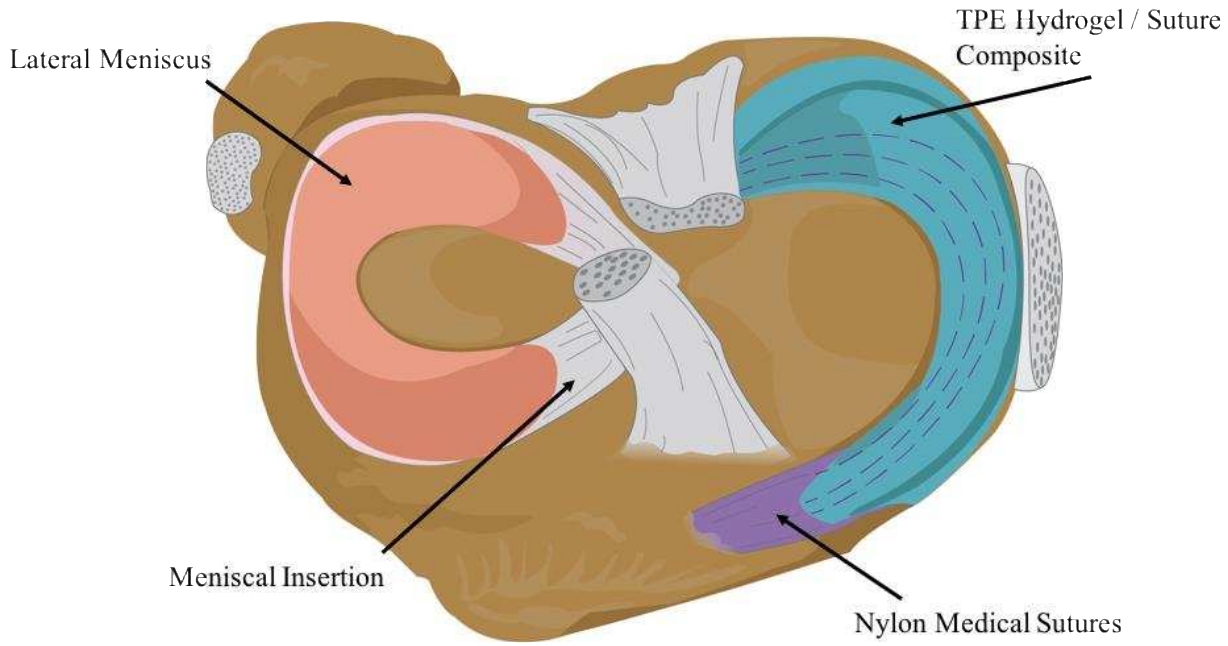

Figure 6.1: (*Left/Lateral*) Transverse and caudal view of tibial plateau demonstrating the natural transition from meniscal body to the insertions in the tibial plateau via the meniscal horn as it occurs in nature. (*Right/Medial*) Proposed approach of using surface treated medical sutures to reinforce the bulk surface treated hydrogel for a means of attachment to the tibial plateau. Surface modified medical sutures (purple) will be run in a circumferential orientation throughout the surface treated hydrogel and, after crosslinking, will form a covalent bond between the hydrogel and the suture.

Figure 6.1 above shows a theoretical depiction of a composite material consisting of our HA surface treated TPE hydrogel covalently bound to nylon medical sutures after being surgically incorporated into the knee joint. If the hydrogel can effectively transmit the vertical load observed in the knee joint into the medical sutures via hoop stress, then the synthetic composite may be able to mimic the tissue in its ability to handle native stresses. While assessment of the mechanical capability of a would-be composite as well as the surgical viability

of an approach like this is necessary, the following study will focus solely on the covalent attachment of a single nylon medical suture to our TPE hydrogels.

Covalent Attachment of Nylon Suture to TPE Hydrogel via the Bonding Intermediary HA

The successful incorporation of HA as a secondary IPCN, discussed in Chapter 4, provided a myriad of benefits, including reduced cytotoxicity as well as an increased modulus in both compression and tension. Further still, this successful incorporation of HA produced the high concentration of chemical functionality, not present in high SOS content regimes, necessary to covalently bond our TPE hydrogel to nylon suture. Notably, this additional chemical functionality produced through the HA surface treatment is restricted to the immediate surface of the hydrogel (Chapter 4) making it seemingly inaccessible to the suture-hydrogel interface which would occur in the bulk of the material. However, if the suture is incorporated into the bulk of the thermoplastic during melt processing, it will generate of a new surface at the suture-polymer interface. Thus, upon swelling, a channel will emerge at the suture-hydrogel interface making the hydrogel surface in this channel, theoretically, subject to the same HA diffusion mechanics observed at the outermost hydrogel surface discussed in Chapter 4. Unfortunately, while our HA surface treated TPE hydrogel may possess the high chemical functionality needed for covalent attachment to a nylon suture, nylon is comprised of a sequence of very stable amide linkages, which do not accommodate covalent attachment without significant chemical modification.

Several chemical modification strategies were considered in order to add the necessary chemical functionality to the surface of the nylon suture. Many of these strategies were built on work by Jia et al. who demonstrated that a strong nucleophile could be generated at the surface

of nylon through the deprotonation of the amide group via the strong base tert-butoxide (tBuOK) (**Figure 6.2**). The generation of this nucleophile makes the amide group susceptible to S_N2 reactions with alkyl halides. Several alkyl halides were considered to add the necessary chemical functionality to nylon, two of which, are presented in the future work section of this chapter. For example, one of these crosslinking methods included the addition of furan and maleimide groups, to the suture and HA respectively, to achieve a reversible Diels-Alder cycloaddition between the HA and the suture upon heating. Another strategy consisted of the addition and methylation of a pendant alkyl amine to generate a strong positive charge at the nylon suture surface, which would in turn, form a recoverable ionic interaction with HA, a natural polyanion.

However, in order to fully utilize the cytocompatible HA surface treatment developed in Chapter 4, as well as preserve the hyaluronan's natural chemical structure as much as possible, it was of particular interest to develop chemistries that promoted crosslinking between nylon and hyaluronan using the same EDC based crosslinking chemistry described in Chapter 4. Therefore, the two chemical functionalities that were of interest to add to the surface of the nylon suture were either a hydroxyl or a primary amine. Both a hydroxyl group and a primary amine will form a stable ester or amide linkage (respectively) with the carboxylic acid of HA when subjected to the EDC chemistry from Chapter 4. One method to add a primary amine at the surface of nylon using the S_N2 reaction mechanics proposed by Jia et al. is through the addition of the alkyl amine 2-bromoethylamine hydrobromide (BEA- HBr) to the deprotonated amide of nylon.[7] (**Figure 6.2**).

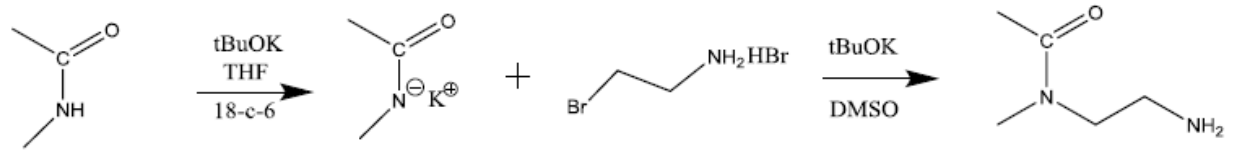

Figure 6.2: Addition of ethyl amine to nylon through deprotonation of the secondary amide of nylon followed by substitution with 2-bromoethylamine.

While these chemical modification strategies used to add functionality to the nylon suture are effective, there was concern that the use of such strong basicity, or in other modification techniques harsh solvent conditions, may impact the bulk mechanical characteristics of the nylon sutures. Therefore, the need to maintain the suture's mechanical integrity, as well as the recognition that covalent attachment of the suture was limited to a surface reaction, led us to focus on strategies that limited modification only to the immediate surface of the nylon suture.

Plasma treatment is a very effective way to add functionality to the immediate surface of polymeric substrates.[8] Plasma surface treatment of polymers takes place when a polymer substrate in a vacuum chamber is exposed to a process gas that is ionized through exposure to radiofrequency (RF) energy. The active species in the ionized gas collide with the polymer substrate and generate reactive free radicals. These free radicals react with the ionized gas to form new species that can form stable bonds with the polymer surface. Plasma surface treatment is solvent free, low temperature, inexpensive and ideal method to quickly add different surface functionality to a polymer substrate by simply changing the source gas for the plasma. Notably, this is all accomplished without impacting the bulk mechanical characteristics of the polymeric substrate being modified.[9] However, it is important to note that some source gases, such as oxygen, can effectively etch the surface of the polymer substrate and generate pore structures. In these systems the surface functionality that is generated is easily rinsed away.

Work by Fisher et al. demonstrated that by using H_2O as a source gas for their plasma modification they could generate stable surface functionality, often for over two years, on polyethersulfone, polysulfone and polyethylene. Fisher et al. also demonstrated that amine functionality could be added to the surface of polycaprolactone and silicon wafers through allyl amine plasma copolymerization.[10] The ability to add hydroxyl or amine functionality only to the immediate surface of the medical sutures without impacting its bulk mechanical characteristics or introducing any harsh solvents appeared ideal in facilitating future covalent bonding between HA and the modified suture via the EDC mediated crosslinking reaction presented in Chapter 4 (**Figure 6.3**).

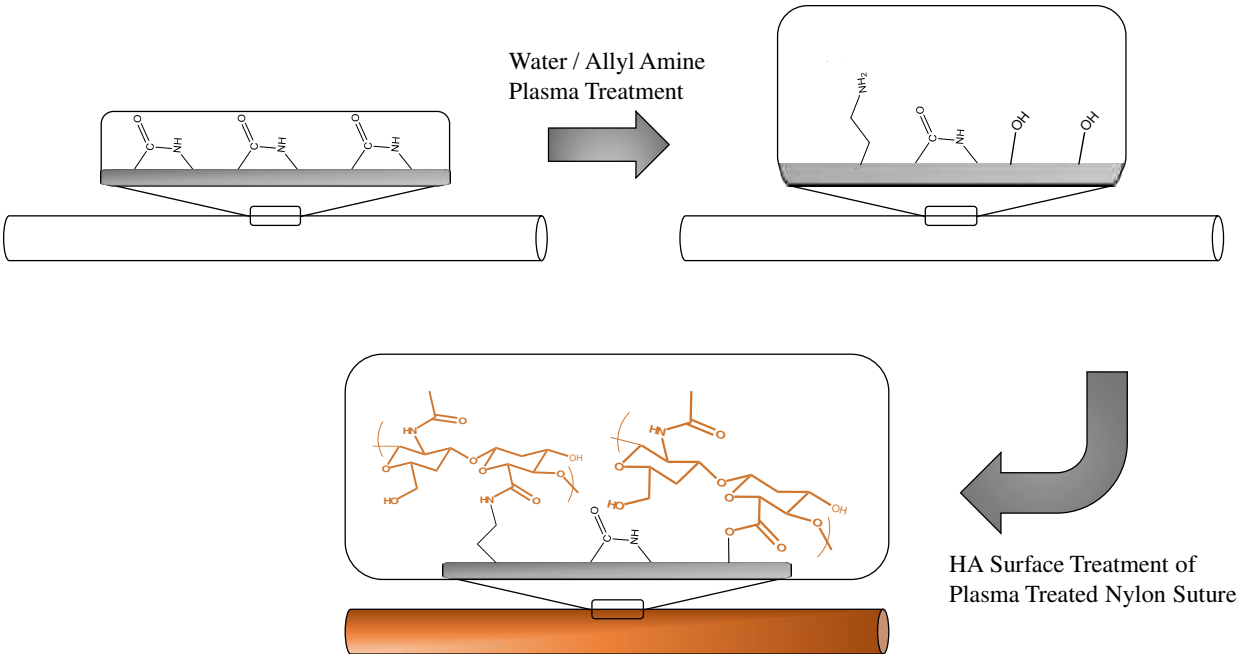

Figure 6.3: The addition of amine and hydroxyl functionality to the immediate surface of nylon medical sutures via H_2O and allyl amine plasma treatment. These reactive function handles provide sites for the covalent attachment of the immediate surface of the nylon medical suture to the binding intermediary HA via an EDC mediated crosslinking reaction.

Figure 6.4 below summarizes the proposed chemical mechanism for the covalent attachment of a modified nylon suture to our TPE hydrogel via the bonding intermediary HA. As EDC is added to the system (SOS/SO, surface modified nylon, and HA), the activated carboxylic

acid of HA will simultaneously (1) form an infinite network within the SOS/SO matrix at both the outermost surface and inner hydrogel-suture surface through ester formation both intra and intermolecularly (2) form an ester linkage with sterically accessible hydroxyl termini of SO and (3) form covalent amide linkages with the amine group of the modified nylon sutures.

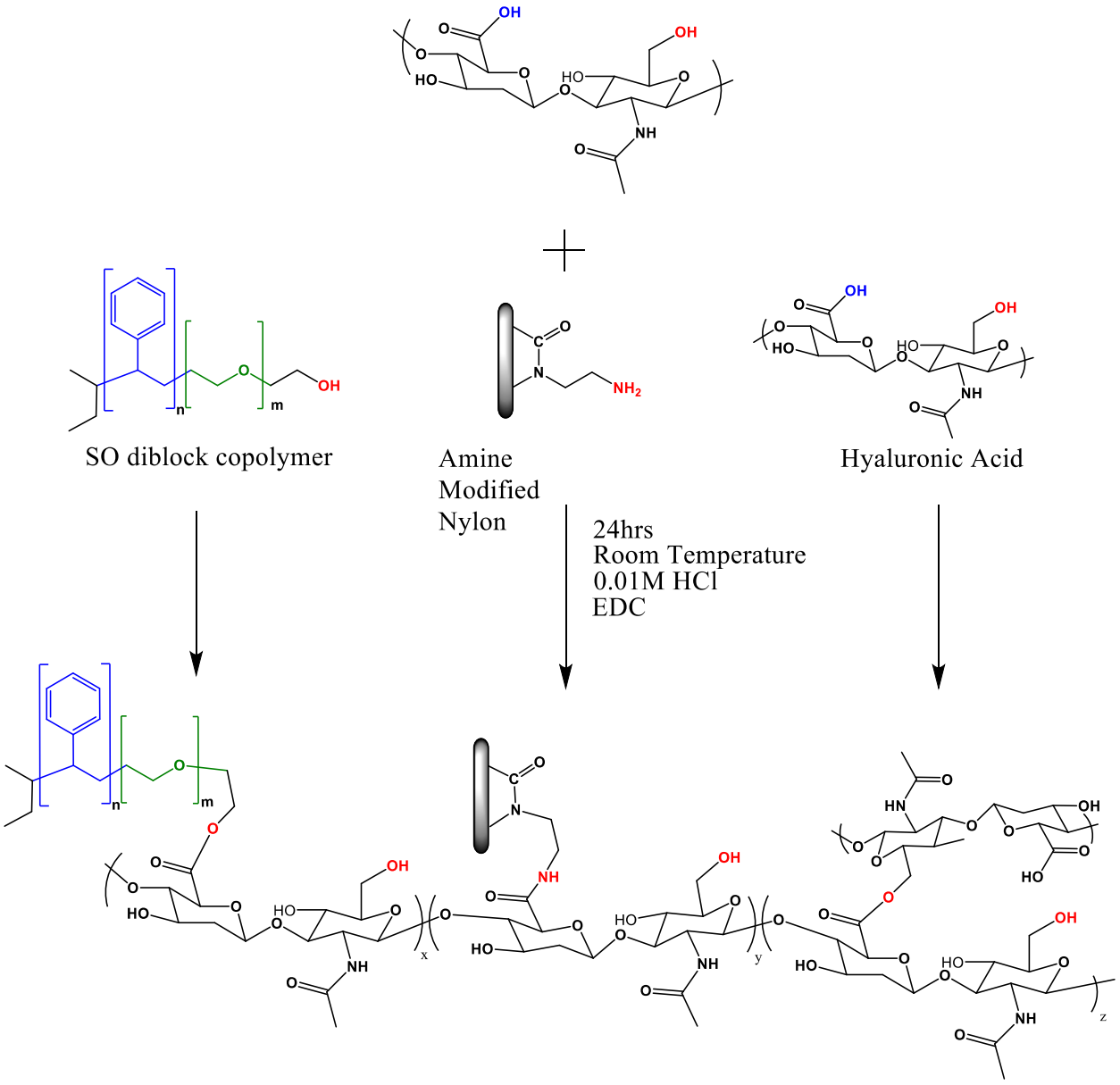

Figure 6.4: Chemical reaction diagram demonstrating how, using EDC, the carboxylic acid of HA can covalently bond to (1) the hydroxyl terminus of an SO chain end to form and ester linkage (2) other HA molecules (both inter and intramolecularly) at the primary alcohol site to form an ester linkage and (3) amine functionalized nylon to form an amide linkage.

Notably, one major difference of fiber incorporation in our TPE hydrogels when compared to the aforementioned conventional hydrogels, is that our TPE hydrogels are composed physically crosslinked nano-domains that self-assemble in the melt (Chapter 3), where conventional hydrogels consist of random crosslinks that are formed in solution. Because of this all dimensions of the dry melt-processed polymer are conserved upon swelling. Thus, when you incorporate a suture into our molten SOS/SO polymer and then let the polymer vitrify around the suture, you generate a negative space of SOS/SO polymer in the space that the suture occupies. Thus, when the hydrogel is swollen the suture shaped hole swells while the suture, obviously, does not, resulting in the generation of a void space between the fiber and the swollen hydrogel. Therefore, the solution based crosslinking techniques used in conventional hydrogels have the advantage that they can be "poured" around the fibers at their fully swollen dimensions before crosslinking.

Thus, the swelling and processing mechanics involved in the production of suture composite with our TPE hydrogels results in multiple effects that should be considered: (1) the bonding of a modified nylon suture to the interior of our hydrogel is actually surface reaction due to the new surface created by the incorporation of the suture in the melt, (2) contact with the immediate surface of the HA surface treated hydrogel may only consist of points of contact between the suture and the inside of a channel and (3) the HA will likely fill this channel and may produce a significantly thick, weak, and brittle neat HA hydrogel. The potential danger in this type of an interaction between the suture and the hydrogel is that as the crosslinked HA within the channel gets further away from the mechanically reinforcing SOS/SO hydrogel surface it loses much of its mechanical integrity as neat HA hydrogels are far softer and brittle than the SOS/SO hydrogel. However, it was theorized that if multiple points of contact between

the suture and the TPE hydrogel could be established along the channel, then it would produce enough covalent bonding to make the force necessary for suture pullout significantly high. **Figure 6.5** demonstrates pictorially how our HA surface treatment, when applied to a SOS/SO polymer with a surface modified nylon suture incorporated in the melt, could make the bonding between our TPE hydrogel and a surface modified nylon suture using HA as a bonding intermediary possible.

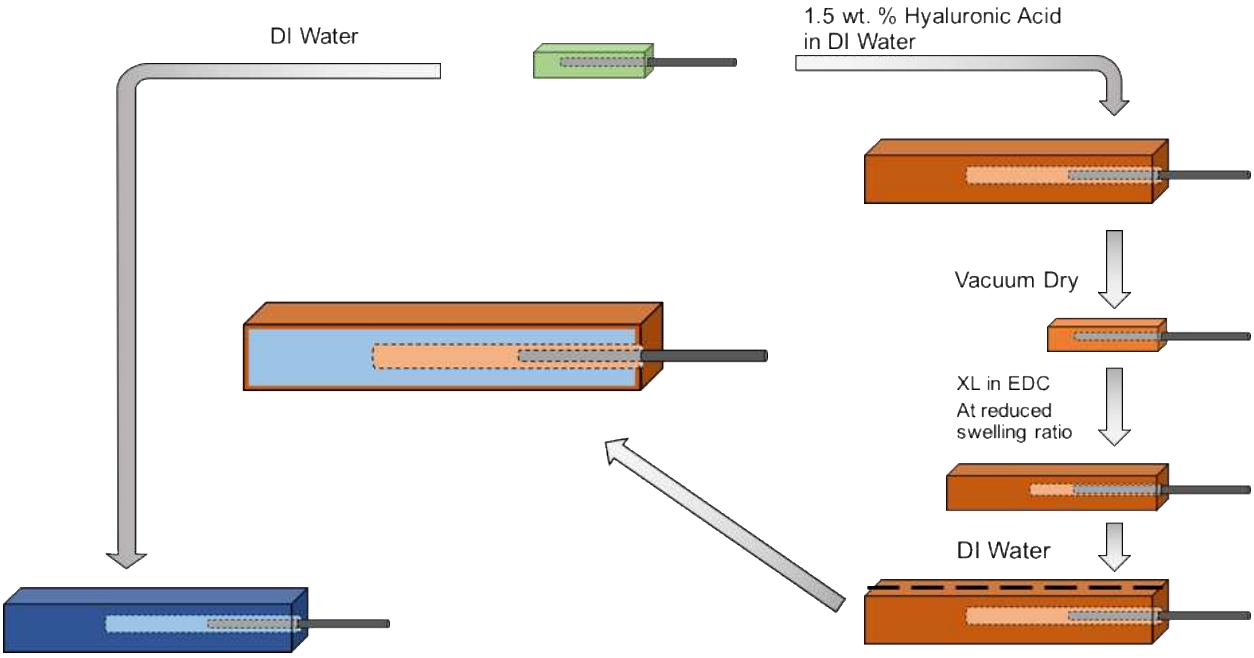

Figure 6.5: Demonstration of using an HA surface treatment to covalently bind our TPE hydrogel to a surface modified nylon suture (right path). Dry SOS/SO polymer is melt processed and vitrified around a plasma modified nylon suture (green). The SOS/SO/nylon assembly is then placed into a 1.5 wt. % solution of HA. The HA diffuses into the outer surface and inner surface region of the hydrogel. The HA swollen SOS/SO/nylon assembly is then vacuum dried. This dry assembly is then exposed to EDC to facilitate ester of amide formation between the carboxylic acid of one HA molecule to either the primary alcohol of another HA molecule or the primary alcohol / amine functionality of the surface modified nylon suture.

The following study documents initial efforts to modify the immediate surface of nylon medical sutures using H_2O plasma modification and allyl amine plasma copolymerization. X-ray photoelectron spectroscopy (XPS) was used to analyze surface functionality and elemental composition of the nylon medical sutures both before and after using H_2O plasma modification.

The chapter then presents the results of suture pullout of the modified and unmodified nylon sutures from our HA surface treated and neat TPE hydrogels.

6.2 RESULTS AND DISCUSSION

6.2.1 Plasma Modification of Nylon Sutures

Briefly, plasma treatment took place in a borosilicate glass barrel inductively coupled RF plasma reactor using H_2O vapor plasmas. Water vapor was added to the reactor while metering valve and reactor pressure were calculated using a capacitance manometer. Nylon sutures (3-0 and 5-0) were wrapped around a tubular glass membrane holder inside of the glass barrel allowing for perpendicular alignment to flow of gas and induction coil. Each end of the suture was secured with a small piece (2 mm x 2 mm) of double sided carbon tape. Treatment conditions were varied in their vapor pressure, RF applied power, treatment time and proximity to the coil region. After treatment samples were characterized for their surface functionality and elemental composition using X-ray photoelectron spectroscopy (XPS).

Figure 6.5 is an XPS spectra of a typical H_2O plasma treatment, demonstrating an increase in the relative amount of hydroxyl groups present on the immediate surface of the treated nylon sutures compared to their neat nylon suture counterpart. Notably, the ratio of O/C at the surface of the H_2O plasma treated samples was 0.79 compared to 0.52 for its unmodified counterpart. These results in conjunction with our knowledge of specific binding energies give us some confidence that at the immediate surface of the nylon suture hydroxyl groups are present that were not present pre-treatment (**Figure 6.6**). What these results do not show is if these hydroxyl groups are buried, inaccessible or if they are primary, secondary or tertiary in nature. The results only indicate that hydroxyl groups are present on the immediate surface of the nylon suture after H_2O plasma treatment.

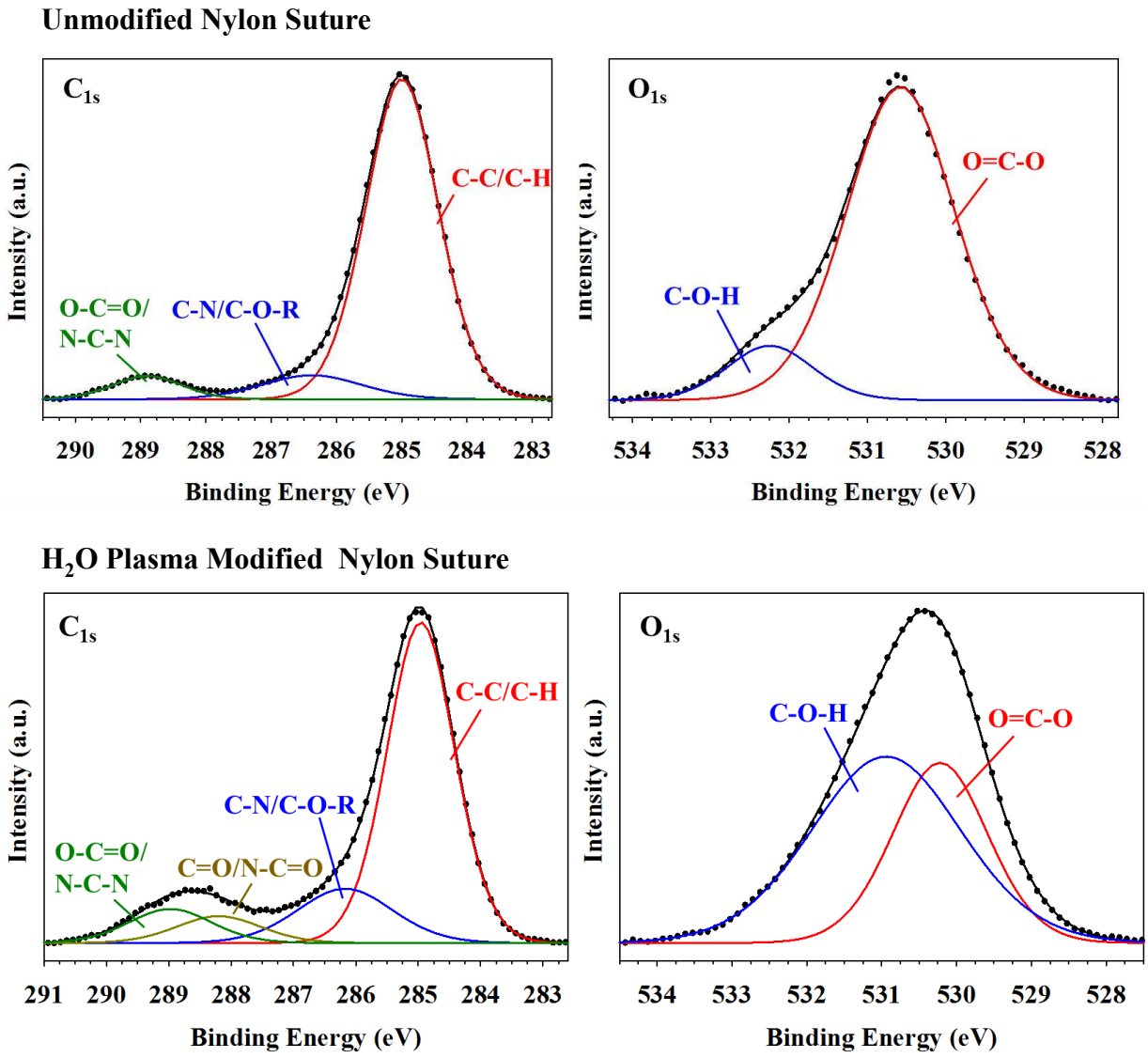

Figure 6.6: XPS spectra results displaying the relative elemental composition of the H_2O treated and untreated medical sutures. These spectra demonstrate that the H_2O plasma treatment resulted in an increase in hydroxyl groups on the modified nylon sutures (bottom) compared to the neat nylon sutures (top).

6.2.2 Nylon suture pullout testing

Untreated as well as either H_2O plasma treated or allyl amine plasma copolymerized nylon sutures were incorporated in the melt state of dry 72 mol% SOS/ 28 mol% SO polymer by (1) placing one layer of SOS/SO polymer into a rectangular mold, (2) placing one nylon suture in the center of the mold halfway up the vertical axis, (3) placing a second layer of SOS/SO

polymer on top of the nylon suture. The assembly was heated to induce self-assembly of the SOS/SO polymer. Once cooled the SOS/SO/nylon suture sample was swollen in a 1.5 wt. % HA aqueous solution for 24 hrs, dried, and then crosslinked at a reduced swelling ratio using EDC crosslinking chemistry described in Chapter 4. The SOS/SO/HA/nylon sample was then allowed to reach equilibrium swelling conditions by being placed into DI water for an additional 24 hours. This process was repeated for samples containing untreated, H_2O plasma treated, and allyl amine plasma treated nylon medical sutures. These treatment groups were compared to a control of an unmodified nylon fiber inside of an unmodified TPE hydrogel. The sample was clamped using ARES torsion rectangular grips such that the bottom grip was placed on the hydrogel below the suture so as not to minimize the impact on the resistance to fiber pullout (**Figure 6.7a**). The top grip was placed on the nylon suture (**Figure 6.7b**), a 2g force was placed on the suture and the top grip moved vertically at rate of 2mm / sec.

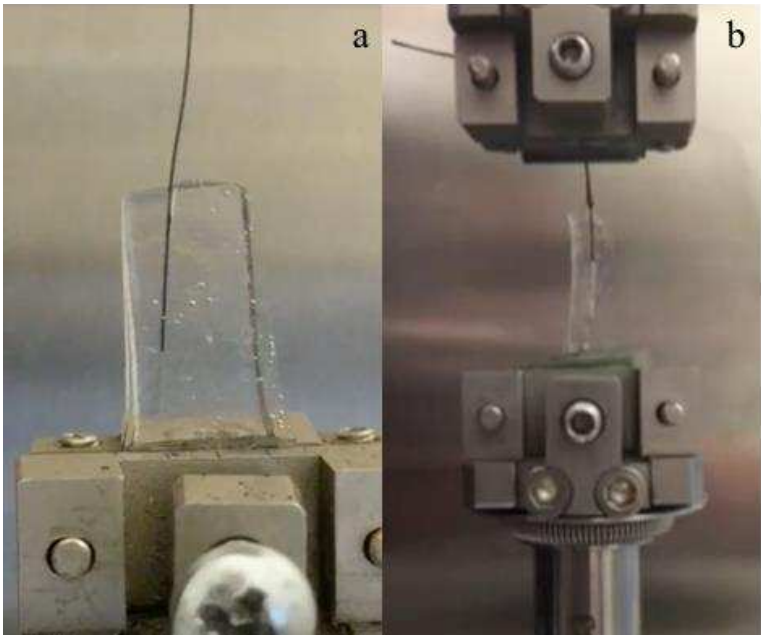

Figure 6.7: Images showing nylon suture position with TPE hydrogel after swelling as well as experimental setup for pullout testing from hydrogel. (a) Typical nylon suture inside of SOS/SO TPE hydrogel demonstrating the relative grip position to the nylon suture position. (b) Experimental setup of a typical nylon suture pullout testing, showing a pullout test mid-run.

The normal force and vertical displacement of the upper grip were recorded as the nylon suture was removed from the hydrogel (**Figure 6.8**). Surprisingly, the experimental data, depicted in **Figure 6.8** below, shows that all samples that were treated with the HA surface treatment appear to have a much lower resistance to suture pullout (0.25 – 1.25 g), than their untreated counterparts (> 4 g) including samples that contained plasma treated nylon sutures. In fact, of the HA treated groups the nylon sutures that were modified using H_2O plasma modification and allyl amine plasma copolymerization actually demonstrated the lowest resistance to suture pullout (**Figure 6.8**). This suggests that if covalent attachment between the modified nylon suture and the HA within the channel of the hydrogel is taking place it may actually result in a reduction to the force needed to remove the suture.

There were three initial hypotheses that were developed to explain the lack of resistance to pullout in HA treated hydrogel-fiber assemblies: (1) the viscous HA solution was not able infiltrate the channel created by the nylon suture and therefore could not act as a binding intermediary (2) the functionalities generated by the plasma surface treatments were inaccessible or buried and did not result in covalent bonding between the plasma treated suture and the HA infinite network and (3) the HA was indeed acting as a binding intermediary between the TPE hydrogel and the plasma treated suture, however, this covalent attachment between HA and the suture was weaker than the hydrophilic / hydrophobic interactions present between an neat TPE hydrogel and a neat medical suture.

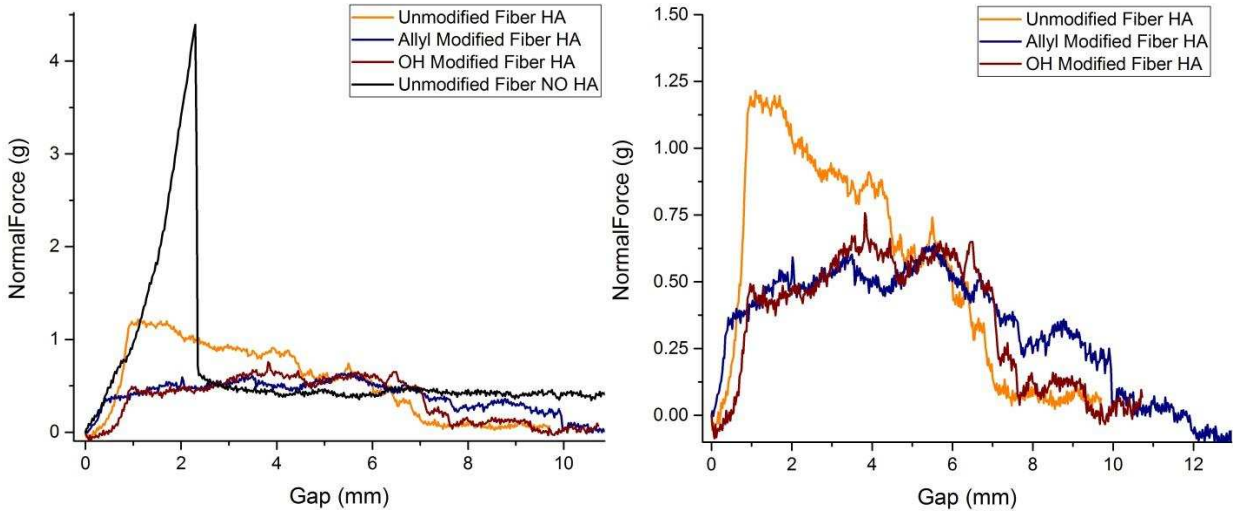

Figure 6.8: Normal force vs. vertical displacement (gap) of all nylon suture and HA surface treatment groups.

In order to assess if the HA was able to covalently bind to a plasma treated nylon medical sutures a qualitative experiment was conducted using the 5-aminofluorescein functionalized HA (HA-F) that was used in Chapter 5. Briefly, both the untreated and plasma treated medical sutures were placed into a viscous solution of HA-F. The HA-F solution was allowed to air dry to produce an HA-F film that contained either a plasma treated or neat medical suture. This HA-

F film containing the plasma treated or neat medical suture was then crosslinked and swollen to equilibrium using the same methods for creating a neat HA hydrogel that were discussed in Chapter 4. The plasma treated or untreated nylon medical suture was then removed from the brittle HA-F hydrogel using a tweezer as they were too weak to be gripped in the same configuration used for the TPE hydrogels. Upon removal of either a plasma treated or untreated nylon suture there was no noticeable mechanical resistance to pullout. **Figure 6.9** below shows an allyl amine plasma treated nylon suture being slowly removed(~ 0.33 cm / s) from a neat HA-F hydrogel. Notably, there is no deformation of the brittle and soft HA-F hydrogel as the suture is removed indicating, at least qualitatively, that there is little to no observable covalent attachment between the suture and the neat HA-F hydrogel that would lead to mechanical resistance. Once removed the plasma treated and untreated medical sutures were observed under a 365nm UV light table and neither the treated or untreated samples showed any fluorescence. This is qualitatively indicative that there is no significant HA layer that is forming on the surface of the nylon suture which would be expected if covalent attachment between the HA and the nylon suture had taken place. This experiment was repeated for H_2O plasma treated and untreated nylon sutures and there was no observable difference in either resistance to pullout or fluorescence of the suture upon removal. This experiment, while not conclusive on the existence of covalent bonding, certainly demonstrated that even if covalent bonding is taking place between the nylon suture and the HA network, it is not significant enough to produce an observable strain let alone failure of even the brittle HA hydrogel.

Figure 6.9: An allyl amine plasma treated nylon suture being slowly (~ 15s) removed from a neat HA-F hydrogel. This series of images demonstrates that there was no observable strain in the HA-F hydrogel upon removal of the theoretically covalently bound nylon suture.

6.3 Conclusion and Possible Future Directions

While this method of adding functionality to the immediate surface of a monofilament nylon medical suture and covalently binding this suture to our TPE hydrogel via the bonding of intermediary HA was ineffective, developing alternative fiber incorporation strategies in order to provide tensile reinforcement and an attachment mechanism for surgeons is critical in the successful development of a synthetic fibrocartilage replacement for the meniscus. There are several avenues to explore moving forward in the development of a fiber composite with our TPE hydrogel.

It may be possible to overcome the apparent preferential or exclusive covalent binding of the carboxylic acid of HA to an adjacent primary alcohol of HA instead of the primary alcohols or allyl amines on the nylon suture surface generated via plasma treatment. One alternative methodology moving forward would be to add complimentary reactive functionality to the HA

and the suture (i.e. adding a reactive functionality to HA that would react exclusively with the modified nylon suture instead of with another adjacent HA repeat unit). This lack of binding specificity may have led to insufficient bond formation between the hyaluronic acid and the modified nylon in the above study. In order to promote bonding specificity between the suture and HA, the following furan-maleimide diels alder chemistry, proposed initially by Schoichet et. al. to covalently bind polyethylene glycol (PEG) to HA[11] , may be adapted to attain binding specificity between the nylon suture and HA. Nimmo and Schoichet proposed an orthogonal crosslinking strategy for HA that does not use any additives and is a one-step coupling event.[11]

Adding furan functionality to HA was accomplished by activating the carboxylic acid of HA with DMTMM, much like the EDC reaction in Chapter 4, to form an activated ester. The amine group of an amine-functionalized furan can then attack the activated ester, leading to the formation of a stable amide linkage between HA and the furan functionality. Schoichet et al. then added a dimaleimide-PEG bridge to crosslink the furan modified HA. **Figure 6.10** demonstrates a modified version of this methodology, where HA is functionalized in the same way that was proposed by Schoichet, except the maleimide functionality is added to HA through the addition of N-(2-Aminoethyl) maleimide. Also, here the nylon suture is modified with a furan functionality using the tBuOK initiated S_N2 reaction proposed by Jia et al. [7] with the alkyl halide furoyl chloride. Once functionalized the suture and the HA will crosslink specifically with each other by simply heating the system. This strategy prevents HA from crosslinking with itself until after a covalent bond between the suture and HA has formed (**Figure 6.10**). NMR analysis would be used confirm the presence of the furan on the nylon with peaks at 6.25 and 7.3. As there is potential here for limited functionalization, XPS would have to be run as well in case NMR is inconclusive.

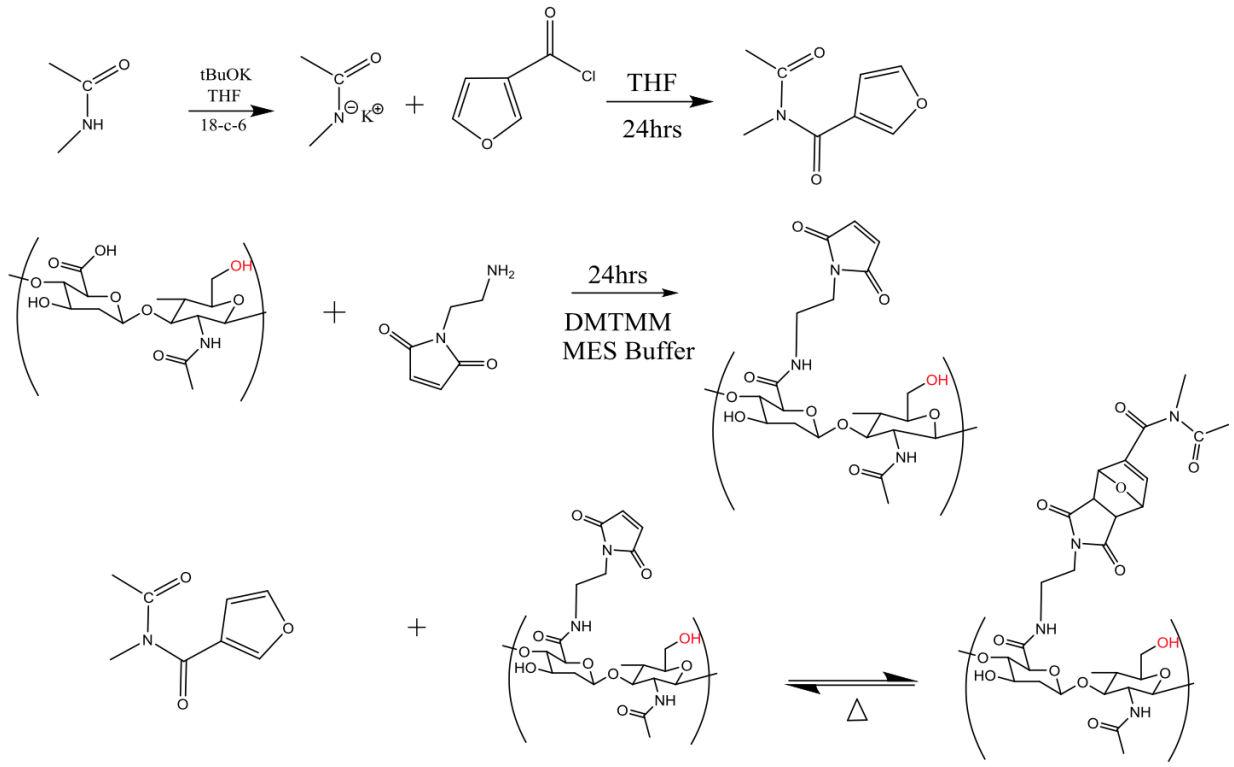

Figure 6.10: Modification of nylon with furoyl chloride. Modification of HA with maleimide. Diels alder coupling of furan functionalized nylon with maleimide functionalized HA.

An additional strategy that promotes binding specificity between nylon and HA is based around the fact that hyaluronic acid is naturally a weak polyanion. Therefore, if the nylon suture can be made cationic, then ionic bonding between the infinite network of HA and the suture can be made possible. The nylon suture can be made cationic by simply adding an additional step to the synthetic scheme proposed in **Figure 6.1**. By methylating the primary amine into a quaternary amine through the methylating agent dimethyl sulfate, you can generate a strong polycation on the surface of the nylon suture (**Figure 6.11**). This has been proven as a successful methylating agent for chitosan to produce positively charged quaternary amines by Assis and de Britto. [12]

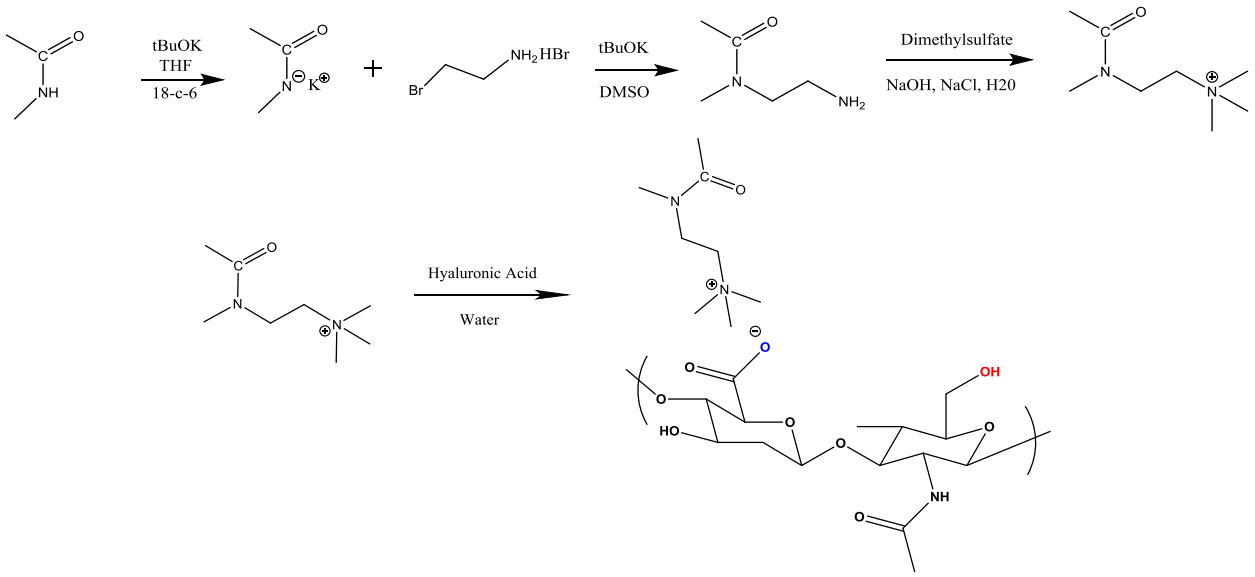

Figure 6.11: Addition of ethyl amine to nylon. Followed by methylation of primary amine. Ionic interaction of the positively charged quaternary amine and the weak polyanion hyaluronic acid.

Notably, nylon is not unique in its ability to be plasma treated and is not the only medical suture material. Silk, for example, has the benefit of possessing reactive functional handles without the need for chemical modification as it is primarily the protein fibroin, which consists of the amino acids glycine, serine and alanine. Serine in particular possesses a primary alcohol that could be utilized as a reactive functional handle for many of the strategies mentioned above without the need for plasma treatment. Cellulose is another fiber that would be of great interest to generate a composite with our TPE hydrogels as it possesses much of the same chemical structure and reactivity of HA without the need for chemical modification.

Finally, it is worth considering adapting our TPE hydrogel system to be compatible with a solution based coupling to ensure maximum contact of the hydrogel and the suture in the swollen state. Work by Huq and Bailey has shown that by (1) modifying our SO diblock with anthracene functionality, (2) heating the system to allow for self-assembly of the SO-anthracene into spherical domains, and (3) dissolving these SO-anthracene micelles in water you have produced a platform that has access to the benefits of a solution based crosslinking system by

simply exposing the SO-anthracene micelle solution to UV light.[13] Perhaps most importantly much of the desirable properties were still observed in these solution based TPE hydrogels including high levels of toughness and elasticity.[13] Notably, hydrogels produced from these SO-anthracene micelle solutions were mechanically softer than their melt processed counterpart, however, with the successful mechanical reinforcement of the fibers this limitation may be overcome.[13] If the suture surface was then modified with anthracene functionality, you would gain access to a system where you can pour the UV-sensitive SO-anthracene micelle solution over the UV-sensitive fiber and simply shine UV light on the system to simultaneously crosslink the SO-anthracene micelles to form SOS while crosslinking the SO-anthracene micelles to the anthracene functionalized fiber.

6.4 EXPERIMENTAL:

Materials and Characterization. Styrene (99%, 4-tert-butylcatechol inhibitor, Aldrich) and ethylene oxide (99.5+%, compressed gas, Aldrich) monomer were each purified by successive vacuum distillations (10–20 mTorr) from dried di-n-butylmagnesium (1.0 M solution in heptane, Aldrich) before use. Both purified styrene and ethylene oxide monomer were stored in glass burettes in the dark, at room temperature (styrene) and 3 °C (ethylene oxide), respectively, before use (typically less than 24 h). Argon degassed cyclohexane (CHX) was purified by passing the solvent over activated alumina followed by Q-5-like supported copper catalyst (Glass Contour, proprietary). Argon degassed tetrahydrofuran (THF) was purified by passing the solvent over activated alumina. High-purity argon (99.998%, Airgas) was passed through additional oxygen and moisture traps prior to use. Glassware and polymerization reactors were flamed under vacuum and backfilled with argon multiple times. All other reagents were used as received. ^{1}H NMR spectra were collected at room temperature in $CDCl_3$ on a Varian Inova 400 MHz Spectrometer (n = 32, delay = 30 s). Size exclusion chromatography (SEC) was performed on a Viscotek GPC-Max chromatography system fitted with three 7.5 x 340 mm Polypore^{TM} (Polymer Laboratories) columns in series, an Alltech external column oven, and a Viscotek differential refractive index (RI) detector. Measurements were performed using a DMF (55 °C) mobile phase (1 mL/min) with PS standards (Polymer Laboratories). Final SO/SOS compositions were confirmed via relative peak integrations in the SEC chromatograms of these blends.

ω-Hydroxy-polystyrene (S-OH). Purified styrene monomer (120 g, 1.14 mol, 20°C) was added to a stirring solution of sec-butyl lithium (10.23 mL, 1.3 M in cyclohexane, Aldrich) and dry, air-free cyclohexane (1 L, 20 °C) in a 2 L reaction vessel. The solution was then raised to 40°C and

stirred continuously for 8 hours. At a reduced pressure of 1 psig, purified ethylene oxide (6.6 g, 0.15 mol, 0 °C, liquid) was added to the reaction vessel. The reaction was held at 40°C for an additional 24 hours, after which all excess ethylene oxide was removed from the reactor under a constant argon flow. The reaction was terminated by acidic methanol (50 mL). The polymer was precipitated in methanol (5 L total), producing a fluffy white solid, and dried under vacuum at room temperature over a 48 h period (yield 116 g, 97%, M_n= 8370 g/mol, PDI = 1.03).

ω-Hydroxy-polystyrene-b-poly(ethylene oxide) (SO). S-OH (7 g, 0.836 mmol) was added to a 2 L reaction vessel containing a glass coated magnetic stir bar. The reactor was evacuated and backfilled with purified argon before adding 1 L of dry, air-free tetrahydrofuran (THF). Concentrated potassium naphthalenide in THF was added to the polymer solution via cannula until a light green color persisted for 30 minutes. The temperature of the reaction mixture was raised to 40 °C and purified ethylene oxide monomer (78.7 g, 1.78 mol, 0 °C) was added under argon (1 psi) to the stirring solution for 48 hours. The reaction was terminated by methanol (50 mL) and the polymer was precipitated in 4 L of pentane, producing a fluffy white solid. The polymer was dried under vacuum at room temperature for 48 hours. (M_n= 107,000 g/mol, PDI = 1.07, f_{PS} = 0.085).

Polystyrene-b-poly(ethylene oxide)-b-polystyrene (SOS). SO (29 g, 0.271 mmol) was placed into a 2 L round bottom reactor vessel that was evacuated and backfilled with purified argon. The SO was allowed to dry under vacuum overnight. The SO was then dissolved in dry THF. A concentrated potassium naphthalenide solution in dry THF was titrated into the reactor until the solution maintained a green color for 30 minutes. α,α′-dibromo-p-xylene (35.8 mg, 0.136 mmol,

0.5 eq) in THF (1.5 mL) was then injected into the reactor over a 12 hour period at a rate of 0.125 mL hr^{-1} using a syringe pump and a 2.5 mL glass syringe. Coupled polymer was recovered through precipitation in 5 L of pentane followed by vacuum filtration. The precipitated polymer was dried overnight under vacuum to produce a fluffy white solid as a blend of coupled (SOS) and uncoupled (SO) block copolymer (52 mol% SOS).

SO/SOS Fractionation. To achieve 72 mol% SOS concentrations used in this study, the 52 mol% produced during the SO coupling reaction was fractionated. Dry SO/SOS polymer (4 g) was dissolved in chloroform (400 ml) and heated to 45 °C. N-hexane (920 ml) was added slowly, keeping the temperature above 40°C. The SOS precipitated and the solution turned cloudy. Upon cooling to room temperature, the solution turned transparent. The solution contained the majority of the SO while the SOS existed as a precipitate. The SOS precipitate was recovered and allowed to dry under vacuum overnight, while the SO in solution was recovered through rotary evaporation.

Plasma surface treatment of nylon suture Plasma treatment took place in a borosilicate glass barrel inductively coupled RF plasma reactor using H_2O vapor plasmas. Water vapor was added to the reactor while metering valve and reactor pressure were calculated using a capacitance manometer. Nylon sutures (5-0) were wrapped around a tubular glass membrane holder inside of the glass barrel allowing for perpendicular alignment to flow of gas and induction coil. Each end of the suture was secured with a small piece (2 mm x 2 mm) of double sided carbon tape. Treatment conditions were varied in their vapor pressure, RF applied power, treatment time and proximity to the coil region. After treatment samples were characterized for their surface

functionality and elemental composition using X-ray photoelectron spectroscopy (XPS). Three types of H_2O treatment were conducted (1) 200 mTorr, 20 W, 2 min 22 cm downstream from coil region (2) 200 mTorr, 20 W, 2 min in the coil region and (3) 200 mTorr, 100 W, 5 min in the coil region. Allyl amine treatments were conducted at 100 mTorr, 50 W, 9 cm downstream from the coil region for 15 min. All testing was done on 5-0 Nylon sutures

Incorporation of suture into polymer Dry 72 mol% SOS polymer was placed in order to halfway fill a rectangular steel mold. A 5-0 nylon medical suture was then centered on the short and long axis of the mold on top of the dry polymer such that half off the hydrogel did not contain the suture and that excess suture 3-4 inches remained outside of the rectangular mold. An equivalent amount of dry SOS 72 mol% polymer was placed over the suture. This assembly was then placed between two Kapton sheets. This assembly was then placed into a Carver Press and heated to 150°C under an applied pressure of ~500 psi for 5 minutes. In some cases multiple compressions were used to remove visible bubbles. Samples were allowed to cool to room temperature before swelling. For tensile testing, test strips measured (3 mm × 8 mm × 1.25 - 1.5 mm deep).

HA surface treatment of nylon suture/SOS/SO The nylon suture/SOS/SO assembly once cooled was subjected to the same treatment that is described in Chapter 4. Briefly, the dry nylon suture/SOS/SO assembly was either swollen in DI water or a solution containing 1.5 wt% sodium hyaluronate in DI water for 24 hours at 4°C. Samples were then removed from their respective swelling solutions, patted dry with a Kimwipe, allowed to dry in air for 24 hours, and their masses were recorded. The amount of hyaluronan inside of the hydrogel was determined

gravimetrically by taking the difference of the dry mass of the polymer before and after being subjected to a swelling and drying cycle. EDC crosslinking solutions consisted of a 4:1 molar equivalence of EDC: hyaluronan repeat unit in 0.01M HCl. Enough solution was added to the dry polymer to produce a swelling ratio of 1.5. These partially swollen hydrogels were then allowed to crosslink for 24 hours. After crosslinking the hydrogels were placed into a semi-infinite solution of DI water for 7 days to remove any loose unbound HA.

Pullout Testing of Nylon Suture from SOS/SO/Nylon/HA hydrogel Samples were clamped using ARES torsion rectangular grips such that the bottom grip was placed on the hydrogel below the suture so as not to minimize the impact on the resistance to fiber pullout. A 2g force initial force was placed on the suture to ensure that the fiber was taught before pullout. The top grip moved vertically at rate of 2mm / sec. The normal force and vertical displacement of the upper grip were recorded as the nylon suture was removed from the hydrogel.

REFERENCES

1. Naficy, S.; Brown, H. R.; Razal, J. M.; Spinks, G. M.; Whitten, P. G. *Australian Journal of Chemistry* **2011,** 64, (8), 1007-1025.

2. Fischenich, K. M.; Lewis, J.; Kindsfater, K. A.; Bailey, T. S.; Donahue, T. L. H. *Journal of Biomechanics* **2015,** 48, (8), 1407-1411.

3. Holloway, J. L.; Lowman, A. M.; Palmese, G. R. *Acta Biomaterialia* **2010,** 6, (12), 4716-4724.

4. King, D. R.; Sun, T. L.; Huang, Y. W.; Kurokawa, T.; Nonoyama, T.; Crosby, A. J.; Gong, J. P. *Materials Horizons* **2015,** 2, (6), 584-591.

5. Ambrosio, L.; De Santis, R.; Nicolais, L. *Proceedings of the Institution of Mechanical Engineers Part H-Journal of Engineering in Medicine* **1998,** 212, (H2), 93-99.

6. Khoushabi, A.; Schmocker, A.; Pioletti, D. P.; Moser, C.; Schizas, C.; Manson, J. A.; Bourban, P. E. *Composites Science and Technology* **2015,** 119, 93-99.

7. Jia, X. Q.; Herrera-Alonso, M.; McCarthy, T. J. *Polymer* **2006,** 47, (14), 4916-4924.

8. Chu, P. K.; Chen, J. Y.; Wang, L. P.; Huang, N. *Materials Science & Engineering R-Reports* **2002,** 36, (5-6), 143-206.

9. Tompkins, B. D.; Dennison, J. M.; Fisher, E. R. *Journal of Membrane Science* **2013,** 428, 576-588.

10. Hawker, M. J.; Pegalajar-Jurado, A.; Hicks, K. I.; Shearer, J. C.; Fisher, E. R. *Plasma Processes and Polymers* **2015,** 12, (12), 1435-1450.

11. Nimmo, C. M.; Owen, S. C.; Shoichet, M. S. *Biomacromolecules* **2011,** 12, (3), 824-830.

12. de Britto, D.; Assis, O. B. G. *Carbohydrate Polymers* **2007,** 69, (2), 305-310.

13. Huq, N. A.; Ekblad, J. R.; Leonard, A. T.; Scalfani, V. F.; Bailey, T. S. *Macromolecules* **2017,** 50, (4), 1331-1341.

[7]APPENDIX 1

DANGLING-END DOUBLE NETWORKS: TAPPING HIDDEN TOUGHNESS IN HIGHLY SWOLLEN THERMOPLASTIC ELASTOMER HYDROGELS

A1.1 INTRODUCTION [8]

The investigation of polymeric based hydrogels has been an attractive research field due to their applicability in a wide range of technologies including separations[1-3], encapsulation matrices, biomedical implants, tissue engineering[4] and drug delivery[5-8]. Of the various hydrogel platforms that have been previously developed for such applications, most are predicated on solution-based polymerization of hydrophilic monomers or random physical or chemical cross-linking of hydrophilic polymers in solution[9-12]. In general, such systems can achieve the high water content essential for use in such applications, however, in cases for which water contents above 80% (g/g) are required, the mechanical properties (toughness in particular) are notoriously substandard.

Our group has been actively developing thermoplastic elastomer (TPE) hydrogels aimed at improving toughness and elasticity in processable, physically crosslinked hydrogels. These TPE hydrogels are fabricated by melt blending sphere-forming[13-15] AB diblock and ABA triblock copolymers followed by vitrification[13, 14] or chemical cross-linking[15] of the isolated spherical

[7] The contents of this appendix have been adapted from a manuscript published in Chemistry of Materials: Chen Guo, Jackson T. Lewis, Vincent F. Scalfani, Miriah M. Schwartz and Travis S. Bailey Chem. Mater., 2016, 28 (6), pp 1678–1690. Chen Guo, Jackson Lewis and Travis S. Bailey developed and designed the experiments. Jackson Lewis performed the experiments. The manuscript and dissertation chapter were written by Chen Guo, Jackson Lewis, Vincent F. Scalfani and Travis S. Bailey.

[8]

domains of block A which form during the self-assembly process (**Figure 6.1**). Each sphere is comprised of several hundred minority component (A) blocks, which are necessarily (by block connectivity) enveloped by a dense brush of equal number majority component (B) blocks, giving rise to the micelle like appearance. Without solvent present, a highly regular and periodic lattice of densely packed micelles is produced. Vitrifying or cross-linking the interior spherical domain (A blocks) allows one to completely preserve the melt state self-assembled structure both on the micro and macroscale. Upon selectively hydrating the majority component (B blocks), the lattice of micelles expands as water penetrates the dense coronal brush layer of each micelle.

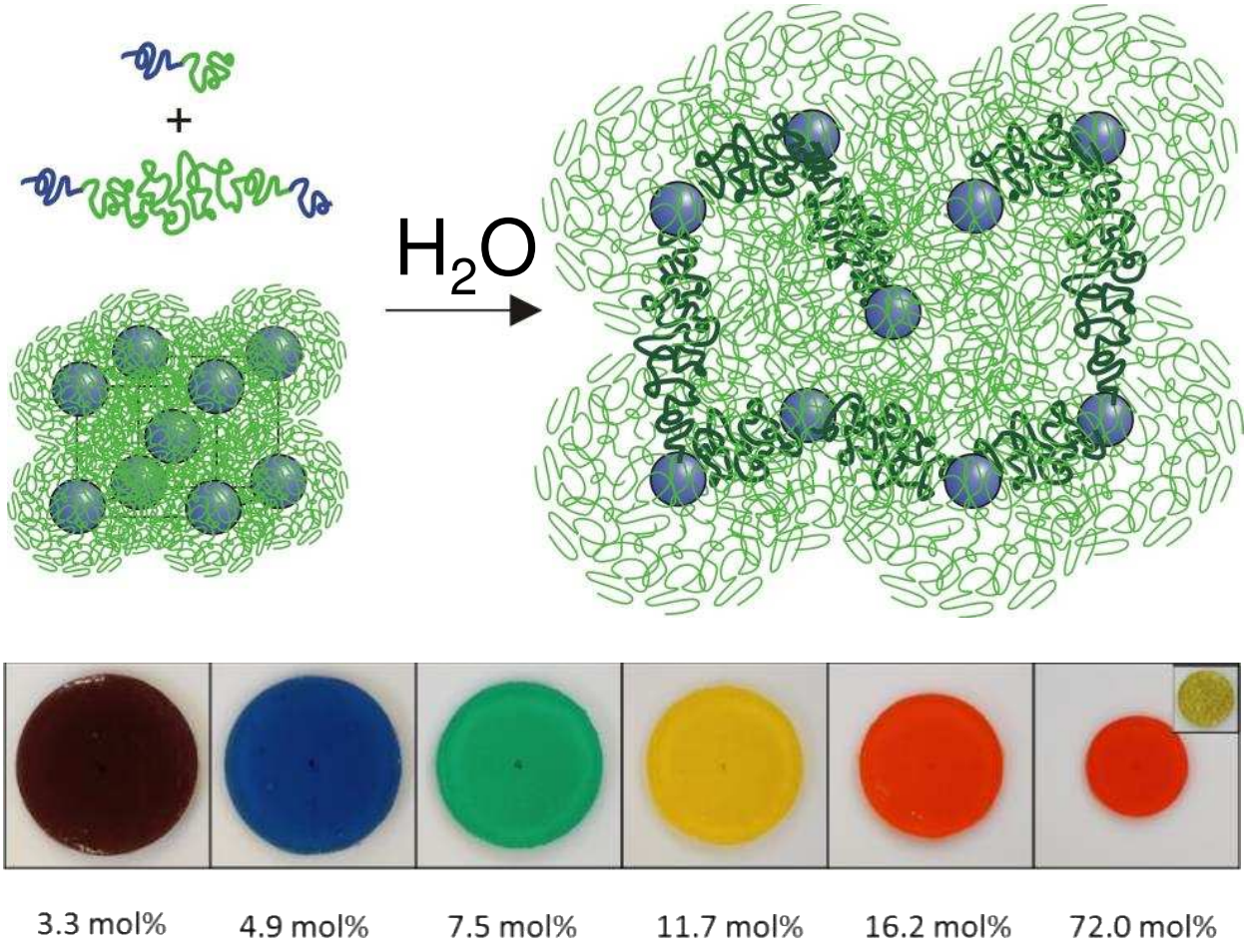

Figure A1.1: Generalized fabrication strategy for block copolymer based hydrogels based on sphere-forming SO diblock and SOS triblock copolymer blends. Constituent block copolymers are pre-assembled in the melt and vitrified prior to swelling. SOS triblock copolymer (in bold)

acts to tether adjacent spherical PS domains. Changing the amount of SOS triblock copolymer (labeled in mol%) influences the equilibrium swelling dimensions due to topological entanglements produced during self-assembly (Figure adapted from Ref. 14)

However, the added ABA triblock copolymer, even at small quantities, acts to tether the individual micelles together into an infinite network; each sphere acting as a junction point in physically cross-linked system. Equilibrium swelling dimensions are determined by the balance of osmotic swelling forces, entropic restoring forces contributed by the ABA tethering midblocks, and the quantity of topological ABA entanglements produced within the network (**Figure A1.1**) during self-assembly.[14]

Our initial investigations of TPE hydrogels, based on sphere-forming polystyrene-*b*-poly(ethylene oxide)/ polystyrene-*b*-poly(ethylene oxide)-b-polystyrene (PS-PEO/PS-PEO-PS or SO/SOS), we found melt-organized blends preserved their original shape, were highly elastic, and easily tunable; the mechanical properties (elastic moduli and compression-decompression were evaluated) of the model SO/SOS hydrogels were controllable through simple adjustment of triblock copolymer (SOS) content, while the overall swelling was controllable through triblock copolymer content, temperature, and midblock molecular weight. However, we also discovered, somewhat unexpectedly, that at low SOS concentrations, the majority of the elastic modulus was produced not by the tethering concentration but through the imposed overlap in the PEO coronal brush layers. That is, the dynamic entanglements among the dangling PEO chain ends were responsible for a considerable fraction of the mechanical response under small-strain dynamic shear. We were inspired by this result to explore the potential of using dangling chain ends, typically discounted within network theory as a mechanical property contributor,[16] as an untapped source of available toughness in highly swollen systems.

One of the most common strategies for improving hydrogel tensile properties is to incorporate a second network to help absorb and distribute stress imposed on the system.

Conventional double-network (DN) hydrogels, usually consist of networks comprised of two distinct hydrophilic polymers, one stiff and brittle and the other soft and ductile. These systems tend to exhibit high toughness in general and have proven quite effective, although the range of water contents where enhanced toughness is achieved can be limited.[17, 18] The fabrication process typically consists of two steps. By adding small amount of cross-linker to a polymerization solution, the first network is made. Then the first network is immersed in the solution where the second network is polymerized and cross-linked. Even though DN hydrogels significantly improve hydrogel mechanical properties, the sol-gel fabrication process is susceptible to producing heterogeneity in local structure in both networks (due to differences in monomer, initiator and cross-linker diffusion rates), and can be challenging to adapt to shape specific hydrogel applications. In addition, unreacted monomer, crosslinker, and small oligiomers or oligiomeric networks can take weeks to be removed, particularly when leaching or cytotoxicity is of concern.

As we demonstrate in this report, the homogeneity in structure provided by melt-state self-assembly of macromolecular block copolymers produces a primary or first network that is inherently quite tough when compared with most hydrogel systems. In fact, these networks are able to absorb strains elastically to a few hundred percent, with the exact modulus exhibited tunable through the triblock copolymer content used in the original melt-state blend. Given these advantages over many hydrogel systems, we focused on the installation of a second network that, instead of altering the mechanical performance directly, would remain largely passive under small strain conditions. That is, the secondary mesh would only become actively engaged when the primary network was approaching its own strain limitations. The goal was to be able to improve the high strain toughness of the hydrogel without impacting the smaller strain

mechanical response of the primary network, previously tuned through triblock copolymer content in the melt blend. Additionally, the goal was to do so without sacrificing the thermoprocessibility of the system.

Our approach is based on exploiting the large number of (in excess of 200)[14] hydroxyl terminated SO diblock copolymers comprising each micellar domain. By converting these hydroxyl groups to clickable alkyne and azide functionalities, we established a means of coupling excess diblock block copolymer to form additional SOS triblock copolymer in situ, after the hydrogel has already reached its equilibrium dimensions. Our hypothesis was that, while the SOS triblock copolymer added in the original melt blend and that formed via Cu(I)-catalyzed coupling in the hydrated state would be molecularly identical (effectively), the stress state of these two triblock copolymer populations would be significantly different. The SOS triblock copolymer present during melt-state self-assembly of the spherical morphology becomes trapped in its current conformation during sample vitrification. Upon exposure to aqueous media, the entropic restoring force in the tethering midblocks of the triblock copolymer population, combined with topological entanglements present among nearby tethers, act to preclude infinite swelling and osmotically driven micelle dispersal. The concentration of topological entanglements scales with triblock copolymer composition, and has a dramatic influence on the equilibrium dimensions (**Figure A1.1**). Effectively, the osmotic driving force to swell is opposed by an equal and opposite force supplied by the entangled triblock copolymer adjoining the spherical PS domains. In contrast, triblock copolymer formed through diblock copolymer coupling at swelling equilibrium produces a population of tethers free of the mechanical stress osmotically imposed on the primary network. Importantly, with the exception of the Cu(I) catalyst specific to this particular choice of chemistry, formation of the DN through the coupling

of dangling chain ends is absent of leachable small molecule reagents or sol fractions intrinsic to most traditional DN hydrogel systems.

Within, we 1) establish the baseline tensile toughness of the SO/SOS TPE hydrogel system, 2) demonstrate the successful incorporation of latent azide and alkyne chain end functionality without network disruption, and 3) exploit that chain end functionality to increase the tensile toughness of high water content (~ 95 mass%) forms of these hydrogels through DN formation.

A1.2 RESULTS AND DISCUSSION

A1.2.1 Block Copolymer Synthesis, Physical Characterization and Blend Formation.

The hydrogel systems used in this study originate from a set of just four distinct block copolymers. One of these four block copolymers, a hydroxyl-terminated PS-PEO diblock copolymer, serves as the parent molecule from which the remaining three block copolymers were derived.

The parent block copolymer, designated SO, was prepared via a two-step anionic polymerization of styrene and ethylene oxide as previously reported.[14, 19, 20] ^{1}H NMR was used to confirm the targeted volume fraction of polystyrene (f_S = 0.13), and SEC confirmed the narrow polydispersity of 1.04. From this parent diblock copolymer the first of the three derivative molecules, a PS-PEO-PS (SOS) triblock copolymer was synthesized. This SOS triblock copolymer was prepared by re-activating the terminal alcohol on SO with potassium naphthalenide and then slowly (several hours) adding, α,α'-dibromo-*p*-xylene as a coupling agent. The coupled triblock copolymer product was found to be a 60:40 (mass%) mixture of SOS:SO via SEC peak integration, which is consistent with other reported coupling yields,[21] including our own prior work.[13] The SOS triblock copolymer was isolated from this mixture

(98+%) using an iterative fractionation process in which chloroform and n-hexane were used as a solvent/non-solvent pair and the temperature was maintained higher than 40 ˚C to avoid (non)solvent-induced PEO crystallization.[13, 21] Importantly, the SOS triblock copolymer formed in this manner has a molecular weight and contour length essentially double that of the SO diblock copolymers used in this study. This was done in order to ensure domain size compatibility between the SO and SOS block copolymers during self-assembly.

Blends formed from these two block copolymers (SO and SOS) comprise the first set of hydrogel materials considered. These hydrogels serve as baseline materials through which the intrinsic tensile properties of the model system, containing only a primary network, could be established. Six SO/SOS blends containing SOS contents ranging from 4.1 to 45.1 mol% were prepared via solution blending in benzene.

Table A1.1: Hydrogel composition and post-swelling click chemistry reaction conversion [a] Molar percentages calculated based on integration of corresponding peaks on GPC traces. [b] The maximum amount of SOS after reaction in the case of stoichiometric reaction between all azide and alkyne functional groups, assuming azide and alkyne functionalities were 100% after SO-azide and SO-alkyne modification. [c] Coupling conversions were calculated as the ratio of newly formed SOS in the hydrogel state to the maximum SOS can be achieved in ideal case (stoichiometric reaction between all azide and alkyne with 100% functionalities on SO-azide and SO-alkyne).

Sample	SOS_{pre} (mol%[a])	SO-X_{pre} (mol%)[a]	SO-azide : SO-alkyne : SO-H[a]	SOS_{max} (mol%)[b]	SOS_{post} (mol%)[a]	Coupling conversion (%)[c]
A1	9.3	90.7	1:1:4	28.8	20.2	60.0
A2					18.4	50.8
A3					21.2	65.0
A4					20.3	60.0
B1	9.8	90.2	1:1:8/5	46.5	29.0	59.4
B2					30.7	63.8
B3					29.8	61.4
B4					22.7	41.9
C1	10.4	89.6	1:1:4/7	69.4	39.7	60.2
C2					42.9	65.3
C3					37.5	56.6
C4					32.4	47.7
D1	8.9	91.1	1:1:0	100	48.0	58.0
D2					48.4	58.4
D3					52.0	62.3
D4					52.1	62.3
D5					45.1	54.8

Solid powder mixtures were recovered via freeze drying the blend solutions. Reported SOS triblock copolymer compositions are based on integration of SEC traces following solution blending. Uniform discs (8 mm diameter, 0.24-0.28 mm thickness, 0.015-0.016g) at each SOS

composition were prepared via melt pressing at 150 ˚C for five minutes. Melt pressing serves both to mold the powders into a homogeneous solid and provide the chain mobility needed for self-assembly into the sphere-based morphology. A LLP of spheres was verified by SAXS for all samples. Detailed analysis of the morphological structure of these materials by SAXS can be found in a previous publication.[14] SEC analysis of samples before and after melt pressing showed no observable sample degradation or change in SOS content.

The second set of materials considered were based on substituting various fractions of the parent (hydroxyl functional) SO diblock copolymer with SO diblock copolymer that had been modified with click functionality (SO-azide; SO-alkyne). In these four component blends, the SOS triblock copolymer continued to serve as the component forming the primary network in the hydrogel. The azide and alkyne functional SO diblock copolymers provided a latent ability to generate more triblock copolymer at a future time, that is, once the vitrified blend had been hydrated and the primary network of triblock copolymer tethers had been established and mechanically engaged.

SO-alkyne and SO-azide were both prepared via straightforward substitution reactions after conversion of the terminal alcohol groups on the parent SO diblock copolymer to their corresponding sodium or potassium alkoxides. To generate SO-azide, the terminal alkoxide was first converted to a mesyl leaving group before displacement in the presence of sodium azide.[22-24] Generation of SO-alkyne was achieved by treatment of the SO alkoxide with propargyl bromide. ^{1}H-NMR was able to confirm transformation of the hydroxyl groups to -alkyne and -mesyl groups to be essentially quantitative given the uncertainty associated with end-group analysis by ^{1}H NMR of large polymer molecules. Quantification of the azide functionalization efficiency was more difficult to ascertain. The methylene protons adjacent to the azide group overlap with

the ethylene oxide backbone and could not be resolved. However, the complete disappearance of the methyl protons of the mesyl group was indicative of a successful substitution reaction with complete mesyl group displacement. In addition, FTIR confirmed the presence of an azide vibration (2110 cm^{-1}) (See supplementary information for the NMR spectra of SO-Ms and SO-azide). While complete functionalization of the SO-azide could not be confirmed, blends involving SO-azide and SO-alkyne were assembled assuming functionalization of both block copolymers was quantitative. The possibility of non-quantitative functionalization and its impact on coupling efficiency is considered in subsequent sections.

Polymer blends containing approximately 8.5 - 10 mol% SOS and varying, equimolar amounts of SO-azide and SO-alkyne were prepared via solution blending (with freeze-drying) from benzene. The SO-azide: SO-alkyne ratio was held constant at 1: 1 and the blend was diluted with reactively inert SO, producing four distinct blends (A_{pre} - D_{pre}) with varying SO-azide/SO-alkyne content as shown in Table 1. Reported SOS triblock copolymer compositions are based on integration of SEC traces following solution blending (**Figure A1.4**, left). Notably, there is some unintended variation in the amount of pre-blended SOS triblock (8.9 - 10.4 mol %) across the four blends, which is attributable to a combination of error associated with massing, SEC peak integration, and local variations in blend composition. Uniform discs (8 mm diameter, 0.24-0.28 mm thickness, 0.015-0.016g) of samples A through D were prepared via melt pressing at 150 ˚C for five minutes. It is well established that azide-alkyne Huigsen cycloadditions can occur at high temperatures with the absence of a metal catalyst.[26] We ran several control experiments before and after melt pressing azide-alkyne functional SO and found no indication of thermally-induced coupling in the SEC traces. Molecular weight degradation was also not observed. Functional group integrity during melt pressing proved difficult to accurately assess (via ^{1}H

NMR, e.g.) given the reduced concentration of end groups in the blends. However, independent melt processing of neat SO-alkyne showed no apparent change in chain end functionality occurred during heating for such short times.

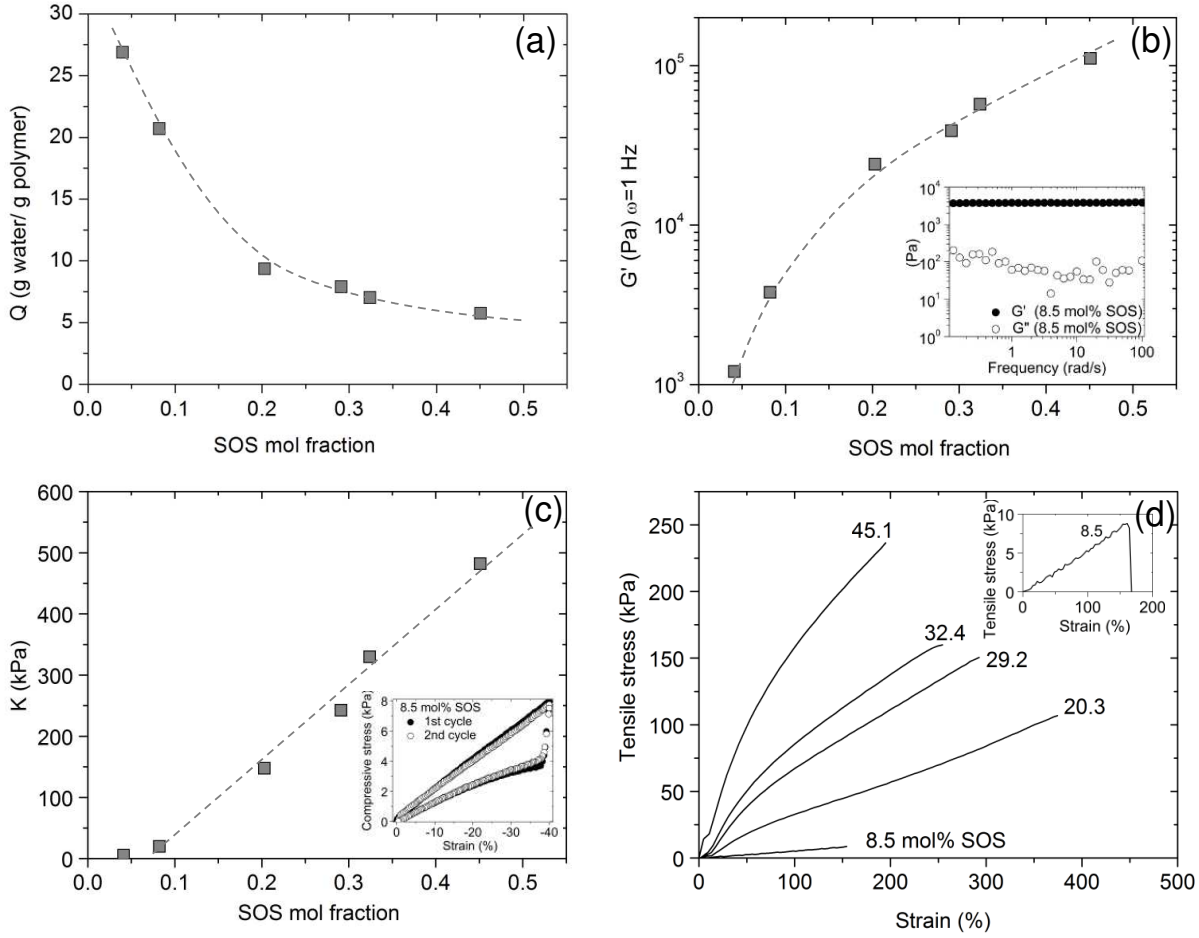

Figure A1.2. Behavior of baseline SO/SOS hydrogels as a function of SOS triblock copolymer composition. (a) Swelling ratio (Q). (b) Elastic modulus (G') under dynamic shear (ω = 1 Hz); (c) Compressive modulus (K) in unconfined compression (strain rate = 20% min^{-1}). (d) Tensile tests, (strain rate = 5 mm s^{-1}). Insets in (b) and (c) describe the dynamic frequency sweep and unconfined compression data for the baseline SO/SOS hydrogel containing 8.5 mol% SOS triblock copolymer. The inset in (d) provides a zoomed representation of the 8.5 mol% SOS hydrogel.

A1.2.2 Baseline Performance of SO/SOS TPE Hydrogels.

Dry polymer discs of SO/SOS blends were swollen in DI water until reaching the equilibrium swollen state (approximately one hour, confirmed by constant mass and size). The

equilibrium swelling ratios (Q's) were calculated based on gravimetric analysis of the discs before and after swelling. As found in our previous study, Q could be altered through environmental temperature in addition to tether (SOS) composition.[14] To eliminate temperature effects, all hydrogels were swollen at room temperature (thermostated 25 °C). **Figure A1.1a** shows the variation in Q with SOS composition for the six SO/SOS blends. The values of Q varied from 5.5 g H_2O/g polymer (45.1 mol% SOS) to 27 g H_2O/g polymer (4.1 mol% SOS). Importantly, the change in equilibrium Q with decreasing SOS composition was entirely consistent with that observed in our prior studies employing this sphere based network,[14, 15] once the significant differences in molecular weight used in those studies are accounted for. A detailed discussion of the influence of SOS composition on hydrogel swelling behavior can be found in a previous publication.[14] Of notable importance is the role that SOS composition and the associated concentration of topologically fixed entanglements play in determining Q. As alluded to in the introduction, polystyrene end blocks of the SOS triblock copolymer become fixed within the spherical domains during sample vitrification. Topological entanglements among nearby tethers are produced during the melt-state self-assembly. Upon exposure to aqueous media, these entanglements act to restrict expansion of the hydrogel. The concentration of topological entanglements scales with triblock copolymer composition, and therefore has a dramatic influence on the equilibrium dimensions and swelling ratio obtainable by the hydrogel (**Figure A1.2a**).

The mechanical properties evaluated in this study include dynamic shear modulus, compressive modulus, tensile strain at break, tensile stress at break, Young's modulus and toughness. All quantities were taken at first fracture. Of this set, the dynamic shear modulus and compressive modulus have been investigated previously for similar SO/SOS based hydrogel

systems.[14] Given the SO and SOS molecules used in this study are of slightly smaller molecular weights, measurements of both moduli were re-measured in order to establish the baseline performance of these particular SO/SOS blends, and provide a means of directly assessing the impact of installing a secondary network of tethers.

Figure A1.2b shows the elastic moduli of all six SO/SOS hydrogels as a function of their SOS triblock copolymer composition. The elastic moduli for hydrogels based on all six blends were found to be independent of frequency over the range of 0.1-100 Hz. Importantly these are small strains (< 3%) experiments maintained in the linear viscoelastic region for each sample. The frequency sweep data for the blend containing 8.5 mol% SOS triblock copolymer is highlighted in the inset of **Figure A1.2b**. The plateau behaviour in modulus is typical of the elastic solids and our hydrogel systems, in particular. The major axes of **Figure A1.2b** plot the elastic modulus (G') (at a shear frequency of 1 Hz) for each of the hydrogels as a function of the SOS triblock copolymer composition. The elastic moduli span a significant range (10^3 to 10^5 Pa), increasing with increasing SOS triblock copolymer composition. This ability to tune the modulus over such a dramatic range using SOS composition is consistent with our previous studies and is a consequence not only of adding additional strands (tethers) between junction points (spheres and topological entanglements) but of increased coronal layer overlap (among PEO chains) imposed by the entanglement restricted swelling.[13, 14]

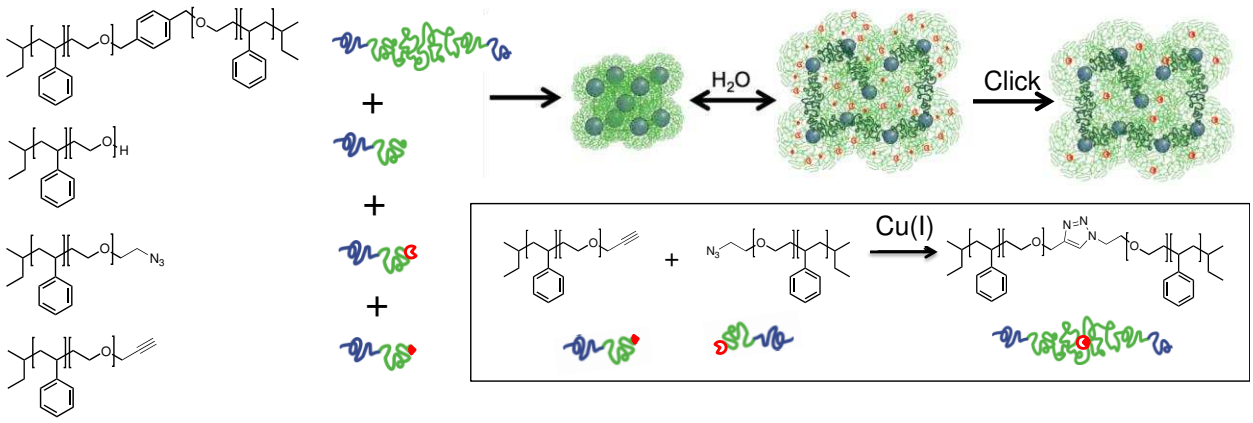

Figure A1.3: Pictorial schematic showing the strategy for introducing a secondary network of SOS triblock copolymer tethers using aqueous phase click chemistry to couple dangling PEO chain ends in situ at swelling equilibrium.

Table A1.2: Hydrogel mechanical properties of baseline TPE hydrogels and post-click DN hydrogels

Sample	SOS_{post} (mol%)	Q (g water/g polymer)	Strain to break (%)	Stress to break (kPa)	Young's modulus (kPa)	Toughness (kJ/m^3)
Baseline SO/SOS Hydrogels	4.1	26.9	-	-	-	-
	8.5	20.7	154	8.7	5.3	6.2
	20.3	9.3	375	107	38	203
	29.2	7.9	293	150	82	246
	32.4	7.0	254	160	110	240
	45.1	5.7	195	237	209	280
A	20.0 ± 1.2	18.5 ± 1.0	287 ± 58	68 ± 21	12.0 ± 1.5	74 ± 33
B	28.1 ± 3.6	18.3 ± 0.7	458 ± 85	163 ± 53	12.5 ± 1.2	269 ± 116
C	38.1 ± 4.4	18.8 ± 0.4	567 ± 56	169 ± 34	11.2 ± 1.5	361 ± 93
D	49.1 ± 3.0	19.2 ± 0.7	479 ± 103	135 ± 30	13.1 ± 1.2	276 ± 127

Figure A1.2c shows the compressive moduli of the six hydrogel samples as a function of SOS triblock copolymer concentration. Unconfined compression/decompression was carried out to 40% strain for each sample at a strain rate of 20% min^{-1}. Each sample was subjected to two continuous compression/decompression cycles, with no delay between cycles. Example stress-strain data for the sample containing 8.5 mol% SOS triblock copolymer is shown in the **Figure A1.2c** inset. The basic cycle shape exhibited by the 8.5 mol% SOS sample was consistent across all hydrogels regardless of SOS triblock copolymer composition, and indicates several shared characteristics of hydrogels constructed using this pre-structured network of tethered spheres.

The modulus under compression remains constant (stress linear in strain) up to 40% strain for all samples. The compressive modulus, indicated by the slope of the compression leg of the cycle is plotted on the major axes of **Figure A1.2c** for each hydrogel as a function of its SOS triblock copolymer composition. Like the dynamic shear modulus, the compressive modulus increases with increasing SOS composition, covering an impressive range spanning two orders of magnitude, from approximately 5.3 kPa (4.1 mol% SOS) to 480 kPa (45.1 mol% SOS). Each hydrogel also exhibits complete elastic recovery (with reproducible hysteresis) such that the first and second compression/decompression cycles are experimentally equivalent.

Figure A1.2d shows the stress-strain behaviour for five of the six baseline SO/SOS TPE hydrogels under tensile strain. The resolution of the normal force transducer used was insufficient to accurately examine the tensile properties of smallest SOS content (4.1 mol%) and therefore weakest hydrogel. As with the dynamic shear modulus and compressive modulus, increasing the SOS triblock copolymer content had a significant influence on the tensile properties exhibited by the hydrogel. Table 2 shows the values for the Young's modulus (initial slope), strain at break, and toughness for the baseline TPE hydrogels as a function of their SOS triblock copolymer content. Interestingly, while the Young's modulus increases quite dramatically with increasing SOS triblock copolymer content, improving from 5.3 to 209 kPa between 8.5 mol% and 45.1 mol% SOS triblock copolymer. The hydrogel toughness seems to also improve with the SOS composition, although the most significant jump takes place between 8.5 mol% and 20.3 mol% SOS triblock copolymer (from 6.2 to 203 kJ m^{-3}). After that the improvement is far less dramatic, with the toughness of the 45.1 mol% SOS sample topping out at 280 kJ m^{-3}. This non-linear dependence on SOS composition suggests a transition in the failure mechanism from one that is quite dependent on the concentration of tethering molecules

at low concentrations to one that is much less dependent at higher concentrations. At low concentrations, the tethering molecules are responsible for absorbing most of the load, and their number appears to be the primary factor limiting the total energy absorbable by the hydrogel. We believe once the concentration of tethering molecules reaches a critical value, the entanglement density produced among them more effectively distributes the load across the entire network and provides a higher overall modulus. However, those entanglements, just as they limit strain produced by osmotic swelling forces (as their number increases), also limit the strain available to the hydrogel under a tensile loading event. As a result, the strain at break decreases as the tether concentration increases above that 20 mol% threshold. We suspect that once the hydrated matrix reaches its strain limit, failure is likely a consequence of bond rupture in the hydrated PEO matrix, rather than chain pull out from, or brittle facture within, the vitrified PS spheres. This hypothesis has yet to be examined.

Clearly, additional SOS triblock copolymer added during the melt-state self-assembly process has considerable influence on hydrogel mechanical properties. The next section of this article is focused on how the installation of additional SOS tethering molecules after equilibrium swelling enhances the toughness exhibited by these hydrogel systems. We chose to focus our efforts on hydrogels with original SOS triblock copolymer compositions in the 9 to 10 mol% range. These hydrogels exhibited significantly high Q values in the range of 18 to 20 g H_2O/g polymer and could be handled easily due to reasonable shear, compressive and tensile moduli, but lacked the toughness of the higher SOS content hydrogels by a significant margin (ca. **Figure A1.2d**, 8.5 mol%). The goal was to use latent azide and alkyne chain end functionality as a means of performing diblock copolymer coupling in situ, once self-assembly, vitrification, and swelling were already complete. The diblock copolymer coupling effectively creates additional

SOS triblock copolymer in the system, but absent of the osmotic stress imposed on the original SOS triblock copolymer present during initial swelling. This strategy is shown pictorially in **Figure A1.3**. It was our hypothesis that this second population of SOS triblock copolymer tethers would serve to improve toughness by extending the strain limitations of the first tether population, given their initial, unstrained state.

A1.2.3 Chemical Characterization and Swelling in "Click" Enhanced Dangling-End DN Hydrogels.

Four blends (A through D), each containing approximately (1) 8.9 to 10.4 mol% SOS triblock copolymer, (2) varying, equimolar amounts of SO-azide and SO alkyne diblock copolymer, and (3) a balance of reactively inert SO diblock copolymer, were prepared. The concentration of SO-azide and SO-alkyne were chosen such that the baseline values of 8.9 – 10.4 mol% SOS present in each sample prior to swelling could be theoretically increased to values ranging from 28.8 mol% (blend A) to 100 mol% (blend D) *aggregate* SOS triblock copolymer in the final hydrogel network (Table 1).

Multiple polymer discs were melt-pressed from each of the blends A through D (Table 1). The discs were individually swollen in excess DI water until reaching equilibrium dimensions (about one hour evident by constant mass and size). The Q values for hydrogel discs formed from each of the blends A through D prior to exposure to Cu(I) catalyst are shown in **Figure A1.5**. The inclusion of SO diblock copolymer that contains terminal azide or alkyne functionality appeared to have no particular influence on the equilibrium swelling dimensions when compared to that expected from baseline SO/SOS type hydrogels with similar SOS triblock copolymer compositions. That is, all hydrogels from the blends exhibited pre-click Q values in the 18 – 20 g H_2O/g polymer range, consistent with an SOS tether content in the 8.9 – 10.4 mol% range. This

behaviour confirmed the hypothesis that the integration of chain end functionality other than the native hydroxyl at the PEO chain end could be done without disruption of the basic network swelling behavior.

Each hydrogel solution (hydrogel in excess DI water) was degassed with argon prior to the addition of sodium ascorbate and copper (II) sulphate. The combination of copper sulfate and sodium ascorbate produces the Cu(I) catalyst in-situ to facilitate the Huisgen cycloaddition reaction between terminal azide and alkyne functional groups of the hydrated PEO blocks.[27] In the absence of oxygen removal from the hydrogel solutions prior to catalyst addition, we observed significant PEO degradation (verified with SEC, data not shown). This is in accordance with reports by the Madras[28] and Crowley groups[29] who observed similar degradation phenomena. Hydrogel samples were left in the catalyst solution for 24 hours prior to removal, followed by sequential dialysis against fresh DI solutions to remove residual catalyst. Preliminary kinetic experiments were used to confirm the 24-hour reaction time was sufficient to reach maximum conversion. Coupling efficiencies were calculated based on the percent of azide (or alkyne) functional groups reacted as quantified through the observed SOS triblock copolymer added to the system following exposure to the Cu(I) catalyst.

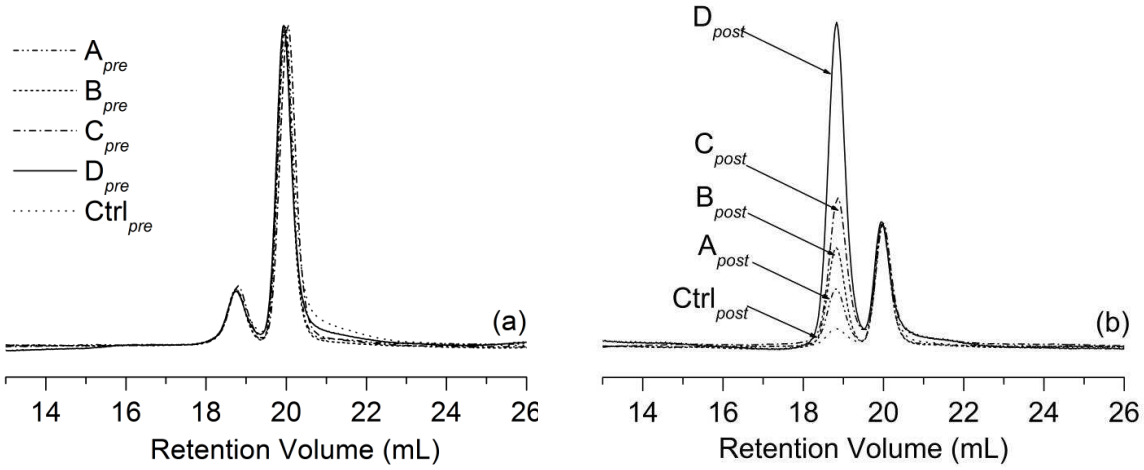

Figure A1.4: Representative SEC data for hydrogels formed from blends A through D (a) before (pre) and (b) after (post) exposure to the Cu(I) catalyst. All SEC traces are normalized to a constant area under the SO-X diblock copolymer peak (right) in order to show the relative amounts of SOS triblock copolymer (left peak) more clearly. Control samples contain only SO and SOS and verify that exposure to the catalyst solution has no degradative effects on the constituent block copolymers.

Representative SEC data is shown in **Figure A1.4** for each of the blends with the results of all coupling reactions summarized in Table 1. Beyond the molecular weight distributions captured in these SEC traces, the data demonstrates the unique ability to deconstruct these TPE hydrogels back into their constituent block copolymer species through simple removal of water and dissolution in an organic solvent. Even after the introduction of the secondary network, the hydrogel remains a physically cross-linked mixture of diblock and triblock copolymer, which can be easily recovered and reprocessed.

Importantly, a control sample composed of only SO diblock and SOS triblock copolymer, absent of any azide/alkyne functionality was also run in parallel, to determine the effect of sodium ascorbate and copper (II) sulfate solution on the constituent polymer species. The SEC traces of the control sample before and after exposure to the catalyst system for 24 hours showed no significant change, suggesting neither degradation nor significant side-reactions occurred (**Figure A1.4**). To ensure that coupling in the sample was homogeneous and not influenced by

diffusion limitations in either copper sulfate or sodium ascorbate, SEC was performed on sections taken from both inner and outer regions of a disc. No significant differences in regional coupling were detected in any samples tested.

SEC analysis of the total SOS triblock copolymer after the post-swelling click chemistry varied from 18.4 - 52.0 mol%, depending on blend. Importantly, these values were reflective of a coupling efficiency that remained almost constant (58.1% ± 6.3%) across all samples despite variation in the amount of azide/alkyne functional polymer present. This is likely indicative that some degree of non-quantitative functionality is present in the initial materials (e.g. PS-PEO-azide at < 100% functionality). However, post-reaction ^{1}H NMR and FTIR seem to indicate both azide and alkyne groups are still present in small amounts, although the size of the block copolymers have made quantification unreliable. We suspect that in addition to non-quantitative functionality in SO-azide (or SO-alkyne), performing the reaction within the context of a fixed morphology is also playing an active role in determining coupling efficiency. On the positive side, the self-assembled sphere morphology uniquely places PEO chains of the corona in close proximity with those belonging to adjacent spherical domains. This structure spatially directs or concentrates terminal azide and alkyne groups into defined regions, which should enhance coupling efficiencies when the number of functional chain ends in the region is high (as it is at low conversions). On the negative side, the reaction volume available to each functional group is constrained by the limited travel available to each PEO chain end, given the opposing end is anchored to a fixed junction point (spherical domain) in the network. As the conversion proceeds to higher values, and residual functional group concentrations diminish, the occurrence of orphaned chain ends is likely. Finally, the preferred location of azide and alkyne functional chain ends during self-assembly process is unknown. It is also possible the sphere morphology

produces a consistent ratio of functional chain ends that loop back and are sequestered deep in the coronal PEO layer, in proximity with the PS domains. Such buried chain ends would have severely hindered mobility and be unable to contribute to the in-situ generation of triblock copolymer. We also note that our polymers are of much greater molecular weight than what is commonly employed in azide/alkyne click reactions (M_n < 30000 g/mol)[27] and that coupling efficiency between high molecular weight species is commonly much lower than that reported for small molecular weight systems. It is unclear at present if the moderate conversion yield is a result of limitations associated with phase separation, morphology, non-quantitative functionality in one or both species, or a combination of these factors.

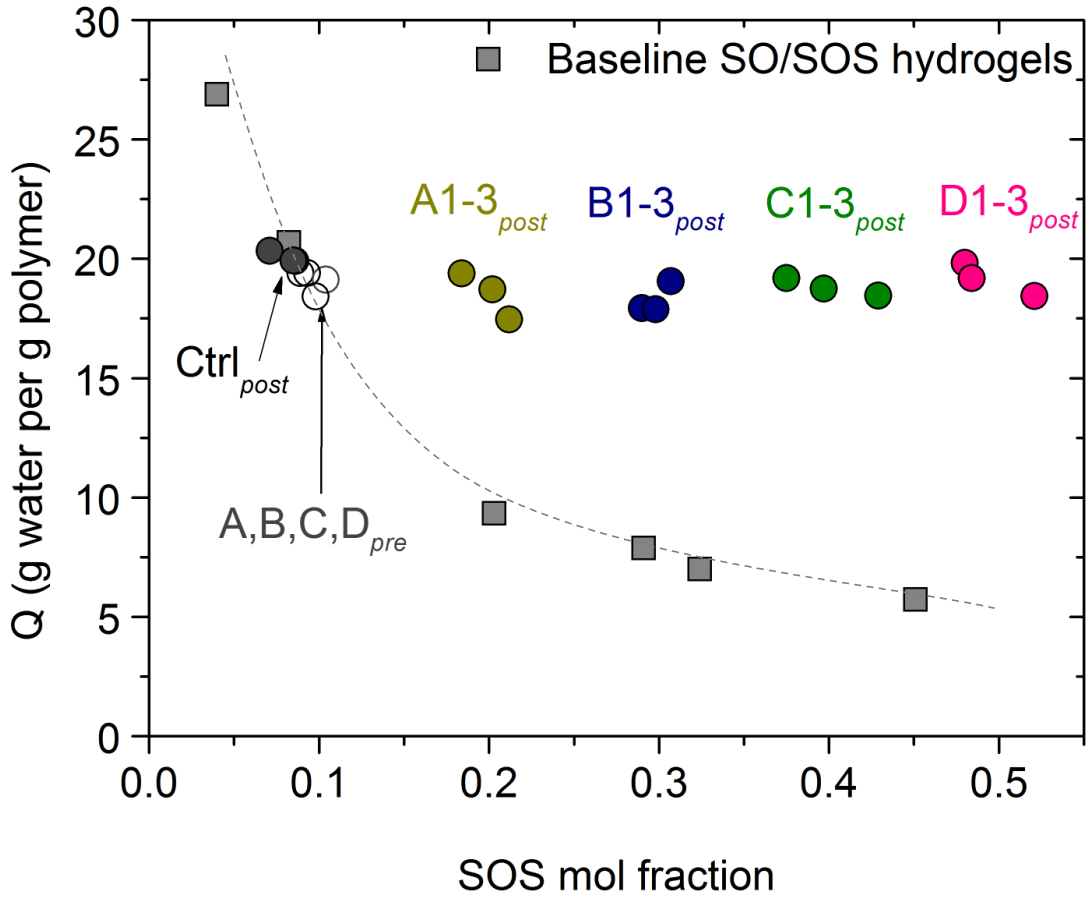

Figure A1.5: Hydrogel swelling ratio (Q) as a function of SOS triblock copolymer composition. Data show the installation of a secondary network of SOS tethers has no impact on the equilibrium swelling ratio determined by the primary SOS network.

The post-click Q values for three hydrogels from each blend type are given in **Figure A1.5** as a function of their new total SOS triblock copolymer compositions. Clearly, the installation of additional SOS triblock copolymer through click coupling under equilibrium swelling conditions has no significant influence on the water content of the hydrogel. That is, the Q values still reflect the SOS triblock copolymer composition present prior to swelling. Q values for the baseline SO/SOS hydrogels are included in **Figure A1.5** and provide a direct comparison between hydrogels of similar *total* SOS triblock copolymer compositions, differing only in the manner in which the triblock copolymer was introduced into the system. To summarize, one can

predetermine water content by selecting the percentage of SOS triblock copolymer used during melt-state self-assembly. The post-swelling click chemistry then provides a means of adding an additional, secondary network of SOS tethers while preserving the original Q values. The impact of this secondary network on the mechanical properties of the hydrogel is the subject of the next section.

A1.2.4 Mechanical Performance of "Click" Enhanced Dangling-End DN Hydrogels.

Figure A1.6 shows the pre-click and post-click elastic moduli of hydrogels formed from the four blends A through D. In addition, the elastic moduli of the six SO/SOS TPE hydrogels are also included for direct comparison of the post-click DN hydrogels with baseline hydrogels of similar SOS content. As a control experiment, baseline SO/SOS hydrogels (no azide or alkyne functionality present) with approximately 8.5 mol% SOS triblock copolymer were soaked in argon degassed catalyst solutions for the standard 24 hour reaction time. Their elastic moduli are also included in **Figure A1.6**. The purpose of those control samples was to establish the effect of the catalyst solution on the mechanical properties of the hydrogel independent from the addition of SOS tethers. As shown in **Figure A1.6**, the elastic moduli after catalyst solution exposure remained very similar to that of the unexposed 8.5 mol% baseline hydrogel (original frequency sweep data is provided in the supplementary information). Thus, the impact of the catalyst solution exposure on elastic modulus was regarded to be negligible.

The effect of adding azide and alkyne chain end functionality (unreacted) towards the elastic modulus of the hydrogel appears to be largely minimal. Examples of the elastic moduli of the four blends prior to the addition of the catalyst solution all appear to fall along the trajectory expected for the baseline SO/SOS hydrogel systems. That is, the chain in functionality in its

uncoupled state has limited to no effect on the elastic properties of the hydrogels under dynamic shear, as expected.

A comparison of the elastic moduli of hydrogels under dynamic shear, containing azide/alkyne functional groups both pre- and post-click reveals an apparent increase in elastic modulus (20 to 40%) upon installation of additional SOS triblock copolymer. However, when compared with baseline TPE hydrogels of similar *total* SOS triblock copolymer compositions, these increases in modulus (as a result of introducing the second network of tethers) are actually quite modest. For example, adding tethers post-swelling to get from 8.9 mol% SOS to 48 mol% SOS triblock copolymer (sample D1) produces an increase in elastic modulus from 4.7 to 6.3 kPa (supplementary data). By comparison, baseline SO/SOS hydrogels with 45.1 mol% SOS triblock copolymer in which the entire population of tethers was introduced during melt-state self-assembly exhibits an elastic modulus of just over 100 kPa. This type of comparison underscores the very limited impact the secondary network, installed post-swelling, has on the small strain shear response of these hydrogels. At small oscillatory strains (< 3%), the secondary network, containing almost four times the number of tethers as the primary network, remains largely passive. This is a direct reflection of the stress free environment under which these tethers are installed. Notably, in a previous study we have shown the elasticity of these hydrogel networks is governed predominately by the degree of PEO coronal overlap with adjacent spherical domains.[13] The small improvement in elastic modulus is likely product of the changes in the way in which adjacent coronal layers are connected, however, without a pronounced difference in coronal layer overlap, the changes detected remain quite modest.

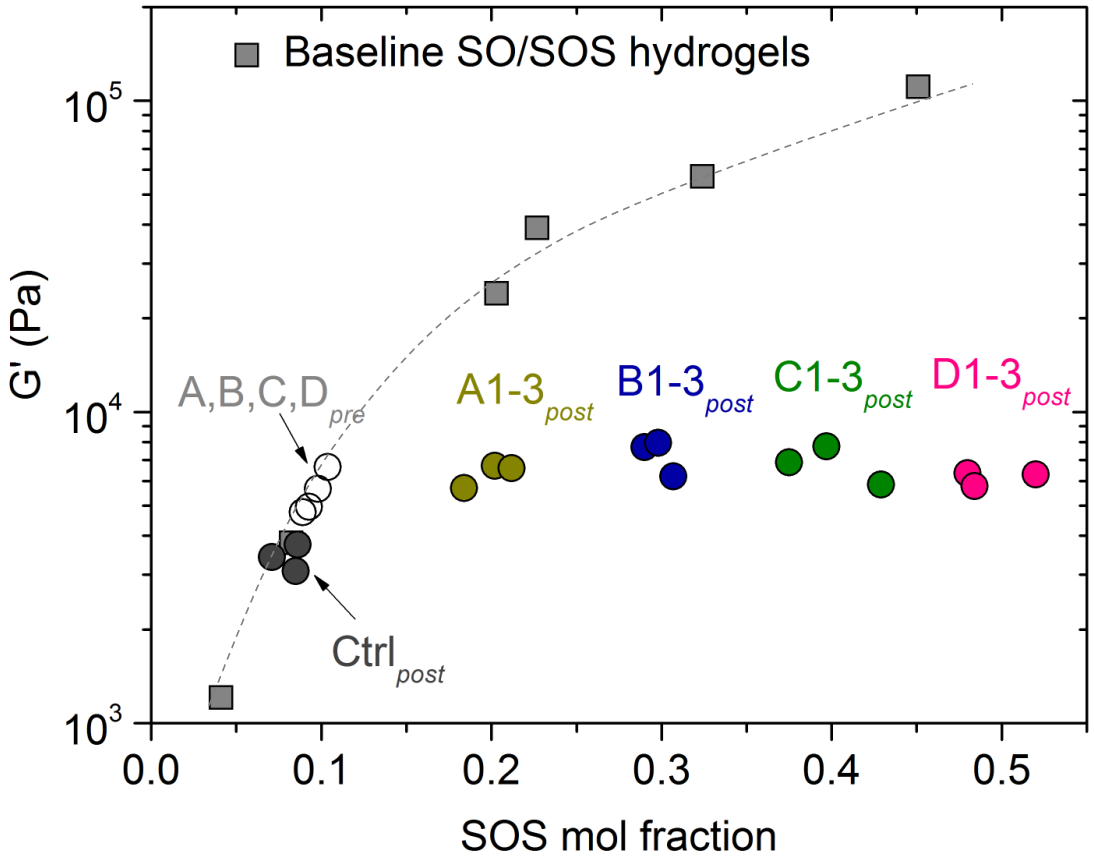

Figure A1.6: Elastic moduli under dynamic shear (ω=1 Hz) as a function of total SOS triblock copolymer composition.

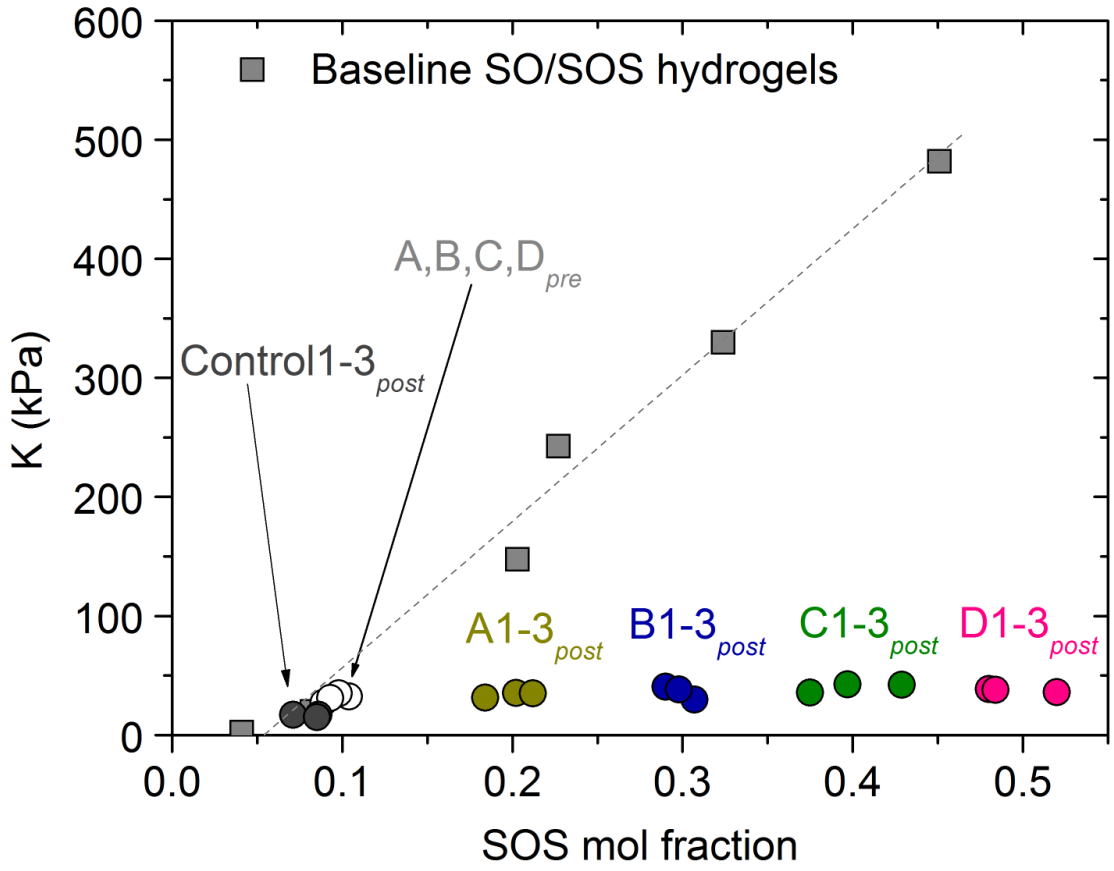

Figure A1.7: Compressive moduli in unconfined compression (strain rate = 20% min^{-1}) as a function of total SOS triblock copolymer composition.

The behaviour of the post-click DN hydrogels in unconfined compression (to 40% strain) produced similar conclusions (**Figure A1.7**). As with the baseline SO/SOS hydrogels, all samples, regardless of treatment, produced linear stress-strain relationships to 40% strain (strain rates at 20% min^{-1}) and exhibited some hysteresis during decompression, but ultimately showed complete elastic recovery with second compression/decompression cycles coinciding the first cycle. Baseline SO/SOS control samples exposed to catalyst solutions for the required 24 hour reaction time performed similarly to unexposed baseline hydrogels in agreement with the previous experiments involving elastic modulus. Pre-click samples gave compressive moduli consistent with those produced by baseline SO/SOS hydrogels of similar SOS triblock

copolymer compositions, also in agreement with the previous experiments involving elastic modulus. The effects of installing the additional SOS triblock copolymer post-swelling resulted in small increases in compressive modulus across all samples when compared with their pre-click counterparts, but as with elastic modulus, the increase was very modest when compared with baseline SO/SOS hydrogels of similar *total* SOS content. Using sample D1 as an example once again, the pre-click (8.9 mol% SOS) and post-click (48.0 mol% SOS) compressive moduli were 27 and 38 kPa respectively, demonstrating the marginal effect of the secondary SOS network on compression response of the hydrogel. By comparison, the baseline SO/SOS hydrogel of 45.1 mol% SOS exhibited a compressive modulus of 482 kPa. Perhaps unexpectedly, the post-click DN data suggest that even at 40% compression, the secondary network of SOS tethers still does not engage to an extent that allows it to contribute significantly to the mechanical response of the hydrogel, even with four times as many tethers as the primary network. The SOS triblock copolymer of the primary network introduced during melt-state self-assembly is still the dominant factor determining compressive properties. Original compression data for the baseline SO/SOS control samples, as well as the pre- and post-click samples A1 – D1 are included in the supplementary information.

The true impact of installing the secondary network of SOS tethers is the stunning enhancement in hydrogel toughness possible while maintaining very high Q values. **Figure A1.8** shows the tensile tests from a series of post-click DN samples A through D. In most cases, multiple test coupons could be tested from each sample disc (i.e.. discs B1, B2 and B3 produced six viable test coupons), with all results from each sample group combined to produce the four plots of **Figure A1.8**. Similar control experiments on baseline SO/SOS hydrogels exposed to the catalyst solution for 24 hours, as well as pre-click blends A through D showed tensile behaviour

similar to that expected for baseline SO/SOS hydrogels of similar SOS content, as expected. However, the post-click blends A through D showed dramatic improvements in virtually all tensile property categories. Table 2 summarizes the basic tensile properties for each of the hydrogel blends A through D, along with analogous data for the performance of the baseline SO/SOS hydrogels. Importantly, each of the hydrogels formed from blends A through D has a swelling ratio in the range of 18 – 20 g H_2O/g polymer, and is therefore comparable with the 8.5 mol% SOS baseline hydrogel.

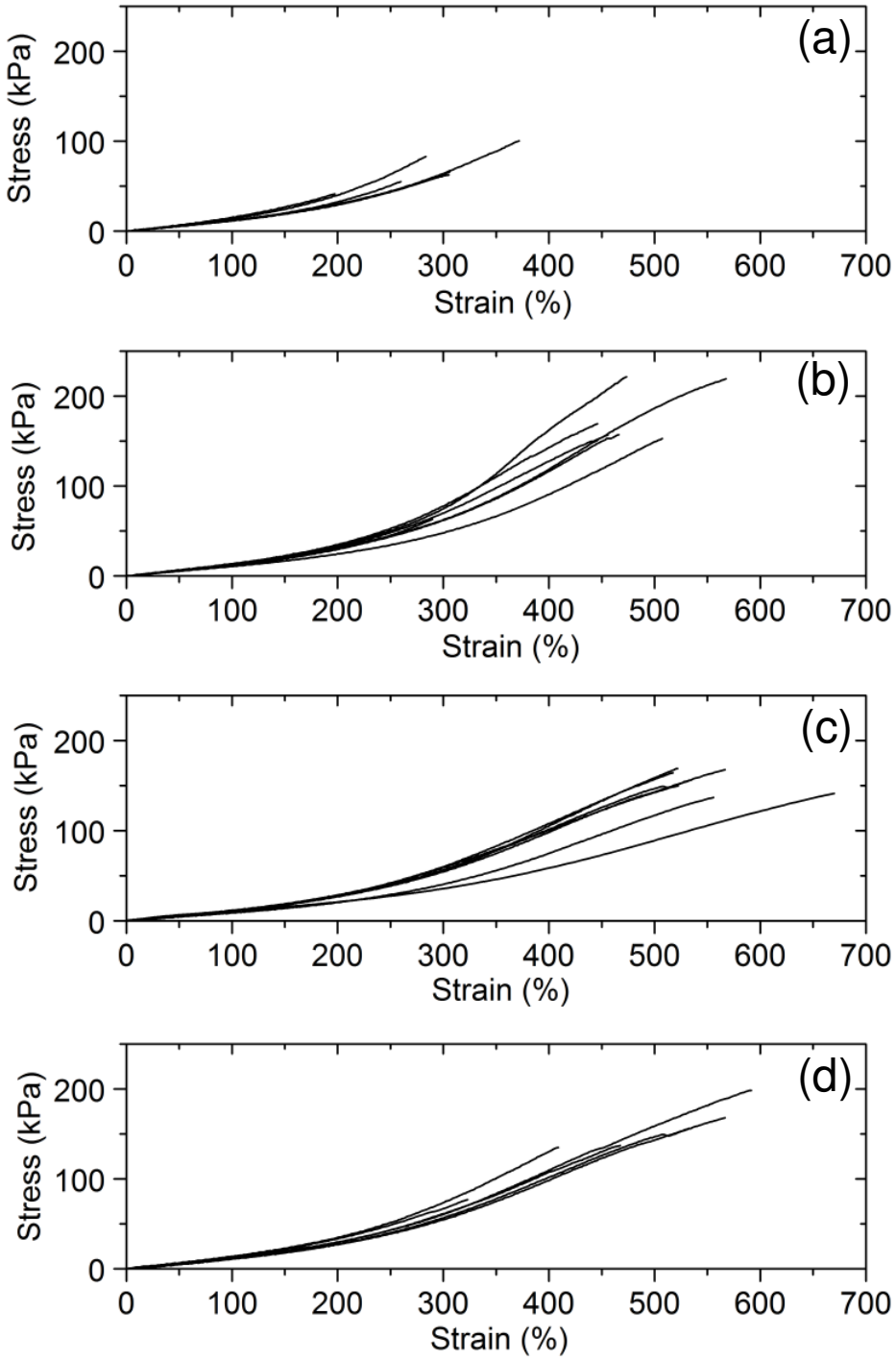

Figure A1.8: (a) – (d) Tensile test results for hydrogels formed from blends A through D, respectively, evaluated after installation of the secondary network of SOS triblock copolymer. Total SOS triblock copolymer compositions can be found in Table 2.

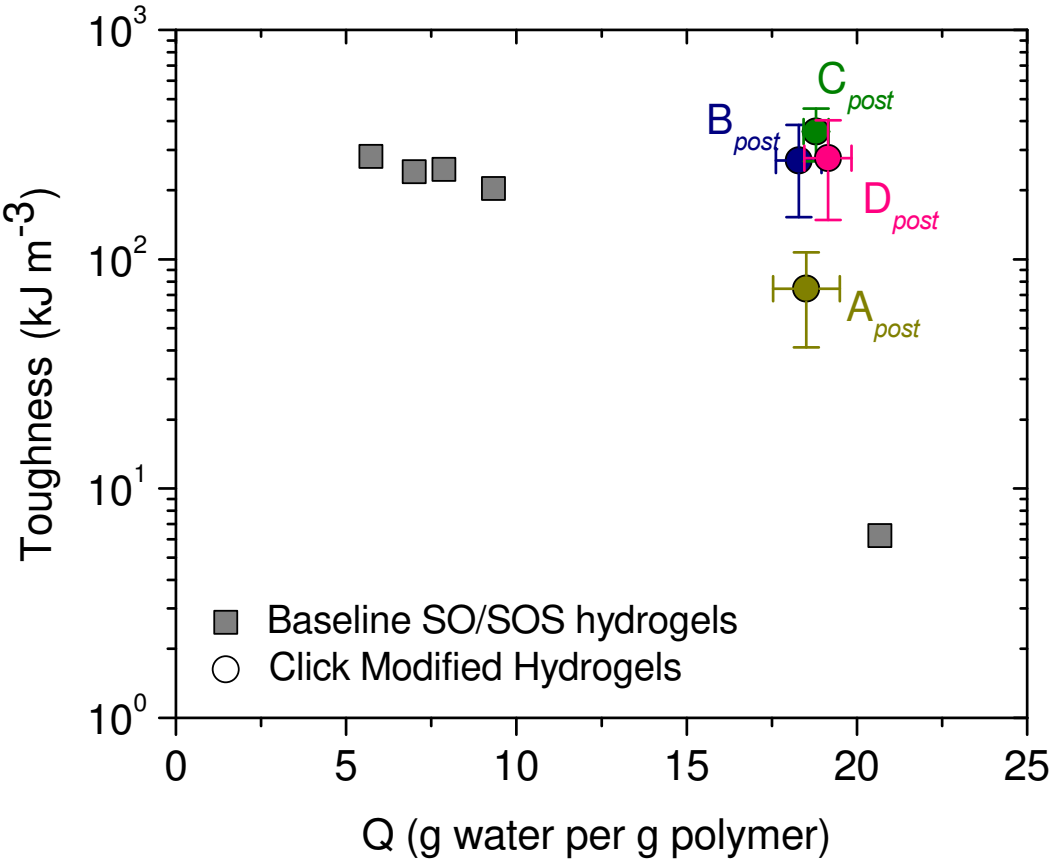

Figure A1.9: Hydrogel toughness as a function of Q. Data show the installation of a secondary network of SOS tethers improves hydrogel toughness while remaining approximately the same Q. The toughness and Q data can be found in Table 2.

One can see immediately from the entries in Table 2 as well as **Figure A1.9** that the addition of the secondary network provides vast improvements in both toughness and stress to break. With only a single, primary network of SOS tethers, the 8.5 mol% SOS hydrogel (~ 95% H_2O by mass) was able to absorb 6.2 kJ m^{-3}. before fracture at stresses as low at 8.7 kPa. With the addition of the secondary network of tethers, both the toughness and stress at break could be improved dramatically, with samples from blend C reaching mean values of 361 kJ m^{-3} (a 58-fold increase) and 169 kPa (a 19-fold increase), respectively. Similarly, the secondary network of SOS tethers provides significant improvements in strain to break (2- to 3-fold) and Young's

modulus (2-fold) when compared with the 8.5 mol% SOS baseline hydrogel of equivalent Q value. Incredibly, the installation of the secondary network, even at the moderate levels produced in the B blends, provides hydrogels with Q values of 18 - 20 g H_2O/g polymer the tensile properties typically available only to hydrogels of *much lower* water content.

We believe the dramatic impact of the secondary SOS network under tension (in comparison to small strain shear or unconfined compression) is a product of its ability to reinforce the primary network at higher strains. Because it is largely formed in an unperturbed state, the topological entanglements of the secondary network require much higher strains to become mechanically engaged. As such, they provide the hydrogel network an improved range over which strain energy can be absorbed by the hydrogel. That is, as the primary network approaches its mechanical limit, it gradually begins to transfer load to the secondary network, extending the strain and stress to break. Consequently, these additional tethers improve the elongation capacity of the hydrogels, quite remarkably. Overall, the post swelling click chemistry provides a means of adjusting the tensile properties of these tethered micelle based hydrogels, in a manner that is largely independent of other mechanical properties.

It should be noted that no particular processing strategies were developed to optimize the tensile performance of these samples. The stress-strain plots in **Figure A1.8** give a sense of the scatter in the tensile response that was typical given simple melt-pressing under atmospheric conditions. Thus the measured tensile properties are almost assuredly influenced by the presence of bubble, grain boundary and edge defects present before and after swelling. As a consequence, the vast improvements in tensile properties reported are likely understated. That is, the potential of the secondary network to enhance the tensile properties of these hydrogel systems may not be fully accessible until processing strategies are optimized to limit focal defects.

Finally, we reiterate the inherent simplicity of this hydrogel network, which is based effectively on a single parent PS-PEO block copolymer. Unlike traditional DN hydrogels, the first and second networks in this system derive from the same molecular constructs, with the elements of the second network intrinsically present, yet held dormant until catalytically activated (in this specific case). The strategy preserves the chemical composition of the hydrogel while employing a stepwise installation process to form two chemically identical tethering populations, each under a different degree of mechanical (osmotic) stress. Importantly, with the exception of the Cu(I) catalyst specific to this particular choice of coupling chemistry, formation of the secondary network by this route could potentially eliminate concerns associated with leaching in traditional DN hydrogel systems. Alternative, catalyst free approaches are currently under development.

A1.3 CONCLUSIONS

The homogeneity in structure provided by melt-state self-assembly of sphere-forming blends of PS-PEO diblock and PS-PEO-PS triblock copolymers produces a primary network of spherical domains that remains incredibly elastic when swollen in water. Such hydrogel networks were able to absorb tensile strains to a few hundred percent, with the exact modulus exhibited tunable through the triblock copolymer composition of the original melt-state blend. By incorporating azide and alkyne functional PS-PEO diblock copolymer into the hydrogel framework, a secondary network of tethers could be reactively installed through in situ coupling of the dangling PEO chain ends. Importantly, the installation of the second network did not influence the equilibrium water content of the hydrogel system. Through mechanical testing of this novel system containing both primary and secondary dangling-end double networks, we were able to establish the passive nature of the secondary network under small strain dynamic

shear and larger strain unconfined compression experiments. However, the presence of the secondary network was able to dramatically improve the high strain tensile properties (strain to break, stress to break, Young's modulus and toughness) of high water content hydrogels. For example, the toughness and stress to break of hydrogels containing 95% (g/g) water was increased nearly 58-fold and 19-fold, respectively, through secondary network installation. This remarkable increase is attributed to the system's ability to gradually transfer load from the primary to the secondary network, directly extending the ability of the system to withstand larger and larger stresses and/or strains. With such vast improvements in tensile properties these unique TPE hydrogel networks have the potential to now rival many of the current DN approaches, particularly when large swelling capacities ($Q > 15$) are required. Perhaps more importantly, the concept of exploiting dangling chain ends as an untapped source of improved toughness can be easily extended to a range of other hydrogels systems beyond the scope of this initial demonstration.

A1.4 EXPERIMENTAL

Materials. Styrene (99%, 4-tert-butylcatechol inhibitor, Aldrich) and ethylene oxide (99.5+%, compressed gas, Aldrich) monomer were each purified by successive vacuum distillations (10–20 mTorr) from dried di-n-butylmagnesium (0.1 mmol g^{-1} monomer, 1.0 M solution in heptane, Aldrich) before use. Both purified styrene and ethylene oxide monomer were stored in glass burettes in the dark, at room temperature (styrene) and 3 ˚C (ethylene oxide), respectively, before use (typically less than 24 h). Argon degassed cyclohexane (CHX) was purified by passing the solvent over activated alumina followed by Q-5-like supported copper catalyst (Glass Contour, proprietary). Argon degassed tetrahydrofuran (THF) was purified by passing the solvent over activated alumina. High-purity argon (99.998%, Airgas) was passed through additional oxygen and moisture traps prior to use. Glassware and polymerization reactors were flamed under vacuum and backfilled with argon (3x). Polymerizations and functionalization reactions were carried out using standard air-free techniques. All other materials were used as received.

Synthesis of PS-PEO diblock copolymer (SO-H) and PS-PEO-PS (SOS) triblock copolymer. SO-H and SOS were prepared as reported previously using two-step anionic polymerization of styrene and ethylene oxide monomers.[14, 19, 20] The fractionation process used for triblock copolymer purification was previously discussed where chloroform and n-hexane were used as solvent/non-solvent system and the temperature was maintained higher than 40 ˚C to avoid PEO crystallization.[13, 21] SEC: (THF, PS std): M_w/M_n=1.04. $M_{n,SO}$ = 70000 g mol^{-1}. M_w/M_n=1.06. $Mn_{,SOS}$ = 140000 g mol^{-1}, (calculated using SO M_n),; δ_H (300 MHz; $CDCl_3$): 6.20-7.26 (b, -C_6H_5,-$OCH_2(C_6H_4)CH_2O$-), 4.55 (s, -$OCH_2(C_6H_4)CH_2O$-), 3.1–4.0 (b, -CH_2CH_2O-

, -CH(C_6H_5)CH_2CH_2O-), 1.0-2.30 (b, -CH_2CH(C_6H_5)-, CH_3CH(CH_2CH_3)-, -CH(C_6H_5)CH_2CH_2O-), 0.5-0.78 (m, CH_3CH(CH_2CH_3)-).

Synthesis of SO-azide.[22, 23] SO-H (5.42 g, 7.8x10-5 mol) was added to a 300 mL flask, which was then evacuated and backfilled with Ar (3x). 100 mL of distilled methylene chloride was then added to dissolve the polymer. The flask was placed to a pre-heated oil bath at 45 ˚C before adding methane sulfonylchloride (MsCl, 0.12 mL, 20 equiv.) and triethyl amine (0.2 mL, 20 equiv.). The reaction was allowed to stir overnight and the crude product was filtered before being precipitated into pentane (1 L). The solid was collected via vacuum filtration and dried under vacuum overnight to produce a white solid. Yield 5.25 g, 95+%. SEC: (THF, PS std): M_w/M_n=1.05. $M_{n,SO\text{-}azide}$ = 70000 g mol^{-1}; δ_H (400 MHz; $CDCl_3$): 6.20-7.26 (b, -C_6H_5, -OCH_2(C_6H_4)CH_2O-), 4.55 (s, -OCH_2(C_6H_4)CH_2O-), 4.2-4.4 (t, -CH_2-SO_3-CH_3), 3.1–4.0 (b, -CH_2CH_2O-, -CH(C_6H_5)CH_2CH_2O-), 2.7 (s, -CH_2-SO_3-CH_3), 1.0-2.30 (b, -CH_2CH(C_6H_5)-, CH_3CH(CH_2CH_3)-, -CH(C_6H_5)CH_2CH_2O-), 0.5-0.78 (m, CH_3CH(CH_2CH_3)-).

SO-Ms (4.75 g, 6.9x10-5 mol) was placed in a 300 mL round bottom flask containing purified DMF under Ar in a pre-heated oil bath at 60 ˚C. After the polymer was completely dissolved, sodium azide (NaN_3, 0.089g, 20 equiv.) was added to the reaction with vigorous stirring. The crude reaction mixture was filtered after an overnight reaction and then precipitated into ethyl ether. The collected powder was then dissolved in chloroform to be washed with DI water. The polymer solution in chloroform was dried using magnesium sulfate and then filtered. White powder was collected though filtration under vacuum after the precipitation into pentane. The polymer was then dried under vacuum at room temperature overnight. Yield 4.2 g, 88%. SEC: (THF, PS std): M_w/M_n=1.05. $M_{n,SO\text{-}azide}$ = 70000 g mol^{-1} (difference between end-groups did not calculated); δ_H (400 MHz; $CDCl_3$): 6.20-7.26 (b, -C_6H_5, -OCH_2(C_6H_4)CH_2O-), 4.55 (s, -

$OCH_2(C_6H_4)CH_2O$-), 3.1–4.0 (b, -CH_2CH_2O-, -$CH(C_6H_5)CH_2CH_2O$-), 1.0-2.30 (b, -$CH_2CH(C_6H_5)$-, $CH_3CH(CH_2CH_3)$-, -$CH(C_6H_5)CH_2CH_2O$-), 0.5-0.78 (m, $CH_3CH(CH_2CH_3)$-)

Synthesis of SO-alkyne.[24] SO-H (6.31 g, 9.1x10-5 mol) was placed into a 500 mL two-neck round bottom flask. Dry THF (250 mL) was added to the flask. The solution was heated in a pre-heated oil bath at 50 ˚C under Ar. Once SO-H was completely dissolved, NaH (0.23 g, 100 equiv.) was added to the solution and stirred for 20 minutes. Propargyl bromide solution in toluene (80 wt%, 0.31 mL, 20 equiv.) was injected to the reaction via an air-free syringe. The reaction was increased to 65 ˚C to reflux overnight. The reaction mixture was filtered and precipitated three times into pentane (1 L). The suspension was filtered and dried under vacuum overnight to give pale yellow powder. Yield 5.65 g, 89%. SEC (THF, PS std): M_w/M_n=1.05. $M_{n,SO\text{-}alkyne}$ = 70000 g mol^{-1} (difference between end-groups did not calculated); δ_H (400 MHz; $CDCl_3$): 6.20-7.26 (b, -C_6H_5, -$OCH_2(C_6H_4)CH_2O$-), 4.55 (s, -$OCH_2(C_6H_4)CH_2O$-), 4.2 (d, -$OCH_2C{\equiv}C$), 3.1–4.0 (b, -CH_2CH_2O-, -$CH(C_6H_5)CH_2CH_2O$-), 2.46 (t, -C≡C*H*), 1.0-2.30 (b, -$CH_2CH(C_6H_5)$-, $CH_3CH(CH_2CH_3)$-, -$CH(C_6H_5)CH_2CH_2O$-), 0.5-0.78 (m, $CH_3CH(CH_2CH_3)$-)

SO/SO-alkyne/SO-azide/SOS blends. Each blend sample was prepared by solution blending (1 g total polymer in 20 mL benzene) the appropriate amounts of SO, SO-alkyne, SO-azide and SOS (10 mol% for all blends) to produce blends containing the specified amount of the "clickable" SO moities. Solutions were frozen using an ethanol/liquid nitrogen slush bath and then dried under vacuum at room temperature overnight.

Dry polymer disk formation. Dry polymer disks with 8 mm diameter and 0.25 mm thickness were melt-pressed using a washer between Teflon covered kapton sheets on a Carver press at 150˚C.

Swelling and in situ coupling protocols (DN formation). Dry polymer disks were placed into a 300 mL round-bottom flasks containing degassed DI water (100 mL) until the equilibrium swelling conditions were reached (~1 hr) at room temperature. Swollen hydrogels at equilibrium state were taken out from the degassed DI water and placed on a teflon surface. After excess water was blotted, the hydrogels were weighed. Then, the hydrogels were placed back into the flasks with freshly degassed water (100 mL) and degassed for another 10 minutes. Copper sulfate solution (0.25 mL, 0.007 M, in degassed DI water) and sodium ascorbate solution (1 mL, 0.009 M, in degassed DI water) were then injected into the flasks via air-free syringes. The reaction was kept at room temperature overnight. Finally, the hydrogels were left in degassed DI water for one hour to wash off the catalyst before any characterization was performed.

Molecular characterization. ^{1}H NMR spectra were collected at room temperature in $CDCl_3$ on a Varian Inova 400 MHz Spectrometer (n = 32, delay = 30 s). Size exclusion chromatography (SEC) was performed on a Viscotek GPC-Max chromatography system fitted with three 7.5 ×340 mm PolyporeTM (Polymer Laboratories) columns in series, an Alltech external column oven, and a Viscotek differential refractive index (RI) detector. S-OH molecular weight and polydispersity, and the polydispersity of the SO and SOS samples were determined using a THF (40 ˚C) mobile phase (1 mL/min) with PS standards (Polymer Laboratories).

Dynamic Shear and Unconfined Compression Testing. The rheology and unconfined compression test results were collected on a TA Instruments ARES rheometer at room temperature using parallel plate geometry with an infinite lower plate and an 8 mm upper plate. The bottom plate was the bottom of an integrated glass cup outfitted with a humidified cover. The swollen hydrogels were placed onto the bottom plate with excess water blotted away. The hydrogel thicknesses were measured on the rheometer and determined by the gap value between the parallel plates when the normal force on the upper plate reached 2 grams force. Since all unstrained hydrogels in this study exceeded 8 mm diameters, the stresses were calculated based on the fixed upper plate dimensions. To eliminate slip between the upper plate and the hydrogel samples during the rheological property measurements, 10% compressive strain was applied on each hydrogel sample. Dynamic frequency sweeps were performed on each sample using a shear strain in the range of 0.15-3% (linear viscoelastic region) over a frequency of 0.1 to 100 rad/s. For unconfined compression tests, the gels were compressed to 40% using a rate of 20%/min. Two compression-decompression cycles were performed to study the possible hysteresis also using the rate of 20%/min during decompression.

Tensile Testing. Tensile tests were carried out on rectangular pieces of hydrogel sample cut to approximately 14 mm width with thickness that varied from 0.442 to 0.875 mm. Multiple test coupons were cut from each hydrogel disc to maximize sample size within a letter group (i.e.. discs B1, B2 and B3 produced six viable test coupons). All tensile tests were run at room temperature using the normal force transducer of a TA ARES rheometer. TA rectangular torsion geometry test fixtures were used as tensile test grips, although the grip surfaces were modified with 600 grit sand paper to eliminate slip. The experimental setup and strain rate used were

similar to that reported Schmidt et al.[25] with some minor adjustments. A strain rate of 5 mm/s was applied until complete hydrogel fracture. The strain rate was chosen to minimize slip while ensuring the maximum travel distance could be covered in less than 0.5 minutes, such that surface evaporation during testing could be minimized. Stress was calculated as the force normalized by the initial cross sectional area of each sample (engineering stress).

Supporting Information. ^{1}H-NMR spectrum of PS-PEO-H, PS-PEO-Ms, PS-PEO-azide and PS-PEO-alkyne, FTIR result of PS-PEO-azide and representative rheological data. This material is available free of charge via the Internet at http://pubs.acs.org

REFERENCES

1. Annette Rösler, G. W. M. V., Harm-Anton Klok, Advanced Drug Delivery Devices Via Self-Assembly of Amphiphilic Block Copolymers. *Advanced Drug Delivery Reviews* **2001,** 53, (1), 95-108.

2. Huang, R.; Kostanski, L. K.; Filipe, C. D. M.; Ghosh, R., Environment-Responsive Hydrogel-Based Ultrafiltration Membranes for Protein Bioseparation. *Journal of Membrane Science* **2009,** 336, (1-2), 42-49.

3. Kim, J. J.; Park, K., Smart Hydrogels for Bioseparation. *Bioseparation* **1998,** 7, (4-5), 177-184.

4. Khademhosseini, A.; Langer, R., Microengineered Hydrogels for Tissue Engineering. *Biomaterials* **2007,** 28, (34), 5087-92.

5. Vinogradov, S. V.; Bronich, T. K.; Kabanov, A. V., Nanosized Cationic Hydrogels for Drug Delivery: Preparation, Properties and Interactions with Cells. *Advanced Drug Delivery Reviews* **2002,** 54, (1), 135-147.

6. Peppas, N. A.; Keys, K. B.; Torres-Lugo, M.; Lowman, A. M., Poly(Ethylene Glycol)-Containing Hydrogels in Drug Delivery. *Journal of Controlled Release* **1999,** 62, (1-2), 81-87.

7. Qiu, Y.; Park, K., Environment-Sensitive Hydrogels for Drug Delivery. *Advanced Drug Delivery Reviews* **2001,** 53, (3), 321-339.

8. Bajpai, A. K.; Shukla, S. K.; Bhanu, S.; Kankane, S., Responsive Polymers in Controlled Drug Delivery. *Progress in Polymer Science* **2008,** 33, (11), 1088-1118.

9. Hoffman, A. S., Hydrogels for Biomedical Applications. *Adv Drug Deliv Rev* **2002,** 54, (1), 3-12.

10. Jeong, B.; Kim, S. W.; Bae, Y. H., Thermosensitive Sol-Gel Reversible Hydrogels. *Adv Drug Deliv Rev* **2002,** 54, (1), 37-51.

11. Nguyen, K. T.; West, J. L., Photopolymerizable Hydrogels for Tissue Engineering Applications. *Biomaterials* **2002,** 23, (22), 4307-14.

12. Hennink, W. E.; van Nostrum, C. F., Novel Crosslinking Methods to Design Hydrogels. *Adv Drug Deliv Rev* **2002,** 54, (1), 13-36.

13. Guo, C.; Bailey, T. S., Tailoring Mechanical Response through Coronal Layer Overlap in Tethered Micelle Hydrogel Networks. *Soft Matter* **2015,** 11, (37), 7345-7355.

14. Guo, C.; Bailey, T. S., Highly Distensible Nanostructured Elastic Hydrogels from Ab Diblock and Aba Triblock Copolymer Melt Blends. *Soft Matter* **2010,** 6, (19), 4807-4818.

15. Scalfani, V. F.; Bailey, T. S., Access to Nanostructured Hydrogel Networks through Photocured Body-Centered Cubic Block Copolymer Melts. *Macromolecules* **2011,** 44, (16), 6557-6567.

16. Hiemenz, P. C.; Lodge, T., *Polymer Chemistry*. 2nd ed.; CRC Press: Boca Raton, 2007; p xvii, 587 p.

17. Yasuda, K.; Ping Gong, J.; Katsuyama, Y.; Nakayama, A.; Tanabe, Y.; Kondo, E.; Ueno, M.; Osada, Y., Biomechanical Properties of High-Toughness Double Network Hydrogels. *Biomaterials* **2005,** 26, (21), 4468-75.

18. Gong, J. P.; Katsuyama, Y.; Kurokawa, T.; Osada, Y., Double-Network Hydrogels with Extremely High Mechanical Strength. *Advanced Materials* **2003,** 15, (14), 1155-+.

19. Quirk, R. P.; Ma, J. J., Characterization of the Functionalization Reaction-Product of Poly(Styryl)Lithium with Ethylene-Oxide. *Journal of Polymer Science Part a-Polymer Chemistry* **1988,** 26, (8), 2031-2037.

20. Hillmyer, M. A.; Bates, F. S., Synthesis and Characterization of Model Polyalkane-Poly(Ethylene Oxide) Block Copolymers. *Macromolecules* **1996,** 29, (22), 6994-7002.

21. Fragouli, P. G.; Iatrou, H.; Hadjichristidis, N., Synthesis and Characterization of Linear Diblock and Triblock Copolymers of 2-Vinyl Pyridine and Ethylene Oxide. *Polymer* **2002,** 43, (25), 7141-7144.

22. Dmitri A. Ossipov, J. H., Poly(Vinyl Alcohol) Based Hydrogels Fromed by Click Chemistry. *Macromolecules* **2006,** 5, (39), 1709-1718.

23. Iyer, S. S.; Anderson, A. S.; Reed, S.; Swanson, B.; Schmidt, J. G., Synthesis of Orthogonal End Functionalized Oligoethylene Glycols of Defined Lengths. *Tetrahedron Letters* **2004,** 45, (22), 4285-4288.

24. Aggour, Y. A.; Tomita, I.; Endo, T., Synthesis and Radical Polymerization of End-Allenoxy Polyoxyethylene Macromonomer. *Reactive & Functional Polymers* **1995,** 28, (1), 81-87.

25. Gaharwar, A. K.; Dammu, S. A.; Canter, J. M.; Wu, C. J.; Schmidt, G., Highly Extensible, Tough, and Elastomeric Nanocomposite Hydrogels from Poly(Ethylene Glycol) and Hydroxyapatite Nanoparticles. *Biomacromolecules* **2011,** 12, (5), 1641-50.

26. Vsevolod V. Rostovtsev, L. G. G., Valery V. Fokin, Barry Sharpless, A Stepwise Huisgen Cycloaddition Process Copper(I)-Catalyzed Regioselective "Ligation" of Azides and Terminal Alkynes. *Angewandte Chemie International Edition* **2002,** 41, (14), 2596-2599.

27. Binder, W. H.; Sachsenhofer, R., 'Click' Chemistry in Polymer and Materials Science. *Macromolecular Rapid Communications* **2007,** 28, (1), 15-54.

28. Vijayalakshmi, S. P.; Raichur, A.; Madras, G., Thermal Degradation of Poly(Ethylene Oxide) and Polyacrylamide with Ascorbic Acid. *Journal of Applied Polymer Science* **2006,** 101, (5), 3067-3072.

29. Crowley, M. M.; Zhang, F.; Koleng, J. J.; McGinity, J. W., Stability of Polyethylene Oxide in Matrix Tablets Prepared by Hot-Melt Extrusion. *Biomaterials* **2002,** 23, (21), 4241-4248.

APPENDIX 2

SUPPLEMENTARY INFORMATION

A2.1 APPENDIX 1 SUPPLEMENTARY INFORMATION [9]

Contents:

(1) ^{1}H-NMR spectrum of PS-PEO-H

(2) ^{1}H-NMR spectrum of PS-PEO-Ms

(3) ^{1}H-NMR spectrum of PS-PEO-azide

(4) ^{1}H-NMR spectrum of PS-PEO-alkyne

(5) FTIR result for PS-PEO-azide

(6) Frequency sweep results (elastic shear moduli) for samples A1 - D1, baseline SO/SOS hydrogels of 4.1 and 20.3 mol% SOS, and a catalyst control sample

(7) Unconfined compression for samples A1 - D1, and a catalyst control sample

[9] The contents of this Appendix contain the supplementary information for Appendix 1 adapted from the publication Dangling-End Double Networks: Tapping Hidden Toughness in Highly Swollen Thermoplastic Elastomer Hydrogels Chem. Mater., 2016, 28 (6), pp 1678–1690 as well as supplementary information for Chapter 3.

A2.1.1 ^{1}H-NMR spectrum of PS-PEO-H

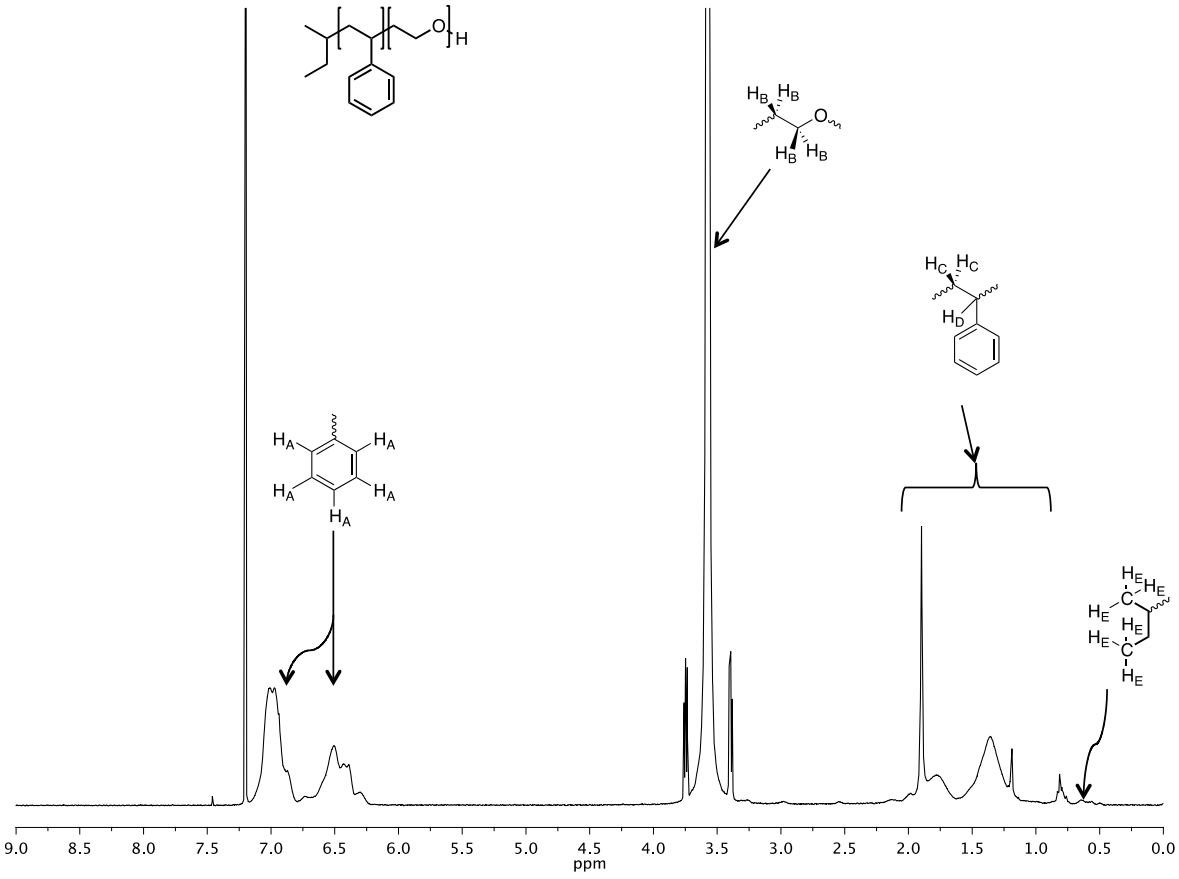

Figure A2.1: ^{1}H-NMR spectrum of PS-PEO-H diblock copolymer. The PS-PEO-PS triblock copolymer, PS-PEO-azide diblock copolymer, and PS-PEO-alkyne diblock copolymer were all generated from the above parent diblock copolymer molecule.

A2.1.2 ^{1}H-NMR spectrum of PS-PEO-Ms

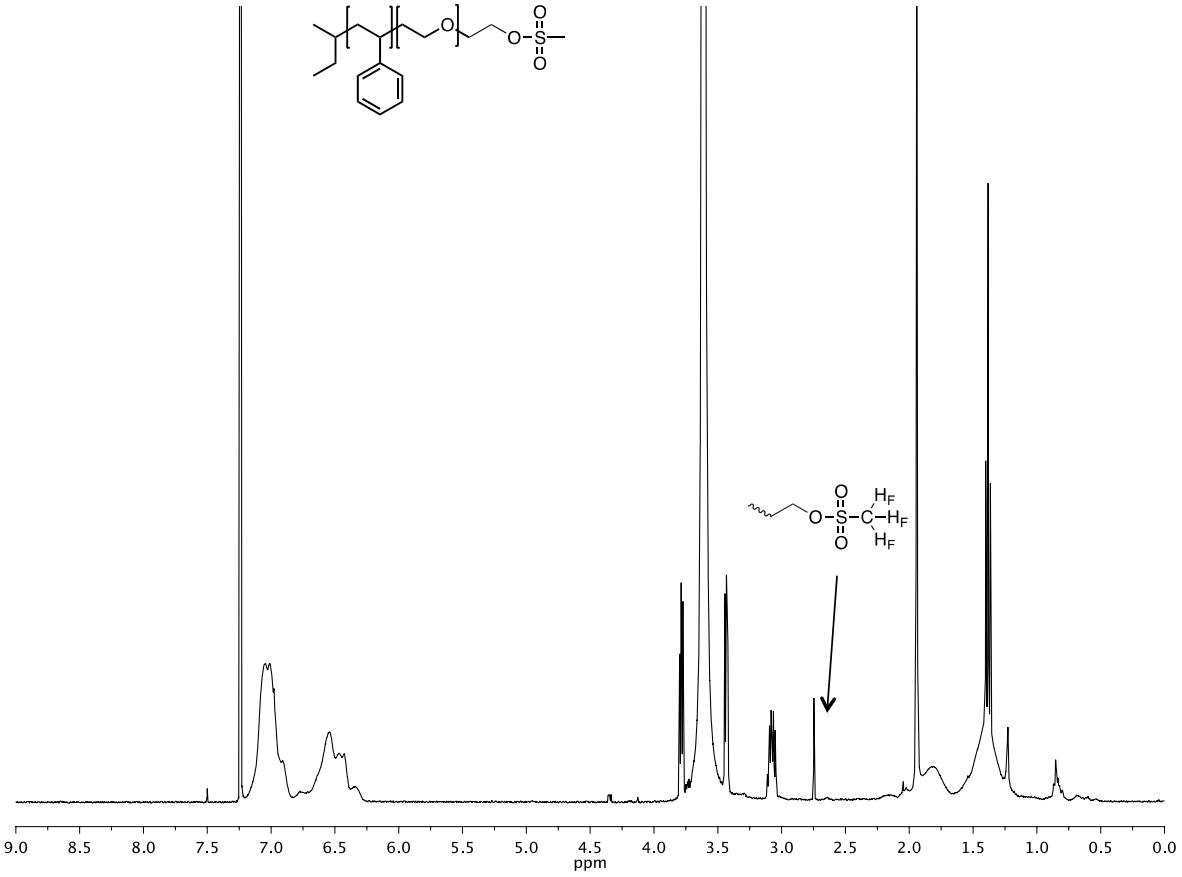

Figure A2.2: ^{1}H-NMR spectrum of PS-PEO-Ms (methanesulfonyl (mesyl)). This compound is the precursor of PS-PEO-azide.

A2.1.3 ^{1}H-NMR spectrum of PS-PEO-azide

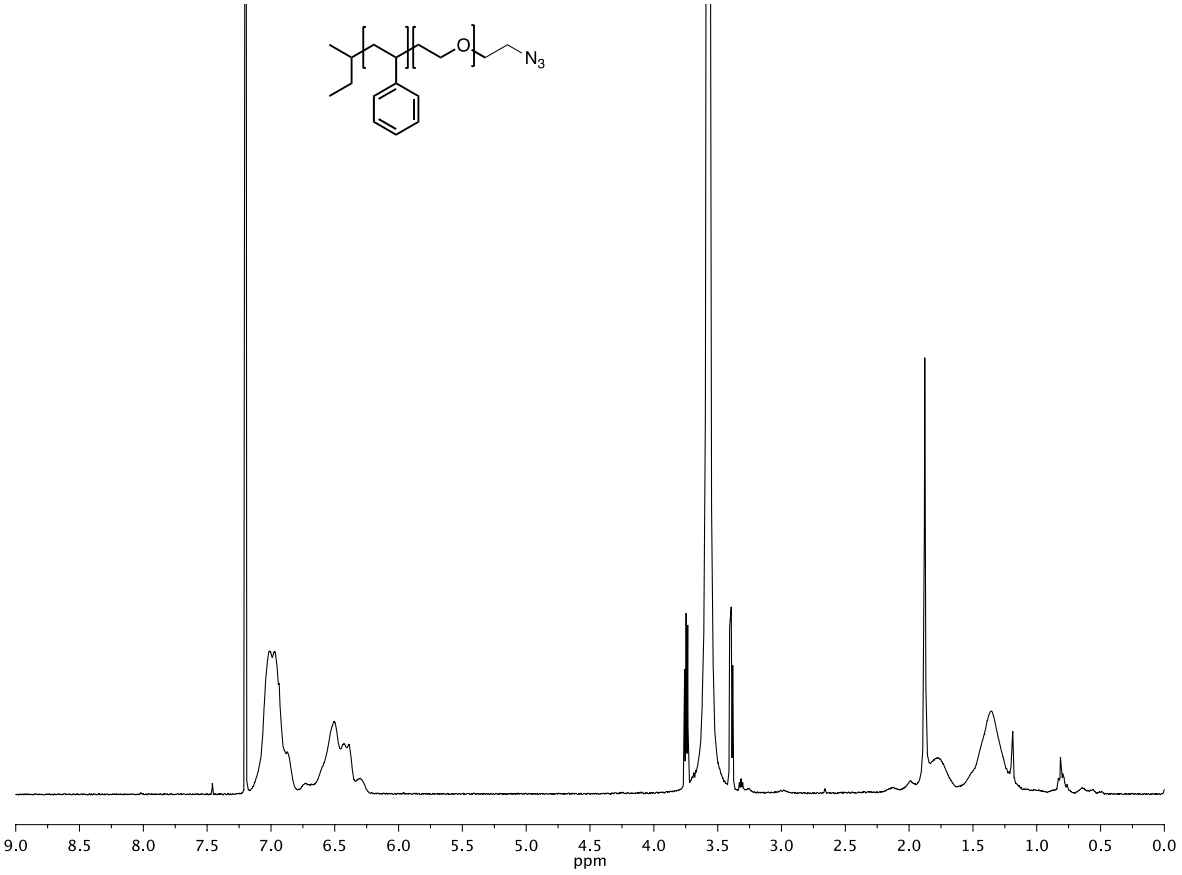

Figure A2.3: ^{1}H-NMR spectrum of PS-PEO-azide. The terminal methylene protons adjacent to the azide end group overlap with the methylene protons of the PEO backbone (4.0-3.2 ppm). Confirmation of azide group functionality is shown in the FTIR spectrum in Figure S5.

A2.1.4 ^{1}H-NMR spectrum of PS-PEO-alkyne

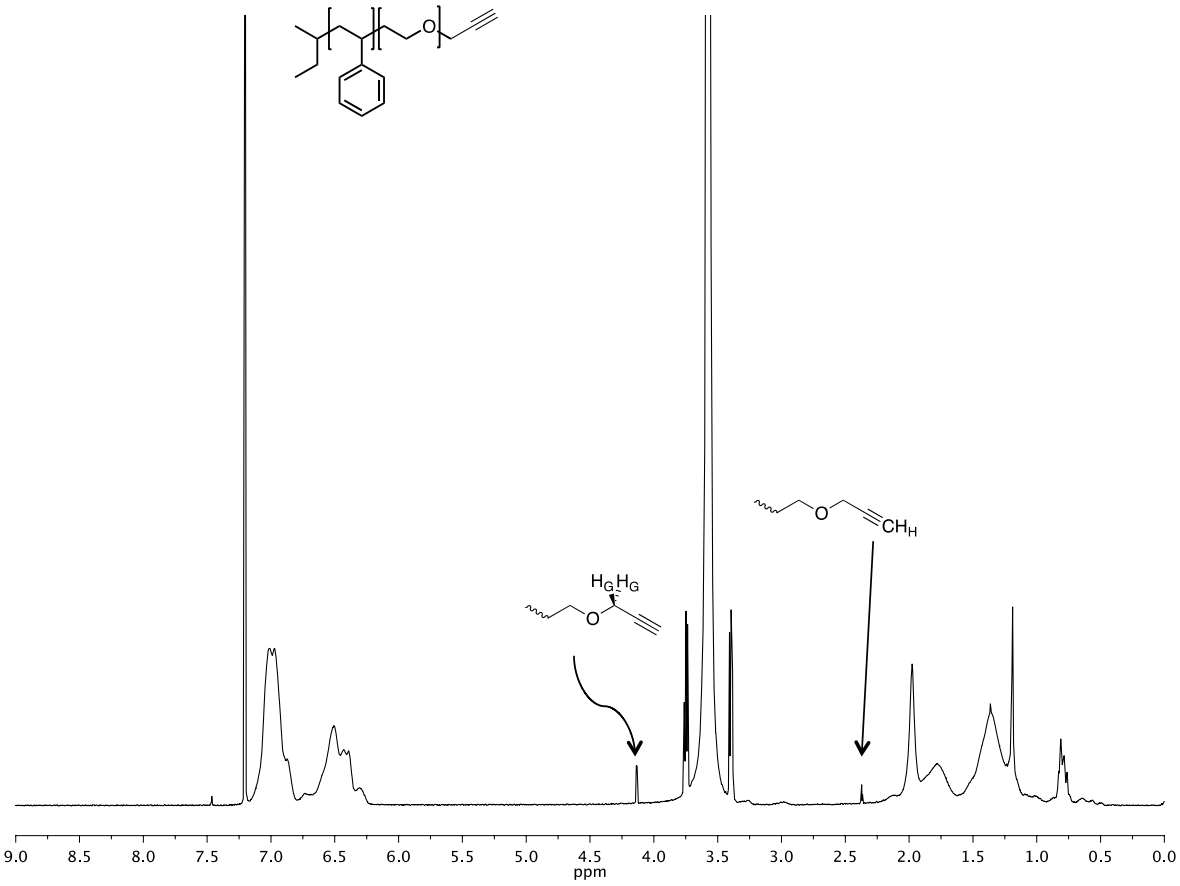

Figure A2.4: ^{1}H-NMR spectrum of PS-PEO-alkyne.

A2.1.5 FTIR spectrum of PS-PEO-azide

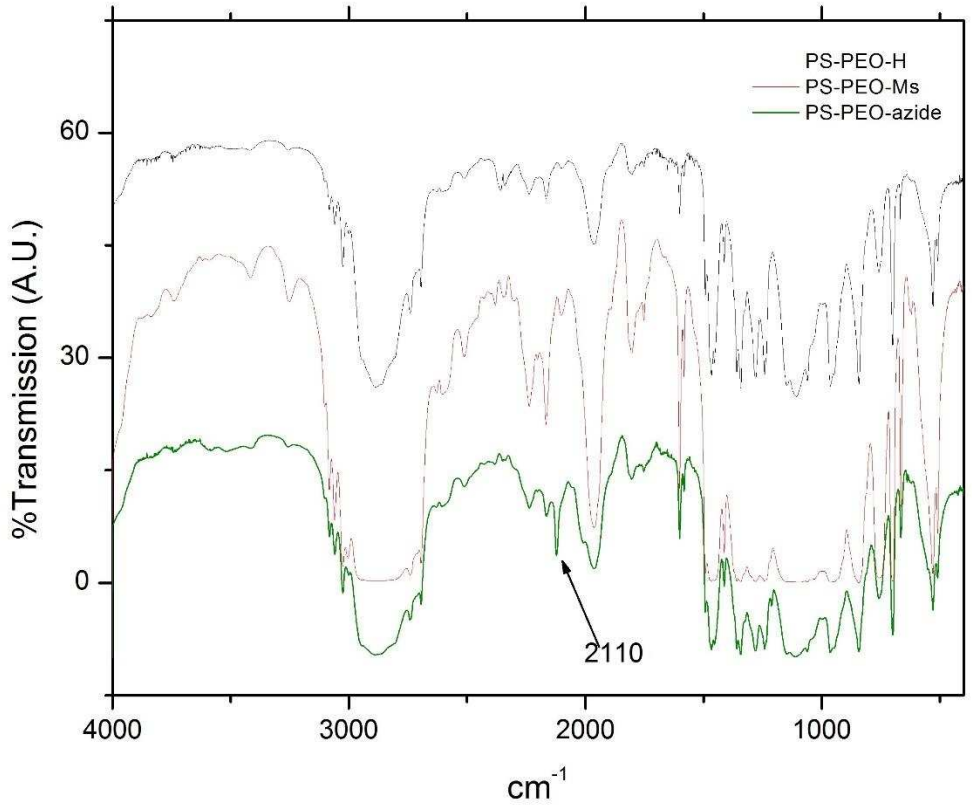

Figure A2.5: FTIR spectra of PS-PEO-H, PS-PEO-Ms and PS-PEO-azide. The characteristic vibration for the azide group is shown at 2110 cm^{-1}.

A2.1.6 Dynamic frequency sweep results (elastic shear moduli) for samples A1 - D1, baseline SO/SOS hydrogels of 4.1 and 20.3 mol% SOS, and a catalyst control sample.

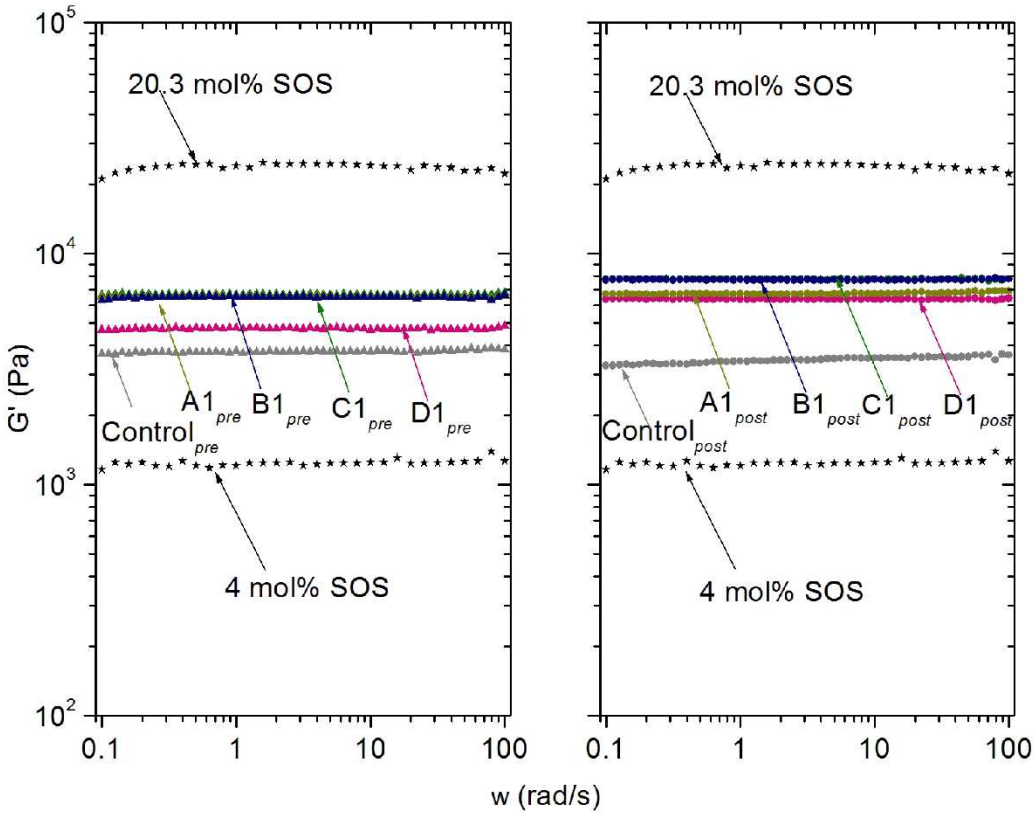

Figure A2.6: Representative dynamic frequency sweep results showing the elastic moduli for samples A1 - D1, two baseline SO/SOS hydrogels of 4.1 and 20.3 mol% SOS, and a baseline SO/SOS hydrogel soaked in catalyst solution for 24 hours (control).

A2.1.7 Unconfined compression for samples A1 - D1, and a catalyst control sample.

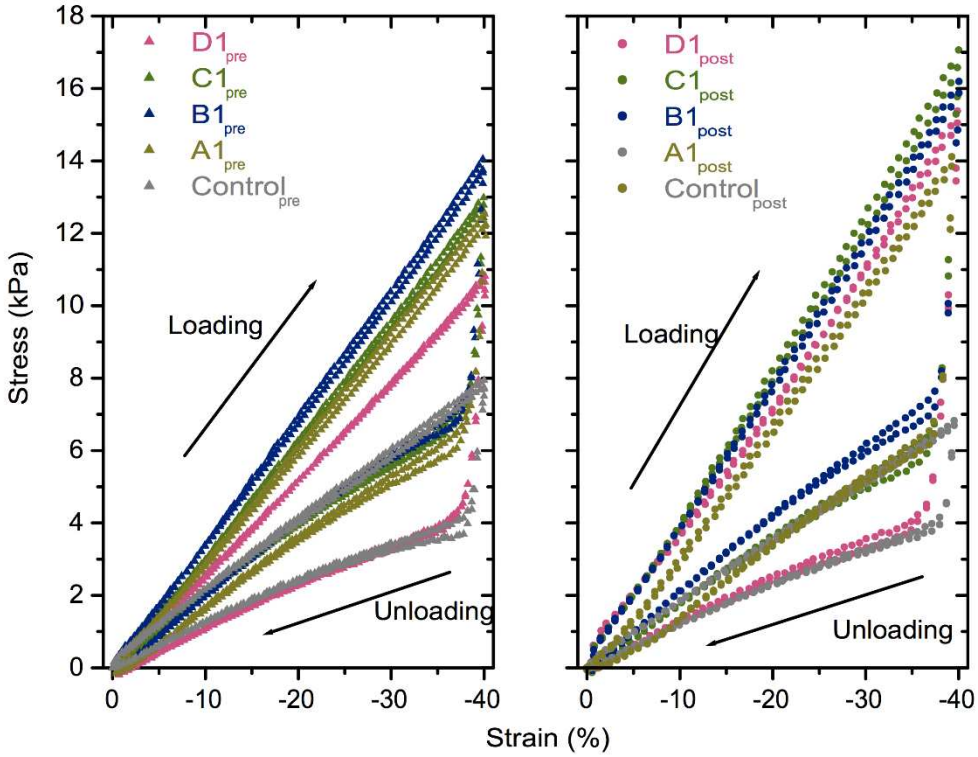

Figure A2.7: Representative unconfined compression results showing the stress-strain relationships for samples A1 - D1, and a baseline SO/SOS control hydrogel soaked in catalyst solution for 24 hours (control).

A2.2 CHAPTER 3 SUPPLEMENTARY INFORMATION

Contents:

A2.2.1 Structural characterization of the SO/SOS blend nanoscale morphology via SAXS

a **b**

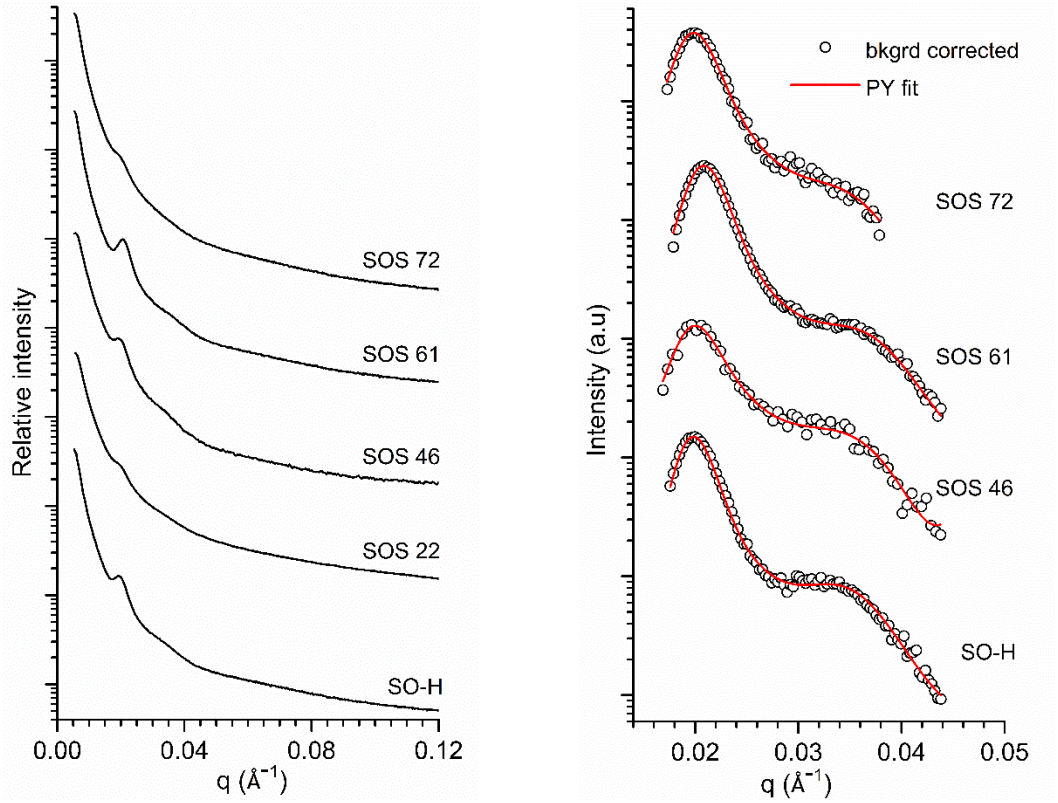

Figure A2.8: a. 1D azimuthally integrated SAXS data for SO-H, SOS 22, SOS 46, SOS 61, and SOS 72 in the melt at 120 °C just prior to vitrification. The primary peak and adjacent broad shoulder are typical scattering signatures for SOS blends exhibiting a liquid-like packing of spheres, as described previously by our group[2, 3] and others.[4, 5, 6, 7, 8] **b.** Fits of the SO-H, SOS 46, SOS 61, and SOS 72 data to a Percus-Yevick hard sphere model[9] for polydisperse spheres confirms a polystyrene core radius of 10.5 nm, with an principal domain spacing of about 30 - 32 nm. While the signal contrast in the SOS 22 scattering data was too weak to perform a reliable Percus-Yevick fit, the coincidence of the principal scattering peak position ($q^* = 0.020$ Å^{-1}) and similarity of the scattering profiles is a strong indication of the structural similarity among all the SOS blends. Such similarity is expected based on our previous experience with these types of blends (used in hydrogel applications), and is an intended byproduct of using "lattice matched" SO and SOS block copolymer compositions.[2, 3]

A2.2.2 Chemical and melt state morphological data of block copolymer blends

Table A2.1: Chemical and melt-state morphological characterization data of block copolymer blends. a Micelle core radius,b Micelle core overall volume fraction, ϕc=(Rc/Rhs)3ϕhs, based on the PY parameters,c Mean aggregation number (i.e., PS chains per sphere), based on the PY parameters,d apparent hard sphere radius,e hard sphere volume fraction

Sample	Tether added (mol%)	q*/Å^{-1}	d*/nm	f_{PS}	Percus-Yevick hard sphere model				
					R_c[a]/nm	ϕ_c[b]	θ_{PS}[c]	R_{hs}[d]/nm	ϕ_{hs}[e]
SO-H	0	0.0198	31.7	0.085	10.5	0.107	337	18.0	0.54
SOS 22	22	0.0197	31.9	0.085	-	-	-	-	-
SOS 46	46	0.0196	32.0	0.085	10.5	0.108	338	17.0	0.46
SOS 61	61	0.0207	30.4	0.085	10.5	0.125	339	17.0	0.53
SOS 72	72	0.0197	31.9	0.085	10.5	0.109	340	17.5	0.50

.

A2.2.3 Swelling data as a function of SOS triblock copolymer concentration, swelling medium, and temperature

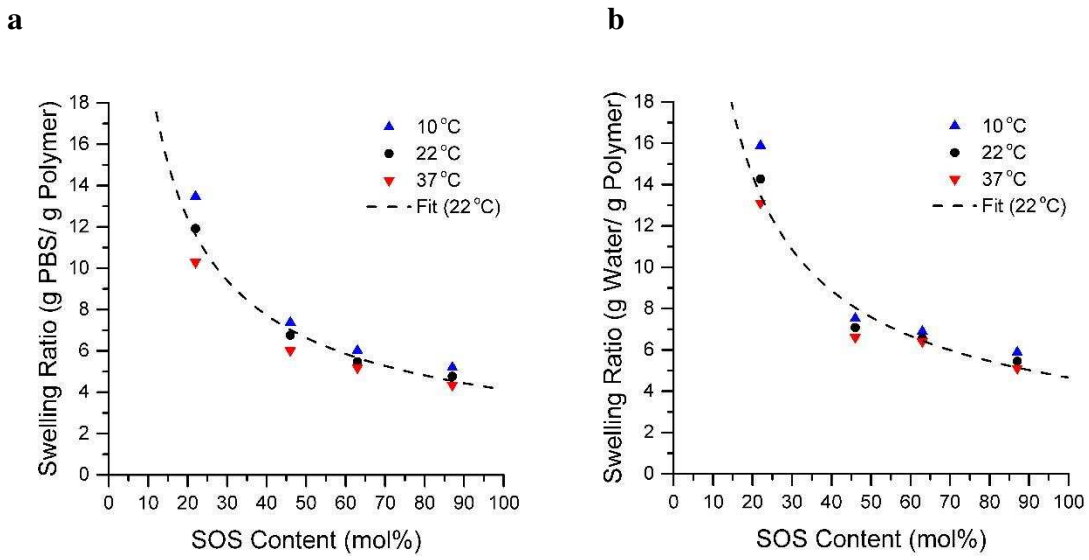

Figure A2.9: a. Gravimetrically determined swelling ratio data in phosphate buffered saline (PBS) for SOS 22, SOS 46, SOS 63, and SOS 87 at 10°C, 22°C, and 37°C with approximate power fit ($95.6(\text{SOS mol\%})^{-0.682}$, $R^2 = 0.99$). **b.** Swelling ratio data in DI water for SOS 22, SOS 46, SOS 63, and SOS 87 at 10°C, 22°C, and 37°C with approximate power fit ($117.2(\text{SOS mol\%})^{-0.701}$, $R^2 = 0.96$). As SOS content increases swelling ratio decreases. Higher SOS content increases the number of trapped topological entanglements produced in the melt, resulting in a restricted ability of the hydrogel to swell. The lower swelling ratio at higher temperatures is due to reduced solubility of the PEO.

A2.2.4 Indentation Relaxation Data

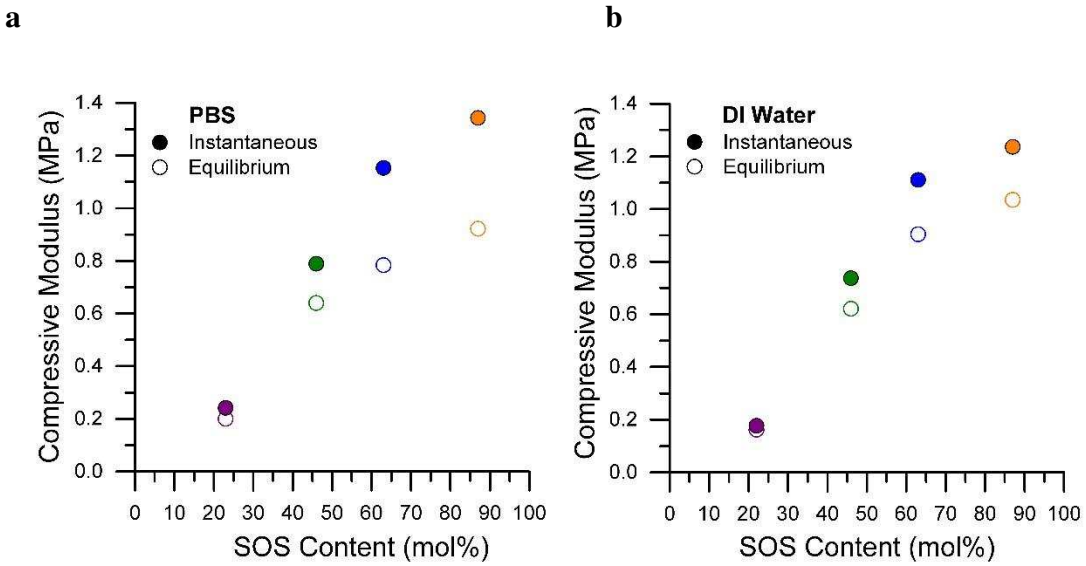

Figure A2.10: a. Indentation relaxation data for SOS 22, SOS 46, SOS 63, and SOS 87 in PBS at room temperature. **b.** Indentation relaxation data for SOS 22, SOS 46, SOS 63, and SOS 87 in DI water at room temperature. All samples were strained to 12% in 1 second and allowed to relax for 300 seconds. As SOS content increases, both the instantaneous and equilibrium moduli increase. As the SOS content increases, the chain density increases, leading to a higher resistance to osmotic flow. This produces the higher initial modulus, which relaxes with flow.

A2.2.5 Sample Identification History

Manuscript ID	Lab Notebook IDs
S-OH	DBW-1-142
SO-H	DBW-1-170
SOS 22	JTL-2-093
SOS 32	JTL-3-010
SOS 46	JTL-2-077
SOS 61	JTL-3-116
SOS 72	JTL-2-113